Universidad de Extremadura

Facultad de Ciencias

Departamento de Física

Transiciones de Fase en Sistemas Desordenados

Phase Transitions in Disordered Systems

Memoria de tesis doctoral

presentada por

Antonio Gordillo Guerrero

Universidad de Extremadura

Facultad de Ciencias

Departamento de Física

Transiciones de Fase en Sistemas Desordenados

Phase Transitions in Disordered Systems

Antonio Gordillo Guerrero

Dirigida por

Juan Jesús Ruiz Lorenzo

Agradecimientos

La elaboración de esta tesis doctoral ha sido únicamente posible gracias al apoyo prestado por muy diversas personas e instituciones, es por ello muy importante para mí hacer una mención a su labor.

Soy muy afortunado al formar parte del grupo investigación Statistical Physics in Extremadura (SPHINX), formado por científicos de primer nivel además de excelentes personas. Su acogida ha sido impecable desde el primer día y he recibido su apoyo en todo momento. Gracias a Andrés Santos, Vicente Garzó, Santos Bravo, Antonio Astillero, Francisco Vega, Mariano López, Enrique Abad, Rafael Borrego, Rene Rohrmann y por supuesto Juan Jesús Ruiz.

Juan Jesús Ruiz tiene más que merecido un párrafo aparte, ha sido el director de este trabajo y es mi principal mentor. Es una persona muy trabajadora, con una formación excelente y grandes habilidades pedagógicas. Además es un director comprensivo y muy accesible. No imagino otro director de tesis mejor. Ha sido un placer trabajar con él durante estos años y espero poder seguir haciéndolo.

Agradezco la ayuda prestada durante estos años por Luis Antonio Fernández y Víctor Martín, de la Universidad Complutense de Madrid. Luis Antonio supone todo un ejemplo de maestría en Física Computacional y de capacidad de trabajo, mientras que Víctor nunca deja de sorprenderme por su capacidad de síntesis. Estoy también en deuda con Ralph Kenna, de la Universidad de Coventry; trabajar con él ha sido agradable y fructífero.

Estoy muy agradecido por el apoyo computacional ofrecido por el Instituto de Biocomputación y Física de Sistemas Complejos (BIFI) de Zaragoza. Resalto la labor de Alfonso Tarancón, su secretario, siempre atento por el buen desarrollo de nuestras investigaciones. El equipo de soporte técnico ha sido excelente; gracias en particular a Guillermo Losilla, Arturo Giner y Fermín Serrano. Los desarrolladores de Ibercivis han hecho un esfuerzo importante en la adaptación y soporte de nuestra aplicación; gracias en concreto a Alejandro Rivero y David Benito.

Mis compañeros del área de Electrónica en la Escuela Politécnica de Cáceres me han facilitado desde el primer día la integración en su equipo docente, siendo siempre comprensivos con mis continuos viajes. Ellos son Horacio González, Ramón Gallardo y Antonio García.

Envío también mi agradecimiento al Departamento de Física y al Departamento de Ingeniería Eléctrica, Electrónica y Automática de la Universidad de Extremadura. Agradezco en particular la labor de sus directores Miguel Jurado y Miguel Ángel Jaramillo, así como de su personal de administración.

Estas páginas de agradecimientos estarían del todo incompletas si no mencionara el apoyo continuo que tengo de mi familia. En especial quiero agradecer a mis padres la educación que me dan a través de su ejemplo. Dedico también estas páginas a mis abuelas y abuelos ya que suponen para mí importantes modelos de buena conducta. Quiero además mencionar a mi hermano Fernando, me gustaría que este trabajo sirviera de motivación para su carrera científica, tiene sobradas capacidades que creo que aún no ha descubierto.

Para la realización de esta tesis ha sido imprescindible la ayuda de mi pareja: Ana Chacón Chamorro. Ha sido todo lo comprensiva que se puede ser con un marido y padre que realiza una tesis doctoral. Sin su apoyo no hubiera podido finalizar este trabajo. Ella cuida y protege con toda su alma a nuestro principal objetivo vital: nuestra hija Julia. A Julia le ruego que me perdone por el tiempo irrecuperable de su primera infancia que no hemos podido disfrutar juntos. Estar con Julia y Ana produce en mí la felicidad más profunda que nunca he sentido.

No puedo dejar de mencionar la ayuda que me ha prestado mi prima Raquel Acosta durante los años vividos entre Cáceres y Badajoz. Desde el primer día me ha abierto las puertas de su casa sin esperar nada a cambio. Me ha dado la posibilidad de aprovechar más mi tiempo y me ha acompañado en mis escasos momentos de ocio. ¡Muchas gracias Prima!

Finalmente mencionar a mis amigos de Badajoz, Zafra y Madrid, así como al Club de Piragüismo de Badajoz. Todos habéis estado ahí cuando os necesitaba.

Cáceres, Septiembre de 2009

A mis padres, responsables de mi educación.

Contents

Capítulo 1

Introducción

Una transición de fase se define como un cambio brusco en la estructura interna y las propiedades de un sistema debido a variaciones en su entorno. Este entorno se caracteriza generalmente por cantidades tales como temperatura, presión, campos electromagnéticos, etc. Los ejemplos más comunes de transiciones de fase son la transición de líquido a gas, de conductor normal a superconductor, o de material paramagnético a ferromagnético. El estudio de las transiciones de fase es de indiscutible interés tanto teórico como tecnológico.

Los estudios teóricos microscópicos de las transiciones de fase implican el estudio de un fenómeno producido por la interacción simultánea de un número enorme ($\sim 10^{23}$) de componentes individuales. Esto forzó el desarrollo de teorías aproximadas que proporcionaban soluciones exactas solo en algunos casos simplificados. Un ejemplo es la teoría de campo medio para transiciones de segundo orden, véase [1] ó [2], introducida por L. D. Landau al final de la década de 1950. La explicación más satisfactoria de los fenómenos críticos fue proporcionada por el *Grupo de Renormalización* (GR), en primer lugar intuido por L. P. Kadanoff [3] y finalmente desarrollado alrededor de 1970 en los importantes artículos de K. G. Wilson [4, 5], ver [6] para una interesante revisión histórica de los logros del GR.

La transición de fase en un sistema puede ser descrita como una discontinuidad en las derivadas de su energía libre respecto a alguna de las variables termodinámicas y pueden ser clasificadas de acuerdo a esto, utilizando la llamada clasificación de Ehrenfest. Si la discontinuidad se presenta en la primera derivada, se denomina transición de fase de primer orden, mientras que si es en la segunda derivada, se denomina transición de fase de segundo orden.

De forma general, las transiciones de fase de primer orden son casi siempre las que involucran un calor latente. Durante dichas transiciones, el sistema absorbe o libera una cantidad fija (y por lo general grande) de energía. Durante el proceso, la temperatura del sistema permanece constante conforme se absorbe o se libera calor. Además, las transiciones de primer orden están asociadas a *regímenes mixtos* en los que algunas partes del sistema han completado la transición, mientras que otras no. Un ejemplo típico de este fenómeno es la coexistencia del régimen de baja temperatura del agua (hielo) y el de alta temperatura (agua líquida); el agua y el hielo pueden coexistir (existen los icebergs).

Las transiciones de fase de segundo orden son continuas en la primera derivada de la energía libre, pero presentan discontinuidades en su segunda derivada. Estas incluyen la transición a la fase ferromagnética en materiales como el hierro, donde la magnetización, que es la primera derivada de la energía libre con respecto a la fuerza del campo magnético aplicado, aumenta de forma continua desde cero conforme la temperatura desciende por debajo de la temperatura de Curie. La susceptibilidad magnética, la segunda derivada de la energía libre respecto al campo, diverge. Este tipo de transiciones no tiene calor latente asociado pero presenta longitudes de correlación infinita. Ejemplos típicos de transiciones de fase de segundo orden son las transiciones paramagnética-ferromagnética y conductor-superconductor. Este tipo de transiciones también se caracteriza por comportamientos en forma de leyes de potencia en el punto de transición (también llamado *punto crítico*) con exponentes no enteros, llamados *exponentes críticos*[1]. Los exponentes críticos están relacionados entre sí por *relaciones de hiperescalado* – conociendo dos de los exponentes, los otros pueden ser deducidos. Sistemas muy diferentes pueden compartir exactamente el mismo conjunto de exponentes críticos y se dice entonces que pertenecen a la misma *Clase de Universalidad* (CU). La CU de un sistema se define por propiedades muy generales tales como la simetría de la interacción microscópica, la dimensionalidad espacial, o la dimensionalidad del parámetro de orden, ver [8] para una revisión exhaustiva de las CU más habituales.

La existencia de un parámetro de orden es también característica de las transiciones de fase. Éste puede ser definido como una cantidad que es nula en una de las fases y no nula en la otra. Refleja el proceso de ruptura de simetría que normalmente tiene lugar a través del punto de transición. Por ejemplo, para la transición paramagneto-ferromagneto un parámetro de orden válido es la magnetización neta (cero en la fase de alta temperatura y no cero en la de baja temperatura), mientras que para la transición líquido-gas es la diferencia de densidad de los dos regímenes que coexisten. Otros tipos de transiciones de fase deben ser descritos por parámetros de orden más complejos.

Simulaciones de Monte Carlo (MC) han resultado ser muy útiles en esta rama de la Mecánica Estadística, ver [9] para una revisión de los métodos más populares. Con ellos, se puede simular la evolución temporal de cada constituyente del sistema para un determinado Hamiltoniano. En nuestro caso, los sistemas se definen en redes de dimensionalidad espacial D, con tamaño lineal L y condiciones de contorno periódicas. En cada nodo de la red se define una variable, llamada *espín*, que toma ciertos valores (dependientes del modelo) que evolucionan con el tiempo.

Un método de MC puede actualizar o bien un solo espín por iteración, como es el caso del algoritmo de Metrópolis o del de baño térmico [9], o bien un grupo de espines, como en el caso de los algoritmos de Wolff [10] o de Swendsen-Wang [11]. Estos últimos son llamados *métodos de clusters*. En las proximidades del punto crítico, se produce el llamado *Decaimiento Crítico*, ver por ejemplo [9]. Los tiempos de

[1]Seguiremos la nomenclatura habitual (ver por ejemplo [7]) para los exponentes críticos: ν es el exponente de la longitud de correlación, α es el del calor específico, β el del parámetro de orden, mientras que ω es el exponente (universal) de correcciones de escala de orden dominante. Un exponente ligeramente distinto, la dimensión anómala η, se define en Ec. (2.72).

relajación del parámetro de orden divergen como una potencia de la longitud de correlación, $\tau \sim \xi^z$, siendo z el denominado *exponente crítico dinámico*. Esto implica que el tiempo necesario para producir configuraciones estadísticamente independientes diverge cerca del punto crítico para un sistema finito como $\tau \sim L^z$. Los métodos de MC de actualización de un único espín tienen un exponente $z \gtrsim 2$. Por lo tanto es muy complicado obtener datos de alta precisión muy cerca del punto crítico en sistemas grandes. Por el contrario, se obtiene un comportamiento dinámico mucho mejor utilizando métodos de MC de actualización de clusters. Con estos últimos, dependiendo del modelo y de la dimensionalidad, se obtienen valores de z entre 0 y 1 [12]. En este trabajo hemos utilizado casi siempre algoritmos de clusters.

Los métodos de actualización de espines incluyen simulaciones dentro del colectivo canónico (a una temperatura fija) y dentro del colectivo microcanónico (a energía fija). Respecto a las simulaciones dentro del colectivo microcanónico, hemos utilizado un método de simulación microcanónico propuesto recientemente que permite la simulación de sistemas de un tamaño nunca antes alcanzado que realizan transiciones de fase de primer orden [13].

Incluso con los recursos de computación de hoy en día, estamos restringidos a simular sistemas con más de 10^{15} órdenes de magnitud menos componentes que los presentes en un sistema macroscópico real (con $\sim 10^{23}$ partículas). Lo único que podemos hacer es simular sistemas con diferentes tamaños y tratar de extrapolar nuestros resultados al Límite Termodinámico ($L \to \infty$). El estudio del comportamiento de escala de los diferentes observables con el tamaño del sistema es llamado Finite-Size Scaling (FSS) y es fundamental para el estudio de las transiciones de fase, véase por ejemplo [7]. En este trabajo hemos usado continuamente técnicas de FFS, además hemos realizado un estudio novedoso del FSS dentro del colectivo microcanónico, veáse el Capítulo 2.

Nuestro objetivo principal es el estudio de los efectos del desorden sobre las transiciones de fase. En concreto, deseamos estudiar el efecto de las impurezas congeladas en la transición de material paramagnético a ferromagnético. La presencia de desorden aleatorio en un sistema produce muchos fenómenos interesantes y físicamente relevantes, lo que ha motivado extensos estudios teóricos y experimentales. Los tipos más característicos de sistema con desorden aleatorio son: vidrios de espín [14, 15], sistemas aleatoriamente anisotrópicos [16–18], sistemas diluidos [19–21] y sistemas con los campos aleatorios [14]. En todos estos casos, existen variables aleatorias que caracterizan el comportamiento del sistema.

Al modelar un sistema con desorden aleatorio se pueden utilizar dos enfoques diferentes. Por un lado, se puede considerar que las variables aleatorias están en equilibrio termodinámico las otras variables dinámicas del sistema. Por lo que las variables aleatorias también serán "dinámicas". Este es el llamado *desorden annealed* y debe ser la elección si deseamos modelar un sistema en el que los tiempos característicos de la dinámica del desorden sean comparables con los tiempos característicos de la dinámica de las variables originales, como sería el caso por ejemplo de una disolución de dos líquidos. Por otro lado, se puede considerar que las variables aleatorias no evolucionan en el tiempo, sino que están congeladas. Es el llamado *desorden congelado*. Ésta última es una alternativa perfectamente válida por ejemplo si

queremos modelar sistemas magnéticos con impurezas. En este caso, el comportamiento magnético se debe a los espines de los electrones no apareados en las capas atómicas exteriores, mientras que las impurezas son átomos sin electrones no apareados. Se sabe que la dinámica de los electrones es órdenes de magnitud más veloz que la dinámica de los núcleos de modo que se puede considerar a los átomos de impurezas congelados en el tiempo. En Ref. [22] se presenta un análisis más detallado de esta cuestión. Cuando se considera el desorden congelado se generan diferentes configuraciones espaciales aleatorias del desorden (llamadas *muestras*). Los espines de cada muestra evolucionarán independientemente mientras que las impurezas permanecen fijas. Para extraer la información de un determinado observable, en primer lugar realizamos el promedio de su evolución temporal en el interior de cada muestra (en lo sucesivo denominado *promedio termal* y denotado por brackets) y luego realizamos el promedio de lo anterior entre todas las muestras (denominado *promedio muestral* y denotado por un suprarrayado), el promedio doble es entonces denotado por $\overline{\langle \cdots \rangle}$.

Uno de los resultados de mayor importancia en el estudio de sistemas desordenados es el criterio de Harris [23], véase el Apéndice A. El criterio señala que si el calor específico en el sistema puro diverge (el exponente crítico α_{puro} es mayor que cero), el desorden cambiará el comportamiento crítico del modelo, es decir, aparecerá una nueva CU. En este caso, se dice que el desorden es *relevante*. Por el contrario, si el calor específico no diverge en el sistema puro ($\alpha_{\text{puro}} < 0$) los exponentes críticos del sistema desordenado no cambiarán. Es este caso, se dice que el desorden es *irrelevante*. En el presente trabajo recomprobaremos la validez del criterio para el modelo de Heisenberg tridimensional con dilución por sitios.

Otra cuestión muy interesante que surge cuando se estudian sistemas diluidos es la cuestión del *autopromedio*. El valor medio de un observable $\mathcal{O}$ en una red de tamaño lineal L es diferente para cada realización del desorden (en nuestro caso, para cada distribución espacial de los sitios no magnéticos), por lo que es una variable estocástica caracterizada por un promedio sobre el desorden $\overline{\mathcal{O}}$ y una varianza $(\Delta\mathcal{O})^2 \equiv \overline{\mathcal{O}^2} - \overline{\mathcal{O}}^2$. Se dice que un sistema exhibe autopromedio para el observable $\mathcal{O}$ si $\Delta\mathcal{O}/\mathcal{O}$ tiende a cero cuando $L \to \infty$. Cuando un sistema diluido no autopromedia los estudios numéricos se hacen muy difíciles: incluso fijando la temperatura crítica al valor correcto para $L \to \infty$, hacer el sistema más grande no proporciona una gran mejora estadística. El autopromedio de las propiedades de los sistemas desordenados genera gran interés, reflejado en numerosos trabajos tanto numéricos [24–26] como analíticos [27–29]. En esta tesis se estudiará el autopromedio tanto de la susceptibilidad del modelo de Heisenberg tridimensional, como del calor latente y la tensión superficial del modelo de Potts tridimensional, ambos modelos con dilución por sitios.

Hemos estudiado numéricamente varios modelos con desorden aleatorio que presentaban importantes cuestiones abiertas. Nuestra colaboración ha producido las publicaciones recogidas en [30–42] aunque en el presente trabajo sólo se presentan los resultados de las referencias [30–35].

La disposición del resto de esta tesis doctoral es la siguiente. En el Capítulo 2 estudiamos las propiedades de escala, tanto del modelo de Potts puro con cuatro

estados ($Q = 4$) en $D = 2$ como del modelo de Ising puro en $D = 3$. Estos modelos realizan transiciones de fase de segundo orden bien conocidas con calores específicos divergentes. Hemos simulado ambos modelos utilizando el método de simulación microcanónico presentado en [13]. Obtuvimos fuertes evidencias de la bondad de dicho método a través de la comparación con los resultados más recientes [8, 43]. El Capítulo 3 lo dedicamos al estudio de los efectos de la dilución en un sistema que realiza una transición de fase de primer orden fuerte: el modelo de Potts tridimensional con $Q = 4$ y $Q = 8$ estados. Utilizando el método de simulación comprobado en el Capítulo 2, fuimos capaces de simular sistemas con más de 10^6 componentes, multiplicando por un factor de 100 el número de componentes de los trabajos más recientes [44–46]. En el Capítulo 4 estudiamos las propiedades de autopromedio del modelo de Heisenberg tridimensional diluido por sitios, donde existen dos escenarios en conflicto que afirman que la susceptibilidad es [27] o no es [28] autopromediante. Además obtendremos información acerca de la validez del criterio de Harris. En el Capítulo 5 exponemos nueva información acerca de los exponentes críticos de los términos logarítmicos del modelo de Ising en cuatro dimensiones con dilución por sitios. Hemos logrado discriminar entre cinco diferentes teorías [47–51] mediante simulaciones numéricas de gran envergadura. Presentamos nuestras conclusiones generales en el Capítulo 6. También se exponen varios apéndices tratando de ampliar la información sobre algunas de las herramientas utilizadas más importantes o innovadoras. En el Apéndice A explicamos con detalle el criterio de Harris. En el Apéndice B presentamos brevemente las técnicas populares del FSS, así como el Método de los Cocientes, una técnica que permite el cálculo de los exponente críticos partiendo de los datos obtenidos en sistemas finitos. En el Apéndice C se describen dos cuestiones muy importantes para la simulación de sistemas dinámicos con métodos de MC: los tiempos de autocorrelación y la estimación de errores. El Apéndice D está dedicado a describir los diferentes métodos para la extrapolación en temperatura de los resultados obtenidos en una simulación canónica mientras que en el Apéndice E se describe la obtención de la construcción de Maxwell, muy útil para el estudio de transiciones de fase de primer orden. En el Apéndice F se describe el enfoque introducido por Lee y Yang para describir las transiciones de fase, formulando su importante teorema. También discutimos en este apéndice de la distribución de los ceros de Lee-Yang sobre el círculo unidad. Por último, dedicamos el Apéndice G a la descripción de la infraestructura de supercomputación IBERCIVIS, que ha sido crucial para completar algunas partes de este trabajo.

Chapter 1

Introduction

A phase transition is defined as a sharp change in the internal structure and properties of a system due to variations in its environment. This environment is usually characterised by quantities such as temperature, pressure, electromagnetic fields, etc. Common examples of phase transitions are the transition from liquid to gas, from normal conductor to superconductor, and from paramagnet to ferromagnet. The study of phase transitions is of major interest both theoretically and technologically.

Theoretical microscopic studies of phase transitions involve the study of a phenomenon produced by the simultaneous interaction of an enormous number ($\sim 10^{23}$) of individual components. This forced the development of approximate theories that produce exact solutions only for some simplified cases. An example is the mean-field theory for second-order phase transitions, see for instance [1] or [2], introduced by L. D. Landau in the late 1950s. The most satisfying explanation of critical phenomena was provided by the *Renormalization Group* (RG) picture, first intuited by L. P. Kadanoff [3] and finally developed around 1970 in the landmark papers of K. G. Wilson [4, 5], see [6] for an interesting historical review of RG achievements.

A phase transition in a system can be described as a discontinuity in the derivatives of its free energy with respect to some thermodynamic variable, and can be classified according to this by using the so-called Ehrenfest classification. If the discontinuity is in the first derivative it is called a first-order phase transition, while if it is in the second derivative it is called a second-order phase transition.

More generally, first-order phase transitions are usually those involving a latent heat. During such a transition, the system either absorbs or releases a fixed (and typically large) amount of energy. During the process, the temperature of the system remains constant as heat is added or released. In addition, first-order transitions are associated with *mixed-phase regimes* in which some parts of the system have completed the transition while others have not. A typical example of this phenomenon is the coexistence of the low temperature regime of water (ice) and the high temperature one (liquid water); water and ice can and do coexist (there exist icebergs).

Second-order phase transitions are continuous in the first derivative but exhibit discontinuities in a second derivative of the free energy. These include the ferro-

magnetic phase transition in materials such as iron, where the magnetisation, which is the first derivative of the free energy with respect to the applied magnetic field strength, increases continuously from zero as the temperature is lowered below the Curie temperature. The magnetic susceptibility, the second derivative of the free energy with respect to the field, diverges. These have no associated latent heats, but present infinite correlation lengths. Examples of second-order phase transitions are the paramagnetic-ferromagnetic and the conductor-superconductor transitions. This kind of transition is also characterised by power-law behaviour at the transition point (also-called *critical point*) with non-integer exponents, thus called *critical exponents*[1]. The critical exponents are related to each other by *hyperscaling relations* – knowing two of the exponents the others can be deduced. Quite different systems can share exactly the same set of critical exponents and are said to belong to the same *Universality Class* (UC). The UC of a system is defined by very general properties such as symmetry of the microscopic interaction, dimensionality of the space, or dimensionality of the order parameter, see [8] for an exhaustive review of the most usual UC's.

The existence of an order parameter is also characteristic of phase transitions. It can be defined as a quantity that is null in one of the phases and non-null in the other, and reflects the symmetry-breaking process that usually takes place across the transition point. For example, for the ferromagnetic-paramagnetic transition a valid order parameter is the net magnetisation (zero in the high temperature phase and non-zero in the low-temperature one), while for the liquid-gas transition it is the density difference of the two co-existing regimes. Other kinds of phase transition must be described by more complex order parameters.

Monte Carlo (MC) simulations have proved very useful in this branch of Statistical Mechanics, see [9] for a review of the most popular methods. With them, one can simulate the evolution in time of each constituent of the system for a given Hamiltonian. In our case the systems are defined on lattices of spatial dimensionality D, with linear size L and periodic boundary conditions. On each node of the lattice we define a variable, called *spin*, that takes on values (depending on the model) that evolve in time.

An MC spin update method can change either just one spin per iteration, as is the case of the Metropolis or heat-bath algorithms [9], or a cluster of spins, as is the case of the Wolff [10] and Swendsen-Wang [11] algorithms. The latter are thus called *cluster methods*. At the critical point is presented the so-called *Critical Slowing Down*, see for example [9]. The relaxation time of the order parameter diverges as a power of the correlation length, $\tau \sim \xi^z$, with z being the *dynamic critical exponent*. This roughly implies that the time needed to produce statistically independent configurations diverges at the critical point for a finite system as $\tau \sim L^z$. Single-spin MC update methods have an exponent $z \gtrsim 2$. Therefore is very hard to obtain high-precision data very close to the critical point on large systems. However,

[1] We follow the standard terminology (see e.g [7]) for the critical exponents: ν is the exponent for the correlation length, α that of the specific heat, β that of the order parameter, while ω is the (universal) leading-order scaling-corrections exponent. A slightly different exponent, the anomalous dimension η, is defined in Eq. (2.72).

cluster MC update methods produce a much better dynamic behaviour. Depending on the model and dimensionality, cluster methods have z values between 0 and 1 [12]. In this work we have used basically cluster methods.

Spin update methods include simulations within the canonical ensemble (at fixed temperatures) and within the microcanonical ensemble (at fixed energies). With respect to simulations in the microcanonical ensemble, we have exploited a recently proposed microcanonical simulation method that allows the simulation of systems with a size never reached before that undergo first-order phase transitions [13].

Even with today's computing resources, we are restricted to simulating systems with more than 10^{15} orders of magnitude fewer components than the real macroscopic system (with $\sim 10^{23}$ particles). The only thing we can do is to simulate systems with different sizes and try to extrapolate the results to the Thermodynamic Limit ($L \to \infty$). The study of the scaling behaviour of the different observables with system size is called Finite-Size Scaling (FSS) and is fundamental for the study of phase transitions, see for example [7]. In this work we have continually used FSS techniques, as well as performing a novel study of FSS within the microcanonical ensemble, see Chap. 2.

Our main objective is the study of the effects of disorder in phase transitions. In particular, we study the effect of quenched impurities on the paramagnet-ferromagnet transition. The presence of random disorder in a system produces many interesting and physically relevant phenomena which have motivated extensive theoretical and experimental studies. The most typical types of system with random disorder are: spin glasses [14, 15], random anisotropic systems [16–18], dilute systems [19–21], and systems with random fields [14]. In all these cases there exist random variables characterising the behaviour of the system.

When modelling a randomly disordered system one can use either of two approaches. On the one hand, one can consider the random variables in thermodynamic equilibrium with the other dynamic variables of the system. Thus the random variables will also be "dynamic". This is the so-called *annealed disorder* and should be the choice if we model a system in which the characteristic times for the dynamics of the disorder are comparable with the characteristic time of the original dynamic variables, as would be the case for example of a solution of two liquids. On the other hand, one can consider that the random variables do not evolve in time, but are frozen. This is the so-called *quenched disorder*. The latter is a perfectly valid alternative for example if we want to model magnetic systems with impurities. In this case the magnetic behaviour is due to the spins of the unpaired electrons in the outer atomic shells while the impurities are whole atoms with no unpaired electrons. It is known that the dynamics of the electrons is orders of magnitude faster than the dynamics of the nuclei, so that we can perfectly consider the impurity atoms as frozen in time. In Ref. [22] there is presented a more detailed discussion of this issue. When considering quenched disorder we will generate different random spatial configurations of the disorder (called *samples*). Within each sample the spins evolve independently but the disorder is fixed. To extract information of a given observable, first we perform the average of its temporal evolution within each sample (in the following called *thermal average* and denoted by angle brackets) and afterwards

we perform the *sample average* (denoted by an overline), the double average is then denoted by $\overline{\langle \cdots \rangle}$.

One of the main results in disordered systems is the Harris criterion [23], see Appendix A. It states that if the specific heat diverges in the pure system (the critical exponent, $\alpha_{\rm pure}$, is greater than zero), the disorder will change the critical behaviour of the model, i.e a new UC will appear. In this case it is said that the disorder is *relevant*. Conversely, if the specific heat does not diverge in the pure system ($\alpha_{\rm pure} < 0$) the critical exponents of the disordered system will not change. In this case it is said that the disorder is *irrelevant*. We will recheck in the present work the validity of the criterion for the three-dimensional site-diluted Heisenberg model.

Another very interesting question arising when studying dilute systems is the issue of *self-averaging*. The mean value of a quantity $\mathcal{O}$ on a lattice of linear size L is different for each realization of the disorder (in our case, for each spatial distribution of the non-magnetic sites). Therefore it is a stochastic variable characterised by an average over the disorder $\overline{\mathcal{O}}$ and a variance $(\Delta\mathcal{O})^2 \equiv \overline{\mathcal{O}^2} - \overline{\mathcal{O}}^2$. It is said that a system is self-averaging for the quantity $\mathcal{O}$ if $\Delta\mathcal{O}/\mathcal{O}$ goes to zero when $L \to \infty$. When a dilute system is not self-averaging, numerical studies become very difficult: even fixing the critical temperature to the correct value for $L \longrightarrow \infty$ making the system larger does not much improve the statistics. The self-averaging properties of disordered systems have generated much interest, reflected in numerous works both numerical [24–26] and analytical [27–29]. In this work we will study the self-averaging properties both of the susceptibility of the three-dimensional site-diluted Heisenberg model and of the latent heat and surface tension of the three-dimensional site-diluted Potts model.

We have numerically studied randomly disordered models presenting important open issues. Our collaboration has produced the papers of Refs. [30–42], although in the present work we only present the results of Refs. [30–35].

The organisation of the rest of this PhD thesis is as follows. In Chapter 2 we study the scaling properties both of the four-state ($Q = 4$) pure Potts model in $D = 2$ and of the pure Ising model in $D = 3$. These models undergo well-known second-order phase transitions with diverging specific heats. We have simulated them using the microcanonical simulation method presented in [13] obtaining strong evidence for the goodness of our approach by comparing it with the most recent results [8,43]. Chapter 3 is devoted to the study of the effects of dilution on a system performing a strong first-order phase transition: the three-dimensional Potts model with $Q = 4$ and $Q = 8$ states. Using the simulation method studied in Chapter 2, we will be able to simulate systems with more than 10^6 components, multiplying by a factor of 100 the number of components reached in the most recent work [44–46]. In Chapter 4 we study the self-averaging properties of the three-dimensional site-diluted Heisenberg model, where there exist two conflicting results stating that the susceptibility is [27] or is not [28] a self-averaging quantity. We will also obtain information about the validity of the Harris criterion. In Chapter 5 we report novel information about the critical exponents of the logarithmic terms of the four-dimensional site-diluted Ising model, we try to discriminate between five different

theories [47–51] by using high-statistics MC simulations. We present our conclusions in Chapter 6. We also present some appendices with the aim of extending some of the most important or innovative tools used. In Appendix A we explain in detail the Harris criterion. In Appendix B we briefly present the popular FSS techniques and the Quotient Method, a technique that allows the computation of critical exponents from data obtained in finite systems. In Appendix C we describe two important issues when simulating dynamical systems with MC methods – autocorrelation times and error estimates. Appendix D is devoted to describing the different methods to temperature-extrapolate the results obtained in a canonical MC simulation, and Appendix E describes the derivation of the Maxwell construction, which is very useful in the study of first-order phase transitions. In Appendix F we describe the approach introduced by Lee and Yang to describe phase transitions, formulating their landmark theorem. We also discuss in this appendix the distribution of the LY-zeros on the unit circle. Finally Appendix G describes the IBERCIVIS computing infrastructure, which has been crucial for the completion of some parts of this work.

Chapter 2

Microcanonical Finite-Size Scaling

2.1 Introduction

The canonical ensemble enjoys a predominating position in Theoretical Physics due to its many technical advantages (convex effective potential in finite systems, easily derived fluctuation-dissipation theorems, etc.). This somewhat arbitrary choice of ensemble is justified by the ensemble equivalence property, which holds in the Thermodynamic Limit (TL) for systems with short-range interactions.

However, in spite of this long-standing bias in favour of the canonical ensemble, the canonical analysis of phase transitions is *not* simpler. The advantages of microcanonical analyses of first-order phase transitions have long been known [13, 52], and indeed become overwhelming in the study of disordered systems [31]. Furthermore, the current interest in mesoscopic or even nanoscopic systems, where ensemble equivalence does not hold, provides ample motivation to study other statistical ensembles, in particular the microcanonical ensemble [53]. Besides, microcanonical Monte Carlo [54] is now as simple and efficient as its canonical counterpart (even microcanonical cluster algorithms are available [13]). Under such circumstances, it is of interest to extend Finite-Size Scaling (FSS) [7, 55–57] to the microcanonical framework for systems undergoing a continuous phase transition.

The relation between the microcanonical and the canonical critical behaviour is well understood only in the TL. A global constraint modifies the critical exponents, but only if the specific heat of the unconstrained system diverges with a positive critical exponent $\alpha > 0$ [58] (however, see [59]). This fact is explained in detail in Sec. 2.2.1. The modification of the critical exponents, termed Fisher renormalization, is very simple. Let L be the system size, and consider an observable O (for instance, the susceptibility) whose diverging behaviour in the infinite-volume canonical system is governed by the critical exponent x_O

$$\langle O \rangle^{\text{canonical}}_{L=\infty,T} \propto |t|^{-x_O} , \quad t = \frac{T - T_\text{c}}{T_\text{c}} . \tag{2.1}$$

Now, let e be the internal energy density and $e_\text{c} = \langle e \rangle^{\text{canonical}}_{L=\infty,T_\text{c}}$. Consider the microcanonical expectation value of the *same* observable O in Eq. (2.1), but now at fixed

energy e. The scaling behaviour (2.1) translates to [1]

$$\langle O\rangle_{L=\infty,e} \propto |e-e_{\rm c}|^{-x_{O,{\rm m}}}\,, \quad x_{O,{\rm m}} = \frac{x_O}{1-\alpha}\,. \tag{2.2}$$

We will denote the microcanonical exponents with the subindex "m". Hence, the Fisher renormalization of the correlation length exponent ν, is $\nu \to \nu_{\rm m} = \nu/(1-\alpha)$, that of the order parameter exponent is $\beta \to \beta_{\rm m} = \beta/(1-\alpha)$, etc. On the other hand, the anomalous dimension, defined in Eq. (2.72), is invariant under Fisher renormalization [58], i.e. $\eta = \eta_{\rm m}$. See also [60] for a recent extension of Fisher renormalization to the case of *logarithmic* scaling corrections.

As for systems of finite size, the microcanonical FSS [61–63] is at the level of an ansatz. This ansatz is obtained from the canonical one merely by replacing the free-energy density by the entropy density, and using Fisher renormalised critical exponents. The microcanonical ansatz reproduces the canonical one [64], and has been the subject of some numerical testing [63,65]. Furthermore, systems undergoing Fisher renormalization (due to some global constraint other than the energy) do seem to obey FSS as well [66].

A difficulty lies in the fact that the current forms of the microcanonical FSS ansatz (FSSA) [61–63] are in a somewhat old-fashioned form. Indeed, they are formulated in terms of quantities such as $e_{\rm c}$ or the critical exponents, which are not accessible in the absence of an analytical solution. In this respect, a great step forward was achieved in a canonical context [67] when it was realized that the finite-lattice correlation length [68] allows one to formulate the FSSA in terms of quantities computable in a finite-lattice. This formulation made it practical to extend Nightingale's phenomenological renormalization [69] to space dimensions $D > 2$ (the so-called quotient method [70]).

Here, we will extend the microcanonical FSSA to a modern form, allowing us to use the quotient method. We will test numerically this extended FSSA in two models with $\alpha > 0$, hence undergoing non-trivial Fisher renormalization, namely

[1] In the particular case of the fixed-energy constraint, Eq. (2.2) follows from (2.1) and from the ensemble equivalence property

$$\langle O\rangle_{L=\infty,e} = \langle O\rangle^{\rm canonical}_{L=\infty,T}\,, \quad \text{if} \quad e = \langle e\rangle^{\rm canonical}_{L=\infty,T}\,.$$

Indeed, it suffices to notice that ($C(T)$ is the canonical specific heat, $C \propto |t|^{-\alpha}$),

$$e - e_{\rm c} = \int_{T_{\rm c}}^{T} {\rm d}T\, C(T) \propto |t|^{1-\alpha} \implies |t| \propto |e-e_{\rm c}|^{\frac{1}{1-\alpha}}\,.$$

The only exponent whose renormalization is not clear at this point, is α itself, for the energy is not a dynamical variable but a parameter in this ensemble. If one chooses to define $\alpha_{\rm m}$ as the critical exponent corresponding to ${\rm d}t/{\rm d}e$, the correspondence with Fisher renormalization, $\alpha_{\rm m} = -\alpha/(1-\alpha)$ becomes complete. In fact, see concluding paragraph in Sect. 2.2.2, the microcanonical ${\rm d}t/{\rm d}e$ behaves as the canonical $1/[{\rm d}e/{\rm d}t]$. Note that in the above expressions we disregarded subdominant terms such as the contribution of the analytical background in the specific heat. Such terms are subdominant only if $\alpha > 0$. In case α were negative, the asymptotic dominance is different. The specific heat at $T_{\rm c}$ is dominated by the analytical background. As a consequence $|t| \sim |e - e_{\rm c}|$ and none of the exponents (not even α) gets renormalised.

the $D = 3$ ferromagnetic Ising model, and the $D = 2$ four-state ferromagnetic Potts model. The Potts model has the added interest of undergoing, in its canonical form, quite strong *logarithmic* corrections to scaling that are nevertheless under relatively strong analytical control [43]. It will therefore be quite a challenge to control the logarithmic corrections in the microcanonical setting.

2.2 Analytical Framework

2.2.1 Fisher Renormalization of Critical Exponents

In 1976, an important paper of M. E. Fisher [58] established a set of elegant relationships describing the effects of constrained hidden variables on the critical exponents. The original theory was developed to explain the significant deviations of the theoretical predictions (basically from the Ising model) from the experimental measurements of critical exponents. These deviations were attributed to some extra "hidden" degrees of freedom, present in the *real* system but not in the oversimplified *ideal* theoretical model. Models (like Ising or Potts) are somewhat gross idealisations of real fluids or magnets, and can be said to lack sufficient internal degrees of freedom. In addition, some experiments are unavoidably different from the ideal system, for example due to the presence of defects or impurities (such as quenched magnetic impurities or non-uniform isotopic composition).

Apart from the exactly soluble models introduced in the original work [58], the formalism introduced by Fisher has provided explanations of numerous phenomena and behaviours, both theoretical and experimental. To cite some examples, there are studies of the phase transition of constrained uniaxial dipolar ferromagnets [71] and of the random-field antiferromagnet with competing interactions [72], efforts made to distinguish between the Random Field Ising Model (RFIM) and the Dilute Antiferromagnetic Model (DAFM) under an applied field [73], and the study of the tricritical point of the Blume-Capel model in three dimensions [74] related with the superfluid λ transition in ^{3}He-^{4}He mixtures in confined films [75]. We would also point to the agreement of Fisher theory with the results for compressible systems, theoretically for both the Ising [77] and the ϕ^4 [78] models and experimentally for ammonium chloride at high pressures [79], see also [76] for a study of the tricritical point in compressible systems.

The situation was described as follows: firstly, there is an "ideal" system with known variables characterised by the ideal critical exponents $\alpha, \beta, \gamma, \ldots$; secondly, the "real" system has some "hidden" degrees of freedom which fluctuate but remain in equilibrium with the known variables; finally, the hidden variables are subject to some form of constraint (for example, the total number of impurity atoms must remain fixed). The critical exponents of the real system are denoted by $\alpha_X, \beta_X, \gamma_X, \ldots$

In the following we will describe the relationships between the two sets of critical exponents (now called Fisher renormalization), following in some points the recent work of Kenna et al. [60] in which there also can be found the corresponding set of relationships for the logarithmic correction exponents. We will focus the discussion on describing the temperature transition in a ferromagnet at the Curie point, although

the results are perfectly valid for other kinds of phase transitions (antiferromagnets, gas-liquid transitions, binary fluids, etc.).

The starting point is the description of the ideal system in terms of the free energy:

$$f = f_0(t, h)\,, \tag{2.3}$$

where $t = (T - T_c)/T_c$ is the reduced temperature and h is the "field". The field is related in general with the order parameter, σ, describing the transition under study through

$$\sigma = \sigma(t, h) = -\left(\frac{\partial f}{\partial h}\right)_t\,, \tag{2.4}$$

that in the ideal case becomes

$$\sigma = \sigma_0(t, h) = -\left(\frac{\partial f_0}{\partial h}\right)_t\,. \tag{2.5}$$

The order parameter can be the magnetisation in a ferromagnet, the sublattice magnetisation in an antiferromagnet, the density in a gas-liquid transition, etc. The ideal system will undergo a phase transition at T_c^0. Thus below this temperature there will be a non-vanishing order parameter (spontaneous magnetisation)

$$\Delta\sigma_0 = \lim_{h\to 0^+} \frac{1}{2}[\sigma_0(t, h) - \sigma_0(t, -h)]\,, \tag{2.6}$$

which vanishes at the critical point as:

$$\Delta\sigma_0 \sim |t|^\beta \qquad , \qquad (t \to 0^-)\,. \tag{2.7}$$

The second field derivative is also described by its corresponding critical exponent

$$\chi_0(t) = \lim_{h\to 0}\left(\frac{\partial \sigma_0}{\partial h}\right)_t \sim |t|^{-\gamma} \qquad , \qquad (t \to 0)\,. \tag{2.8}$$

Finally the critical behaviour of the specific heat

$$c_0(t) \sim |t|^{-\alpha} \qquad , \qquad (t \to 0)\,, \tag{2.9}$$

means that, in the absence of a field, the ideal free energy behaves for small t as

$$f_0(t, 0) = \mathcal{A}_{0\pm} + \mathcal{A}_{1\pm}|t| + \mathcal{A}_{2\pm}|t|^2 + \mathcal{B}_\pm|t|^{2-\alpha} + \mathcal{O}(|t|^3)\,, \tag{2.10}$$

where the $\pm$ depends on the sign of t.

We assume that the real system is derived from the ideal system by the introduction of a new "hidden" thermodynamic variable x which is the conjugate of a force u, such that the thermodynamic potential becomes $f = f(t, h, u)$, with

$$x(t, h, u) = \left(\frac{\partial f}{\partial u}\right)_{t,h}\,. \tag{2.11}$$

The constraint in the hidden variable is written as

$$x(t,h,u) = X(t,h,u)\,, \tag{2.12}$$

where $X(t,h,u)$ is assumed to be an analytical function. Let us introduce the basic hypothesis (suggested in part by the analytical results of some soluble models [58]) that the free energy of the constrained system can be written in terms of the ideal free energy f_0 as

$$f(t,h,u) = f_0(t^*(t,h,u), h^*(t,h,u)) + g(t,h,u)\,, \tag{2.13}$$

where t^*, h^*, and g are analytic functions of their arguments. I.e., we assume that the total free energy consists of a "regular background" contribution $g(t,h,u)$ plus a "singular contribution" derived from the ideal free energy $f_0(t,h)$ by a smooth transformation of the temperature, t, and the field, h, to the modified versions t^* and h^*. Furthermore, the transition must remain ideal if observed at fixed force u, and the ideal free energy $f_0(t,h)$ is recovered when $u = 0$.

To simplify the discussion we assume that the hidden degrees of freedom are neutral in the sense that they do not bias the value of the external field at the transition. I.e., the transition still occurs at $h = 0$ and

$$h^*(t,h,u) = h\mathcal{J}(t,h,u)\,. \tag{2.14}$$

With the previous assumptions, one can obtain from Eqs. (2.6), (2.13), and (2.14) that the order parameter of the constrained system behaves as

$$\Delta\sigma = \Delta\sigma_0(t^*(t,0,u))\mathcal{J}(t,0,u)\,, \tag{2.15}$$

where we have made use of the continuity of all the analytical functions for $h \to 0$ including the internal energy of the ideal system, $e_0 = \partial f_0/\partial t$.

We can calculate the internal energy for zero field using Eq. (2.10) as

$$e_0(t,0) = \frac{\partial f_0(t,0)}{\partial t} = A_0 + A|t| + B|t|^{1-\alpha} + \cdots\,, \tag{2.16}$$

with $A_0 = \pm\mathcal{A}_{1\pm}$, $A_1 = 2\mathcal{A}_{2\pm}$ and $B = \pm(2-\alpha)\mathcal{B}_\pm$ and where $\cdots$ represents higher-order terms.

We can also obtain from Eqs. (2.11) and (2.13) for $h \to 0$

$$x(t,0,u) = \frac{\partial f(t,0,u)}{\partial u} = \frac{\partial f}{\partial t^*}\frac{\partial t^*}{\partial u} + \frac{\partial f}{\partial h^*}\frac{\partial h^*}{\partial u} + \frac{\partial g}{\partial u} \tag{2.17}$$

$$= e_0(t^*,0)\frac{\partial t^*(t,0,u)}{\partial u} + \frac{\partial g(t,0,u)}{\partial u}\,, \tag{2.18}$$

where we used the fact that

$$\frac{\partial h^*}{\partial u} = h\frac{\partial \mathcal{J}}{\partial u} = \mathcal{O}(h)\,. \tag{2.19}$$

Provided that t^* is a smooth function, it can be expanded for $h = 0$ around the real critical point $T = T_c$ and $u = u_c$,

$$t^*(t, 0, u) = a_1\mu + a_2\tau + \cdots , \tag{2.20}$$

with $\mu = u - u_c$ and $\tau = T - T_c$. The absence of constant terms in the above expansion is due to Eq. (2.15) because $\Delta\sigma(t^*(t_c, 0, u_c)) = 0$ fixes the temperature in the constrained system so that $t^*(t_c, 0, u_c) = 0$.

Then to first order

$$\frac{\partial t^*(t, 0, u)}{\partial u} = a_1 + \cdots , \tag{2.21}$$

which inserted into Eq. (2.18) with Eq. (2.16) gives

$$x(t, 0, u) = a_1A_0 + a_1A|t^*| + a_1B|t^*|^{1-\alpha} + \frac{\partial g(t, 0, u)}{\partial u} + \cdots . \tag{2.22}$$

We can also expand the constraint, Eq. (2.15), about the real critical point $u = u_c$ and $T = T_c$

$$X(t, 0, u) = X(t_c, 0, u_c) + d_1\mu + d_2\tau + \cdots . \tag{2.23}$$

In addition, from Eq. (2.20)

$$\mu = \frac{1}{a_1}t^*(t, 0, u) - \frac{a_2}{a_1}\tau + \cdots . \tag{2.24}$$

Using the above equation, we can insert Eqs. (2.22) and (2.23) into (2.12) to obtain the main result

$$a_1^2(A|t^*| + B|t^*|^{1-\alpha}) = d_1t^* + (a_1d_2 - d_1a_2)\tau . \tag{2.25}$$

If $\alpha < 0$, the regular term dominates and $|t^*| \propto |\tau|$, resulting in the absence of Fisher renormalization, in which case the critical exponents of the transition remain unchanged. On the contrary, if $\alpha > 0$, one obtains the central result

$$|t^*| \propto |\tau|^{1/(1-\alpha)} . \tag{2.26}$$

That means that a deviation from the critical point of τ in the real system is equivalent to a deviation t^* in the ideal system, these deviations being related by Eq. (2.26). Then the real system approaches the transition more slowly than the ideal one. The internal energy of the real system for $h = 0$ is

$$e(t, 0, u) = \frac{\partial f(t, 0, u)}{\partial t} = e_0(t^*, 0)\frac{\partial t^*(t, 0, u)}{\partial t} + \frac{\partial g(t, 0, u)}{\partial t} \tag{2.27}$$

$$= (A_0 + A|t^*| + B|t^*|^{1-\alpha})\frac{\partial t^*(t, 0, u)}{\partial t} + \frac{\partial g(t, 0, u)}{\partial t} \tag{2.28}$$

$$= (A_0 + A|\tau|^{1/(1-\alpha)} + B|\tau|)\frac{\partial t^*(t, 0, u)}{\partial t} + \frac{\partial g(t, 0, u)}{\partial t} , \tag{2.29}$$

where the only possible singular contributions to the specific heat stem from the terms within parentheses. The specific heat of the constrained system is then

$$c(t,0,u) = \frac{\partial e(t,0,u)}{\partial t} \sim |\tau|^{\alpha/(1-\alpha)}\,, \tag{2.30}$$

and therefore the singular behaviour of the specific heat has been replaced for a cusp-like one, i.e., it remains finite due to the presence of the constrained hidden variable. Then the Fisher renormalization for the exponent of the specific heat is

$$\alpha_X = -\frac{\alpha}{1-\alpha}\,. \tag{2.31}$$

We can obtain analogously the renormalization for other critical exponent as:

$$\sigma \sim |t^*|^{\beta} \sim |\tau|^{\beta/(1-\alpha)} \quad , \quad \beta_X = \frac{\beta}{1-\alpha}\,, \tag{2.32}$$

$$\chi \sim |t^*|^{-\gamma} \sim |\tau|^{-\gamma/(1-\alpha)} \quad , \quad \gamma_X = \frac{\gamma}{1-\alpha}\,, \tag{2.33}$$

$$\xi \sim |t^*|^{-\nu} \sim |\tau|^{-\nu/(1-\alpha)} \quad , \quad \nu_X = \frac{\nu}{1-\alpha}\,. \tag{2.34}$$

The critical exponent η is defined at just the critical point and therefore is invariant [2]

$$\eta_X = \eta\,. \tag{2.35}$$

If the standard power-law scaling behaviour of the main quantities is modified by multiplicative logarithmic correction, i.e,

$$c_0(t) \sim |t|^{-\alpha}|\log|t||^{\hat{\alpha}}\,, \tag{2.36}$$

$$m_0(t) \sim |t|^{\beta}|\log|t||^{\hat{\beta}} \quad \text{for } t<0\,, \tag{2.37}$$

$$\chi_0(t) \sim |t|^{-\gamma}|\log|t||^{\hat{\gamma}}\,, \tag{2.38}$$

$$\xi_0(t) \sim |t|^{-\nu}|\log|t||^{\hat{\nu}}\,, \tag{2.39}$$

$$m_0(h) \sim |h|^{\frac{1}{\delta}}|\log|h||^{\hat{\delta}} \quad \text{for } t=0\,, \tag{2.40}$$

$$\mathcal{G}_0(x,t) \sim x^{-(D-2+\eta)}(\log x)^{\hat{\eta}} G\left(\frac{x}{\xi(t)}\right) \quad \text{for } t \ll 1\,, \tag{2.41}$$

then Eq. (2.10) is naively changed to give:

$$f_0(t,0) = \mathcal{A}_{0\pm}+\mathcal{A}_{1\pm}|t|+\mathcal{A}_{2\pm}|t|^2+\mathcal{O}(|t|^3)+\mathcal{B}_{\pm}|t|^{2-\alpha}|\log|t||^{\hat{\alpha}}\left\{1+\mathcal{O}\left(\frac{\log|\log|t||}{\log|t|}\right)\right\}\,. \tag{2.42}$$

And therefore it can be obtained the equivalent of Eq. (2.25) for the logarithmic case

$$a_1^2(A|t^*|+B|t^*|^{1-\alpha}|\log|t^*||^{\hat{\alpha}}) = d_1 t^* + (a_1 d_2 - d_1 a_2)\tau\,. \tag{2.43}$$

The above equation produces the following results:

[2] This can also be obtained from the scaling relationship $(2-\eta)\nu = \gamma$. If ν and γ are renormalised, η remains unchanged.

- If $\alpha < 0$, or $\alpha = 0$ and $\hat{\alpha} < 0$, the regular term dominates and $|t^*| \propto |\tau|$, leading to the absence of Fisher renormalization.

- If $\alpha > 0$, or $\alpha = 0$ and $\hat{\alpha} > 0$, one obtains the modified central result

$$|t^*| \propto |\tau|^{1/(1-\alpha)} |\log|\tau||^{-\hat{\alpha}/(1-\alpha)} , \tag{2.44}$$

  which produces the renormalization of the individual exponents of the logarithms:

$$\hat{\alpha}_X = -\frac{\hat{\alpha}}{1-\alpha} , \tag{2.45}$$

$$\hat{\beta}_X = \hat{\beta} - \frac{\beta\hat{\alpha}}{1-\alpha} , \tag{2.46}$$

$$\hat{\gamma}_X = \hat{\gamma} + \frac{\gamma\hat{\alpha}}{1-\alpha} , \tag{2.47}$$

$$\hat{\nu}_X = \hat{\nu} + \frac{\nu\hat{\alpha}}{1-\alpha} . \tag{2.48}$$

  Again, no renormalization takes place for the exponents $\hat{\eta}_X = \hat{\eta}$ and $\hat{\delta}_X = \hat{\delta}$.

2.2.2 The Microcanonical Ensemble

The first step in the construction of the ensemble is an extension of the configuration space. We add $N(= L^D)$ real momenta, p_i, to our N original variables, σ_i (named spins here) [13,54]. Note that this extended configuration, $\{\sigma_i, p_i\}$, appears in many numerical schemes (consider, for instance, Hybrid Monte Carlo [80] simulations in Lattice Gauge Theory). We shall work in the *microcanonical* ensemble for the $\{\sigma_i, p_i\}$ system.

Let $\mathcal{U}$ be the original spin Hamiltonian (i.e., Eq. (2.82) in our case). Our total energy is [3]

$$\mathcal{E} = \sum_{i=1}^{N} \frac{p_i^2}{2} \; + \; \mathcal{U} \quad (e \equiv \mathcal{E}/N \,, \; u \equiv \mathcal{U}/N) \,. \tag{2.49}$$

The momenta contribution,

$$N\kappa \equiv \sum_{i=1}^{N} \frac{p_i^2}{2} , \tag{2.50}$$

is necessarily positive, and it is best thought of as a "kinetic" energy. In this mechanical analogue, the original spin Hamiltonian $\mathcal{U}$ can be regarded as a "potential" energy.

[3] Note that this microcanonical ensemble exactly matches the conditions in the original Fisher work [58]: the momenta are some *hidden* degrees of freedom in thermal equilibrium with the spins, and a global constraint is imposed. It is also curious to rederive the results in Sec. 2.2.2 considering Γ momenta per spin (in this work $\Gamma = 1$, while Lustig [54] always considered $\Gamma = 3$). If one takes the limit $\Gamma \to \infty$, at fixed N, the canonical probability is recovered for the spins.

The canonical partition function is ($\beta \equiv 1/T$)

$$Z_N(\beta) = \int_{-\infty}^{\infty} \prod_{i=1}^{N} \mathrm{d}p_i \sum_{\{\sigma_i\}} \mathrm{e}^{-\beta\mathcal{E}} = \left(\frac{2\pi}{\beta}\right)^{\frac{N}{2}} \sum_{\{\sigma_i\}} \mathrm{e}^{-\beta\mathcal{U}}\,, \tag{2.51}$$

where $\sum_{\{\sigma_i\}}$ denotes summation over spin configurations. Hence, the $\{p_i\}$ play the role of a Gaussian thermostat. The $\{p_i\}$ are statistically uncorrelated with the spins. Since $\langle\kappa\rangle_{L,\beta}^{\mathrm{canonical}} = 1/(2\beta)$, one has $\langle e\rangle_{\beta}^{\mathrm{canonical}} = \langle u\rangle_{\beta}^{\mathrm{canonical}} + 1/(2\beta)$.

Furthermore, given the statistical independence of κ and u, the canonical probability distribution function for e, $P_{\beta}^{(L)}(e)$, is merely the convolution of the distributions for κ and u:

$$P_{\beta}^{(L)}(e) = \int_0^{\infty} \mathrm{d}\,\kappa\; P_{\beta}^{(L),\kappa}(\kappa)\, P_{\beta}^{(L),u}(e-\kappa)\,. \tag{2.52}$$

In particular, note that for spin systems on a finite lattice, $P_{\beta}^{(L),u}(u)$ is a sum of (order N) Dirac δ functions. Now, since the canonical variance of κ is $1/(\beta\sqrt{2N})$, roughly $\sqrt{N}$ discrete u-levels, with $u \sim e - 1/(2\beta)$, give the most significant contribution to $P_{\beta}^{(L)}(e)$. We see that the momenta's kinetic energy provides a natural smoothing of the comb-like $P_{\beta}^{(L),u}(u)$. Once we have a conveniently smoothed $P_{\beta}^{(L)}(e)$, we may proceed to the definition of the entropy.

In a microcanonical setting, the crucial role is played by the entropy density, $s(e,N)$, given by

$$\exp[Ns(e,N)] = \int_{-\infty}^{\infty} \prod_{i=1}^{N} \mathrm{d}p_i \sum_{\{\sigma_i\}} \delta(Ne - \mathcal{E})\,. \tag{2.53}$$

Integrating out the $\{p_i\}$ using the Dirac delta function in (2.53) we get

$$\exp[Ns(e,N)] \;=\; \frac{(2\pi N)^{\frac{N}{2}}}{N\Gamma(N/2)} \sum_{\{\sigma_i\}} \omega(e,u,N)\,, \tag{2.54}$$

$$\omega(e,u,N) \;\equiv\; (e-u)^{\frac{N-2}{2}}\theta(e-u)\,, \tag{2.55}$$

where Γ is the gamma function and the step function, $\theta(e-u)$, enforces $e > u$. Equation (2.54) suggests defining the microcanonical average at fixed e of any function of e and the spins, $O(e,\{\sigma_i\})$, as [54]

$$\langle O\rangle_e \equiv \frac{\sum_{\{\sigma_i\}} O(e,\{\sigma_i\})\,\omega(e,u,N)}{\sum_{\{\sigma_i\}} \omega(e,u,N)}\,. \tag{2.56}$$

We use Eq. (2.54) to compute $\mathrm{d}s/\mathrm{d}e$ [13]:

$$\frac{\mathrm{d}s(e,N)}{\mathrm{d}e} \;=\; \langle\hat{\beta}(e;\{\sigma_i\})\rangle_e\,, \tag{2.57}$$

$$\hat{\beta}(e;\{\sigma_i\}) \;\equiv\; \frac{N-2}{2N(e-u)}\,. \tag{2.58}$$

Bearing in mind the crucial role of the generating functional in Field Theory (see e.g. [7]), we extend the definition (2.53) by considering a linear coupling between the spins and a site dependent source field h_i:

$$\exp[Ns(e,\{h_i\},N)] = \int_{-\infty}^{\infty} \prod_{i=1}^{N} \mathrm{d}p_i \sum_{\{\sigma_i\}} \mathrm{e}^{\sum_i h_i\sigma_i} \delta(Ne - \mathcal{E})\,, \tag{2.59}$$

where $\mathcal{E} = Ne$ is still given by Eq. (2.49), without including the source term. In this way, the microcanonical spin correlation functions follow from derivatives of $s(e,\{h_i\},N)$:

$$\begin{aligned} \left.\frac{\partial[N\,s]}{\partial h_k}\right|_{e,\{h_i\},N} &= \langle\sigma_k\rangle_{e,\{h_i\}}\,, \\ \left.\frac{\partial^2[N\,s]}{\partial h_k \partial h_l}\right|_{e,\{h_i\},N} &= \langle\sigma_k\sigma_l\rangle_{e,\{h_i\}} - \langle\sigma_k\rangle_{e,\{h_i\}}\,\langle\sigma_l\rangle_{e,\{h_i\}}\,. \end{aligned} \tag{2.60}$$

In particular, if the source term is uniform $h_i = h$ we observe that the microcanonical susceptibility is given by standard fluctuation-dissipation relations, see Ref. [7] and Eq. (2.89) below.

Ensemble equivalence

Equation (2.53) ensures that the *canonical* probability density function for e is

$$P_\beta^{(L)}(e) = \frac{N}{Z_N(\beta)} \exp[N(s(e,N) - \beta e)]\,, \tag{2.61}$$

hence, Eq. (2.57),

$$\log P_\beta^{(L)}(e_2) - \log P_\beta^{(L)}(e_1) = N \int_{e_1}^{e_2} \mathrm{d}e\, \left(\langle\hat{\beta}\rangle_e - \beta\right)\,, \tag{2.62}$$

where log means natural logarithm everywhere in this work.

The relation between the canonical and the microcanonical spin-values is given by

$$\langle O\rangle_\beta^{\text{canonical}} = \int_{-\infty}^{\infty} \mathrm{d}e\, \langle O\rangle_e\, P_\beta^{(L)}(e)\,. \tag{2.63}$$

Now, Eqs. (2.61) and (2.63) imply that the canonical mean value will be dominated by a saddle-point at e^{SP},

$$\langle\hat{\beta}\rangle_{e_{L,\beta}^{\mathrm{SP}}} = \beta\,, \tag{2.64}$$

which can be read as yet another expression of the Second Law of Thermodynamics, $T\mathrm{d}s = \mathrm{d}e$.

The condition of thermodynamic stability (namely that $\langle\hat{\beta}\rangle_e$ be a monotonically decreasing function of e) ensures that the saddle point is unique and that e^{SP} is

a maximum of $P_\beta(e)$. Under the thermodynamic stability condition and if, in the large L limit,

$$\left.\frac{\mathrm{d}\langle\hat{\beta}\rangle_e}{\mathrm{d}e}\right|_{e^{\mathrm{SP}}_{L,\beta}} < 0\,, \tag{2.65}$$

the saddle point approximation becomes exact:

$$e^{\mathrm{SP}}_{L=\infty,\beta} = \langle e\rangle^{\mathrm{canonical}}_{L=\infty,\beta}\,, \tag{2.66}$$

and we have ensemble equivalence:

$$\langle O\rangle_{L=\infty,e^{\mathrm{SP}}_{L=\infty,\beta}} = \langle O\rangle^{\mathrm{canonical}}_{L=\infty,\beta}\,. \tag{2.67}$$

It follows that the microcanonical estimator

$$C_{\mathrm{m}}(L,e) = \frac{1}{\mathrm{d}\langle\hat{\beta}\rangle_{e,L}/\mathrm{d}e}\,, \tag{2.68}$$

evaluated at $e^{\mathrm{SP}}_{L=\infty,\beta}$ will tend in the large-L limit to minus the canonical specific heat. Thus, if the critical exponent α is positive, Eq. (2.65) will fail precisely at e_{c}. Hence, Eq. (2.67) can be expected to hold for all e but e_{c} (or for all β but β_{c}).

Double-peaked histogram

The situation can be slightly more complicated if $P_{\beta_{\mathrm{c}}}(e)$ presents two local maxima, remindful of phase coexistence. This is actually the case for one of our models – the $D = 2$, four-state Potts model [81]. From Eq. (2.62) it is clear that the solution to the saddle-point equation (2.64) will no longer be unique. We borrow the following definitions from the analysis of first-order phase transitions (where true phase coexistence takes place) [13]:

- The rightmost root of Eq. (2.64), $e^{\mathrm{d}}_{L,\beta}$, is a local maximum of $P^{(L)}_\beta$ corresponding to the "disordered phase".
- The leftmost root of Eq. (2.64), $e^{\mathrm{o}}_{L,\beta}$, is a local maximum of $P^{(L)}_\beta$ corresponding to the "ordered phase".
- The second rightmost root of Eq. (2.64), $e^{*}_{L,\beta}$, is a local minimum of $P^{(L)}_\beta$.

Maxwell construction yields the finite-system critical point, $\beta_{\mathrm{c},L}$, see Fig. 2.9 and Appendix E:

$$0 = \int_{e^{\mathrm{o}}_{L,\beta_{\mathrm{c},L}}}^{e^{\mathrm{d}}_{L,\beta_{\mathrm{c},L}}} \mathrm{d}e\, \left(\langle\hat{\beta}\rangle_e - \beta_{\mathrm{c},L}\right)\,, \tag{2.69}$$

and the finite-system estimator of the "surface tension"

$$\Sigma^L = \frac{N}{2L^{D-1}} \int_{e^{*}_{L,\beta_{\mathrm{c},L}}}^{e^{\mathrm{d}}_{L,\beta_{\mathrm{c},L}}} \mathrm{d}e\, \left(\langle\hat{\beta}\rangle_e - \beta_{\mathrm{c},L}\right)\,. \tag{2.70}$$

Of course, in the large-L limit and for a continuous transition, $\Sigma^L \to 0$, $\beta^L_{\mathrm{c}} \to \beta_{\mathrm{c}}$ and $e^{\mathrm{d}}_{L,\beta_{\mathrm{c},L}}, e^{\mathrm{o}}_{L,\beta_{\mathrm{c},L}} \to e_{\mathrm{c}}$, as we will see.

2.2.3 Our Microcanonical Finite-Size Scaling Ansatz

Usually, the Microcanonical FSSA takes an entropy density scaling form [61–63]. In close analogy with the canonical case, one assumes that $s(e, \{h_{\vec{x}}\}, N)$ can be divided into a regular part and a singular term $s_{\rm sing}(e, \{h_{\vec{x}}\}, N)$. The regular part is assumed to converge for large L (recall that $N = L^D$) to a smooth function of its arguments. Hence, all critical behaviour comes from $s_{\rm sing}(e, \{h_{\vec{x}}\}, N)$. Note as well that we write $\{h_{\vec{x}}\}$, instead of $\{h_i\}$, to emphasise the spatial dependence of the sources (supposedly very mild [7]). Hence,

$$s_{\rm sing}(e, \{h_{\vec{x}}\}, N) = L^{-D} g\left(L^{\frac{1}{\nu_{\rm m}}}(e - e_{\rm c}), \{L^{y_h} h_{\vec{x}}\}\right) . \tag{2.71}$$

Here, g is a very smooth function of its arguments, while $y_h = 1 + \frac{D-\eta}{2}$ is the canonical exponent, see e.g. [7], which does not get Fisher-renormalised. Corrections to FSS due to irrelevant scaling fields, have not played a major role in several previous analysis [61–63] (in [63] only analytical scaling corrections were considered), but will be important for our precision tests. Leading order corrections were, however, explicitly considered in Ref. [66].

We will propose here alternative forms of the ansatz (2.71), more suitable for a numerical work where neither $e_{\rm c}$ nor the critical exponents are known beforehand.

Our first building block is the infinite-system microcanonical correlation length, $\xi_{\infty,e}$. Indeed, ensemble equivalence implies that, in an infinite system, the long-distance behaviour of the microcanonical spin-spin propagator $G(\vec{r}; e) = \langle \sigma_{\vec{x}} \sigma_{\vec{x}+\vec{r}} \rangle_e - \langle \sigma_{\vec{x}} \rangle_e \langle \sigma_{\vec{x}+\vec{r}} \rangle_e$ behaves for large $\vec{r}$ as in the canonical ensemble (close to a critical point $\xi_{\infty,e}$ is large, so that rotational invariance is recovered in our lattice systems):

$$G(\vec{r}; e) = \frac{A}{r^{D-2+\eta}} {\rm e}^{-r/\xi_{\infty,e}} , \tag{2.72}$$

where A is a constant. In particular, note that ensemble-equivalence implies that the anomalous dimension η does not get Fisher-renormalised. We expect $\xi_{\infty,e} = \xi_{\infty,T}^{\rm canonical}$ if the correspondence between e and T are fixed through $e = \langle e \rangle_{L=\infty,T}^{\rm canonical}$.

The basic assumption underlying the FSSA is that the approach to the $L \to \infty$ limit is governed by the dimensionless ratio $L/\xi_{\infty,e}$. Hence, our first form of the microcanonical FSSA for the observable O whose critical behaviour was discussed in referring to Eq. (2.2) is

$$\langle O \rangle_{L,e} = L^{\frac{x_{O,\rm m}}{\nu_{\rm m}}} f_O(L/\xi_{\infty,e}) + \cdots . \tag{2.73}$$

In the above, the ellipsis stands for scaling-corrections, while the function f_O is expected to be very smooth (i.e., differentiable to a large degree or even analytical). A second form of the microcanonical FSSA is obtained by substituting the scaling behaviour $\xi_{\infty,e} \propto |e - e_{\rm c}|^{-\nu_{\rm m}}$:

$$\langle O \rangle_{L,e} = L^{\frac{x_{O,\rm m}}{\nu_{\rm m}}} \tilde{f}_O\left(L^{1/\nu_{\rm m}}(e - e_{\rm c})\right) + \cdots . \tag{2.74}$$

Again, $\tilde{f}_O$ is expected to be an extremely smooth function of its argument [4]. In particular, this is the form of the ansatz that follows from Eq. (2.71) by differentiating with respect to e or from the source terms.

However, the most useful form of the microcanonical FSSA is obtained by applying Eq. (2.73) to the finite-lattice correlation length $\xi_{L,e}$, obtained in a standard way (see Ref. [7]) from the finite-lattice microcanonical propagator. We expect $\xi_{L,e}/L$ to be a smooth, one-to-one function of $L/\xi_{\infty,e}$, that can be inverted to yield $L/\xi_{\infty,e}$ as a function of $\xi_{L,e}/L$. Hence, our preferred form of the FSSA is

$$\langle O \rangle_{L,e} = L^{\frac{x_{O,\mathrm{m}}}{\nu_\mathrm{m}}} \left[F_O\left(\frac{\xi_{L,e}}{L}\right) + L^{-\omega} G_O\left(\frac{\xi_{L,e}}{L}\right) + \cdots \right] . \tag{2.75}$$

Here, F_O and G_O are smooth functions of their arguments and ω is the first universal scaling corrections exponent.

It is important to note that exponent ω does not get Fisher-renormalised. Indeed, let us consider an observable O with critical exponent x_O at a temperature T such $e = \langle e \rangle^{\mathrm{canonical}}_{L=\infty,T}$. Now, ensemble equivalence tells us that $O^{\mathrm{canonical}}_{L=\infty,T} = O_{L=\infty,e}$ and that $\xi^{\mathrm{canonical}}_{L=\infty,T} = \xi_{L=\infty,e}$. Eliminating T in favour of $\xi^{\mathrm{canonical}}_{L=\infty,T}$, see e.g. [7], we have

$$O^{\mathrm{canonical}}_{L=\infty,T} = \xi^{x_O/\nu}_{L=\infty,e} [A_0 + B_0 \xi^{-\omega}_{L=\infty,e} + \cdots] , \tag{2.76}$$

where A_0 and B_0 are scaling amplitudes. It follows that $\omega_\mathrm{m} = \omega$, and that $x_O/\nu = x_{O,\mathrm{m}}/\nu_\mathrm{m}$.

The Quotient Method

Once we have Eq. (2.75), it is straightforward to generalise the quotient method [70]. In Appendix B we also describe how it should be modified in the presence of (multiplicative) logarithmic corrections to scaling.

Let us compare data obtained *at the same* value of e for a pair of lattices $L_1 = L$ and $L_2 = sL$ with $s > 1$. We expect that a single e_{c,L_1,L_2} exists such that the correlation-length in units of the lattice size coincides for both systems:

$$\frac{\xi_{L,e_{\mathrm{c},L_1,L_2}}}{L} = \frac{\xi_{sL,e_{\mathrm{c},L_1,L_2}}}{sL} . \tag{2.77}$$

Hence, if we compare now in the two lattices the observable O in (2.75), precisely at $e_{\mathrm{c},L,sL}$, we have

$$\frac{\langle O \rangle_{sL,e_{\mathrm{c},L_1,L_2}}}{\langle O \rangle_{L,e_{\mathrm{c},L_1,L_2}}} = s^{\frac{x_{O,\mathrm{m}}}{\nu_\mathrm{m}}} \left[1 + A_{O,s} L^{-\omega} + \cdots \right] , \tag{2.78}$$

where $A_{O,s}$ is a non-universal scaling amplitude. One considers this equation for fixed s (typically $s = 2$), and uses it to extrapolate to $L = \infty$ the L-dependent estimate of the critical exponents ratio $x_{O,\mathrm{m}}/\nu_\mathrm{m}$. At the purely numerical level, it

[4] Note that the microcanonical weight (2.55) is *not* analytical at each energy level of the spin Hamiltonian.

needs to be noted as well that there are strong statistical correlations between the quotients in (2.77) and in (2.78), that reduces the statistical errors in the estimate of critical exponents. These errors can be computed via a jack-knife method, see e.g. [7].

In this chapter, we shall compute the critical exponents from the following operators (χ is the susceptibility, while ξ is the correlation length, see Sec. 2.3 for definitions):

$$\chi \;\rightarrow\; x_O = \nu_{\rm m}(2-\eta)\,, \tag{2.79}$$

$$\partial_e \xi \;\rightarrow\; x_O = \nu_{\rm m} + 1\,. \tag{2.80}$$

The L dependence of $e_{{\rm c},L,s}$ follows from Eq. (2.74) as applied to ξ_L/L for the two lattice sizes L and sL [7, 55]:

$$e_{{\rm c},L,s} = e_{\rm c} + B\frac{1-s^{-\omega}}{s^{1/\nu_{\rm m}}-1}L^{-(\omega+\frac{1}{\nu_{\rm m}})} + \cdots\,, \tag{2.81}$$

where B is again a non-universal scaling amplitude. In particular, if one works at fixed s, $e_{{\rm c},L,sL}$ tends to $e_{\rm c}$ for large L as $L^{-(\omega+\frac{1}{\nu_{\rm m}})}$ [5].

2.3 The Model

We will define here the model and observables of a generic D-dimensional Q-state Potts model. The numerical study was done for two instances of this model: the three-dimensional Ising ($Q=2$) model, and the two-dimensional $Q=4$ Potts model.

We place the spins $\sigma_i = 1, \ldots, Q$ at the nodes of a hypercubic D-dimensional lattice with linear size L and periodic boundary conditions.

The Hamiltonian is

$$\mathcal{U} = -\sum_{\langle i,j\rangle} \delta_{\sigma_i\sigma_j}\,, \tag{2.82}$$

where $\langle i,j\rangle$ denotes first nearest neighbours and δ_{ij} is the Kronecker delta. For a given spin, σ, we define the normalised Q-vector $\vec{s}$, whose q-th component is

$$s_q = \sqrt{\frac{Q}{Q-1}}\Big(\delta_{\sigma q} - \frac{1}{Q}\Big)\,. \tag{2.83}$$

A Q components order parameter for the ferromagnetic transition is

$$\vec{\mathcal{M}} = \frac{1}{L^D}\sum_i \vec{s}_i\,, \tag{2.84}$$

where i runs over all the lattice sites. We will now consider microcanonical averages. The spatial correlation function is

$$\begin{aligned} C(\boldsymbol{r}'-\boldsymbol{r}) &= \Big\langle \vec{s}(\boldsymbol{r})\cdot\vec{s}(\boldsymbol{r}')\Big\rangle_e \\ &= \frac{Q}{Q-1}\Big\langle \delta_{\sigma(\boldsymbol{r})\sigma(\boldsymbol{r}')} - \frac{1}{Q}\Big\rangle_e\,. \end{aligned} \tag{2.85}$$

[5] Note that, Eq. (2.74) tells us that, if the energy histogram is double-peaked, see Sec. 2.2.2, the histogram maxima will tend to $e_{\rm c}$ only as $L^{-1/\nu_{\rm m}}$.

Our definition for the correlation length at a given internal energy density e, is computed from the Fourier transform of C

$$\hat{C}(\boldsymbol{k}) = \sum_{\boldsymbol{r}} C(\boldsymbol{r})\, \mathrm{e}^{\mathrm{i}\boldsymbol{k}\cdot\boldsymbol{r}} \,, \tag{2.86}$$

at zero and minimal ($\|\boldsymbol{k}_{\min}\| = 2\pi/L$) momentum [7, 68]:

$$\xi(e, L) = \frac{\sqrt{\hat{C}(0)/\hat{C}(\boldsymbol{k}_{\min}) - 1}}{2\sin(\pi/L)} \,. \tag{2.87}$$

Note that $\hat{C}$ can be easily computed in terms of the Fourier transform of the spin field, $\hat{s}(\boldsymbol{k})$, as

$$\hat{C}(\boldsymbol{k}) = L^D \big\langle \hat{s}(\boldsymbol{k}) \cdot \hat{s}(-\boldsymbol{k}) \big\rangle_e \,, \tag{2.88}$$

and that the microcanonical magnetic susceptibility is

$$\chi = L^D \langle \vec{\mathcal{M}}^2 \rangle_e = \hat{C}(0) \,. \tag{2.89}$$

For the specific case of the Ising model, the traditional definitions, using $S_i = \pm 1$ (recall that $s_i = \pm 1/\sqrt{2}$), are related with those of the general model through:

$$\begin{aligned} \mathcal{U}^{\mathrm{Ising}} &= -\sum_{<i,j>} S_i S_j = 2\mathcal{U} - 3L^D \,, \\ \beta^{\mathrm{Ising}} &= \beta/2 \,, \\ \chi^{\mathrm{Ising}} &= 2\chi \,. \end{aligned} \tag{2.90}$$

Notice that for $D = 2$ this model undergoes a phase transition at $\beta_c = \log(1 + \sqrt{Q})$ which is of second order for $Q \leq 4$ and first order for $Q > 4$ [82].

2.4 Numerical Results

2.4.1 Methods

We have simulated systems of several sizes in a suitable range of energies (see Table 2.1). To update the spins we used a Swendsen-Wang (SW) version of the microcanonical cluster method [13]. This algorithm depends on a tunable parameter, κ, which should be as close as possible to $\langle \hat{\beta} \rangle_e$ in order to maximise the acceptance of the SW attempt (SWA). This requires a start-up using a much slower Metropolis algorithm for the determination of κ. In practice, we performed cycles consisting of 2×10^3 Metropolis steps, a κ refresh, 2×10^3 SWA, and a further κ refresh. We require an acceptance exceeding 60% to finish these pre-thermalization cycles fixing κ for the following main simulation, where only the cluster method is used.

In both cases studied, we observed a very small autocorrelation time for all energy values at every lattice size. In the largest lattice for the four-state Potts model we also considered different starting configurations: hot, cold, and mixed (strips). Although the autocorrelation time is much smaller, for safety we decided to discard the first 10% of the Monte Carlo history, using the last 90% for taking measurements.

Model	L	$N_{\rm m}(\times 10^6)$	$N_{\rm e}$	Energy range
$Q=2,\ D=3$	8	20	42	$[-0.8,-0.9]$
	12	20	42	$[-0.8,-0.9]$
	16	20	49	$[-0.8,-0.9]$
	24	20	25	$[-0.845,-0.875]$
	32	20	16	$[-0.87,-0.860625]$
	48	20	10	$[-0.87,-0.860625]$
	64	5	10	$[-0.870625,-0.865]$
	96	5	10	$[-0.870625,-0.865]$
	128	5	7	$[-0.869375,-0.865625]$
$Q=4,\ D=2$	32	1024	61	$[-1.2,-0.9]$
	64	128	61	$[-1.2,-0.9]$
	128	32	41	$[-1.08,-0.98]$
	256	32	24	$[-1.08,-1.005]$
	512	25.6	32	$[-1.07,-1.01]$
	1024	6.4	30	$[-1.06,-1.02]$

Table 2.1: Simulation details for the two models considered. For each lattice size L we show the number of measurements $N_{\rm m}$ at each energy and the total number of simulated energies uniformly distributed over the displayed energy range $N_{\rm e}$. For the $Q=4,\ D=2$ model, the values of $N_{\rm m}$ reported were reached only at specific energies near the peaks of the Maxwell construction, where additional energy values were simulated.

2.4.2 $D=3$ Pure Ising Model

In Fig. 2.1 (upper panel) we show a scaling plot of the correlation length (in lattice size units) against $(e-e_{\rm c})L^{1/\nu_{\rm m}}$. For the susceptibility we plot $\chi \sim L^{2-\eta}$ (lower panel). If the data followed the expected asymptotic critical behaviour with microcanonical critical exponents they should collapse into a single curve. In Fig. 2.1 we have used the canonical critical quantities from Refs. [83,84] transformed to the microcanonical counterparts using Eq. (2.2). From the plot it is clear that important scaling corrections exist in both cases for the smallest lattices, although they are mainly eliminated in the largest systems.

To obtain the microcanonical critical exponents we used the quotient method, see Sec. 2.2.3. The clear crossing points of the correlation length for different lattice sizes can be seen in Fig. 2.2. The determination of the different quantities at the crossings, and the position of the crossing itself, requires one to interpolate the data between consecutive simulated energies. We found that the method of choice, given the high number of energy values available, is to fit, using the least squares method, a selected number of points near the crossing to a polynomial of appropriate degree. Straight lines do not provide good enough fits. However, second and third order polynomials give compatible results. In practice, we fitted a second-order polynomial using the nine points nearest to the crossing, also comparing the results

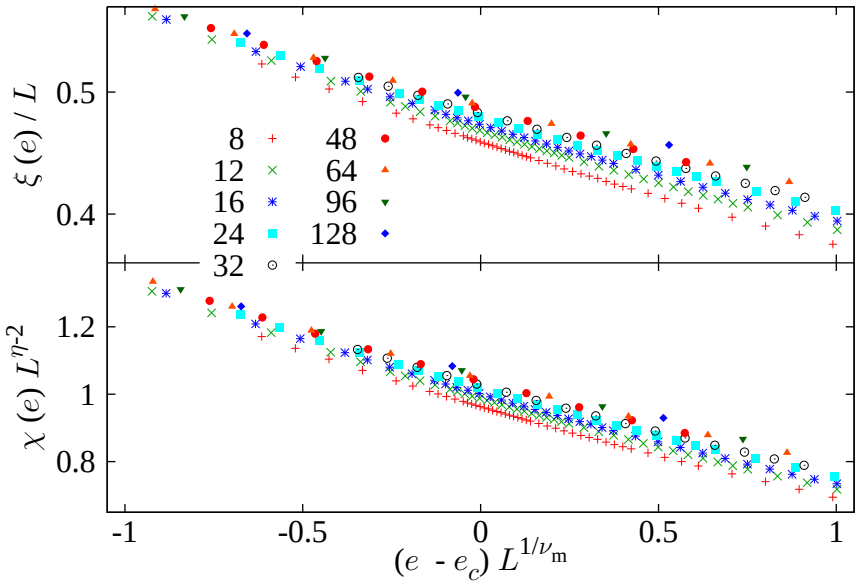

Figure 2.1: Scaling plot of the correlation length (in lattice size units) and the scaled susceptibility for the three-dimensional Ising model. We used the critical values, $e_c = -0.867433$ and $\nu_m = 0.7077$. Notice the strong scaling corrections for small systems as well as the data collapse for the largest ones.

with those using the seven nearest points that turn out to be fully compatible. For error determination we always used a jack-knife procedure, see Appendix C.

L	$e_{c,L,2L}$	$\xi_{L,e_{c,L,2L}}/L$	ν_m	η_m
8	−0.861831(12)	0.44922(3)	0.8033(42)	0.0564(2)
12	−0.865010(10)	0.46106(5)	0.7968(31)	0.0492(4)
16	−0.866020(6)	0.46710(5)	0.7717(22)	0.0469(4)
24	−0.866767(3)	0.47411(4)	0.7665(11)	0.0437(3)
32	−0.867034(4)	0.47813(6)	0.7594(13)	0.0425(5)
48	−0.867228(2)	0.48278(5)	0.7492(5)	0.0412(3)
64	−0.867302(2)	0.48555(11)	0.7457(16)	0.0397(8)

Table 2.2: Lattice size dependent estimates of critical quantities for the microcanonical $D = 3$ Ising model. The displayed quantities are: crossing points $e_{c,L,2L}$ for the correlation length in units of the lattice size, ξ/L itself at those crossing points, and the estimates of the correlation length exponent ν_m and the anomalous dimension η_m. All quantities were obtained using parabolic interpolations.

The numerical estimates for e_c, $\xi_{L,e_c}/L$ and the critical exponents ν_m and η_m, obtained using the quotient method for lattice pairs $(L, 2L)$ are given in Table 2.2. Our small statistical errors allow one to detect a tiny L evolution. An extrapolation to infinite volume is clearly needed.

Before continuing, let us recall our expectations as obtained by applying Fisher renormalization to the most accurate determination of *canonical* critical exponents known to us [$\nu_{\rm m} = \nu/(1-\alpha) = \nu/(D\nu - 1)$]:

$$\nu_{\rm m} = 0.7077(5) \text{ (from } \nu = 0.6301(4) \text{ [8]}) \,, \tag{2.91}$$

$$\eta_{\rm m} = \eta = 0.03639(15) \text{ [85]} \,, \tag{2.92}$$

$$\omega = 0.84(4) \text{ [8]} \,. \tag{2.93}$$

Besides, although non-universal, let us take $e_{\rm c} = -0.867433(12)$ [6].

The results obtained from an extrapolation using only leading order scaling corrections were:

- $e_{\rm c} = -0.867397(6)$, $\omega + 1/\nu_{\rm m} = 1.918(26)$
  (we obtained a good fit for $L \geq L_{\rm min} = 12$, with χ^2/d.o.f. $= 0.39/3$, C.L.=94%, where "d.o.f." stands for *degrees of freedom* and "C.L." for *confidence level* [7]).

- $\xi_{e_{\rm c},L}/L = 0.5003(12)$, $\omega = 0.581(27)$
  ($L_{\rm min} = 12$, χ^2/d.o.f. $= 0.12/3$, C.L.=99%).

- $\nu_{\rm m} = 0.714(28)$, $\omega = 0.53(30)$
  ($L_{\rm min} = 8$, χ^2/d.o.f. $= 3.16/4$, C.L.=53%).

- $\eta_{\rm m} = 0.0391(15)$, $\omega = 1.21(24)$
  ($L_{\rm min} = 8$, χ^2/d.o.f. $= 0.96/4$, C.L.=92%).

The main conclusions that we draw from these fits are: (i) the exponents are compatible with our expectations from Fisher renormalization, (ii) sub-leading scaling corrections are important given the tendency of the fits to produce a too low estimate for ω (see below), and (iii) the estimates from canonical exponents (themselves obtained by applying the high-temperature expansion to improved Hamiltonians [8,85]) are more accurate than our direct computation in the microcanonical ensemble.

We can, instead, take an opposite point of view. If we take the central values in Eqs. (2.91, 2.92, 2.93) as if they were exact, we can obtain quite detailed information on the amplitudes for scaling corrections:

- We find an excellent fit to $\nu_{\rm m}(L, 2L) = \nu_{\rm m} + A_1 L^{-\omega} + A_2 L^{-2\omega}$, for $L_{\rm min} = 16$: χ^2/d.o.f. $= 1.53/3$, C.L.=68%, with $A_1 = 1.38(7)$ and $A_2 = -7.6(1.1)$. This confirms our suspected strong sub-leading corrections. Indeed, according to these amplitudes A_1 and A_2, only for $L \approx 130$ the contribution of the (sub-leading) quadratic term becomes 10% of that of the leading one.

[6] For the $3D$ Ising model at criticality, $u_{\rm c}^{\rm Ising} = -0.990627(24)$ [83], and $\beta_{\rm c}^{\rm Ising} = 0.2216546(2)$ [84], we obtain for our Potts representation of the Ising model $e_{\rm c} = (u_{\rm c}^{\rm Ising} - D)/2 + 1/(4\beta_{\rm c}^{\rm Ising})$.

[7] The confidence level is the probability that χ^2 would be larger than the observed value, supposing that the statistical model is correct. As a rule, we consider a fit not good-enough whenever C.L.$< 10\%$.

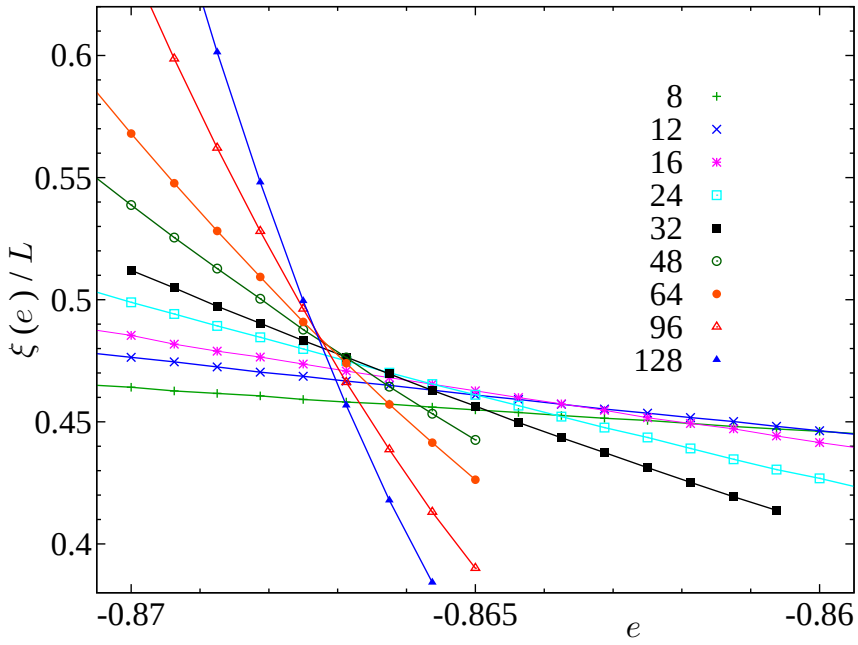

Figure 2.2: Crossing points of the correlation length in lattice size units for the three-dimensional Ising model. The error bars are in every case smaller than the point sizes. The values of the different quantities at the crossing as well as the critical exponents are given in Table 2.2.

- In the case of $\eta_{\rm m}(L, 2L) = \eta_{\rm m} + B_1 L^{-\omega} + B_2 L^{-2\omega}$, for $L_{\rm min} = 8$: $\chi^2/\text{d.o.f.} = 2.4/5$, C.L.=79%, we have $B_1 = 0.101(10)$ and $B_2 = 0.07(7)$. Sub-leading scaling corrections are so small that, within our errors, it is not clear whether or not $B_2 = 0$.

The quite strong scaling corrections found for $\nu_{\rm m}$ may cast some doubt on the extrapolation for $\xi_{L,e_{\rm c}}/L$, the only quantity that we cannot double check with a canonical computation. To control this, we proceed to a fit including terms linear and quadratic in $L^{-\omega}$ with $\omega = 0.84(4)$. We get

$$\frac{\xi_{L,e_{\rm c}}}{L} = 0.4952(5)(7),$$

with $L_{\rm min} = 12$, $\chi^2/\text{d.o.f.} = 2.17/3$, C.L.=54%. Here, the second error is due to the quite small uncertainty in ω. It is remarkable that the contribution to the error stemming from the error in ω is *larger* than the purely statistical one.

The canonical specific-heat

Previous numerical studies of microcanonical FSS [61–63] focussed on the specific heat. Although we show all across this paper that a complete microcanonical FSS analysis can be based only on the spin propagator, the specific heat can be certainly studied within the present formalism.

As discussed in Sect. 2.2.2 (see also [13]), the canonical specific heat can be estimated from the microcanonical estimator $C_{\rm m}(L, e)$ defined in Eq. (2.68). The expected FSS behaviour for $C_{\rm m}(L, e_{{\rm c},L,2L})$ is

$$C_{\rm m}(L, e_{{\rm c},L,2L}) = L^{\alpha/\nu}[A_0 + A_1 L^{-\omega} + \cdots] + B\,. \tag{2.94}$$

Here, A_0 and A_1 are scaling amplitudes, while B is a constant background usually termed *analytical correction to scaling*, stemming from the non-singular part of the free-energy [7]. It is usually disregarded as it plays the role of a subleading scaling-correction term. Yet, a peculiarity of the $D = 3$ Ising model is that B is anomalously large (see e.g. [63]) and needs to be considered.

In Fig. 2.3, we reproduce the analysis of Bruce and Wilding [63], where the amplitude A_1 in Eq. (2.94) was fixed to zero by hand. In this way, if we consider the range of lattice sizes $8 \le L \le 64$ (in [63] only $L \le 32$ was considered), we obtain $B = -35.01(11)$ but with an untenable $\chi^2/\text{d.o.f} = 227/5$. Our value of B is, nevertheless, quite close to the result $B = -34.4(4)$ reported in [63] (unfortunately, these authors provided no information on fit-quality).

Once the arbitrary constraint $A_1 = 0$ is removed, we do obtain an acceptable fit, $\chi^2/\text{d.o.f} = 0.68/4$. Perhaps unsurprisingly, the estimate of B is largely changed, once a nonvanishing A_1 is allowed: $B = -24.4(7)$.

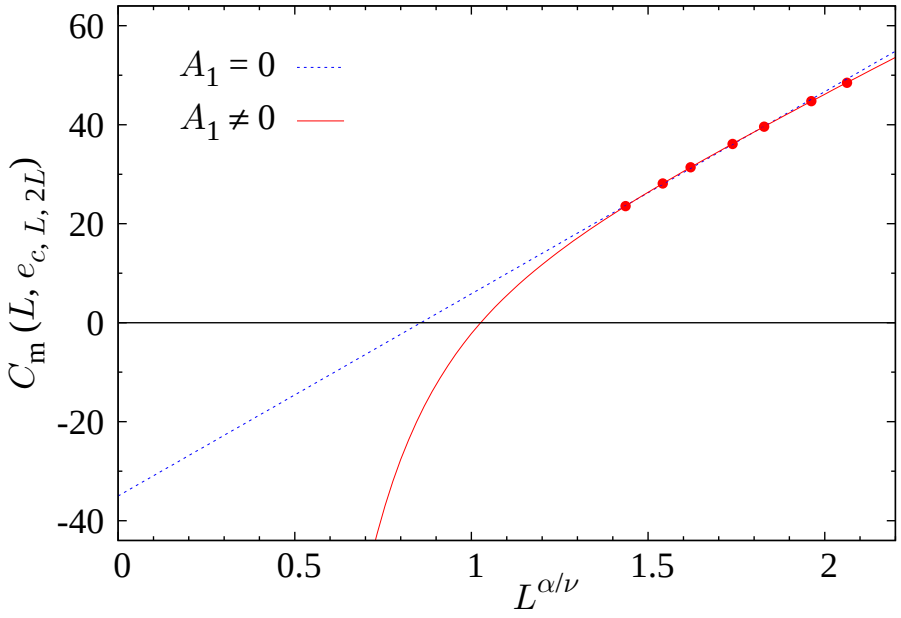

Figure 2.3: Microcanonical estimate of the specific heat, $C_{\rm m}(L, e)$, at $e_{{\rm c},L,2L}$ for the $D = 3$ Ising model, as a function of the system size. The numerical estimates of exponents α/ν and ω were taken from Ref. [8]. The error bars are in every case smaller than the point sizes. The solid line is a fit to Eq. (2.94) (fitting parameters: A_0, A_1 and B), the dashed one is obtained by constraining the fit to $A_1 = 0$.

2.4.3 $D = 2$, $Q = 4$ Pure Potts Model

The $Q = 4$, $D = 2$ Potts model involves two peculiarities that will be explored here. First, it suffers from quite strong logarithmic scaling corrections. And second, it displays pseudo-metastability [81], an ideal playground for a microcanonical study.

The study of the FSS for the $Q = 4$, $D = 2$ Potts model [43], based on the analysis of the Renormalization Group (RG) equations [86], reveals the presence of multiplicative logarithmic scaling corrections. This is one of the possible forms that scaling corrections can take in the limit $\omega \to 0$, and is a major nuisance for numerical studies. A very detailed theoretical input is mandatory to safely perform the data analysis. We shall make here an educated guess for the *microcanonical* form of the scaling corrections, based purely on ensemble equivalence and the *canonical* results.

From ensemble equivalence we expect

$$e - e_{\rm c} \sim C(L, \beta_{\rm c}) \Delta\beta_L \ , \tag{2.95}$$

where $C(L, \beta_{\rm c})$ is the finite-lattice canonical specific heat at $\beta_{\rm c}$, and $\Delta\beta = \beta_{\rm c}^{(L)} - \beta_{\rm c}$ is the inverse-temperature distance to the critical point of any L-dependent feature (such as the temperature maximum of the specific heat, etc.). We borrow from Ref. [43] the leading FSS behaviour for these quantities:

$$C(L, \beta_{\rm c}) \sim \frac{L}{(\log L)^{3/2}} \quad , \quad \Delta\beta_L \sim \frac{(\log L)^{3/4}}{L^{3/2}} \, . \tag{2.96}$$

Thus, we have:

$$e(L) - e_c(\infty) \sim L^{-1/2} (\log L)^{-3/4} \ . \tag{2.97}$$

This result can be derived as well by considering only the leading terms of the first derivative of the singular part of free energy with respect to the thermal field, ϕ ($\propto \beta - \beta_{\rm c}$) [43]:

$$\frac{\partial f_{\rm sing}(\phi, h, \psi)}{\partial \phi} \approx \frac{4}{3} D_{\pm} |\phi|^{1/3} (-\log|\phi|)^{-1} + D_{\pm} |\phi|^{4/3} (-\log|\phi|)^{-2} \frac{1}{\phi} \, . \tag{2.98}$$

The above equation describes the energy of the system, and its leading term is

$$e - e_{\rm c} \sim \frac{4}{3} D_{\pm} \frac{|\phi|^{1/3}}{\log|\phi|} \ , \tag{2.99}$$

but

$$\phi \approx C'_{\pm} L^{-3/2} (\log L)^{3/4} \ , \tag{2.100}$$

so it is direct to obtain again Eq. (2.97). Hence, we are compelled to recast Eq. (2.74) as

$$\langle O \rangle_{L,e} = L^{\frac{x_{O,\rm m}}{\nu_{\rm m}}} \tilde{f}_O \left(L^{1/2} (\log L)^{3/4} (e - e_{\rm c}) \right) + \cdots \, . \tag{2.101}$$

Furthermore, from the canonical analysis [43], we expect multiplicative logarithmic corrections to the susceptibility (that do not get Fisher renormalised). Furthermore, the ellipsis in (2.101) stands for corrections of order $\log\log L / \log L$ and $1/\log L$ [43].

We first address in the next subsection the direct verification of Eq. (2.101) using the quotient method. We then consider the pseudo-metastability features.

Scaling plots and critical exponents

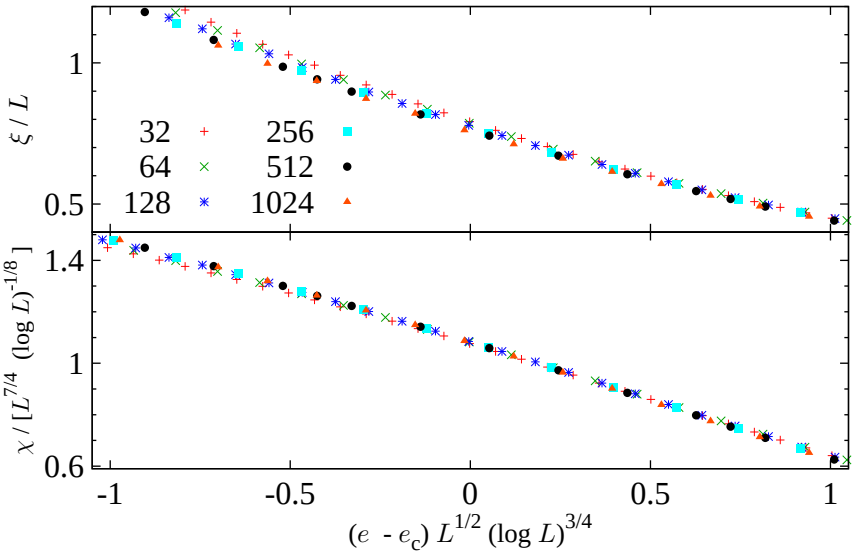

Figure 2.4: Graphical demonstration of Eq. (2.101) as applied to the microcanonical $D = 2$, $Q = 4$ Potts model: both the correlation length in units of the lattice size (**top**) and the scaled susceptibility, $\overline{\chi}$ in Eq. (2.102) (**bottom**), are functions of the scaling variable $(e - e_c)L^{1/2}(\log L)^{3/4}$.

We start with a graphical demonstration of Eq. (2.101): ξ/L as a function of $(e-e_c)L^{1/2}(\log L)^{3/4}$ should collapse onto a single curve (the deviation will be larger for small L values due to neglected scaling corrections of order $\log\log L/\log L$ and $1/\log L$) [8]. Similar behaviour is expected for the scaled susceptibility [43]:

$$\overline{\chi} = \frac{\chi}{L^{7/4}(\log L)^{-1/8}} \,. \tag{2.102}$$

Note that ξ/L does not need an additional logarithmic factor. These expectations are confirmed in Fig. 2.4, especially for the larger system sizes (that are subject to smaller scaling corrections).

We can check directly the importance of the multiplicative logarithmic corrections for the susceptibility by comparing χ and $\overline{\chi}$ as a function of ξ/L, see Fig. 2.5. The improved scaling of $\overline{\chi}$ is apparent. We observe as well that the largest corrections to scaling are found at and below the critical point (around $\xi/L \approx 1.0$).

The scaling proposed for the susceptibility in Ref. [43] can also be checked from our values at $e_{c,L,2L}$. Considering $\chi \sim L^{7/4}$ (our data is fully supportive of this point) we can plot $\log(\chi/L^{7/4})$ versus $\log\log L$. We obtain a linear fit for the data with $L > 64$ with a slope $-0.132(3)$ (χ^2/n.d.f. $= 7.5/1$), see the dashed line in

[8] We obtain the exact e_c in the thermodynamic limit from $\beta_c = \log(1+\sqrt{Q})$ [87], and $u_c = -(1+Q^{-1/2})$ [82] by applying $e_c = u_c + 1/(2\beta_c)$.

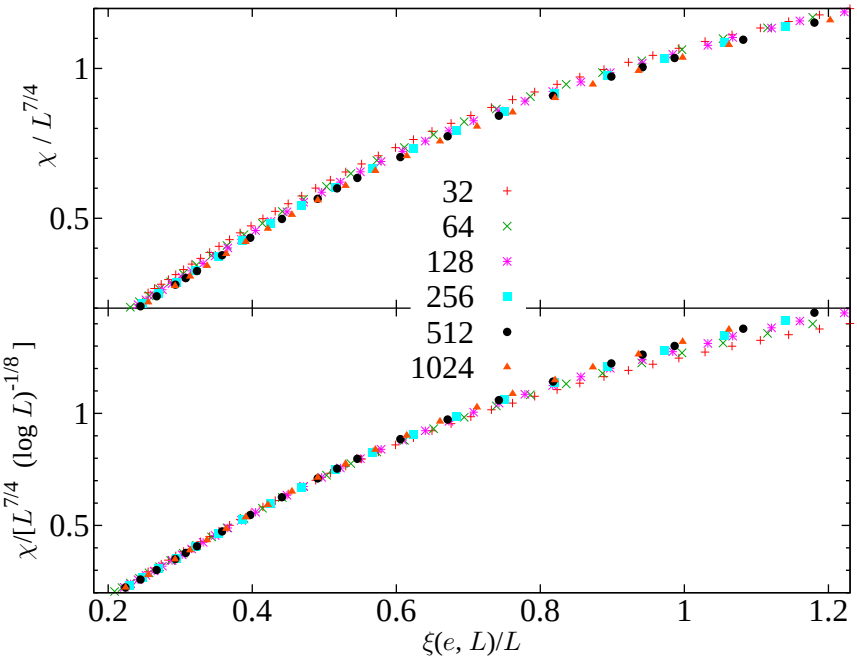

Figure 2.5: Comparison of the scaling for the naively scaled susceptibility $\chi L^{-7/4}$ (**top**) and for $\overline{\chi}$, defined in Eq. (2.102), (**bottom**), as a function of the correlation length in units of the lattice size, for the microcanonical $D = 2$, $Q = 4$ Potts model.

Fig. 2.4.3, which can be compared with the expected value $-1/8$ [43]. The large value of χ^2/d.o.f. can be ascribed to the presence of higher order correction terms. In fact the whole scaling behaviour for the susceptibility is [43]

$$\chi \sim L^{7/4} (\log L)^{-1/8} \left(1 + A \frac{\log\log L}{\log L} + B \frac{1}{\log L} + \cdots \right) , \tag{2.103}$$

and we can use this form for a least-square fit. Fixing both the leading and the logarithmic exponents we estimate $A = 0.80(7)$ and $B = -0.48(3)$ using all the lattice sizes with χ^2/d.o.f. $= 2.9/2$, see the solid line in Fig. 2.4.3. Therefore our data set is fully supportive of the behaviour proposed in Ref. [43], including the subleading additive logarithmic corrections.

We now proceed to the numerical computation of critical exponents. We shall use the quotient method, modified as described in Appendix B. From Fig. 2.7, we can see that the crossing points can be well obtained using parabolic interpolations of the nine points around the estimated crossing energies, as done in Sec. 2.4.2. We checked that the results do not depend on the interpolating polynomial degree by comparing with interpolations using cubic curves. We also compared with the results obtained using only seven points around the crossing obtaining again full agreement.

The critical exponents obtained are listed in Table 2.3. They may be compared with the exact ones [82] ($\nu = 2/3$, $\alpha = 2/3$ and $\eta = 1/4$):

$$\nu_{\rm m} = 2 \qquad ; \qquad \eta = \eta_{\rm m} = \frac{1}{4} . \tag{2.104}$$

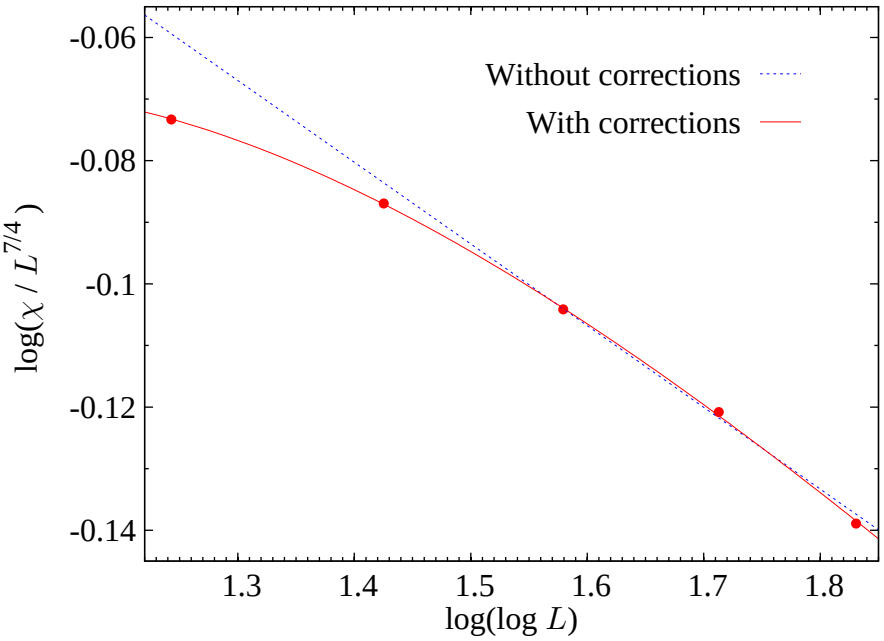

Figure 2.6: Logarithmic scaling behaviour of the susceptibility at the critical point. The error bars are in every case smaller than the point sizes. The dashed line do not include the subleading additive terms of Eq. (2.103) while the solid line do.

Comparing with our computed exponents, we obtain an acceptable agreement. In the case of the microcanonical ν exponent, ν_{m}, after adding the correction for the quotient method in the presence of logarithms, the agreement is fairly good. We can see a clear trend towards the exact value for all the lattice sizes except the largest (2.5 standard deviations away), which is probably due to a bad estimate of the huge temperature derivatives of the correlation length. In the case of the microcanonical η exponent, η_{m}, which must be the same as the canonical one, we can see clearly the tendency to the analytical value $\eta_{\mathrm{m}} = 0.25$. We must stress the importance of adding the corrections described in Appendix B to the quotient method.

Critical point, latent heat, and surface tension

It has been known for quite a long time that the $D = 2$, $Q = 4$ Potts model on finite lattices shows features typical of first-order phase transitions [81]. For instance, see Fig. 2.8, the probability distribution function for the internal energy, $P_\beta(e)$, displays two peaks at energies e_{d} (the coexisting *disordered* phase) and e_{o} (the energy of the *ordered* phase) separated by a minimum at e^*. Of course, since the transition is of second order, e_{c} is the common large L limit of e_{d}, e_{o} and e^*.

We discussed in Sec. 2.2.2 how the Maxwell construction is used to estimate the canonical critical point $\beta_{\mathrm{c},L}$, as well as e_{d}, e_{o} and the associated surface tension. This procedure is outlined in Fig. 2.9. The numerical results are listed in Table 2.4, where we can see that $\beta_{\mathrm{c},L}$ is a monotonically increasing function of L continuously

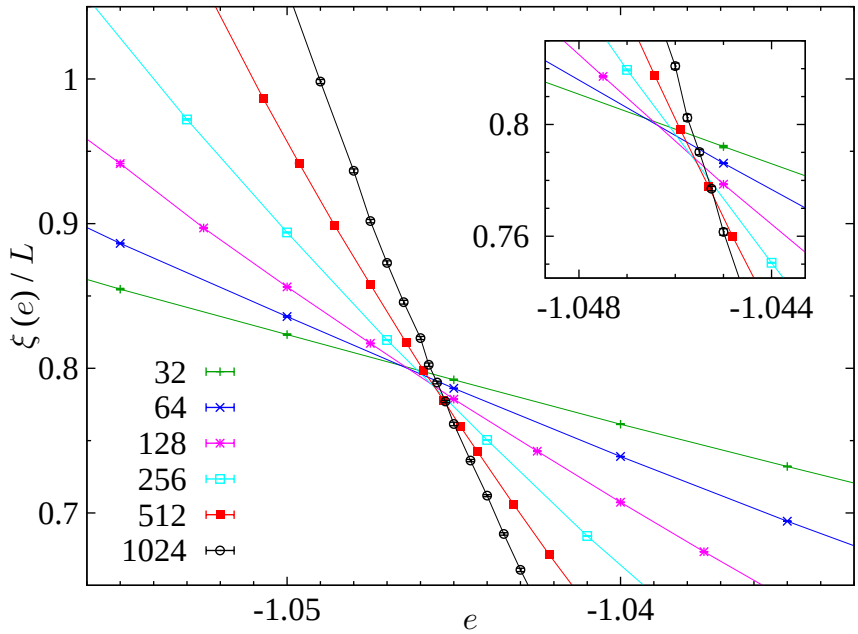

Figure 2.7: Correlation length in lattice size units for the $D = 2$, $Q = 4$ Potts model. The values of the different quantities at the crossings for lattices L and $2L$, as well as the corresponding estimates for critical exponents, are given in Table 2.3. The inset is a magnification of the critical region.

approaching the analytical value $\beta_c = \log(1+\sqrt{Q}) = 1.0986122\ldots$ [87]. A jack-knife method [7] was used to compute the error bars for all the quantities in Table 2.4.

To perform a first check of our data, we observe that $\beta_{c,L}$ is a typical *canonical* estimator of the inverse critical temperature. As such, it is subject to standard canonical FSS, where the main scaling corrections come from two additive logarithmic terms [43]:

$$\beta_{c,L} - \beta_c = a_1 \frac{(\log L)^{3/4}}{L^{3/2}} \left(1 + a_2 \frac{\log\log L}{\log L} + a_3 \frac{1}{\log L}\right) . \qquad (2.105)$$

From our data in Table 2.4, we obtain $a_1 = -0.44(7)$, $a_2 = -1.15(72)$, and $a_3 = 2.28(26)$, and a good fit ($L_{\min} = 128$, χ^2/d.o.f. $= 0.28/1$, C.L.=60%).

As for the L dependence of e_d and e_o, we try a fit that considers the expected scaling correction terms [43]:

$$e_{c,o,L} - e_c = a_1 L^{-1/2} (\log L)^{-3/4} \left(1 + a_2 \frac{\log\log L}{\log L} + a_3 \frac{1}{\log L}\right) . \qquad (2.106)$$

Our results for e_o are: $a_{1o} = -2.03(20)$, $a_{2o} = -1.65(27)$, and $a_{3o} = -2.08(41)$, with a fair fit quality ($L_{\min} = 32$, χ^2/d.o.f. $= 2/3$, C.L.=57%). We obtain for e_d: $a_{1d} = 2.02(14)$, $a_{2d} = 0.93(37)$, and $a_{3d} = -2.93(34)$, with a fair fit as well ($L_{\min}$=32, χ^2/d.o.f. $= 0.84/3$, C.L.=84%). These two fits are shown in Fig. 2.10.

For the surface tension, one notes in Table 2.4 a non-monotonic behaviour. Furthermore, we lack any theoretical input with which to attempt a fit. We thus turn to

L	$e_{\mathrm{c},L,2L}$	$\xi_{L,e_{\mathrm{c},L,2L}}/L$	ν_{m}	ν'_{m}	η_{m}	η'_{m}
32	−1.04659(5)	0.8016(5)	1.534(6)	1.998(10)	0.2663(9)	0.2334(9)
64	−1.04633(2)	0.7990(3)	1.554(8)	1.957(12)	0.2638(6)	0.2360(6)
128	−1.04579(1)	0.7909(3)	1.578(5)	1.938(7)	0.2639(5)	0.2398(5)
256	−1.04548(2)	0.7836(5)	1.643(12)	1.987(17)	0.2615(11)	0.2402(11)
512	−1.04519(2)	0.7734(9)	1.602(31)	1.895(42)	0.2617(21)	0.2427(21)

Table 2.3: Crossing points of the correlation length in lattice size units as a function of the energy for pairs of lattices $(L, 2L)$. Using the original quotient method [7] we obtain the microcanonical critical exponents, listed in Columns 4 and 6, while the corrected ones (Columns 5 and 7) are labelled with primed symbols, see Appendix B.

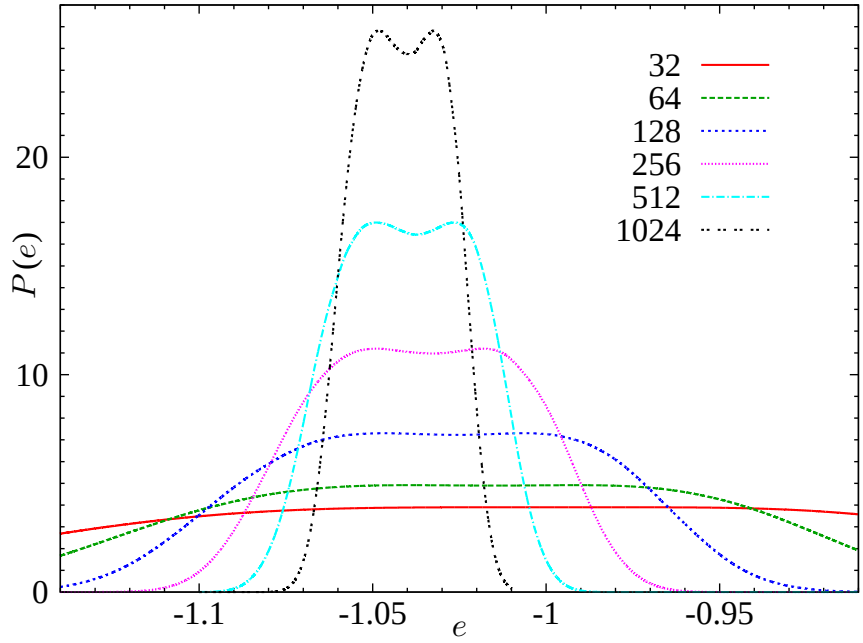

Figure 2.8: *Canonical* probability distribution function for the energy density, $P_\beta^{(L)}(e)$, as reconstructed from microcanonical simulations of the $D = 2$, $Q = 4$ Potts model for different system sizes. The L-dependent critical point $\beta_{\mathrm{c},L}$ is computed using the Maxwell rule, Sec. 2.2.2 (note the equal height of the two peaks enforced by Maxwell construction). The system displays an apparent latent heat that becomes smaller with increasing L, and vanishes in the large L limit.

a variant of the quotient method. Were Σ to follow pure power-law scaling, $\Sigma \propto L^b$, the exponent b would be obtained as:

$$\frac{\Sigma(L_1)}{\Sigma(L_2)} = \left(\frac{L_1}{L_2}\right)^b \Longrightarrow b = \frac{\log[\Sigma(L_1)/\Sigma(L_2)]}{\log(L_1/L_2)}\,. \tag{2.107}$$

The effective exponent b obtained from our data is given in Table 2.5. We observe that it is clearly negative (as it should be since Σ vanishes for a second-order phase

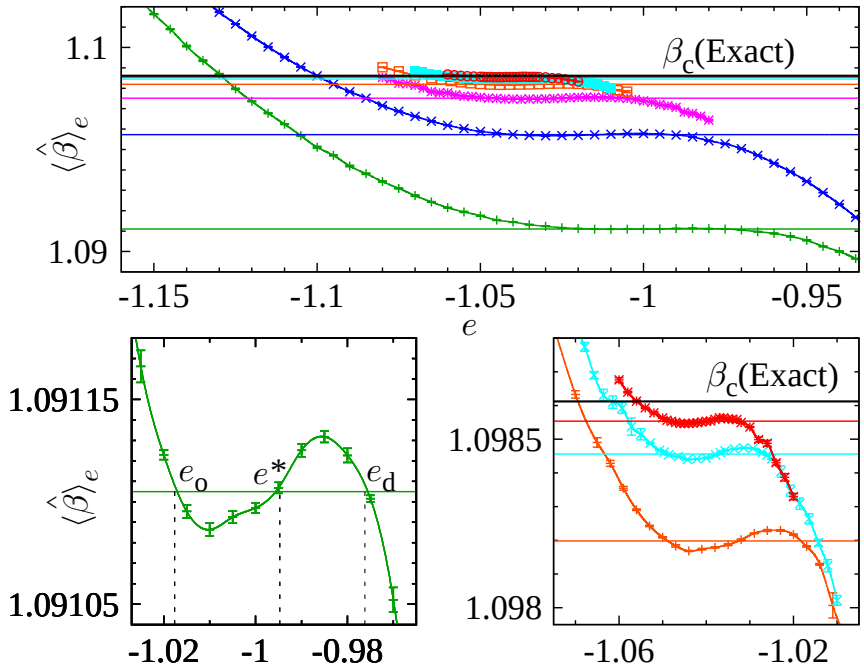

Figure 2.9: **Top:** From the microcanonical mean values $\langle\hat{\beta}\rangle_{e,L}$ for the $D = 2$, $Q = 4$ Potts model, we estimate the size dependent *canonical* inverse critical temperature $\beta_{c,L}$ (horizontal lines) for all the simulated lattice sizes, ranging from $L = 32$ (lower) to $L = 1024$ (upper). We show as well the analytical prediction (uppermost horizontal line). **Bottom-left:** Example of Maxwell construction for our $L = 32$ data. The e-integral of $\langle\hat{\beta}\rangle_{e,L} - \beta_{c,L}$ from e_o to e_d vanishes. **Bottom-right**: Zoom of upper panel showing only data for lattice sizes $L = 256$ (lower curve), $L = 512$ (middle curve), and $L = 1024$ (upper curve).

L	$\beta_{c,L}$	e_o	e_d	$\Sigma \times 10^5$
32	1.0911070(20)	-1.0175(4)	-0.9760(2)	0.47(2)
64	1.0957256(14)	-1.0392(3)	-0.9915(2)	2.77(7)
128	1.0975150(10)	-1.0463(3)	-1.0062(5)	4.10(15)
256	1.0981989(5)	-1.0489(2)	-1.0183(3)	3.92(8)
512	1.0984570(3)	-1.0490(1)	-1.0266(2)	3.28(11)
1024	1.0985539(3)	-1.0483(3)	-1.0325(1)	2.09(17)

Table 2.4: Using the Maxwell construction, we compute for the $D = 2$, $Q = 4$ Potts model the L-dependent estimates of the (inverse) critical temperature $\beta_{c,L}$, the energies of the coexisting ordered e_o, and disordered e_d phases, as well as the surface tension Σ.

transition). An asymptotic estimate, however, seems to require the simulation of larger systems.

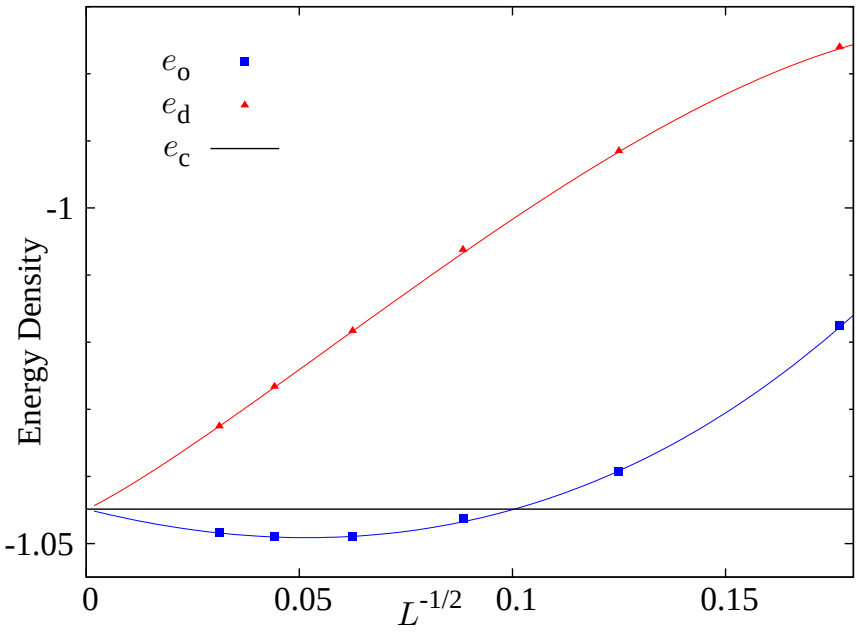

Figure 2.10: System size dependent estimates of the energies of the "coexisting" ordered (e_o, blue squares) and disordered (e_d, red circles) phases of the $D = 2$, $Q = 4$ Potts model, as a function of $L^{-1/2}$. The lines are fits to the expected analytical behaviour Eq. (2.106). The horizontal line corresponds to the asymptotic value, e_c.

(L_1, L_2)	$b_{\rm eff}(\Sigma)$
(32,64)	2.56(7)
(64,128)	0.56(6)
(128,256)	−0.065(60)
(256,512)	−0.257(57)
(512,1024)	−0.650(127)

Table 2.5: Effective exponent obtained using Eq. (2.107) for the surface tension.

We have just seen that, up to scaling corrections, $e_d^{(L)}$ and $e_o^{(L)}$ correspond to (different) L-independent values of the argument of the scaling function $\tilde{f}_\xi$ in Eq. (2.101). Hence we expect that $\xi(e_d)/L$ and $\xi(e_o)/L$, see Table 2.6, approach non-vanishing, different values in the large L limit. The FSS corrections are expected to be additive logarithms [43]

$$\frac{\xi}{L} = a + \frac{b}{\log L}\,. \tag{2.108}$$

The results are:

$$\frac{\xi(e_o)}{L} = 1.28(1) - \frac{2.28(5)}{\log L}\,, \tag{2.109}$$

L	$\xi(e_o)/L$	$\xi(e_d)/L$	$\overline{\chi}(e_o)$	$\overline{\chi}(e_d)$	$\xi^{\rm canonical}/L$	$\overline{\chi}^{\rm canonical}$
32	0.637(2)	0.453(1)	0.907(2)	0.647(1)	0.990(3)	1.287(3)
64	0.732(3)	0.396(1)	1.025(3)	0.545(2)	0.995(2)	1.310(2)
128	0.799(5)	0.357(4)	1.106(5)	0.472(7)	1.001(3)	1.331(3)
256	0.866(6)	0.335(3)	1.182(6)	0.429(5)	1.001(5)	1.343(5)
512	0.915(4)	0.315(2)	1.238(4)	0.392(4)	1.014(8)	1.366(8)
1024	0.953(15)	0.302(2)	1.279(13)	0.367(3))	0.997(21)	1.353(22)

Table 2.6: Correlation length in units of the lattice size and the RG invariant $\overline{\chi}$ defined in Eq. (2.102), for several L values, as computed in the microcanonical $D = 2$, $Q = 4$ Potts model. The values of the energy density correspond to the ordered (e_o) and disordered (e_d) phases. For comparison we also display in the last two columns the *canonical* results at β_c obtained in Ref. [43].

($L_{\rm min} = 32$, χ^2/d.o.f. $= 4.2/3$, C.L.=22%), and

$$\frac{\xi(e_d)}{L} = 0.159(4) - \frac{0.98(2)}{\log L}\,, \tag{2.110}$$

($L_{\rm min} = 32$, χ^2/d.o.f. $= 3.3/3$, C.L.=37%).

A very similar analysis can be performed for the scaled susceptibility, Eq. (2.89), at e_d and e_o. In order to deal with the multiplicative logarithms of the susceptibility, we used $\overline{\chi}$ defined in Eq. (2.102).

Fitting our data set to the logarithmic form

$$\overline{\chi} = A + B\frac{\log\log L}{\log L}\,, \tag{2.111}$$

obtained in Ref. [43], we obtain a good fit in the ordered phase energy, e_o:

$$\overline{\chi}(e_o) = 2.41(5) - 4.00(15)\frac{\log\log L}{\log L}\,, \tag{2.112}$$

with $L_{\rm min} = 128$, χ^2/d.o.f. $= 3.10/2$, C.L.=21%. However, the extrapolation for the susceptibility defined in the disordered phase energy, e_d, is a nonsensical negative value.

We can also fit the data to the logarithmic form also used in Ref. [43]:

$$\overline{\chi} = A + \frac{B}{\log L}\,, \tag{2.113}$$

finding:

$$\overline{\chi}(e_o) = 1.643(5) - \frac{2.55(2)}{\log L}\,, \tag{2.114}$$

($L_{\rm min} = 32$, χ^2/d.o.f $= 7.44/4$, C.L.=11%), and

$$\overline{\chi}(e_d) = 0.094(7) + \frac{1.87(37)}{\log L}\,, \tag{2.115}$$

($L_{\min} = 64$, $\chi^2/\text{d.o.f} = 2.94/3$, C.L.=37%) . For comparison, we recall that Ref. [43] reports two different fits for $\overline{\chi}$, depending on the logarithmic corrections they used:

$$\overline{\chi}^{\text{canonical}} = 1.673(33) - 1.056(98)\frac{\log\log L}{\log L}\,, \tag{2.116}$$

$$\overline{\chi}^{\text{canonical}} = 1.454(13) - \frac{0.600(55)}{\log L}\,. \tag{2.117}$$

2.5 Conclusions

We have formulated the Finite Size Scaling Ansatz (FSSA) for microcanonical systems in terms of quantities accessible in a finite lattice. This form allows to extend the phenomenological renormalization approach (the so-called quotient method) to the microcanonical framework.

Our FSSA was subjected to strong numerical testing. We performed extensive microcanonical numerical simulations in two archetypal systems in Statistical Mechanics: the three-dimensional Ising model and the two-dimensional four-state Potts model. The two models present a power-law singularity in their canonical specific heat, implying non-trivial Fisher renormalization when passing to the microcanonical ensemble. A microcanonical cluster method works for both models, hence allowing us to study very large system sizes ($L = 128$ in $D = 3$ and $L = 1024$ in $D = 2$).

In the case of the Ising model, we obtained precise determinations of the critical exponents that provide strong evidence for our extended microcanonical FSS ansatz.

For the Potts model, very strong logarithmic corrections (both multiplicative and additive) plague our data. Fortunately, we have a relatively strong command over these corrections from canonical studies [43]. Our data can be fully rationalised using the scaling corrections suggested by the theoretical analysis [43].

Chapter 3

Quenched Disorder Effect on a First-Order Phase Transition

3.1 Introduction

Although first-order phase transitions are by far the more frequent in nature, not much is known about the consequences of adding impurities to systems that in the pure case undergo this type of transition. This is due to the fact that there exist inherent difficulties for their study.

One of the intrinsic problems in simulating first-order phase transitions is that in this case two or more phases coexist at the critical temperature. The system changes from the high temperature phase to the low temperature one by building an interface of size L, where L is the lattice size. The energy cost of such a mixed configuration is ΣL^{D-1} (with Σ being the surface tension and D the spatial dimension). Therefore, when doing simulations using the canonical ensemble (at fixed temperatures), the probability of reaching such mixed configurations is attenuated by a factor $\exp[-\Sigma L^{D-1}]$, and as a result the natural time scale of the simulation grows with the system size L as $\exp[\Sigma L^{D-1}]$. This huge obstacle to simulating large systems is called *Exponential Critical Slowing Down* (ECSD).

Up to now, no solution for ECSD has been found in canonical simulations. This has motivated the popularity of simulations within the microcanonical ensemble (at fixed energy), see Sec. 2.2.2. Some simulation methods within this ensemble consider the canonical probability density function (pdf) of the energy as a constant within the energy interval $e^{\mathrm{o}} < e < e^{\mathrm{d}}$ (e^{o} and e^{d} being the energy densities of the coexisting ordered and disordered phases respectively). This led to these methods being called *flat-histogram methods* [88–91]. The canonical probability minimum in the energy gap ($\propto \exp[-\Sigma L^{D-1}]$) is achieved by means of an iterative parameter optimisation. In flat-histogram methods the system performs an energy random walk in the energy gap. The elementary step being of order L^{-D} (a single spin-flip), one naively expects a tunnelling time from e^{o} to e^{d} of order L^{2D} spin-flips. But the (one-dimensional) energy random walk is not Markovian, and these methods still suffer ECSD [92]. In fact, for the standard benchmark (the $Q=10$ Potts model [82] in $D=2$), the barrier

of 10^4 spins was reached in 1992 [88], while the largest simulated system (to the best of our knowledge) had 4×10^4 spins [89].

ECSD in flat-histogram simulations is probably understood [92]: on its way from e^{d} to e^{o}, the system undergoes several (four in $D = 2$) "transitions". First comes the condensation transition [92, 93], at a distance of order $L^{-D/(D+1)}$ from e^{d}, where a macroscopic droplet of the ordered phase is nucleated. Decreasing e, the droplet grows to the point that, for periodic boundary conditions, it reduces its surface energy by becoming a strip [94], see the figures in [13] (in $D=3$, the droplet becomes a cylinder, then a slab [95]). At lower e the strip becomes a droplet of *disordered* phase. Finally, at the condensation transition close to e^{o}, we encounter the homogeneous ordered phase.

In this work we will study a prototypical model of a strong first-order phase transition, the three-dimensional Potts model with $Q > 3$ states. There are numerous experimental systems which can be mapped by this model. For instance, the $Q = 4$ pure case in two dimensions describes the adsorption of N_2 molecules on Kr in graphite layers [96]; in three dimensions it describes the behaviour of FCC antiferromagnetic lattices (NdSb, NdAs, and CeAs, for example) with the magnetic field pointing in the $\langle 1, 1, 1\rangle$ direction [97]. The site-diluted $Q = 4$ case in two dimensions models the effect of oxygen impurities on a sample of nickel where hydrogen molecules are adsorbed [98]. In the dilute three-dimensional case we are not aware of any experimental realization.

It is known [13, 46] that the pure three-dimensional Potts model undergoes a first-order phase transition in the pure case for $Q \geq 3$. On the contrary, it has been been found [44] that for strong dilution the system performs a second-order phase transition. A direct question is the following: what is the exact dilution that causes the order of the transition to change? What is more, are we absolutely sure that first-order phase transitions exist in the presence of dilution? This is still an important open problem in Statistical Mechanics, and also one with implications in very technical fields such as highly correlated electron systems (e.g., high temperature superconductors or colossal magnetoresistance oxides) where phase coexistence and chemical disorder play crucial roles [99].

The question in the previous paragraph can be considered exactly solved in two dimensions [100]: even the most insignificant amount of impurities is enough to switch the phase transition from first-order to second-order (for the Universality Classes see [101]). In $D = 3$ the most useful physical picture is provided by the Cardy-Jacobsen conjecture [101]: considering a ferromagnetic system undergoing a first-order phase transition for a pure sample, with T being the temperature and p the concentration of magnetic sites, a critical line, $T_{\mathrm{c}}(p)$, separates the ferromagnetic and the paramagnetic phases in the (T, p) plane. In $D=3$ a critical concentration is expected to exist, $1 > p_{\mathrm{c}} > 0$, such that the phase transition is of first order for $p > p_{\mathrm{c}}$ and of second order for $p < p_{\mathrm{c}}$ (at p_{c} one has a *tricritical point*). When p approaches p_{c} from above, the latent heat must vanish with the critical exponent of the magnetisation in the Random Field Ising Model (RFIM). Also the surface tension, Σ, vanishes at p_{c}, while the correlation length $\xi(T_{\mathrm{c}}(p))$ diverges, with critical

exponents related to those of the RFIM[1]. The main objection to this argument is that the Cardy-Jacobsen conjecture relies on a mapping from the (large Q) disordered Potts model [82] onto the RFIM (two unsolved models in $D = 3$). As a result, if the $D = 3$ RFIM phase transition turned out to be of first order [104], the conjecture would not be valid.

The $D = 3$ problem has already been numerically studied [44–46]; large regions of the critical line $T_c(p)$ were found to be second order. Unfortunately, the study of the tricritical point as well as that of the first-order part of the critical line seemed beyond hope, mainly due to two factors. Firstly, an important difficulty arises from the long-tailed pdf's encountered when comparing the specific heat or the magnetic susceptibility of different samples at $T_c(p)$ [46]. Note that diverging-variance pdf's arise from the common practice of defining the quenched free energy at temperature T as the average of the sample's free energy at T [22], which is dominated by rare events[2]. Secondly, the other factor has been described above – the simulation of a sample of linear size L with previous methods is intrinsically difficult: the required simulation time grows exponentially with L^{D-1} [92] due to the ECSD. These two factors have limited previous work [45, 46] to $L \leq 25$.

To overcome these two difficulties, on the one hand we propose two alternative methods of performing the sample average, both of which reproduce the correct Thermodynamic Limit, avoiding the diverging-variance pdf's, and providing complementary information, and on the other we exploit a novel microcanonic Monte Carlo method [13], which allows one to study the system entropy directly. This method, combined with a slightly modified typical cluster algorithm [11,13], permits accurate studies of systems with more than 10^6 spins (when the previous methods can only handle 10^4). In our case the method will allow us to simulate systems of size up to $L = 128$ in the case $Q = 4$, $D = 3$, also making it possible to perform a Finite-Size Scaling (FSS) study of the *elusive* tricritical point as well as the associated critical behaviour.

The highly accurate numerical study presented in this chapter has only been possible due to our capability of using different supercomputing facilities simultaneously:

- For the $Q = 4$ case: on the Mare-Nostrum machine of BSC (Barcelona Supercomputing Centre) we used 160 000 computation hours (PowerPC 2.3 GHz processors); on the BIFI (Instituto de Biocomputación y Física de Sistemas Complejos de Zaragoza) cluster we used 250 000 hours (Xeon Dual Core 3.40

[1]The expected exponents β and ν of the tricritical point [101] are: $\beta = \beta_{\rm RFIM}$ and $1/\nu = D - \theta_{\rm RFIM} - \beta_{\rm RFIM}/\nu_{\rm RFIM}$ or (modified hyperscaling relation of the RFIM) $\nu = \nu_{\rm RFIM}/(2 - \alpha_{\rm RFIM} - \beta_{\rm RFIM})$. The surface tension goes to zero with an exponent $\mu = (D-1)\nu$ [102]. Taking the critical exponents of the Gaussian RFIM: $\beta_{\rm RFIM} = 0.00(5)$, $\nu_{\rm RFIM} = 1.1(2)$ and $\theta_{\rm RFIM} = 1.53(1)$ [103], the exponents for the tricritical point should be: $\nu \simeq 1.5$, $\beta \simeq 0$ and $\mu \simeq 3$.

[2]Equilibrium phase-coexistence in a sample of N spins occurs for a temperature interval of width $\sim N^{-1}$ [105], where the specific heat is $C \sim N$. Yet the *sample-averaged* C scales at most as $N^{1/2}$ [106] because the sample dispersion of the critical temperatures leads to the critical region having a width $\sim N^{-1/2}$ around $T_c(p)$. For any fixed temperature within the critical region, only a fraction $\sim N^{-1/2}$ of the samples displays $C \sim N$.

GHz processors); and on computers (mostly Pentium 2.6 GHz) located in the UEX (Universidad de Extremadura) and UCM (Universidad Complutense de Madrid) we used 65 000 and 160 000 hours respectively. As a result we estimate that the computational resources used for this part are equivalent to 60 years of a single last generation (Pentium 2.5 GHz) processor.

- For the $Q = 8$ case: we used mostly the IBERCIVIS infrastructure, see Appendix G, from which we obtained the huge number of approximately 300 years of a single last generation (Pentium 2.5 GHz) processor. In addition we made extensive use of the BIFI cluster, from which we obtained around 40 years of equivalent simulation time. We also used local resources in Badajoz but they can be disregarded compared to the aforementioned enormous numbers.

3.2 Analytical Framework

In this section we briefly review the main analytical results on first-order phase transitions with disorder. They have been taken from Ref. [100], where it was demonstrated that for $D \leq 2$ even the smallest amount of impurities (whether in the bonds or in the fields) destroys the discontinuities of the first derivatives of the free energy making the transition continuous (of second order type), and from Ref. [101] where, after relating the dilute Potts model with the RFIM, it was found that for $D > 2$ there must exist a region in the phase diagram where the transition continues to be of the first order type even in the presence of disorder. This region will end up in a tricritical point.

3.2.1 Aizenman-Wehr Theorem

In Ref. [100], it was demonstrated that for $D \leq 2$ the presence of quenched random fluctuations in the structural parameters (external field h, temperature T, ...) produces the elimination of the first-order character of the phase transitions; in other words, it eliminates the discontinuities in the thermodynamic expectation values of the conjugate quantities (magnetisation if the disorder is in the field, energy if the disorder is in the temperature, etc.).

The problem was solved for the general case of spin variables $\sigma = \{\sigma_x\}$ located on a D-dimensional lattice whose Hamiltonian is the sum of an ordered term (translation-invariant and non-random) and a fluctuating term with quenched randomness, represented in the following by a collection of independent random variables $\{\eta\}$. Some examples of this form are:

1. *Random field (RF) models*

$$H(\sigma) = -\frac{1}{2}\sum_{x,y} J_{x-y}\sigma_x\sigma_y - \sum_x (h_x + \epsilon\eta_x)\sigma_x\,, \tag{3.1}$$

where, in the ferromagnetic RFIM, $\sigma \in \mathbb{Z}^2$ and $J \geq 0$. In the $O(N)$ model, σ_x are N-component unit vectors with a rotation-invariant distribution.

In RF models the spins are subjected to a fluctuating magnetic field composed of two terms: one uniform (h), and the other random, with the order of magnitude of ϵ. We assume that the random fields η_x are independently distributed with a probability measure $\nu(d\eta)$ (with averages denoted by $\mathcal{A}(f) \equiv \int f \nu(d\eta)$) that fulfil:

$$\mathcal{A}(\eta) = 0 \qquad , \qquad \mathcal{A}(\eta^2) > 0 \,, \tag{3.2}$$

and

$$\mathcal{A}(e^{s\eta}) < \infty \qquad , \qquad \forall s < \infty \,. \tag{3.3}$$

2. *Random bond (RB) models*

   For example, the Q-state Potts model, with $\sigma \in \{1, \ldots, Q\}$ and with Hamiltonian with bond disorder

$$H_1(\sigma) = -\frac{1}{2} \sum_{x,y} (J_{x-y} + \epsilon_{x-y} \eta_{x,y}) \delta_{\sigma_x, \sigma_y} \,, \tag{3.4}$$

   or with site disorder

$$H_2(\sigma) = -\frac{1}{2} \sum_{x,y} (1 + \epsilon\eta_x + \epsilon\eta_y) J_{x-y} \delta_{\sigma_x, \sigma_y} = H_0(\sigma) - \sum_x \epsilon\eta_x \sum_y J_{x-y} \delta_{\sigma_x, \sigma_y} \,. \tag{3.5}$$

3. *Spin-glass models*

   For example, the Ising model with Hamiltonian

$$H(\sigma) = -\frac{1}{2} \sum_{|x-y|=1} \eta_{x,y} \sigma_x \sigma_y - \sum_x (h + \epsilon\eta_x) \sigma_x \,. \tag{3.6}$$

In general, all the above models can be unified in a Hamiltonian of the form

$$H(\sigma) = H_0(\sigma) + \sum_a \sum_x (h_a + \epsilon_a \eta_{a,x}) g_a(T_x \sigma) \,, \tag{3.7}$$

where the index a may parameterise pair-interaction terms of a given range or other multiple-spin terms, g_a are bounded functions of the spin configuration, T_x are translation operators (not to be confused with the temperature $T \equiv 1/\beta$), and $\eta_{a,x}$ are a collection of random variables satisfying the conditions (3.2) and (3.3), with an identical distribution within each a class.

The free energy, F, is derived from the finite volume partition function Z_V. By standard thermodynamic arguments, for almost every configuration of the disorder parameters $\{\eta_{a,x}\}$ the limit

$$\lim_{V \to \infty} \frac{T}{V} \log[Z_V(T, \{h\}, \{\epsilon\}, \{\eta\})] = F(T, \{h\}, \{\epsilon\}) \tag{3.8}$$

converges to a non-random function in the Thermodynamic Limit. In other words, the free energy self-averages.

In addition, it is known that the free energy is convex in $\{h\}$, for fixed T and $\{\epsilon\}$, and therefore their directional derivatives exist; any discontinuity of those corresponds to a first-order phase transition. One can define the following order parameter:

$$M_a(T,\{h\},\{\epsilon\}) = \frac{1}{2}\left[\frac{\partial}{\partial(h_a+0)} - \frac{\partial}{\partial(h_a-0)}\right] F(T,\{h\},\{\epsilon\})\,. \tag{3.9}$$

In the case of the ferromagnetic RFIM:

$$M(T,h,\epsilon) = \frac{1}{2}\left[\mathcal{A}(\langle\sigma_0\rangle_+) - \mathcal{A}(\langle\sigma_0\rangle_-)\right]\,, \tag{3.10}$$

where with "+" and "−" we denote the extremal Gibbs states ("pure phases") constructed via choices of the boundary conditions (+ or −).

The following is the main result for the general case, see Ref. [100] for its demonstration:

Theorem. *In a $D \leq 2$ system with quenched disorder, described by a Hamiltonian of the general type of Eq. (3.7) with nearest neighbour interaction (this can be extended to longer range interactions) and with a continuous (non-atomic) probability measure $\nu(d\eta)$ is*

$$M_a(T,\{h\},\{\epsilon\}) = 0 \qquad \forall\ T \geq 0, \{h\}, \{\epsilon\} \text{ and } a \text{ for which } \epsilon_a > 0\,. \tag{3.11}$$

In the disordered Potts case, where the transition is due to a change in temperature, the free energy F is also convex in T for $\{h\}$ and $\{\epsilon\}$ fixed and therefore its partial temperature derivative exists. We can define in this case the latent heat as

$$L = \frac{1}{2}\left(\left.\frac{\partial}{\partial T}\right|_{T_c^+} - \left.\frac{\partial}{\partial T}\right|_{T_c^-}\right) F\,, \tag{3.12}$$

which is the order parameter for this first-order phase transition. In an analogous way it can be demonstrated that $L = 0$ for $D \leq 2$.

3.2.2 Cardy-Jacobsen Theory

The following results are based on a mapping between the Random Bond (RB) model (such as the dilute Potts model) and the Random Field (RF) model (such as the RFIM), see [101]. Firstly we will summarise the main properties of the latter model.

Random Field Ising Model (RFIM)

It is defined by the Hamiltonian

$$H = -J\sum_{i,j} s_i s_j + \sum_i h_i s_i + h\sum_i s_i\,, \tag{3.13}$$

h_i being quenched random variables satisfying $\overline{h_i} = 0$ and $\overline{h_i^2} = \Delta^2$. The pdf of h_i, $p(h_i)$, can be chosen[3] Gaussian or bimodal ($\pm\Delta$).

There are some important general theoretical results concerning this model:

1. Dimensional reduction

   A D-dimensional system with a random field is equivalent to a system with $D-2$ dimensions without the random field [108]. Therefore the lowest critical dimension is $D_c^{\text{inf}} = 3$ because for the pure Ising model it is $D_c^{\text{inf}} = 1$. This result can be obtained by using supersymmetry arguments or through perturbation theories. Nevertheless, dimensional reduction seems to fail specifically for this model [109], although it is a valid result for many other models.

2. Imry-Ma argument

   Starting from $T \backsimeq 0$ in the RFIM and considering that the fundamental low temperature ferromagnetic state is $s_i = +1$, we can analyse what happens if we form a "droplet" with radius R with $s_i = -1$ [110], see Fig. 3.1.

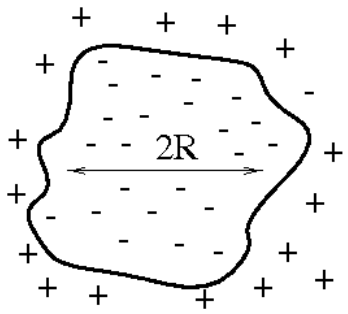

Figure 3.1: "Droplet" with different sign within an almost fully ordered Ising model. We study what is the effect of this perturbation depending on the dimension of the space.

This "droplet" will present an interface with an energy cost

$$\Delta E = JR^{D-1} \sim R^{D-1}\,. \tag{3.14}$$

There is also an energy variation due to the random field within the "droplet"

$$\Delta E_H = \sum_{i \in R} h_i\,, \tag{3.15}$$

which, by the definition of the random field, will fulfil

$$\delta \equiv \sqrt{\overline{\Delta E_H^2}} = \pm (R^D h_{RF}^2)^{1/2} \sim R^{\frac{D}{2}} \quad , \qquad h_{RF}^2 \equiv \Delta^2\,. \tag{3.16}$$

[3] Some controversy exists about the influence of this choice on the universality class of the model, see [107] and references therein.

We can always choose a point in the lattice where $\delta < 0$, so that the energy balance between ΔE and ΔE_H produces the following results depending on the dimensionality of the space:

- For $D > 2$ the fundamental low temperature state is stable. Consequently the low temperature ferromagnetic phase exists and a phase transition at finite temperature can be found.
- For $D < 2$ the fundamental state is not stable and there will exist no phase transition.
- For $D = 2$ we are in the marginal case. In Ref. [111] it was demonstrated that the rugosity of the interface (which is obviously not flat) destabilises the ferromagnetic state, see Fig. 3.2. This result is included in the Aizenman-Wehr theorem.

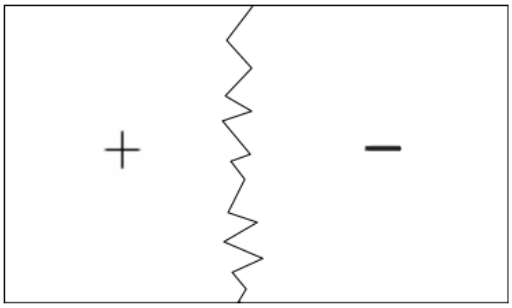

Figure 3.2: Rough interface for a two-dimensional Ising model.

The rugosity of the interface in $D = 2$ produces the energy [111]

$$E = -C\frac{h_{RF}^2}{J} R \log R \,, \tag{3.17}$$

with $C > 0$, which makes the ferromagnetic state unstable. By defining (for $D = 2$)

$$J(L) = JL - C\frac{h_{RF}^2}{J} L \log L = JL(1 - Cw_{RF}^2 \log L) \quad \text{with: } w_{RF}^2 \equiv \frac{h_{RF}^2}{J^2} \,, \tag{3.18}$$

with L being the linear lattice size, we can obtain [109]

$$\frac{dJ(L)}{d\log L} = J(L)(1 - Cw_{RF}^2) + O(w_{RF}^4) \,, \tag{3.19}$$

which is the Renormalization Group (RG) equation for the coupling J. We can easily obtain the remaining RG equations by taking into account that h has dimensions of R^D, h_{RF}^2 has dimensions of R^D, and J has dimensions of R^{D-1}. Therefore it will be to leading order

$$\begin{cases} \dfrac{dh_{RF}}{dl} = \frac{D}{2} h_{RF} \qquad , \qquad l \equiv \log(b)\,, \\ \dfrac{dh}{dl} \;= Dh\,, \\ \dfrac{dJ}{dl} \;= J[(D-1) - Cw_{RF}^2] \longleftarrow \text{(generalising to dimension } D)\,. \end{cases} \tag{3.20}$$

In addition, by definition, $w_{RF} \equiv h_{RF}/J$ and therefore

$$\frac{dw_{RF}}{dl} = -\frac{\epsilon}{2} w_{RF} + Cw_{RF}^3 \;, \quad \text{with:} \quad \epsilon \equiv D - 2\,. \tag{3.21}$$

If $D > 2$ then $\epsilon > 0$ and the RG flow has a non-trivial *random* fixed point (with $w \sim \epsilon^{\frac{1}{2}} \neq 0$) in agreement with [110]. Using these results, the phase diagram for the RFIM can be obtained, see Fig. 3.3.

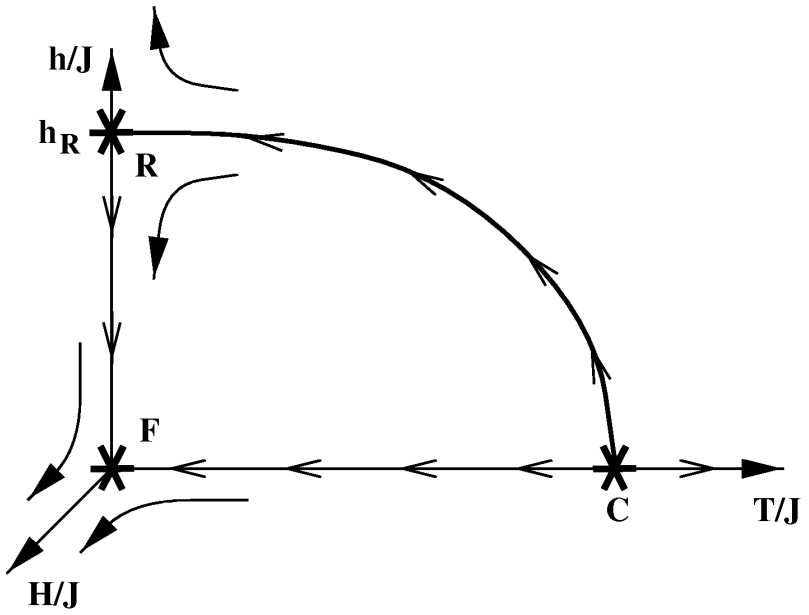

Figure 3.3: RG flows for the RFIM for $D > 2$.

Cardy-Jacobsen mapping

In the case of a pure system undergoing a first-order phase transition there will be coexistence of a (generally unique) disordered phase and the (generally non-unique) ordered phases. The internal energies U_1 and U_2 of these two phases differ by the latent heat. Consider, see Ref. [101], a large (say horizontal) interface between the disordered phase and one of the ordered ones, with surface tension Σ. If $\Sigma \gg 1$,

there will be a really small number of isolated bubbles of the opposite phase above or below the main interface. The free energy of these bubbles is proportional to their areas multiplied by the surface tension.

On the other hand, let us consider an Ising model and build an interface between the two possible ordered phases (all spins taking the values ± 1). At a very low temperature, there will basically exist no "bubbles" above or below the interface and the surface tension will be $\sim 2J$, where J is the reduced coupling of the Hamiltonian. In the limit $\Sigma \sim 2J \gg 1$, these two interface models will be *identical*.

We will analyse the effect of disorder in these two models. In the first one, we introduce random bonds (disorder coupled with the energy) while in the second we introduce a random field (disorder coupled with the magnetisation). The changes in the energy due to the introduction of the disorder are:

1. Random Field:
$$\sum_{r^>} h(r) - \sum_{r^<} h(r)\,, \tag{3.22}$$
where the sums are defined over all the points above ($>$) or below ($<$) the interface.

2. Random bonds
$$U_1 \sum_{r^>} \delta x(r) + U_2 \sum_{r^<} \delta x(r) = \frac{1}{2} L \left(\sum_{r^>} \delta x(r) - \sum_{r^<} \delta x(r) \right) + \text{ const.}\,, \tag{3.23}$$
with $\delta x(r)$ being the local impurities density, $L = U_1 - U_2$ is the latent heat, and the final constant is independent of the interface location[4]. The latter equation has the same form as that corresponding to the random field.

Therefore the thermal variables of the random bond system are related to the magnetic variables of the RFIM by the following mapping:

Random Bond		Random Field
Σ/kT_c	$\Longleftrightarrow$	J/kT
$(L/kT_c)x$	$\Longleftrightarrow$	h_{RF}/kT
$(T-T_c)L$	$\Longleftrightarrow$	HM

(3.24)

[4]The energy can be split in the following way, Δ being the difference between the two sides of Eq. (3.23):

$$\Delta = \frac{1}{2}U_2 \sum_{r^<} \delta x(r) + \frac{1}{2}U_1 \sum_{r^>} \delta x(r) + \frac{1}{2}U_1 \sum_{r^<} \delta x(r) + \frac{1}{2}U_2 \sum_{r^>} \delta x(r) =$$

$$\frac{1}{2}U_1 \left[\sum_{r^<} \delta x(r) + \sum_{r^>} \delta x(r) \right] + \frac{1}{2}U_2 \left[\sum_{r^<} \delta x(r) + \sum_{r^>} \delta x(r) \right] =$$

$$\frac{1}{2}U_1 \sum_{\forall i} \delta x_i + \frac{1}{2}U_2 \sum_{\forall i} \delta x_i$$

which is independent of the interface location.

The last relationship is between the "field" $(T-T_c)$ and a uniform external field H, which helps to distinguish between the two phases (in the same way as $(T-T_c)$). One of the possible problems of this mapping is its use of the local energy density as a kind of order parameter. However it can be made completely explicit, for example for the Q-state Potts model, through the mapping to the random cluster model where $\Sigma \sim L \sim \log Q,\ Q \to \infty$, see Ref. [101].

Explicit relationship with the Potts model

We can now derive [101] the specific relationship of the previous section with the Q-state Potts model with quenched disorder, with Hamiltonian

$$\mathcal{H} = -\sum_{<i,j>} K_{ij}\delta_{s_i s_j}\,, \tag{3.25}$$

where the sum extends only over nearest neighbours. The ferromagnetic couplings K_{ij} are quenched random variables, taking the values K_1 and K_2, each with probability $\frac{1}{2}$; in other words, their pdf is

$$p(K_{ij}) = \frac{1}{2}\delta(K_{ij}-K_1) - \frac{1}{2}\delta(K_{ij}-K_2)\,. \tag{3.26}$$

When $(e^{K_1}-1)(e^{K_2}-1)=1$ this model is, on average, self-dual, and, if the transition is unique, is at its critical point [112]. It is useful to parameterise the model through

$$u_{ij} = (e^{K_{ij}}-1) = Q^{\frac{1}{2}+w_{ij}}\,, \tag{3.27}$$

with $w_{ij} = \pm w$. $w \geq 0$ measures the strength of the randomness, with $w=0$ being the case without disorder. We can solve for K_{ij}

$$K_{ij} = \log(1+Q^{\frac{1}{2}+w_{ij}})\,, \tag{3.28}$$

and consider the limit $Q \to \infty$ to approximate

$$K_{ij} = \log(1+Q^{\frac{1}{2}+w_{ij}}) \simeq \log(Q^{\frac{1}{2}+w_{ij}}) = \left(\frac{1}{2}+w_{ij}\right)\log Q\,. \tag{3.29}$$

By substituting in the Hamiltonian we obtain

$$\mathcal{H} = -\frac{1}{2}\log Q \sum_{<i,j>}\delta_{s_i s_j} - \log Q \sum_{<i,j>} w_{ij}\delta_{s_i s_j}\,, \tag{3.30}$$

where the first term corresponds to an ordered model while the second term corresponds to a disordered one. Therefore the term added to the pure model is

$$\mathcal{H}_{\text{added}} \sim \sum_{<i,j>} w_{ij}\log Q\ \delta_{s_i s_j}\,. \tag{3.31}$$

We will work in the following in two dimensions; i.e. the label i identifying the lattice sites means $i \equiv (x,y)$, with (x,y) being Cartesian coordinates. Using the

same arguments as in the previous section, if an interface divides the space into two parts, denoted by ">" and "<", then

$$\mathcal{H}_{\text{added}} \sim \sum_{>} w \log Q + \sum_{<} w \log Q \,, \tag{3.32}$$

noting that within each of these two homogeneous regions $\delta_{s_i s_j} = 1$. Each of the two terms of Eq. (3.32) is

$$\sum_{<} w \log Q = \frac{1}{2}\left(\sum_{>} + \sum_{<}\right) + \frac{1}{2}\left(\sum_{<} - \sum_{>}\right) \,, \tag{3.33}$$

but, as in the previous section, the term $(\sum_{>} + \sum_{<})$ does not depend on the interface position and as a consequence

$$\frac{1}{2}\left(\sum_{>} - \sum_{<}\right) w \log Q \tag{3.34}$$

is an analogue of the random field term of Eq. (3.22). Therefore we obtain the relationship

$$h_{RF} \longleftrightarrow \frac{1}{2} w \log Q \,. \tag{3.35}$$

In addition, following Ref. [82], when $Q \to \infty$, the surface tension is:

$$\Sigma \sim \frac{1}{4} \log Q \,. \tag{3.36}$$

But as was seen in Sec. 3.2.2 for the RFIM $\Sigma \sim 2J$, and therefore we have the relation

$$J \longleftrightarrow \frac{1}{8} \log Q \,. \tag{3.37}$$

Finally, while a uniform field in the RF model distinguishes between the two phases, in the RB model this is the task of the reduced temperature $t \equiv \frac{T - T_c}{T}$; provided that t is coupled to the energy density we can make the identification

$$h \longleftrightarrow \frac{1}{4} t \log Q \,. \tag{3.38}$$

To summarise, the mapping between the Potts model and the RFIM is:

RFIM		Q-state Potts model
J	$\Longleftrightarrow$	$\frac{1}{8} \log Q$
h	$\Longleftrightarrow$	$\frac{1}{4} t \log Q$
h_{RF}	$\Longleftrightarrow$	$\frac{1}{2} w \log Q$

(3.39)

We can use this mapping to derive the RG equations for the Potts model starting from those for the RFIM [109], see Eq. (3.20). We will denote for the sake of clarity

the w used in Eq. (3.35) as $w_{RB} \equiv w$, to distinguish between this w_{RB} and the w_{RF} defined in Eq. (3.18). Therefore from Eqs. (3.35) and (3.37) one obtains

$$w_{RB} = \frac{2h_{RF}}{\log Q} = \frac{h_{RF}}{4J} \,. \tag{3.40}$$

But $w_{RF} = h_{RF}/J$, hence

$$w_{RB} = \frac{1}{4} w_{RF} \,, \tag{3.41}$$

and therefore the RG equation for w_{RF} is also valid for w_{RB}, i.e.,

$$\frac{dw_{RB}}{dl} = -\frac{\epsilon}{2} w_{RB} + A w_{RB}^3 \quad , \quad \text{with:} \quad \epsilon \equiv D - 2 \quad , \quad l \equiv \log(b) \,. \tag{3.42}$$

From the last RG equation of Eq. (3.20) and from Eq. (3.37), one easily derives the RG relation

$$\frac{d(\log Q)^{-1}}{dl} = -(\log Q)^{-1}[(D-1) - A w_{RB}^2] \,. \tag{3.43}$$

Finally, using again Eq. (3.20) and Eq. (3.38), one obtains:

$$\frac{dt}{dl} = t(1 + A w_{RB}^2) \,. \tag{3.44}$$

Summarising, the set of RG equations for the Q-state Potts model with quenched disorder is:

$$\begin{cases} \dfrac{dw_{RB}}{dl} = -\frac{\epsilon}{2} w_{RB} + A w_{RB}^3 \quad , \quad \text{with} \quad \epsilon \equiv D - 2 \quad , \quad l \equiv \log(b) \,, \\ \dfrac{dt}{dl} = t(1 + A w_{RB}^2) \,, \\ \dfrac{d(\log Q)^{-1}}{dl} = -(\log Q)^{-1}[\epsilon + 1 - A w_{RB}^2] \,. \end{cases} \tag{3.45}$$

We can now analyse the stability of the fixed points of the RG transformations to trace the phase diagram of the model. To simplify we make the change

$$\hat{Q} \equiv \frac{1}{\log Q} \,. \tag{3.46}$$

Then the fixed points of the RG transformation are the Gaussian one:

$$\hat{Q} = t = w_{RB} = 0 \,, \tag{3.47}$$

and the tricritical one:

$$\hat{Q} = t = 0 \quad , \quad w_{RB} = \sqrt{\frac{\epsilon}{2A}} \,. \tag{3.48}$$

The Jacobian matrix for the transformation is

$$J = \begin{pmatrix} -\frac{\epsilon}{2} + 3Aw_{RB}^2 & 0 & 0 \\ 2Atw_{RB} & 1 + Aw_{RB}^2 & 0 \\ 2A\hat{Q}w_{RB} & 0 & -(\epsilon + 1 - Aw_{RB}^2) \end{pmatrix}$$

which evaluated at the Gaussian point is

$$J|_{\text{Gauss}} = \begin{pmatrix} -\frac{\epsilon}{2} & 0 & 0 \\ 0 & 1 & 0 \\ 0 & 0 & -(\epsilon + 1) \end{pmatrix}$$

resulting in that at the Gaussian fixed point the "fields" w_{RB} and Q are irrelevant while t is relevant. At the tricritical (TC) point, the Jacobian will be

$$J|_{TC} = \begin{pmatrix} \epsilon & 0 & 0 \\ 0 & 1 + \frac{\epsilon}{2} & 0 \\ 0 & 0 & -(1 + \frac{\epsilon}{2}) \end{pmatrix}$$

and therefore w_{RB} and t are relevant "fields" while Q is irrelevant. For $D > 2$ the eigenvalues are

$$\begin{aligned} y_w = \epsilon > 0 \quad &\Longrightarrow \quad \text{Relevant} \\ y_t = 1 + \frac{\epsilon}{2} \quad &\Longrightarrow \quad \text{Relevant} \\ y_Q = -\left(1 + \frac{\epsilon}{2}\right) \quad &\Longrightarrow \quad \text{Irrelevant} \end{aligned}$$

The (Q, w) plane of the phase diagram is depicted in Fig. (3.4). In the pure system, for $Q > Q_2$ there is a phase transition with non-vanishing latent heat controlled by a fixed point at infinite Q. For $D > 2$ it will continue into the shaded region bounded by a line of tricritical points whose exponents are related to those of the RFIM [101]. It also may be shown that the latent heat vanishes as $(w_c - w)^{\beta_{\text{RF}}}$ as the line RQ_2 is approached from below. Let us note also that $Q = 1$ corresponds to the percolation model, where the disorder is irrelevant ($\alpha \approx -0.64$), while $Q = 2$ corresponds to an Ising model, where the phase transition is always of second order but the disorder is relevant ($\alpha \approx 0.1118$). Therefore there exists a Q_1, with $1 < Q_1 < 2$, at which the sign of α changes. In addition, for $Q > Q_2 = 2 + \epsilon$ the transition becomes first order.

Above the line RQ_2, as w grows the RG equations lose validity. In addition the surface tension goes to zero and the mapping between the two models disappears. Nevertheless, for $Q \to \infty$ the mapping remains exact and the flow goes to infinite w. But this can not happen for finite Q because this is the percolation limit $K_1/K_2 = 0$, at which the disorder is relevant [113]. Therefore there should exist [101] another line of stable fixed points emerging from P_1, which control the universal continuous transition for large, but finite, values of w and Q.

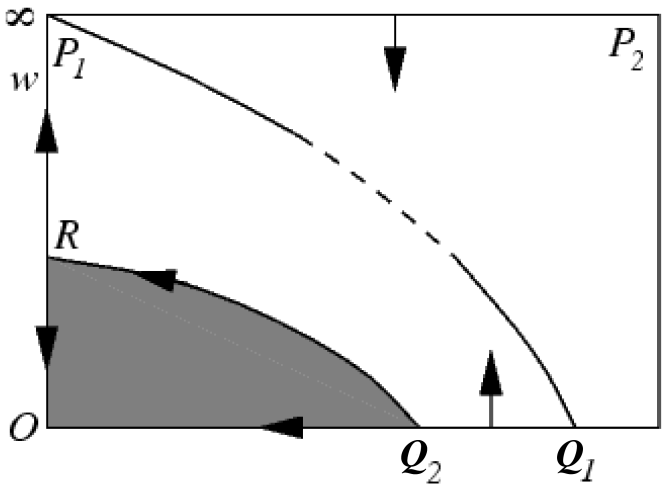

Figure 3.4: Phase diagram of the dilute Potts model with Q states for $D > 2$, obtained in Ref. [101]. Q grows towards the left; w is a measure of the disorder strength, $w = 0$ being the pure case. The latent heat do not vanishes within the shaded region while outside the transition is continuous. P_1 and P_2 are the percolation thresholds.

3.3 The Model

In the three-dimensional site-diluted Q-state Potts model [82] the spins, σ_i, take the values $\sigma_i = 1, \ldots, Q$ and are defined at the nodes of a cubic lattice with probability p. We consider only nearest neighbour interaction and periodic boundary conditions. Therefore the Hamiltonian takes the form:

$$\mathcal{H}^{\text{spin}} = -\sum_{\langle i,j \rangle} \epsilon_i \epsilon_j \delta_{\sigma_i \sigma_j} \,, \tag{3.49}$$

with ϵ_i being quenched occupation variables ($\epsilon_i = 0$ or 1 with probability $1 - p$ and p respectively)[5], and $\langle i, j \rangle$ denoting nearest neighbours. Each one of the specific disorder realizations ($\{\epsilon\}$ spatial distribution) is called a *sample*. The pure system is recovered for $p = 1$, and is known to undergo a first-order phase transition for $Q \geq 3$ [13, 46] generally regarded as *very strong*.

A valid order parameter for the model is the magnetisation density (a Q-dimensional vector) defined as

$$M_q = \frac{1}{V} \sum_i \epsilon_i \left[\frac{Q\delta_{\sigma_i,q} - 1}{\sqrt{Q(Q-1)}} \right] \,, \tag{3.50}$$

[5]To reduce statistical fluctuations, we kept only the spins in the percolating cluster [114] that control the critical behaviour. However, in the most interesting region ($p \gtrsim 0.9$) this correction is quite small.

with $V = L^3$ being the volume and L the linear size of the system. We can define the magnetic susceptibility as

$$\chi = V|M|^2 \,. \tag{3.51}$$

A well-behaved definition for the correlation length in a finite system is obtained from the correlation function as [7]

$$\xi \equiv \left(\frac{\overline{\chi}/\overline{F} - 1}{4\sin^2(\pi/L)} \right)^{\frac{1}{2}} \,, \tag{3.52}$$

where

$$\overline{F} \equiv \frac{V}{3} \overline{\langle |F(2\pi/L,0,0)|^2 + |F(0,2\pi/L,0)|^2 + |F(0,0,2\pi/L)|^2 \rangle} \,, \tag{3.53}$$

and where we denote the thermal averages with brackets while the sample average is overlined. In addition

$$F(\boldsymbol{k}) \equiv \frac{1}{V} \sum_{\boldsymbol{r}} e^{\mathrm{i}\boldsymbol{k}\cdot\boldsymbol{r}} \epsilon_{\boldsymbol{r}} \sigma_{\boldsymbol{r}} \,. \tag{3.54}$$

In this work we use the microcanonical simulation method defined in Ref. [13], see also Sec. 2.2.2, so that, by using the Maxwell construction, see Appendix E, we can directly obtain some quantities characteristic of the phase transition. Firstly the critical temperature is fixed by the definition of the Maxwell construction: the e-integral of $\beta_{\{\epsilon\}}(e) - 1/T_{\mathrm{c}}$ from e_{d} to e_{o} must vanish, where e is the energy density and $\beta_{\{\epsilon\}}(e)$ was defined in Eq. (2.58). This fact also implies that

$$s_{\mathrm{d}} - s_{\mathrm{o}} = (e_{\mathrm{d}} - e_{\mathrm{o}})/T_{\mathrm{c}} \,, \tag{3.55}$$

s being the entropy density. The latent heat is defined directly as

$$\Delta e = e_{\mathrm{d}} - e_{\mathrm{o}} \,. \tag{3.56}$$

Finally the surface-tension, Σ, is $L^2/2$ times the integral of the positive part of $\beta_{\{\epsilon\}}(e) - 1/T_{\mathrm{c}}$, see Ref. [13].

3.4 Numerical Results

We have studied numerically two cases of the three-dimensional site-diluted Potts model: the four-state ($Q=4$) and the eight-state ($Q=8$) cases. Both cases undergo a well-known [82] strong first-order phase transition in the pure case; the strength of the first-order character of the phase transition will grow with Q. In both cases a softening of the discontinuities of the first derivatives of the free energy is expected to appear with increasing dilution. The critical concentration, p_c, at which the character of the phase transition switches to second order will depend on Q, being smaller for increasing Q.

3.4.1 Methods

Simulation method

To update the Potts spins of our systems, we used a microcanonical version [13] of the Swendsen-Wang (SW) [11] cluster method. For disordered systems, SW updates loosely connected regions properly [51] and does not require tedious parameter tuning. The microcanonical cluster method, which is not rejection-free, depends on a tunable parameter, κ. In order to maximise the acceptance of the SW attempt (SWA), κ should be chosen as close as possible to $\beta_{\{\epsilon\}}(e)$. After every e change, we performed cycles consisting of 10^3 Metropolis steps, a κ refresh, then 10^3 SWAs, and a new κ refresh. The cycling was stopped, and κ fixed, when the SWA acceptance exceeded 60%. We then performed a number of SWAs depending on the lattice size, taking measurements every 2 SWAs.

For $Q = 4$ we performed thermalization checks that included comparisons of hot and cold starts or even mixed configurations (bands and strips [13]). We checked that the Maxwell construction obtained for the pure case of the largest system ($L = 128$) does not depend on the initial configuration, after discarding a part of the initial Monte Carlo history.

In the $Q = 8$ case, reaching the thermodynamic equilibrium is a far more complicated task, especially on the first-order side of the phase diagram. For a first-order phase transition, it is known that metastable states do exist. These states can have a very long life even when they are not the true equilibrated states. This is most dramatic for large systems in which the simulation times are intrinsically longer. Therefore the thermalization issue in this case deserves a special treatment that will be described in Sec. 3.4.3.

Sample averaging methods

For a disordered system, one has to analyse a set of functions $\beta_{\{\epsilon\}}(e)$ corresponding to a large enough number of samples. There are two natural possibilities. On the one hand, one can use the Maxwell construction for each sample extracting T_c, e_d, e_o and Σ, and then considering their sample average, median, or even their pdf, see Fig. 3.6. This is the most usual approach.

On the other hand, one can compute the sample average of the (inverse) temperature defined at each simulation energy, e, $\beta(e) = \overline{\beta_{\{\epsilon\}}(e)}$, and then perform the Maxwell construction on it (i.e., take the sample average of $s(e)$, rather than the sample average of the free energy at fixed T).

We found empirically that the two sample averagings are equivalent in the first-order piece of the critical line. This is hardly surprising, because the internal energy as a function of T is a self-averaging quantity, for all temperatures but the critical one. Therefore, also e_d, e_o, and T_c are self-averaging properties in the first-order part of the critical line.

While the first method offers more information, it is computationally more demanding (it requires high accuracy for each sample). The method featuring $\beta(e)$

can be used as well in the second-order part of the critical line, but its merit in that region is yet to be investigated.

3.4.2 $D = 3$, $Q = 4$ Site-Diluted Potts Model

For $Q = 4$ we investigated the phase transition for several p values in the range $0.75 \leq p \leq 1$. As a rule, we found that at fixed p the latent heat is a monotonically decreasing function of L, see Fig. 3.7. For each p value, we simulated $L = 16$, 32, 64, and 128 (for a given p, we did not consider larger lattices once the latent heat vanished). For all pairs (p, L) we simulated 128 samples. Also, some intermediate p values were added for the FSS study, see Fig. 3.8, and we raised to 512 the number of samples for ($L = 16$ and 32, $p = 0.86$ and 0.875).

General behaviour

Following the procedure of Sec. 3.4.1 we performed sample averages of the Maxwell constructions for each L and p. In Fig. 3.5 one can see the general behaviour of the Maxwell constructions as the spin concentration, p, varies: while for large p ($p \approx 0.95$) we can form the Maxwell construction for every system size, it softens with decreasing p up to a point, p_c, at which both latent heat and surface tension vanish. This p_c depends on the system size.

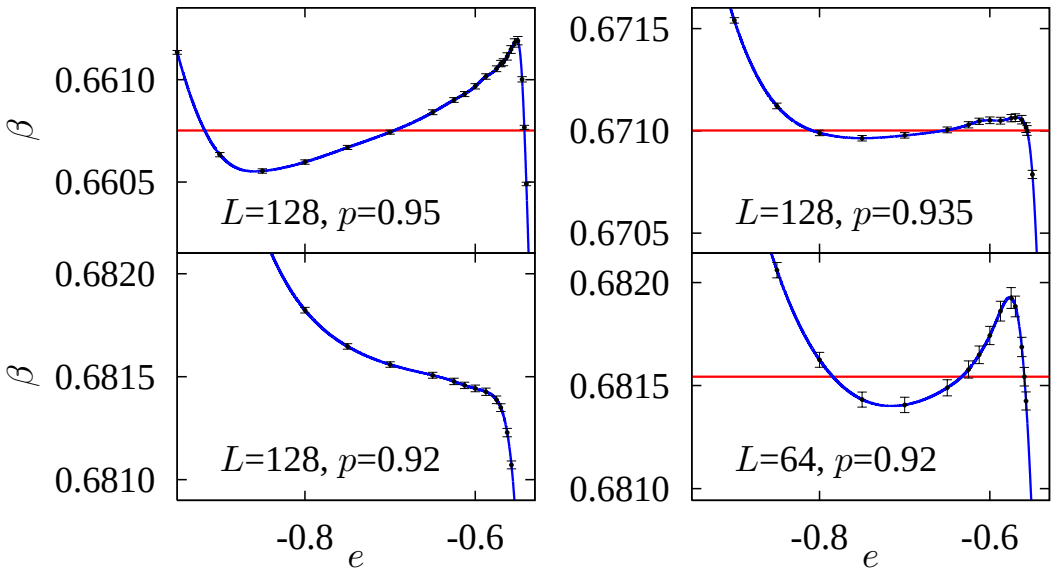

Figure 3.5: Sample-averaged e-derivative of the entropy, $\beta(e)$, for several lattice sizes, L, and spin concentrations, p. Metastability requires a non-decreasing $\beta(e)$. The horizontal line marks the critical (inverse) temperature $1/T_c$, obtained through Maxwell construction. At fixed L the surface tension increases for increasing p. Note that, for a fixed dilution, a seemingly first-order transition ($L = 64$, bottom-right), may actually be of second order if studied on larger lattices ($L = 128$, bottom-left).

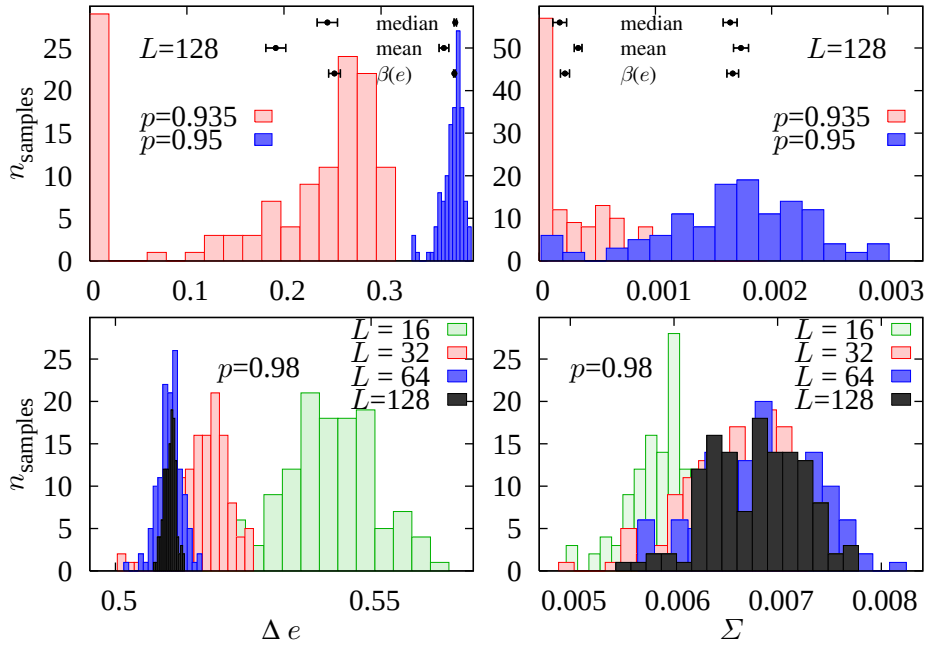

Figure 3.6: Histograms for the sample-dependent latent heat $\Delta_{\{\epsilon\}}e = e_{\rm d} - e_{\rm o}$ (**left**) and surface tension, Σ(**right**). In the top panels we show results in the largest lattice, where two very close spin concentrations behave very differently. The three types of horizontal lines drawn (indicating central value and statistical error) correspond, from top to bottom, to the median, the mean, and the value obtained from $\beta(e)$. In the lower panels we show the histograms for $p = 0.98$ and different L's (note the difference in the horizontal scales with the upper part). As can be seen, the latent heat is self-averaging while the surface tension is not.

As was said before, for each sample we can define the different thermal-averaged quantities, and then determine their mean, median, or pdf. We can also compute the sample-average $\beta(e) = \overline{\beta_{\{\epsilon\}}(e)}$, and then perform the Maxwell construction on it. We compared the two approaches for this model both for the latent heat and for the surface tension, see Fig. 3.6. We found that the two approaches are equivalent, although the second one requires less statistical accuracy for each sample and is therefore less numerically demanding. Also from Fig. 3.6 (top row) we can see that as the dilution is slightly decreased (the tricritical point is reached), a great number of samples present vanishing latent heat and surface tension; the transition has become continuous. Finally we found that within the first-order part of the phase diagram ($p = 0.98$) the width of the histograms of the latent heat decreases as the lattice size increases; this is the definition of a self-averaging quantity. On the contrary, we can not see this behaviour for the surface tension and therefore we can state that it is not self-averaging.

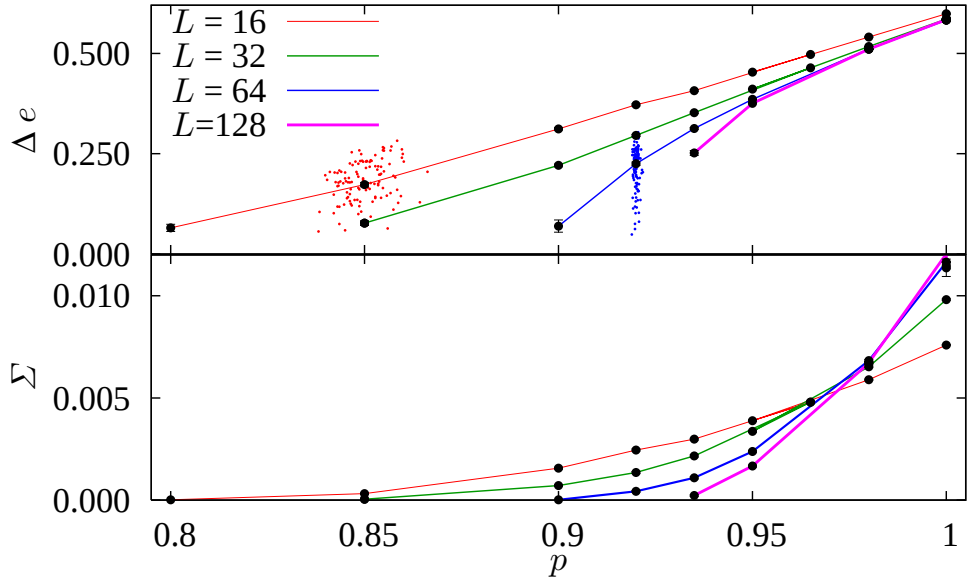

Figure 3.7: **Top:** Latent heat as obtained from $\beta(e)$ as a function of spin concentration for several lattice sizes (lines are linear interpolations). Data for $p = 1$ and $L = 128$ were taken from Ref. [13]. To illustrate the sample dispersion, we also show the scatter-plot of $(N/L^D, \Delta_{\{\epsilon\}}e)$ for the 128 samples at $L = 16$ $p = 0.85$ and $L = 64$ $p = 0.92$. **Bottom:** As the top panel, but for the surface tension.

Latent heat and surface tension

Our results for the behaviour of the latent heat and the surface tension obtained from $\beta(e)$ as the dilution changes are shown in Fig. 3.7. The apparent location of the tricritical point (i.e., the p where both Δe and Σ vanish) shifts to higher p for increasing L rather fast. For lattice sizes comparable with those of previous work [46], $L = 16$, we obtain a sizeable value $p_c^{L=16} \approx 0.75$, but the estimate of p_c increases very rapidly with L. An extrapolation to $L \to \infty$ is called for.

The pdf's for Δe and Σ, Fig. 3.6, display an interesting L evolution. When the $\beta(e)$ changes behaviour from non-monotonic ($L = 64$, Fig. 3.5, bottom-right) to monotonic ($L = 128$, Fig. 3.5, bottom-left), the two pdf's becomes enormously wide[6], see the top panels in Fig 3.6. This arises because for many $L = 128$ samples the curve $\beta_{\{\epsilon\}}(e)$ is becoming flat, or even monotonically decreasing (i.e., $\Delta e = \Sigma = 0$), while no such behaviour was seen for $L = 64$. Only for $p = 0.98$ does the width of the pdf's for Δe scale as $L^{-D/2}$, as expected for a self-averaging quantity, see Fig. 3.6 – bottom-left. The surface-tension is *not* self-averaging, see Fig. 3.6 – bottom-right.

Finite Size Scaling study

From Figs. 3.5, 3.6, and 3.7 one cannot rule out that $p_c \neq 1$: a disordered first-order transition would not exist. Fortunately we can solve this dilemma by consider-

[6]The estimates for Δe and Σ are consistent with the *median* of their (non-Gaussian) pdf's.

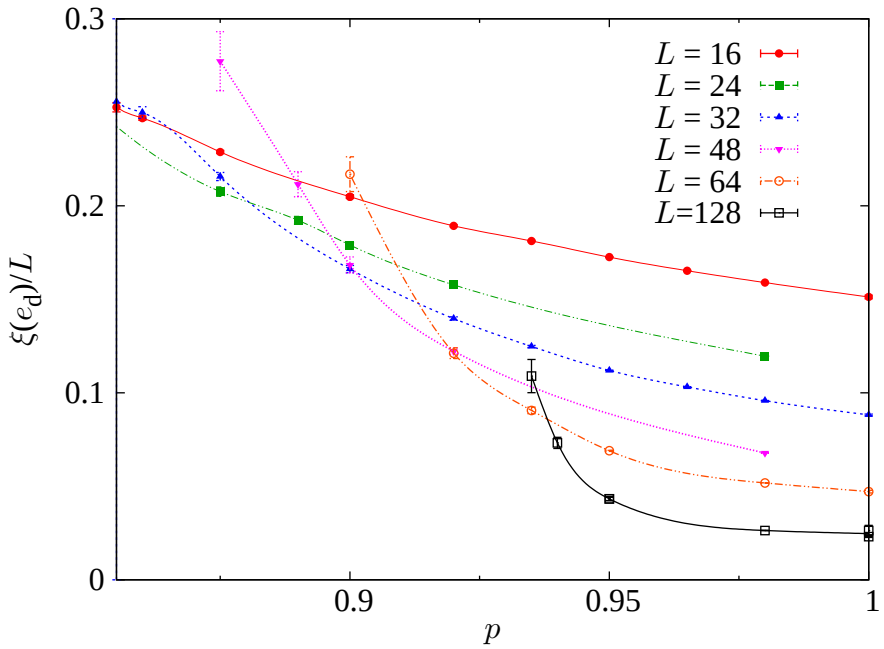

Figure 3.8: Correlation length in units of the lattice size in the $Q = 4$ case, at phase coexistence for the paramagnetic phases, e_d, as a function of concentration, p, for several system sizes, L (lines are cubic spline interpolations for data at fixed L).

ing the correlation length, obtained from the *sample-averaged* correlation function, Eq. (3.52).

We take the correlation length in units of the lattice size at e_d (see Fig. 3.8), and e_o (see Fig. 3.9), as obtained from $\beta(e)$ (a jack-knife method [7] takes care of the statistical correlations). For all $p < p_c$, one expects that both $\xi(e_d)/L$ and $\xi(e_o)/L$ tend to non-vanishing and different limits for large L[7]. For $p > p_c$, $\xi(e_d)/L$ is of order $1/L$, while $\xi(e_o)/L \sim L^{D/2}$. For a fixed L, with increasing p, the behaviour goes from a second-order type to first-order (see Fig 3.5). Hence, a FSS approach [7] is needed.

Consider the curves of $\xi(e_d)/L$ versus p for different L, see Fig. 3.8. There is a unique concentration, $p^{L,2L}$, where the correlation lengths in units of the lattice size coincide for pairs of lattices of sizes L and $2L$. One has [8]

$$p^{L,2L} \approx p_c + A_d L^{-x} \,. \tag{3.57}$$

An exactly analogous result holds for $\xi(e_o)/L$, see Fig. 3.9. Since A_d and A_o are quite different, see Fig. 3.10, a combined fit of all the data yields an accurate estimate of

[7] We have checked numerically that this is indeed the case for the $D = 2$, $Q = 4$, pure Potts model (a prototypical example of a second-order phase transition with a double-peaked canonical pdf for e at T_c), see Sec. 2.4.3.

[8] The tricritical point has no basin of attraction for the RG flow in the (T, p) plane. Although two relevant scaling fields are to be expected, the Maxwell construction allows us to eliminate one of them and hence we use the formulae for a standard critical point.

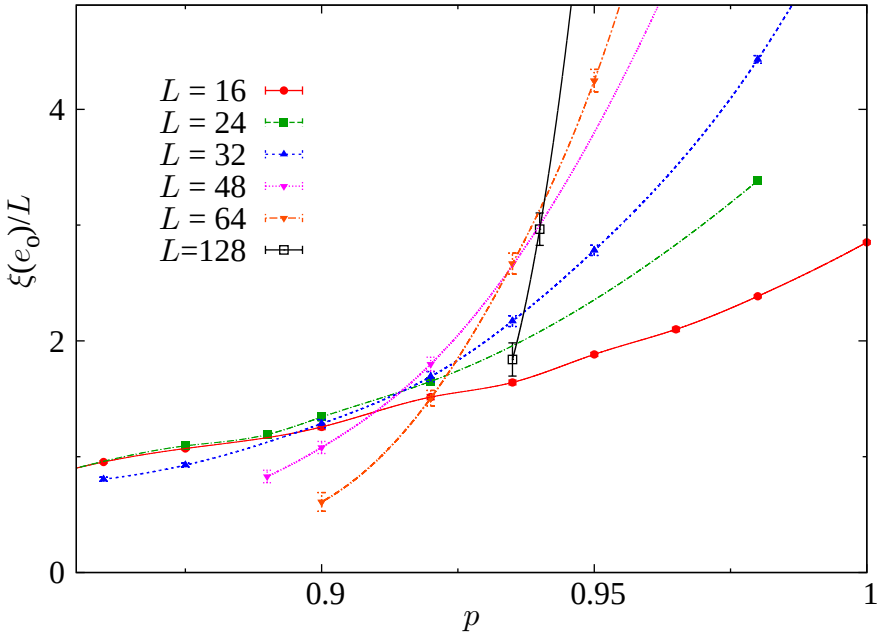

Figure 3.9: Correlation length in units of the lattice size in the $Q = 4$ case, at phase coexistence for the ferromagnetic phases, e_o, as a function of concentration, p, for several system sizes, L.

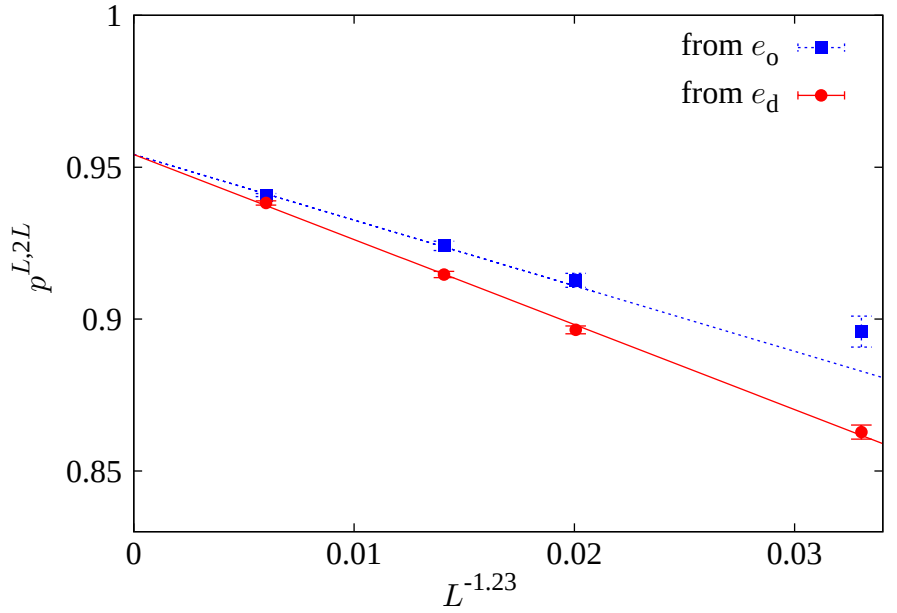

Figure 3.10: Spin concentration where the values of ξ/L (data from Figs. 3.8 and 3.9) coincide for lattices L and $2L$ versus $1/L^x$, see Eqs. (3.57) and (3.58). Lines are a combined fit for x, p_c, A_d, and A_o.

the location of the tricritical point:

$$p_{\rm c} = 0.954(3), \quad x = 1.23(9), \quad \frac{\chi^2}{\text{d.o.f.}} = \frac{4.23}{3}, \quad \text{C.L.} = 24\% \,. \tag{3.58}$$

Of course, due to higher-order scaling corrections, Eq. (3.57) should be used only for lattices larger than some $L^{\rm min}$ [70]. The fit χ^2 was acceptable taking $L_{\rm d}^{\rm min} = 12$ and $L_{\rm o}^{\rm min} = 16$ (for the sake of clarity we do not display data for $L = 12$ in the figures). Therefore we can conclude that $p = 0.98$ is definitively in the first-order part of the critical line.

We now look at ξ/L at $p^{L,2L}$, see Figs. 3.8 and 3.9. Consider $\xi(e_{\rm d})/L$ as a function of (L, p), see Fig. 3.11. Its salient features are:

1. For fixed L, $\xi(e_{\rm d})/L$ is a decreasing function of p (while $\xi(e_{\rm o})/L$ is increasing).

2. For fixed p, $\xi(e_{\rm d})/L$ has a minimum (while $\xi(e_{\rm o})/L$ has a maximum) at a crossover length scale, $L_{\rm cr}(p)$, that separates the first-order type of behaviour from the second-order type, see Figs. 3.8 and 3.9.

3. At the crossing point $p^{L,2L}$ we have $L < L_{\rm cr}(p^{L,2L}) < 2L$.

4. At least within the range of our simulations, $L_{\rm cr}(p)$ is an increasing function of p.

A standard scaling argument, combined with (1–4), yields that $\xi(e_{\rm d})/L$ at $p^{L,2L}$ is of order $1/L_{\rm cr}(p^{L,2L})$ ($\xi(e_{\rm o})/L \sim L_{\rm cr}^{D/2}$). If $L_{\rm cr}(p)$ diverges at $p_{\rm c}$, $\xi(e_{\rm d})/L$ at $p^{L,2L}$ should tend to zero for large L, which is indeed consistent with our data.

3.4.3 $D = 3$, $Q = 8$ Site-Diluted Potts Model

We also present in this chapter some of the preliminary results of our study of the eight-state ($Q = 8$) site-diluted Potts model using basically the same methodological approach as in the $Q = 4$ case. First, however, it has to be stressed that there are two important differences in this case:

- We used chiefly another kind of computing platform. While the $Q = 4$ case was entirely simulated on typical cluster facilities, i.e., the BSC and BIFI, the $Q = 8$ case case was simulated on IBERCIVIS, a distributed computing platform based on BOINC, see Appendix G. This change in platform involved both advantages and disadvantages. By using IBERCIVIS, we were able to outperform broadly all previous statistical accuracies both in the number of samples (we were able to simulate up to 2000 samples of a system with 64^3 spins) and in the number of dilution levels (around ten for each system size). In addition, we did more than 3×10^6 Swendsen-Wang steps at each energy of a system with 64^3 spins. In particular, with IBERCIVIS we obtained more than 300 years of computation time in less than a year of wall clock time. This would have been hard to achieve using a traditional cluster facility.

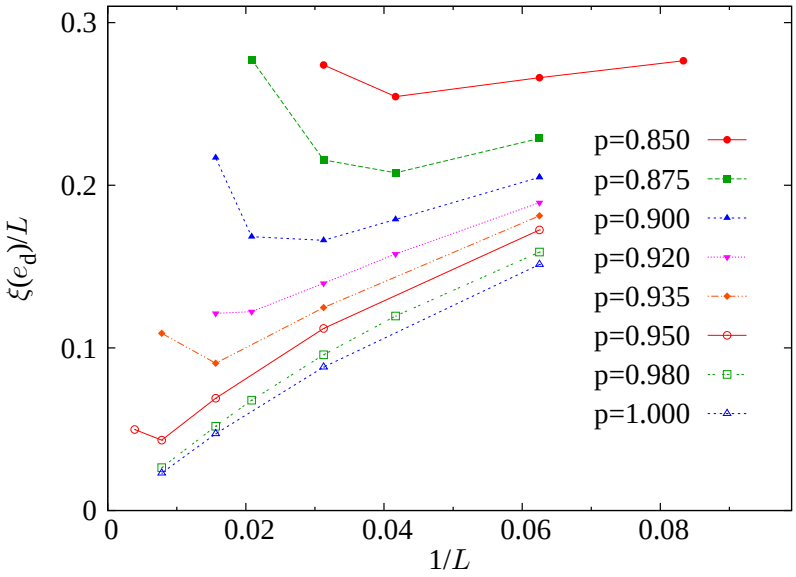

Figure 3.11: Correlation length at e_d in units of the lattice size, for fixed dilutions as a function of the inverse lattice size. For fixed $p < p_c$, $\xi(e_d)/L$ has a minimum at a crossover length scale, $L_{cr}(p)$, that separates the first-order type of behaviour from the second-order type.

On the other hand, the use of IBERCIVIS, a novel infrastructure, led to numerous unusual problems in the adaptation and stabilisation of the original code to the new computing paradigm, see again Appendix G. The huge output of the computations has to be carefully analysed, and a major effort must be made to identify all the possible error sources. For example, the connection of the individual parts of each BOINC job is an extremely delicate issue, and the development of a secure mechanism for the detection of corrupted outputs is fundamental.

- It is known that the pure Potts model undergoes a first-order phase transition for $Q > 2$ in three dimensions [82], with the strength of the first-order character being larger as Q grows. Therefore the $Q = 8$ case will show more evidently the features of this kind of transition (i.e., latent heat, metastabilities, phase coexistence, etc.). This fact has pros and cons. The main benefit is that if we want to see a first-order phase transition in the presence of disorder, the first-order region in the phase diagram is expected to be larger for $Q = 8$ than for $Q = 4$, in other words p_c will be smaller. This will mean stronger evidence for the main result of this chapter – first-order phase transitions do exist in the presence of disorder in three-dimensional systems.

  On the contrary, the stronger first-order character of the transition produces much more palpable metastability effects. This is a huge problem in Monte Carlo simulations, because exponential autocorrelation times will grow sub-

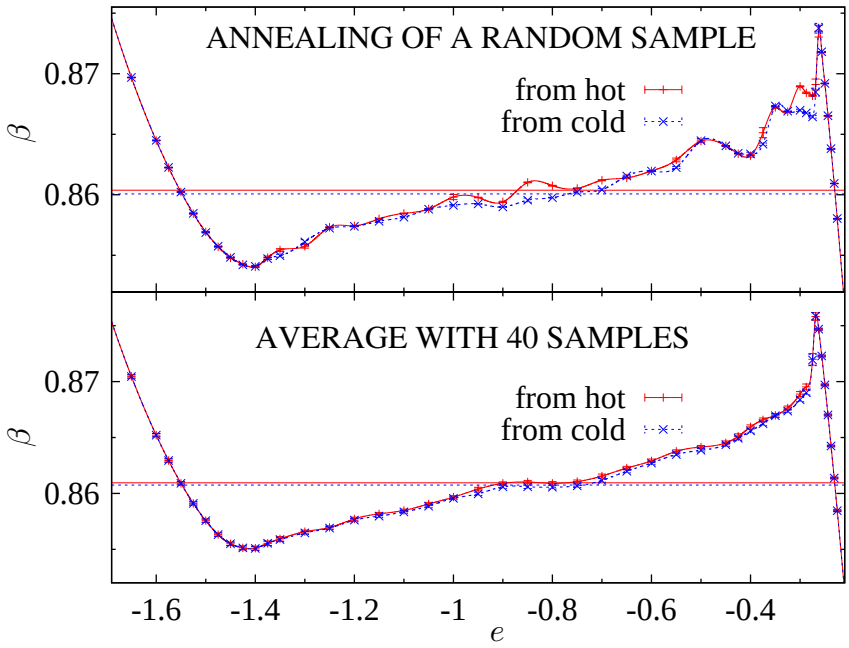

Figure 3.12: Comparison of the different "energy walks" for the system with $L = 48$ and $p = 0.95$. The upper part correspond to the Maxwell construction of a random sample. Note the clear difference between the walk starting from hot (red solid line) and cold (blue dashed line). The lower part shows the softening of the difference as the sample average (with 40 samples) is performed. Horizontal lines mark the corresponding estimates of β_c.

stantially, see Appendix C and Ref. [115], making thermalization really hard to achieve for large systems at given values of their internal energy. This fact restricted us to thermalizing systems with "only" 64^3 spins on the first-order side of the phase diagram, compared with the $Q = 4$ case for which we were able to thermalize systems with up to 128^3 spins. Anyway we plan to study the first-order side of the transition by making estimates of the errors due to not having reached the asymptotic states of the system.

For $Q = 8$ we simulated the model for p values in the range $0.65 \leq p \leq 1$. For each p value, we simulated $L = 12$, 16, 24, 32, 48, 64, and 96 (for a given p, we did not consider larger lattices once the latent heat vanished). Finally, we disregarded our simulations for $L = 96$ because of the impossibility of thermalization in a reasonable time. For all pairs (p, L) we simulated at least 500 samples.

To check the thermalization of the systems we compared simulations of the same samples (distribution of the vacancies), performing annealings starting from both random configurations at high temperatures and cold (all the spins in the same state) configurations at low temperatures. As we performed our "energy walk" we found that for energies corresponding to pure states (with no "islands" of the other phase) both annealings will agree fully. However, between e_o and e_d there will exist some

energies where the two annealings will produce different estimates of the observables (especially for the largest lattices). These energies are precisely those at which the system switches between the different configurations of the "islands", for example from a "droplet" to a "strip". In the case that the thermal averages of the different observables from the two annealings were similar, we would be fairly confident of the equilibration of the system. If they were not, we could at least estimate the error due to the lack of thermalization from their difference.

In Fig. 3.12 we plot the comparison of the annealings of the system with 48^3 spins and $p = 0.95$. The system is clearly undergoing a first-order phase transition. The simulation of *each sample* used in Fig. 3.12 took around three days of a last generation Pentium *I*7 3.0 GHz core and are clearly not thermalized! With this in mind, it is clear that on the first-order side of the phase diagram the simulations must be really long in time to reach equilibrated states. As was said before, this fact will critically restrict us in simulating large systems.

Due to the lack of mixed phases, thermalization is quite easy to achieve on the second-order side of the phase diagram. No metastability will exist and the cluster update method will work very well.

Therefore the approach to the problem must be very different depending on the dilution of the system. If the dilution is weak, the systems will undergo first-order phase transitions and we will not be able to simulate large systems. Nevertheless we can estimate the latent heat and the surface tension to obtain the exponents of their scaling, always taking into account the possibility of unequilibrated systems. On the contrary, if the dilution is important, since the systems will undergo second-order phase transitions, we will be able to equilibrate large systems (with 64^3 spins) and to obtain accurate results for the tricritical point location. In this work we present only the latter study, i.e., the study of the exact location of the tricritical point. The study of the first-order side will be left for further research.

General behaviour

First we outline the behaviour of the model, which is very similar to that of the $Q = 4$ case although the first-order character is stronger. Firstly, by taking the sample average of the Maxwell constructions, see Sec. 3.4.1, we can obtain for each system size the behaviour of the model as the dilution changes, see Fig. 3.13 for the system with $L = 24$. Note that in this case we obtain clean Maxwell constructions up to $p = 0.800$. The system is undergoing (on average) a first-order phase transition even with 20% of vacancies! It is also remarkable that in the pure case, $p = 1$, the Maxwell construction is smooth, without flat parts or strong steps between consecutive energies.

By representing the same plot for a larger system, see Fig. 3.13 for the $L = 48$ case, we find that Maxwell constructions can not be formed for dilutions less than $p = 0.850$. As was said in Sec. 3.4.2, the apparent tricritical point depends on the system size (a FSS study is again called for). We can also see that the Maxwell construction in the pure case presents flat parts and clear steps in the temperature. They are due to the existence of clear mixed regimes with droplet or strip-like

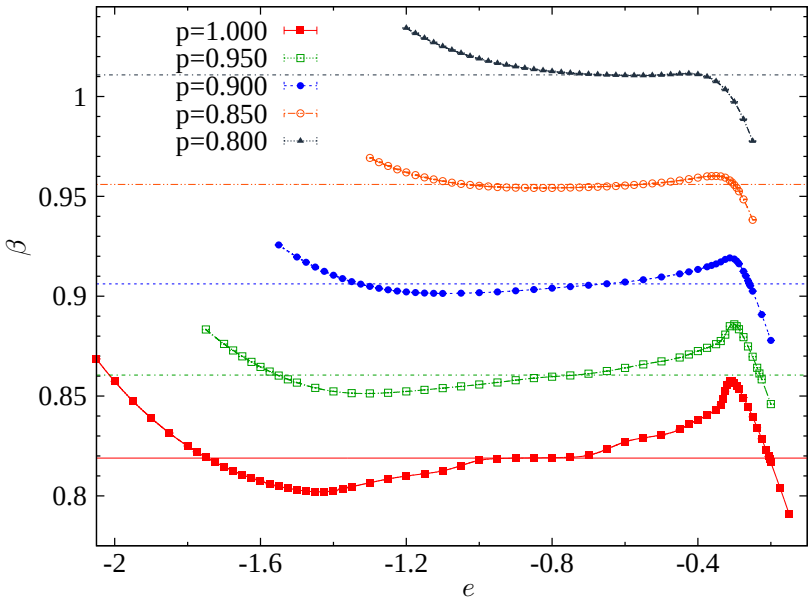

Figure 3.13: Maxwell constructions for the system with $L = 24$ as a function of the spin concentration, p. In the dilute cases, each point represents the average of the temperature for 500 samples. Note that for this size we can form the construction even for $p = 0.800$.

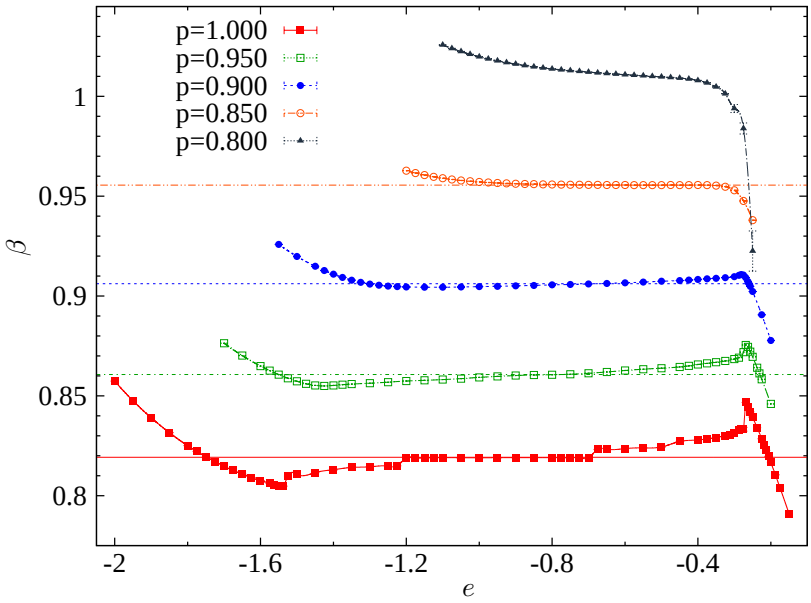

Figure 3.14: Maxwell constructions for the system with $L = 48$ as a function of the spin concentration, p. In the dilute cases, each point represents the average of the temperature for 500 samples. Note that we can form the construction only up to $p = 0.850$, the transition has become of first order between $p = 0.850$ and $p = 0.800$.

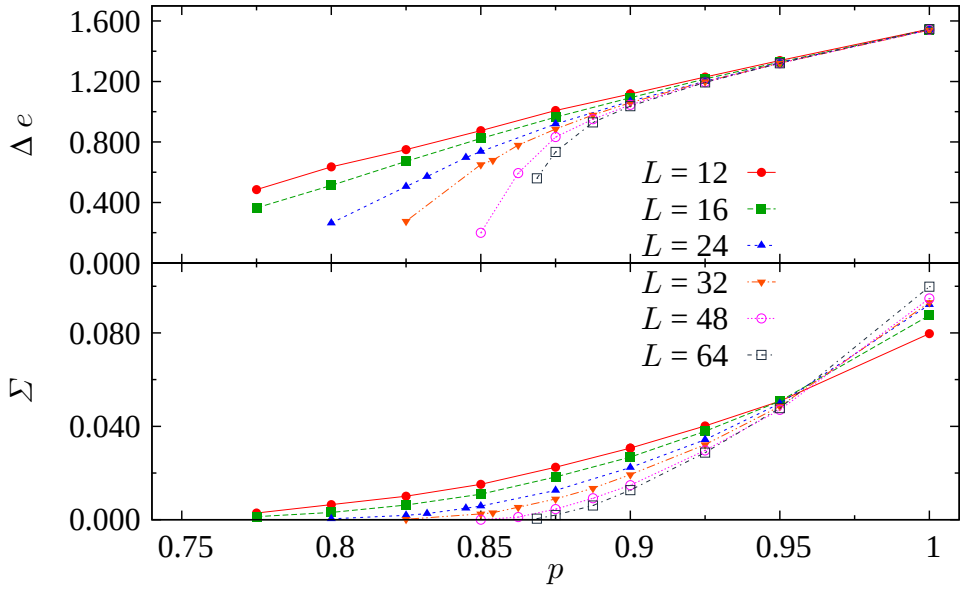

Figure 3.15: **Top:** Latent heat as obtained from the averaged Maxwell construction as a function of p for each simulated lattice size (lines are linear interpolations) for the $Q = 8$ case. **Bottom:** As in the top panel, but for the surface tension.

configurations in which the internal energy basically does not change over a range of energy densities. This is also manifest in the case of the mildly dilute samples prior to the sample-averaging process. The location of the flat parts and the steps is by far the part of the "energy walk" that is most sensitive to the metastability effects; it is really difficult for any Monte Carlo spin update method to perform properly with configurations of this kind.

Again we can plot the entire behaviour of the latent heat and the surface tension as a function of the system size and the dilution, see Fig. 3.15. This figure must be compared with that corresponding to the $Q = 4$ case, Fig. 3.7. While in the $Q = 4$ case the tricritical dilution is clearly above $p = 0.95$, this is not so for $Q = 8$. The data for both the latent heat and the surface tension show the clear trend of the tricritical dilution towards larger values as the number of Potts states grows. The points in Fig. 3.15 corresponding to large values of the dilution and the lattice size ($p > 0.925,\ L > 32$) are possibly not fully equilibrated, so special treatment of the data is needed to obtain accurate information of the scaling in this part of the phase diagram. This will be done in future work.

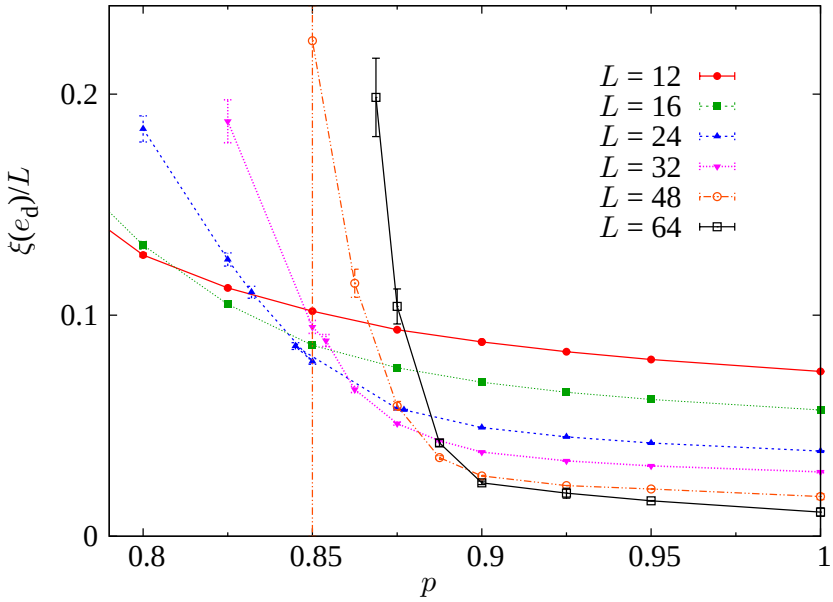

Figure 3.16: Correlation length for the $Q = 8$ case in units of the lattice size, at phase coexistence for the paramagnetic phases, e_d, as a function of concentration for several system sizes, L. The huge error bar for $L = 48$, $p = 0.85$ is due to the enormous sample-to-sample dispersion of this observable close to the tricritical point.

Behaviour of the model on the second-order side

From Fig. 3.15, while one can not obtain an accurate estimate of $p_c \neq 1$, one can again consider the correlation length obtained from the *sample-averaged* correlation function, Eq. (3.52). We use then the same approach as we used in Sec. 3.4.2 computing the crossings of the correlation length in units of the lattice size at e_d, see Fig. 3.16, and e_o, see Fig. 3.17, as obtained from $\beta(e)$.

As was done in Sec. 3.4.2, we define $p^{L,2L}$ as the crossing points of the correlation length $\xi(e_d)$ (in lattice size units) for pairs of lattices with L and $2L$. We can fit these points again to the form of Eq. (3.57) to obtain the value of the tricritical dilution p_c. Fitting our data set in e_d, see Fig. 3.16, we obtain:

$$p_{c,\,e_d} = 0.915(1), \quad x = 1.14(28), \quad \frac{\chi^2}{\text{d.o.f.}} = \frac{1.5}{2}, \quad \text{C.L.} = 47\%\,, \tag{3.59}$$

which is a perfectly valid fit producing a value for p_c clearly less than unity. Using the same approach for the crossings of $\xi(e_o)$, see Fig. 3.17, we obtain a valid fit with parameters

$$p_{c,\,e_o} = 0.910(2), \quad x = 0.95(49), \quad \frac{\chi^2}{\text{d.o.f.}} = \frac{1.1}{2}, \quad \text{C.L.} = 58\%\,. \tag{3.60}$$

Finally we can fit both data series to the form (3.57) sharing the same coefficients p_c and x. To get an acceptable value for the χ^2 of the fit we had to disregard the

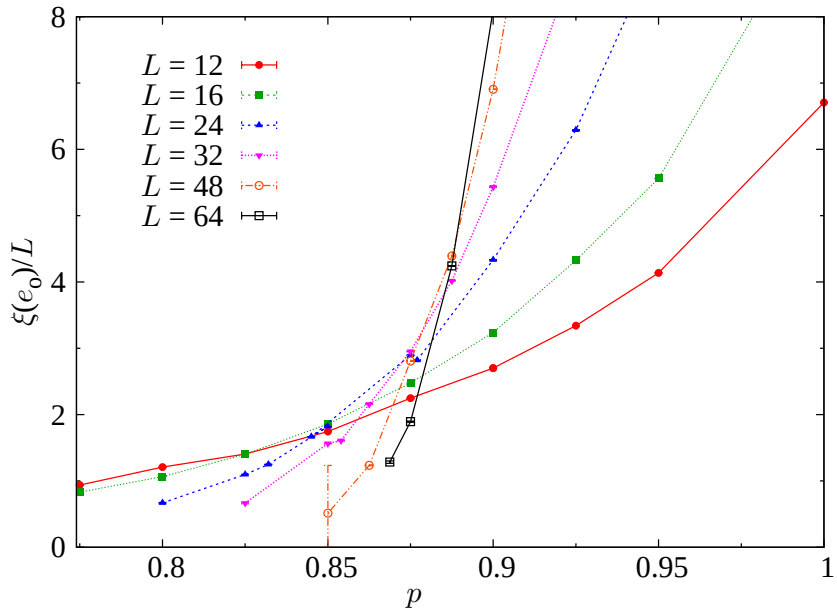

Figure 3.17: Correlation length for the $Q = 8$ case in units of the lattice size, at phase coexistence for the ferromagnetic phases, e_o, as a function of concentration for several system sizes, L.

data with $L < 16$ for $\xi(e_d)$ and $L < 24$ for $\xi(e_o)$ obtaining the fitting parameters:

$$p_{c,\,\text{joined}} = 0.922(1), \quad x_{\text{joined}} = 0.93(47), \quad \frac{\chi^2}{\text{d.o.f.}} = \frac{1.50}{2}, \quad \text{C.L.} = 47\%\,. \qquad (3.61)$$

A plot of all the above fits is shown in Fig. 3.18. Therefore we can firmly conclude that $p = 0.925$ is in the first-order part of the critical line for the three-dimensional Potts model with $Q = 8$. This is another result that reinforces our main conclusion of the previous section, i.e., first-order phase transitions do exist in $D = 3$.

3.5 Conclusions

In this chapter we have performed a detailed study of the effects of quenched disorder on a three-dimensional system undergoing a first-order transition in the pure case. We studied the site-diluted version of both the $Q = 4$ and the $Q = 8$ Potts model, a model undergoing a prototypically strong first-order transition, with the strength being proportional to the value of Q. A small degree of dilution smooths the transition up to the point of becoming second order at a tricritical point, p_c. We observed strong finite-size effects in both the location of the tricritical point and the behaviour of the most relevant quantities (latent heat, surface tension, correlation length, etc.). A delicate FSS analysis allowed us to firmly conclude that $p_c < 1$, with $p_c = 0.954(3)$ and $p_c = 0.922(1)$ in the $Q = 4$ and $Q = 8$ cases respectively. We are then able to claim that (quenched) disordered first-order transitions

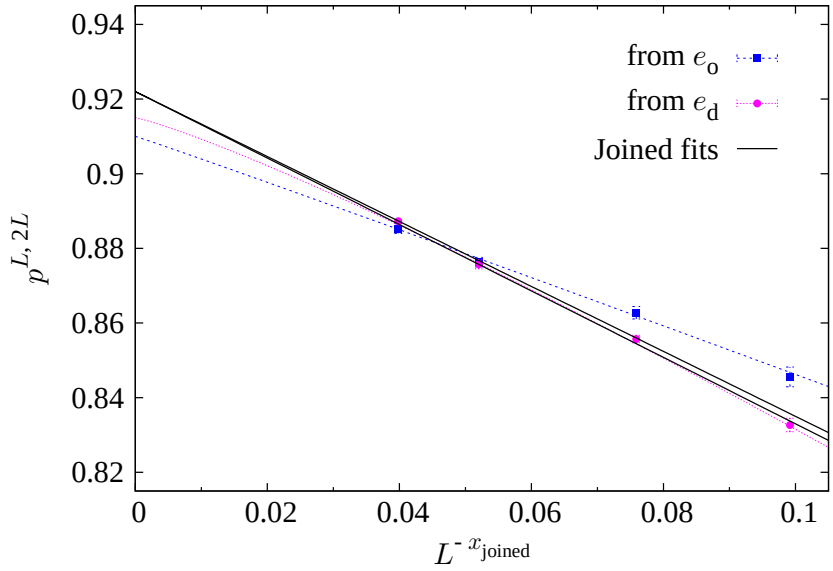

Figure 3.18: Spin concentration where values of ξ/L (data from Figs. 3.16 and 3.17) coincide for lattices L and $2L$ versus $1/L^{x_{\rm joined}}$, see Eq. (3.61). Solid lines are the combined fit, while the dashed and dotted curves correspond to the individual fits of the crossing of $\xi(e_{\rm d})$ and $\xi(e_{\rm o})$ respectively, Eqs. (3.59) and (3.60).

do exist in three dimensions, although quenched disorder is unreasonably effective in smoothing the transition (we speculate that the percolation mechanism for colossal magnetoresistance proposed in [99] could be fairly common in $D=3$).

We also observed that, for a given $p < p_{\rm c}$, a crossover length scale $L_{\rm cr}(p)$ exists such that for $L < L_{\rm cr}(p)$ the behaviour is of first-order type. The asymptotic second-order behaviour appears only for $L > L_{\rm cr}(p)$.

In the $Q = 4$ case, we also verified that the latent heat is a self-averaging quantity for random first-order phase transitions while the surface tension is not. We will try to verify this point for the $Q = 8$ case in future work.

All these results were made possible first by a new definition of the quenched average that avoids long-tailed pdf's [46], and second by the use of a recently introduced microcanonical Monte Carlo method that features the entropy density rather than the free energy [13].

As further research, we will obtain novel information on the scaling of some quantities on the first-order part of the critical line in the $Q = 8$ case. To perform this analysis, we will have to deal with systems that are not fully equilibrated. The characterisation of the effects due to the metastable states will be done by comparing pairs of simulations performing annealings from hot and cold states.

Chapter 4

The Site-Diluted Heisenberg Model in Three Dimensions

4.1 Introduction

The three-dimensional Heisenberg model is the most general representation of the interaction of the spins within an isotropic magnetic material, where isotropic means that the magnetisation does not have any preferential direction to point to. Besides, other popular models such as the Ising or XY models describe materials with a plane or axis of easy magnetisation, as is the case for instance of hexagonal lattices where the magnetisation usually chooses as preferential orientation either the c axis (correctly described then by the Ising model) or its orthogonal plane (an XY model is then correct).

The three-dimensional site-diluted Heisenberg model correctly describes the experimental behaviour of a large number of real dilute magnetic materials, see Table 4.1, so we will be able to compare our numerical results with some experimental estimates.

In this model, according to the Harris criterion [23], see Appendix A, the disorder is irrelevant. We want to check this point through numerical simulation by measuring critical exponents and different cumulants for different values of the dilution. If they do not depend on the dilution and agree with the pure case values, they will all belong to the same Universality Class (UC) and the Harris criterion will be re-verified.

In addition we will study the self-averaging properties of the model computing at criticality the quantity R_χ, which will be defined below and is a measure of the self-averageness of the susceptibility. We will show results strongly supporting that this R_χ cumulant is zero at the critical point, but only taking into account the scaling corrections. This runs against some theoretical predictions [28] but supports others [27, 29].

We will obtain high-precision measurements of the observables for each lattice size near the critical point, so it will be necessary to take into account their finite-size effects in order to obtain asymptotic results. This implies estimating the correction to scaling exponents, whose leading term is denoted ω, related to irrelevant operators in the Renormalization Group (RG) language. To this end, we will use the shift of

Ref.	Material	γ	β	δ
$[116]_{1994}$	$Fe_{10}Ni_{70}Bi_{19}Si$	1.387(12)	0.378(15)	4.50(5)
$[116]_{1994}$	$Fe_{13}Ni_{67}Bi_{19}Si$	1.386(12)	0.367(15)	4.50(5)
$[116]_{1994}$	$Fe_{16}Ni_{64}Bi_{19}Si$	1.386(14)	0.360(15)	4.86(4)
$[117,118]_{1995}$	$Fe_{20}Ni_{60}P_{14}B_6$	1.386(10)	0.367(10)	4.77(5)
$[117,118]_{1995}$	$Fe_{40}Ni_{40}P_{14}B_6$	1.385(10)	0.364(5)	4.79(5)
$[119]_{1997}$	$Fe_{91}Zr_9$	1.383(4)	0.366(4)	4.75(5)
$[119]_{1997}$	$Fe_{89}CoZr_{10}$	1.385(5)	0.368(6)	4.80(4)
$[119]_{1997}$	$Fe_{88}Co_2Zr_{10}$	1.389(6)	0.363(5)	4.81(5)
$[119]_{1997}$	$Fe_{84}Co_6Zr_{10}$	1.386(6)	0.370(5)	4.84(5)
$[120]_{1999}$	$Fe_{1.85}Mn_{1.15}Si$	1.543(20)	0.408(60)	4.74(7)
$[120]_{1999}$	$Fe_{1.50}Mn_{1.50}Si$	1.274(60)	0.383(10)	4.45(19)
$[121]_{1999}$	$MnCr_{1.9}In_{0.1}S_4$	1.39(1)	0.36(1)	4.814(14)
$[121]_{1999}$	$MnCr_{1.8}In_{0.2}S_4$	1.39(1)	0.36(1)	4.795(10)
$[122]_{2000}$	$Fe_{86}Mn_4Zr_{10}$	1.381(12)	0.361	
$[122]_{2000}$	$Fe_{82}Mn_8Zr_{10}$	1.367(12)	0.363	
$[123]_{2001}$	$Fe_{84}Mn_6Zr_{10}$	1.37(3)	0.359	4.81(4)
$[123]_{2001}$	$Fe_{74}Mn_{16}Zr_{10}$	1.39(5)	0.361	4.86(3)

Table 4.1: Experimentally-obtained critical exponents of materials which are expected to be described by the three-dimensional site-diluted Heisenberg model with quenched disorder. Table from Ref. [8]. The results we obtain in this work are: $\gamma = 1.398(6)$, $\beta = 0.370(2)$, and $\delta = 4.775(5)$.

the crossing points both for the Binder cumulant and for the correlation length for lattice pairs of different sizes near the critical point. This study will also provide estimates of the asymptotic critical temperature value. We will also check that including the correction to scaling terms is crucial for the comparison of the values we obtain for the critical exponents with those of other workers.

The simulations of this chapter were done mainly on the BIFI cluster. This consists of Xeon Dual Core 64-bit 3.40 GHz processors, with 2 GB of shared RAM. We used around fifty nodes for nine months making a total of around 17 years of computation time.

4.2 Analytical Framework

The self-averaging (SA) of the susceptibility is defined in terms of:

$$R_\chi \equiv \frac{\overline{\langle \mathcal{M}^2 \rangle^2} - \overline{\langle \mathcal{M}^2 \rangle}^2}{\overline{\langle \mathcal{M}^2 \rangle}^2} \quad , \tag{4.1}$$

with $\mathcal{M}$ being the total magnetisation. The susceptibility is self-averaging if $R_\chi \to 0$ as $L \to \infty$.

In Ref. [27], the following picture was found:

1. Away from the critical temperature: $R_\chi = 0$. On the basis of the RG or using general statistical arguments, one can find that $R_\chi \propto (\xi/L)^d$ in a finite geometry, L being the system size and ξ the correlation length which is finite for $T \neq T_c$. Then $R_\chi \to 0$ as $L \to \infty$. This is called *Strong SA*.

2. At the critical temperature, a RG analysis opens up two possible scenarios:

   - Models in which according to the Harris criterion the disorder is relevant ($\alpha_{\text{pure}} > 0$): $R_\chi \neq 0$. The susceptibility at the critical point is not self-averaging. In particular, Ref. [27] shows that under these conditions R_χ is proportional to the fixed-point value of the coupling which induces the disorder in the Hamiltonian, which controls the new UC. This is called *No SA*.
   - Models in which according to the Harris criterion the disorder is not relevant ($\alpha_{\text{pure}} < 0$): $R_\chi = 0$. The susceptibility at the critical point is self-averaging. In a finite geometry R_χ scales as $L^{\alpha/\nu} \to 0$, where α and ν are the critical exponents of the pure system, which are the same in the disordered one. This is called *Weak SA*.

The observable R_χ has been measured in other dilute models, for example in the four-dimensional dilute Ising model, see Ref. [51]. In this model a Mean Field computation and a numerical one found a non-zero value for R_χ although the dilute model was shown to belong to the same UC as the pure model, contradicting the conclusions of Ref. [27]. One can claim that the logarithms involved in the upper critical dimension make the numerical analysis difficult. In particular it was found analytically in the mean field that $R_\chi = 0.31024$ and numerically that $R_\chi \in [0.15, 0.32]$. Because of the logarithms, it was impossible to make an infinite volume extrapolation for the numerical values of R_χ. Notice that in this model the only fixed point is the Gaussian one (all the values of the couplings are zero) and, following Ref. [27], R_χ should be zero.

In addition a two-loop field theory calculation done in Ref. [28] predicts a non-zero value for R_χ for the dilute Heisenberg model (in which the disorder is irrelevant, $\alpha_{\text{pure}} = -0.134$, see Ref. [124]). The two-loop field theoretical prediction for α in the pure case was $\alpha_{\text{pure}} > 0$, so that apparently this work is consistent with the findings of Ref. [27]. The starting point in Ref. [28] was the mean field computation done in Ref. [51], modifying it to take into account the vector degrees of freedom, introducing the fluctuations using the Brezin-Zinn-Justin (BZJ) method, Ref. [125]. They found analytically $R_\chi = 0.022688$ for the vector channel and universally (independent of the dilution for all $p < 1$). It is important to remark that in the BZJ method one fixes from the beginning the temperature of the system to the infinite volume critical value, working in a finite geometry, so in order to compute R_χ in this scheme the

following sequence of limits is used:

$$R_\chi^* = \lim_{L\to\infty} \lim_{T\to T_c} R_\chi(L,T)\,, \tag{4.2}$$

where R_χ^* is the infinite volume extrapolation at criticality of $R_\chi(L,T)$, and T_c is the infinite volume critical temperature of the system. The other possible limit sequence that can be computed is:

$$\lim_{T\to T_c} \lim_{L\to\infty} R_\chi(L,T)\,, \tag{4.3}$$

which is zero even when the disorder is relevant since $R_\chi \propto L^{-d}$ as $T \neq T_c$.

Hence, in order to test these discrepancies we simulated numerically the site-diluted three-dimensional Heisenberg model computing R_χ^* in the vector and tensor channels. To perform this programme, in particular in doing the infinite volume extrapolations of cumulants and exponents, a proper use of the corrections to scaling is really important.

4.3 The Model

The Heisenberg site-diluted model in three dimensions is defined in terms of O(3) spin variables placed at the nodes of a cubic three-dimensional lattice, with Hamiltonian

$$H = -\beta \sum_{<i,j>} \epsilon_i \epsilon_j \boldsymbol{S_i} \cdot \boldsymbol{S_j}\,, \tag{4.4}$$

where the $\boldsymbol{S_i}$ are three-dimensional vectors of unit modulus, and the sum is extended only over nearest neighbours. The disorder is introduced by the random variables ϵ_i which take value unity with probability p and zero with probability $1-p$. An actual $\{\epsilon_i\}$ configuration will be called a *sample*.

In addition, as done in Ref. [126], we define a tensorial channel associated with the vector $\boldsymbol{S}$ through the traceless tensor

$$\tau_i^{\alpha\beta} = S_i^\alpha S_i^\beta - \frac{1}{3}\delta^{\alpha\beta}\,, \qquad \alpha,\beta = 1,2,3\,. \tag{4.5}$$

We define the total nearest-neighbour energy as

$$\mathcal{E} = \sum_{\langle i,j\rangle} \epsilon_i \epsilon_j \boldsymbol{S_i} \cdot \boldsymbol{S_j}\,, \tag{4.6}$$

and the normalised magnetisation for both channels as

$$\mathcal{M} = \frac{1}{V} \sum_i \epsilon_i \boldsymbol{S_i}\,, \tag{4.7}$$

$$\mathcal{M}_T^{\alpha\beta} = \frac{1}{V} \sum_i \epsilon_i (S_i^\alpha S_i^\beta - \frac{1}{3}\delta^{\alpha\beta})\,, \tag{4.8}$$

with $V = L^3$ and L is the linear lattice size. Because of the finite probability of reaching every minimal value for the free energy, the thermal average of Eqs. (4.7) and (4.8) is zero in a finite lattice. Therefore, we have to define the order parameters as the O(3) invariant scalars

$$M = \overline{\left\langle \sqrt{\mathcal{M}^2} \right\rangle} \quad , \quad M_T = \overline{\left\langle \sqrt{\mathrm{tr}\mathcal{M}_T^2} \right\rangle} . \tag{4.9}$$

Notice that the mean value of a non-invariant O(3) observable is automatically zero.

We also define the two susceptibilities as:

$$\chi = V\overline{\langle \mathcal{M}^2 \rangle} \quad , \quad \chi_T = V\overline{\langle \mathrm{tr}\mathcal{M}_T^2 \rangle} . \tag{4.10}$$

A very useful quantity is the Binder parameter, defined as

$$g_4^V = 1 - \frac{1}{3}\frac{\overline{\langle \mathcal{M}^4 \rangle}}{\overline{\langle \mathcal{M}^2 \rangle}^2} \quad , \quad g_4^T = 1 - \frac{\overline{\langle (\mathrm{tr}\mathcal{M}_T^2)^2 \rangle}}{3\overline{\langle \mathrm{tr}\mathcal{M}_T^2 \rangle}^2} . \tag{4.11}$$

Another kind of Binder parameter, meaningless for the pure system, can be defined as

$$g_2^V = \frac{\overline{\langle \mathcal{M}^2 \rangle^2} - \overline{\langle \mathcal{M}^2 \rangle}^2}{\overline{\langle \mathcal{M}^2 \rangle}^2} \quad , \quad g_2^T = \frac{\overline{\langle \mathrm{tr}\mathcal{M}_T^2 \rangle^2} - \overline{\langle \mathrm{tr}\mathcal{M}_T^2 \rangle}^2}{\overline{\langle \mathrm{tr}\mathcal{M}_T^2 \rangle}^2} , \tag{4.12}$$

and these are the quantities we use to estimate the self-averaging properties of the susceptibility (R_χ) in both channels.

A very convenient definition of the correlation length in a finite lattice is, see Ref. [68],

$$\xi = \left(\frac{\chi/F - 1}{4\sin^2(\pi/L)} \right)^{\frac{1}{2}} , \tag{4.13}$$

where F is defined in terms of the Fourier transform of the magnetisation

$$\boldsymbol{\mathcal{F}}(\boldsymbol{k}) = \frac{1}{V}\sum_{\boldsymbol{r}} e^{\mathrm{i}\boldsymbol{k}\cdot\boldsymbol{r}} \epsilon_{\boldsymbol{r}} \boldsymbol{S}_{\boldsymbol{r}} \tag{4.14}$$

as

$$F = \frac{V}{3}\overline{\langle |\mathcal{F}(2\pi/L,0,0)|^2 + |\mathcal{F}(0,2\pi/L,0)|^2 + |\mathcal{F}(0,0,2\pi/L)|^2 \rangle} . \tag{4.15}$$

The same definition is also valid in the tensorial case. This definition is very well behaved for the FSS method we have employed, see Ref. [126]. Finally, we measure the specific heat as

$$C = V^{-1}\overline{\langle \mathcal{E}^2 \rangle - \langle \mathcal{E} \rangle^2} . \tag{4.16}$$

4.4 Numerical Results

4.4.1 Methods

The lattice sizes L we have studied are $8, 12, 16, 24, 32, 48, 64$, and, only in the pure model, $L = 96$. We have simulated five values of the dilution apart from the pure case, $p = 1$. These values are $p = 0.97,\ 0.95,\ 0.9,\ 0.7$, and 0.5.

Between each measurement of the observable described in Sec. 4.3, firstly, we update the spin variables using a Metropolis method over 10% of the individuals spins, chosen at random, then we perform a number (increasing with L) of cluster updates using a Wolff method – see Ref. [7]. This is our elementary Monte Carlo step (EMCS). The number of clusters traced (or Wolff updates) between measurements was chosen to yield a good value of the self-correlation time, see Ref. [7], in our case always $1 < \tau < 2$ (τ being the integrated autocorrelation time of the energy, see Appendix C).

In order to work in thermally equilibrated systems, we perform a great number of EMCSs before starting measurements. We start the simulation always from random (hot) distributions of the spin variables, although we have checked that the averages do not change if we begin from cold configurations (i.e., all spins pointing in the same direction). In particular, we took 4×10^6 measurements for the pure model, discarding about 10^5 of the first measurements for $L = 8$ and increasing this number with the lattice size. For every lattice size, we performed 2×10^4 quenched disorder realizations in the dilute models (except for $p = 0.97$ and $p = 0.95$ with only 10^3 realizations) taking 100 measurements per sample after equilibration, in accordance with Ballesteros et al. [51] who demonstrated that the best approach to minimising the statistical error is to simulate a great number of samples with just a few measurements in each one.

To measure the critical exponents, we use the so-called quotient method [70], which allows great statistical accuracy, see Appendix B. Therefore, firstly we needed to estimate by successive simulations the β point where

$$\frac{\xi(2L, \beta, p)}{2L} = \frac{\xi(L, \beta, p)}{L} \ , \tag{4.17}$$

for each pair of lattices $(L, 2L)$. Then we used re-weighting techniques to fine-tune this condition. These re-weighting techniques are used to β extrapolate the observables and calculate their β derivatives, always before the sample averaging is performed. The equations used are, see Appendix D,

$$\langle \mathcal{O} \rangle (\beta + \Delta\beta) = \langle \mathcal{O} e^{\Delta\beta\mathcal{E}} \rangle / \langle e^{\Delta\beta\mathcal{E}} \rangle \ , \tag{4.18}$$

$$\partial_\beta \overline{\langle \mathcal{O} \rangle} = \overline{\partial_\beta \langle \mathcal{O} \rangle} = \overline{\langle \mathcal{O}\mathcal{E} - \langle \mathcal{O} \rangle \langle \mathcal{E} \rangle \rangle}. \tag{4.19}$$

These extrapolations are biased. For instance, the expectation value of equation (4.19), when the averages are calculated with N_m measurements is

$$\overline{\left(1 - \frac{2\tau}{N_m}\right) \partial_\beta \langle \mathcal{O} \rangle} \ . \tag{4.20}$$

Hence, we have to correct this bias, see again Appendix D. An example of the effect of this correction is found in Fig. 4.1: a major bias affects the uncorrected numerical data, and the importance of taking this effect into account is clear. In addition, it is clear that the recipe of Ref. [51] is working perfectly for $N_m = 100$, which is the number of measurements per sample we have taken in this work. Therefore, we are very confident that all the data presented in this work are not biased due to the re-weighting technique.

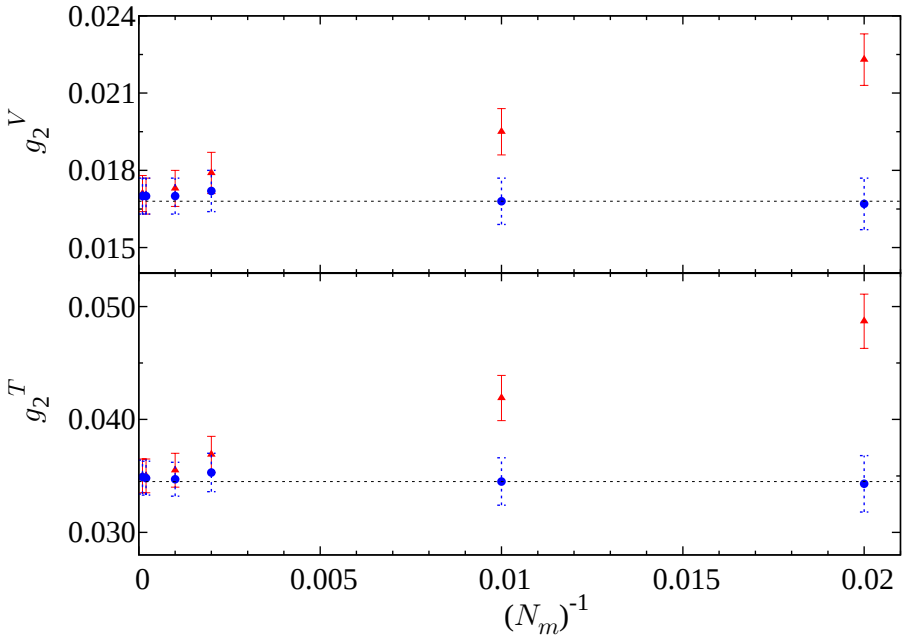

Figure 4.1: The g_2 cumulant in both channels for $L = 64$, $p = 0.9$ with 1000 samples, $\beta_{\text{simulation}} = 0.79112$, re-weighted at $\beta = 0.79082$ as a function of $1/N_m$, with N_m being the number of measurements in each sample. We report data with $N_m = 50, 100, 500, 1000, 5000$, and 10000. The data without the bias correction proposed in Ref. [51] are marked with triangles while the corrected ones are marked with circles. We also mark with the dotted lines the selection used in this work (which corresponds to $N_m = 100$). Notice the importance of the correction of the bias if one performs re-weighting with the data.

Also, we tried to use the solution for the bias obtained in Ref. [127], where each sample is split into four parts, but the results were poor. This was due to the small number of measurements we take in each sample (10^2), which leads to large differences between the averages in each quarter.

To compute errors in the averages we used a jack-knife method, see Appendix C. We defined twenty jack-knife blocks for the pure model in a *single* sample and one block for *each* sample in the dilute ($p < 1$) models.

The calculated observables and critical exponents sometimes present, instead of a stable value, a monotonically decreasing one. For η, there is found this type of evolution with increasing L, but it is clearly weaker than for ν, see Tables 4.5–4.12.

In these cases an infinite volume extrapolation is called for. If hyperscaling holds, we expect finite-volume scaling corrections proportional to $L^{-\omega}$. This issue will be addressed in the next subsection.

4.4.2 The Scaling Exponent ω

As will be seen in Tables 4.5 to 4.12 in Sec. 4.4.4, there are evident finite volume effects, especially for the thermal exponents and the cumulants (g_4 and g_2). So we have to use the equation

$$\left.\frac{x_O}{\nu}\right|_{\infty} - \left.\frac{x_O}{\nu}\right|_{(L,2L)} \propto L^{-\omega}\,, \tag{4.21}$$

which is a consequence of the scale hypothesis first derived in Ref. [128]. Consequently, choosing a good value for ω is a crucial question.

Exact results and RG calculations tell us that the disorder, being irrelevant in this model, induces scaling corrections with an exponent $\alpha/\nu \simeq -0.188$ (in L) [8]. In addition to this new scaling correction one must have that of the pure model, which is related to the coupling of the $(\phi^2)^2$ term in the Ginzburg-Landau theory. This exponent is assumed to be 0.8 [129, 130] (for the pure model). Hence, the leading correction is the exponent induced by the disorder. We will try to check this scenario by computing the 'leading' correction to the scaling exponent from the numerical data.

First of all, we tried to estimate ω just by considering it as another tunable parameter in Eq. (4.21) applied to some physical quantities. In these fits, as a first approximation, we disregarded the possible correlations between the data for different L values. The results are presented in Table 4.2. If we perform a weighted averaging with these results we obtain $\omega = 1.07(9)$ for the pure model and $\omega = 0.92(9)$, $\omega = 0.81(7)$, and $\omega = 0.88(4)$ for the dilute model with $p = 0.9, 0.7$, and 0.5 respectively, in very good agreement with the value of the scaling correction exponent of the pure model. However, we think this method is not very consistent because of the variability of the results from one quantity to another as seen in Table 4.2.

Another approach, following Ref. [131], is to study the crossing points of scaling functions (such as ξ/L and g_4) measured in pairs of lattices with sizes L and sL. The deviation of these crossing points from the infinite volume critical coupling will behave as

$$\Delta\beta(L, sL) \equiv \beta(L, sL) - \beta_c(\infty) \propto \frac{1 - s^{-\omega}}{s^{\frac{1}{\nu}} - 1} L^{-\omega-\frac{1}{\nu}}\,. \tag{4.22}$$

With this method we need an additional estimate for the thermal exponent ν. We used, following [124], the value $\nu = 0.7113(11)$ for the pure model (notice the really small error in ν, so that we will discard it in the following), which is also a valid value for the dilute models because of the validity of the Harris criterion, and as can be checked with the data below. We fixed $s = 2$. In this approach, we only use the crossing points in the vectorial channel because they are cleaner.

$\mathcal{O}$	$\omega_{p=1.0}$	$\omega_{p=0.9}$	$\omega_{p=0.7}$	$\omega_{p=0.5}$
η_{χ^V}	1.45(52)	—	—	—
η_{M^V}	1.62(80)	—	—	—
η_{χ^T}	—	—	1.2 (1.1)	0.68(46)
η_{M^T}	—	—	—	0.73(46)
$\nu_{\partial_\beta g_4^V}$	—	—	—	—
$\nu_{\partial_\beta \xi^V}$	2.30(61)	—	—	0.62(47)
$\nu_{\partial_\beta g_4^T}$	—	—	—	—
$\nu_{\partial_\beta \xi^T}$	2.12(52)	1.76(60)	1.09(40)	1.34 (27)
ξ^V/L	1.08(21)	1.21(31)	0.61(12)	0.45(10)
ξ^T/L	—	—	1.55(76)	1.64(17)
g_4^V	0.85(14)	2.00(61)	1.21(15)	1.19(13)
g_4^T	1.06(14)	—	1.35(33)	1.41(42)
g_2^V	—	0.81(16)	0.89(9)	0.94(7)
g_2^T	—	—	0.63(12)	0.72(10)
$\bar{\omega}_{\text{weighted}}$	1.07(9)	0.92(9)	0.81(7)	0.88(4)

Table 4.2: ω values from the $L \to \infty$ extrapolations of some quantities. The last row gives the weighted average of each column. We disregarded data with error bars larger than 100% of the values themselves. Those disregarded data are shown in the table as —.

Extrapolating these crossing points using Eq.(4.22), we can plot the minimum of the χ^2 of the fit as a function of ω obtaining the upper part of Fig. 4.2 and the whole of Fig 4.3. To carry out these extrapolations we must take into account that the measurements of the crossing points are correlated in pairs, so that we have to use the χ^2 definition that includes the whole self-covariance matrix

$$\chi^2_x \;=\; \sum_{l=1}^{N}\sum_{m=1}^{N}(x_l - \text{fit})(\text{cov}^{-1})_{l,m}(x_m - \text{fit})\,, \tag{4.23}$$

with N being the number of crossing points, that is to say, the number of simulated L values minus two; x_l is the value obtained for the observable x (in our case the coupling) at the crossing point for L_l and $2L_l$, and "fit" is the value fitted to the form of Eq. (4.22) (or to another scaling form) for L_l. In addition

$$(\text{cov})_{l,m} = \langle x_m x_l\rangle - \langle x_m\rangle\langle x_l\rangle \tag{4.24}$$

can also be defined in terms of jack-knife blocks, see Ref. [7], as

$$(\text{cov})_{l,m} = \frac{N_b - 1}{N_b}\sum_{i=1}^{N_b}(x_{l,i}^{\text{J-K}} - \langle x_l\rangle)(x_{m,i}^{\text{J-K}} - \langle x_m\rangle)\,, \tag{4.25}$$

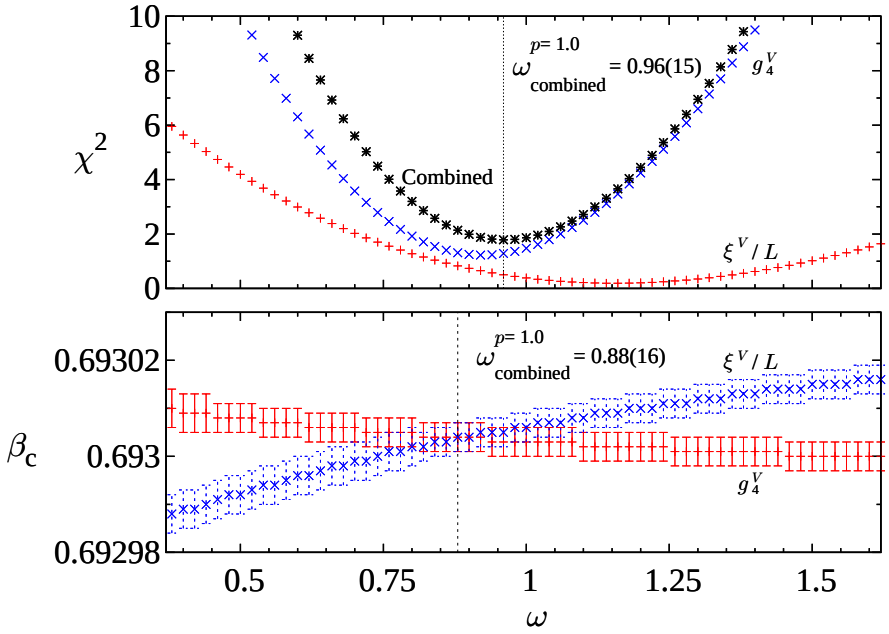

Figure 4.2: **Top:** χ^2 as a function of ω deduced from the fits to $L \to \infty$, Eq. (4.22), for the crossing point of ξ/L and g_4 for the $(L,\, 2L)$ pair for the pure model. Also shown is the combined χ^2, whose minimum is marked with the dotted line. **Bottom:** Extrapolated $\beta_c(\infty)$ as a function of ω. The point where the two observables give the same extrapolated value is marked with the dashed line.

where N_b is the number of jack-knife blocks, $x_{l,i}^{\text{J-K}}$ are block variables, where the first subindex runs over L values while the second one runs over jack-knife blocks, and $\langle x_l \rangle$ is the average of all block variables given $L = L_l$.

Also, following Ref. [131], we can do a combined fit in ω of the crossing points of ξ^V/L and g_4^V by defining

$$\chi^2_{\text{combined}} = \chi^2_{\xi^V/L} + \chi^2_{g_4^V} \,, \tag{4.26}$$

using Eq. (4.23) to calculate each of the right-hand-side terms and searching for the minimum of χ^2_{combined}. We can obtain the error in ω by searching for the point ω_1 at which $\chi^2_{\text{combined}}(\omega_1) = \chi^2_{\text{combined}}(\omega_{\text{min}}) + 1$, so that the error is $\Delta\omega = |\omega_{\text{min}} - \omega_1|$. The results for these combined fits are shown in the upper part of Fig. 4.2 and in the whole of Fig. 4.3. With this method we find the values

$$\omega = 0.96(15) \,, \tag{4.27}$$

for the pure model and

$$\omega = 2.29(70) \,, \quad 0.84(17) \,, \quad 0.64(13) \,, \tag{4.28}$$

for the dilute models with $p = 0.9,\ 0.7,$ and 0.5 respectively, in agreement with the value obtained in the pure model [124, 126, 129, 130], except in the $p = 0.9$ case

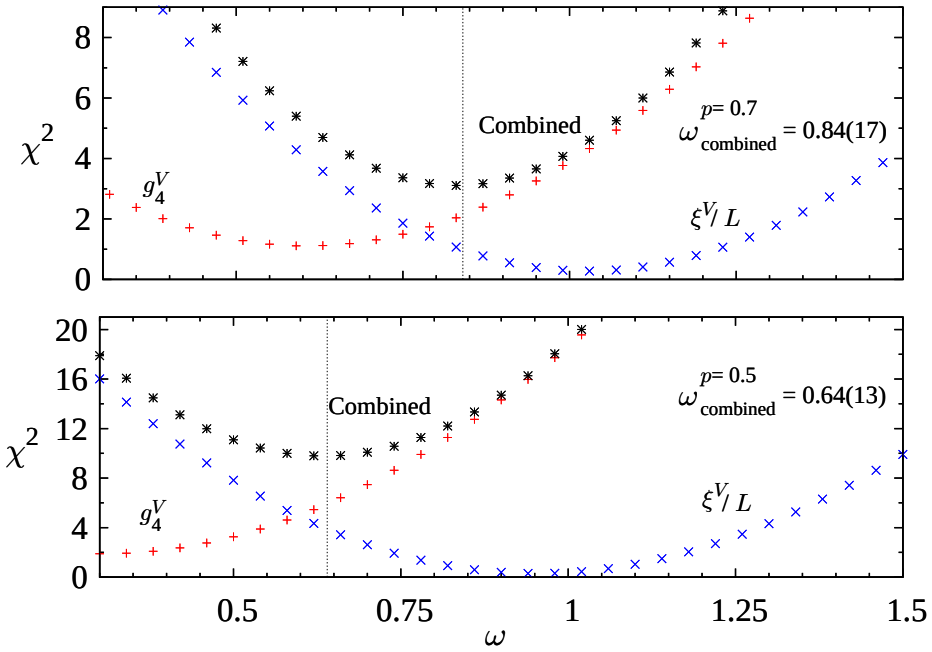

Figure 4.3: **Top:** χ^2 as a function of ω for the dilute ($p = 0.7$) model. Also shown is the combined χ^2. **Bottom:** χ^2 as a function of ω for the dilute ($p = 0.5$) model.

for which the value is two standard deviations away from $\omega = 0.8$ [129, 130]. One possibility is that we are computing the leading correction to the scaling exponent but with a large error. Another possibility is that in the $p = 0.9$ model the coefficient of the leading correction to the scaling vanishes or is very small. This result and the change in the slope of the g_4 data for $p < 1$ with respect to the $p = 1$ ones, as can be seen in Table 4.3, constitute evidence for the possible *improved action* found for $p = 0.9$, see Ref. [127]. Therefore the ω exponent that we are measuring in this case could correspond to the third irrelevant operator, instead of the second one (remember that following RG the first one is $\alpha/\nu \simeq -0.188$).

In addition, as also was done in Ref. [131], we were able to estimate the correct value for ω as that producing the same $\beta_c(\infty)$ value for both the crossings of ξ/L and g_4, as can be seen in the lower part of Fig. 4.2 marked with the dotted line at $\omega = 0.88$. This approach only works for the pure model in which such a point is found. With another p value the $\beta_c(\infty)$ estimates from ξ/L and g_4 do not cross each other.

In conclusion, we have shown that our data (for both the pure and the dilute models) are fully compatible with the value $\omega = 0.80(1)$ obtained previously both numerically and analytically for the pure model [1]. In addition, since the error bars in ω are really small (1% of error) we have discarded the uncertainty in ω in the analysis presented in this work. Since the error bars in the extrapolated quantities are much

[1]Field theoretical approaches (both fixed dimension and ϵ-expansion) provide very accurate values for ω: 0.782(13) and 0.794(18) (respectively) [129]. Recent numerical simulations provide the values 0.775(13) and 0.799(13) [130] and 0.64(13) and 0.71(15) [126].

larger than the uncertainty caused by the error bars in ω, we fixed $\omega = 0.80$. The extrapolations obtained in the rest of the chapter are all obtained using this value.

Finally, it is interesting to note that in the analysis presented in this subsection we have seen no traces of the leading correction to the scaling exponent even for the strongest dilution we have simulated, which should be $\alpha/\nu \simeq -0.188$. One can explain this fact by assuming that the amplitudes of this scaling correction exponent are really small, so that we are seeing only the next-to-leading scaling correction.

4.4.3 Self-Averaging of the Susceptibility

Having checked that the value $\omega = 0.80$ describes the corrections to the scaling for both the pure and the dilute models, we can try to extrapolate the values of g_2 to infinite volume.

Numerical results for g_2 and g_4 in both channels are presented in Table 4.3 for both pure (only g_4) and dilute models.

p	L	g_2^V	g_2^T	g_4^V	g_4^T
1.0	8	0	0	0.62243(4)	0.5216(1)
	12	0	0	0.62172(5)	0.5189(2)
	16	0	0	0.62152(6)	0.5181(2)
	24	0	0	0.62100(5)	0.5166(2)
	32	0	0	0.62092(3)	0.5162(1)
	48	0	0	0.62066(5)	0.5156(2)
0.9	8	0.0327(4)	0.0576(7)	0.6151(2)	0.5102(3)
	12	0.0273(3)	0.0518(6)	0.6163(1)	0.5104(3)
	16	0.0253(3)	0.0499(6)	0.6166(1)	0.5100(3)
	24	0.0226(3)	0.0453(6)	0.6168(1)	0.5098(3)
	32	0.0208(2)	0.0421(5)	0.6171(1)	0.5100(3)
0.7	8	0.0780(8)	0.1406(16)	0.6061(3)	0.4994(6)
	12	0.0610(6)	0.1177(13)	0.6108(2)	0.5039(5)
	16	0.0512(5)	0.1009(11)	0.6131(2)	0.5064(4)
	24	0.0423(4)	0.0868(10)	0.6150(2)	0.5077(4)
	32	0.0371(4)	0.0770(9)	0.6160(2)	0.5089(4)
0.5	8	0.1130(11)	0.2061(24)	0.6006(4)	0.4999(8)
	12	0.0834(8)	0.1600(18)	0.6072(3)	0.5047(6)
	16	0.0702(7)	0.1395(16)	0.6107(3)	0.5070(6)
	24	0.0553(6)	0.1138(13)	0.6138(2)	0.5085(5)
	32	0.0474(5)	0.0980(11)	0.6151(2)	0.5095(4)

Table 4.3: Cumulants for the O(3) model. The first column is the spin density p. All the cumulants are calculated at the crossing points of ξ/L for L and $2L$. The averages were computed using 10^4 samples (except in the $p = 1$ case).

p	L	g_2^V	g_2^T	g_4^V	g_4^T
0.97	8	0.0108(6)	0.0181(13)	0.6201(4)	0.5187(10)
	12	0.0102(6)	0.0189(14)	0.6195(4)	0.5164(10)
	16	0.0084(6)	0.0158(12)	0.6201(4)	0.5159(10)
	24	0.0072(5)	0.0146(11)	0.6206(4)	0.5162(9)
	32	0.0074(5)	0.0152(12)	0.6206(4)	0.5152(10)
0.95	8	0.0179(10)	0.0290(18)	0.6180(5)	0.5158(11)
	12	0.0167(9)	0.0329(20)	0.6182(5)	0.5116(12)
	16	0.0150(9)	0.0286(18)	0.6181(5)	0.5129(11)
	24	0.0117(7)	0.0228(14	0.6186(4)	0.5135(11)
	32	0.0118(7)	0.0251(17)	0.6193(4)	0.5140(10)

Table 4.4: Cumulants for the O(3) model with high p values (very soft dilution). In this case the cumulants are computed averaging 10^3 samples.

First of all, we will try to check the non-zero g_2 scenario with the correction to the scaling exponent fixed to that obtained in the previous section. We found that it is possible, using the form of Eq. (4.21) (performing a combined fit) to extrapolate the values of g_2 to a value (depending only on the channel) which is independent of the dilution, and near the analytical prediction of reference [28]. However, simulations at dilutions $p = 0.95$ and $p = 0.97$ do not follow the scaling found for $p \leq 0.90$ (see Table 4.4). Hence, as a whole our numerical data do not support the scenario $g_2 \neq 0$, see Figs. 4.4 and 4.5 for the two channels. Notice, see also Table 4.4, that all the values for these two lowest dilutions are smaller than the extrapolated point and they are decreasing (for both channels and taking into account the error bars).

Secondly, we will check the $g_2 = 0$ scenario. To do this, we extrapolate g_2 using the form proposed in Ref. [27] ($g_2 \backsim L^{\alpha/\nu}$) *but* also including the term $L^{-\omega}$, i.e. we fit to:

$$g_2 = aL^{\alpha/\nu} + bL^{-\omega} \,. \tag{4.29}$$

We obtain the fits shown in Figs. 4.6 and 4.7 for the two channels. The χ^2 of these fits are really good. Hence, we have obtained strong evidence supporting this $g_2 = 0$ scenario. Notice that the introduction of the two scaling correction exponents has been of paramount importance for obtaining a very good χ^2 for all the fits. The numerical data, for the simulated lattice size, do not follow the one-term dependence $g_2 \propto L^{\alpha/\nu}$.

4.4.4 Critical Exponents and Cumulants

In this subsection we will check the consistency of the ω exponent obtained in the text by means of the computation of critical exponents and cumulants. In addition, we will check whether or not these sets of exponents are universal by comparing different dilutions with the pure model. In this analysis we will use the data for $p = 0.9, 0.7$, and 0.5.

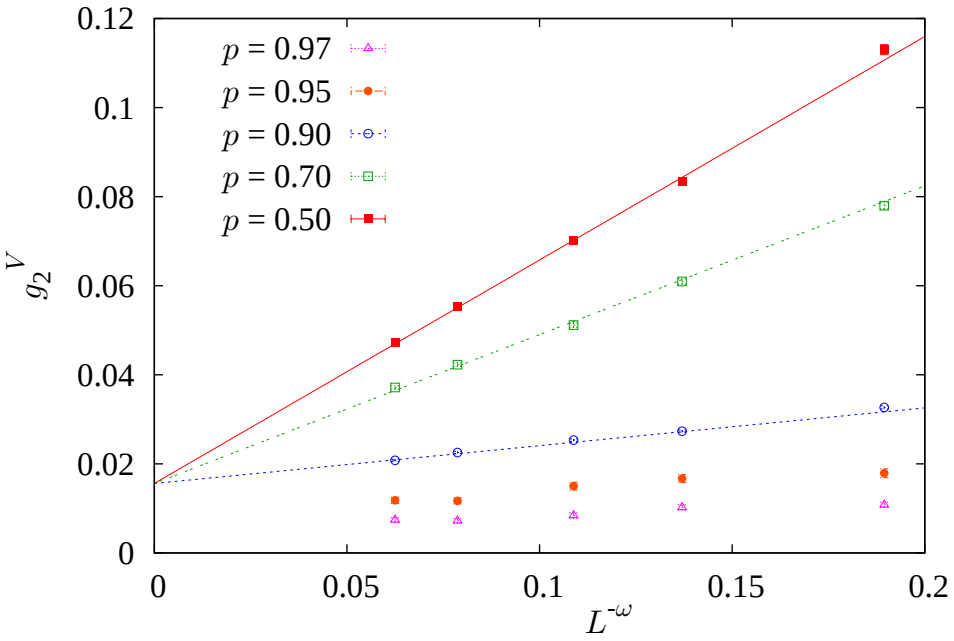

Figure 4.4: Combined extrapolation to $L \to \infty$ for the g_2 cumulant of the vectorial susceptibility. Extrapolations were carried out by choosing a common value for the first term of Eq. (4.21) for all dilutions and by minimising the combined χ^2. We disregarded the data with $L = 8$ to obtain a good value for the χ^2.

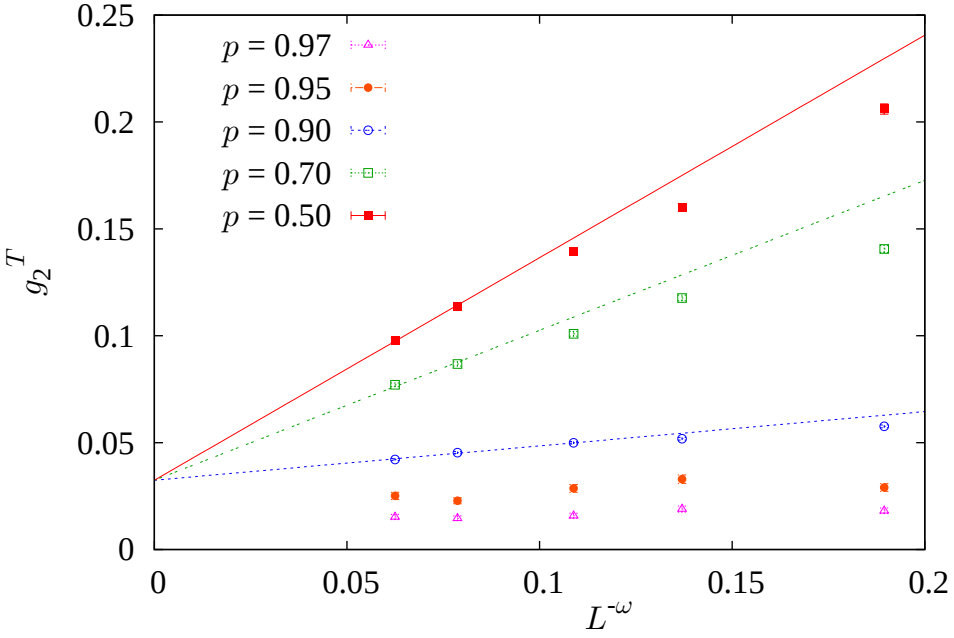

Figure 4.5: Combined extrapolation to $L \to \infty$ for the g_2 cumulant of the tensorial susceptibility, for the form of Eq. (4.21).

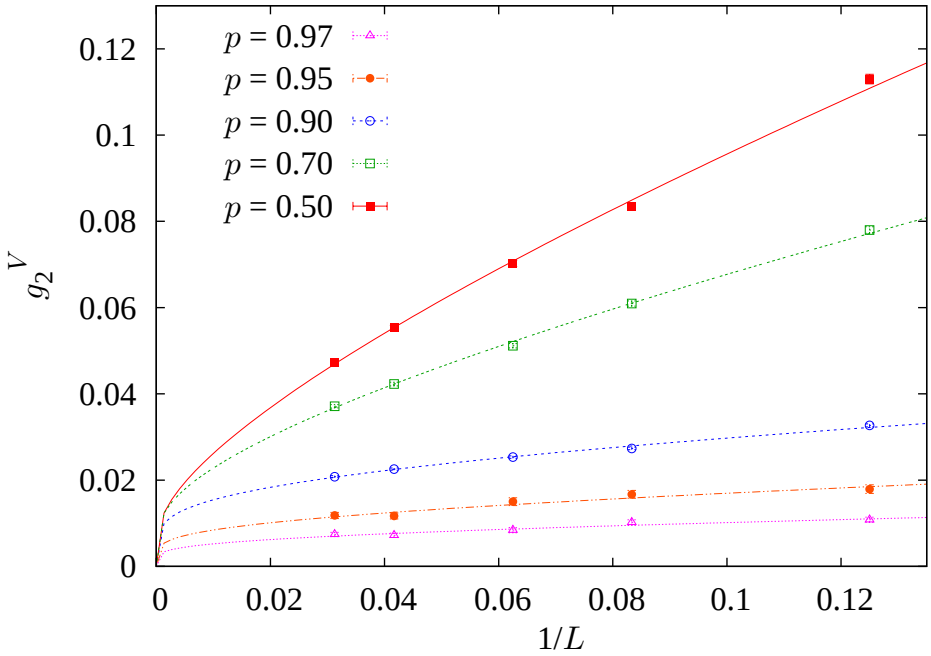

Figure 4.6: Extrapolation to $L \to \infty$ for the g_2 cumulant of the vectorial susceptibility. The fitting function is in this case given in Eq. (4.29).

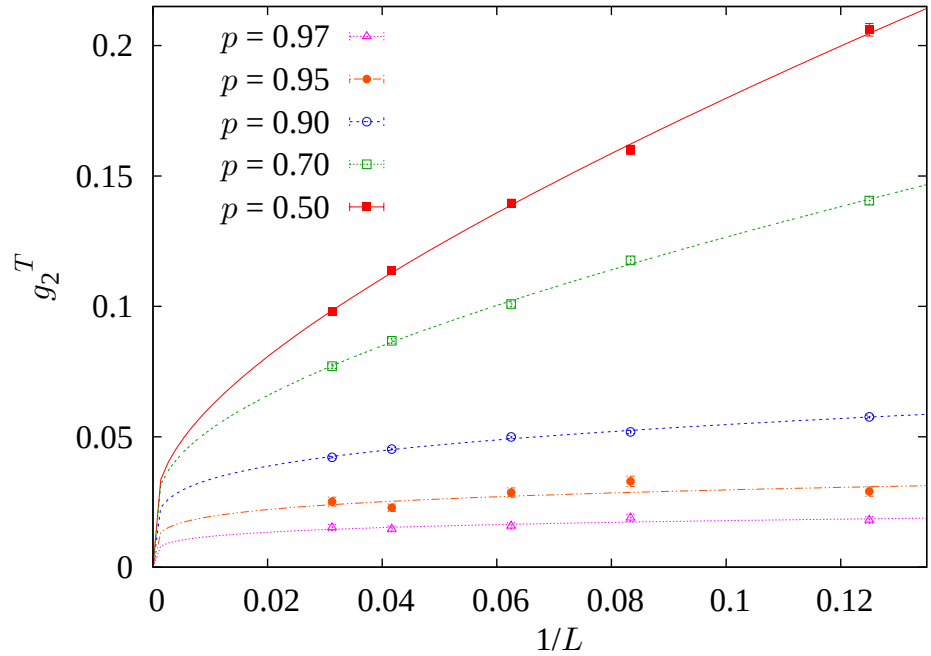

Figure 4.7: Extrapolation to $L \to \infty$ for the g_2 cumulant of the tensorial susceptibility for the fitting form $g_2 = aL^{\alpha/\nu} + bL^{-\omega}$.

Equation (B.8) applied to the quantities $\partial_\beta \xi$, $\partial_\beta g_4$, M, and χ yields respectively the critical exponents $1+1/\nu$, $1/\nu$, $(D-2+\eta)/2$, and $2-\eta$. Their numerical results are given in Tables 4.5 and 4.6 for the pure model, Tables 4.7 and 4.8 for the $p = 0.9$ case, Tables 4.9 and 4.10 for $p = 0.7$, and Tables 4.11 and 4.12 for $p = 0.5$. We also carried out combined extrapolations for all p values by fixing the same value of the extrapolated exponents for every p value. Some of these fits are shown in Figs. 4.8 to 4.11, and the compared results are presented in Tables 4.13 and 4.14.

The combined extrapolation of the Binder cumulant g_4 is given in Table 4.15. The agreement of our results with those obtained in Refs. [124] (numerical for the pure model) and [28] (analytical) is really very good. We also obtain complete agreement with previous numerical estimates of the pure model critical exponents, see Ref. [124].

We obtain non-universal critical exponents and cumulants if instead of $\omega = 0.8$ we use $\omega = -\alpha/\nu$ as the correction to scaling exponent. In addition, the dilution dependent exponents and cumulants are clearly different from the pure ones. Furthermore, this scenario does not change if we fit the data using both $-\alpha/\nu$ and $\omega = 0.8$.

	η		η_T	
L	χ	M	χ_T	M_T
8	0.0301(7)	0.0319(8)	1.4301(12)	1.4343(13)
12	0.0339(7)	0.0353(8)	1.4324(11)	1.4352(12)
16	0.0348(7)	0.0358(8)	1.4310(11)	1.4335(12)
24	0.0361(6)	0.0367(7)	1.4293(9)	1.4307(10)
32	0.0369(7)	0.0374(7)	1.4289(11)	1.4300(12)
48	0.0373(6)	0.0378(7)	1.4271(9)	1.4280(10)
$L \to \infty$	0.0391(9)	0.0390(10)	1.4250(13)	1.4249(15)
χ^2/d.o.f	0.138/3	0.354/3	1.047/3	1.952/3
C.L.	0.987	0.950	0.790	0.582

Table 4.5: Magnetic exponents for the pure O(3) model. The last three rows correspond to the $L \to \infty$ extrapolation (disregarding data with $L = 8$).

	ν			
L	$\partial_\beta g_4^V$	$\partial_\beta \xi^V$	$\partial_\beta g_4^T$	$\partial_\beta \xi^T$
8	0.7016(30)	0.7217(13)	0.6846(41)	0.7306(14)
12	0.7033(32)	0.7162(14)	0.6931(49)	0.7188(13)
16	0.7028(35)	0.7123(16)	0.6830(56)	0.7118(17)
24	0.7061(37)	0.7123(17)	0.6908(47)	0.7112(18)
32	0.7081(35)	0.7121(19)	0.7022(61)	0.7116(23)
48	0.7101(41)	0.7118(19)	0.7125(61)	0.7085(21)
$L \to \infty$	0.7109(38)	0.7071(19)	0.7082(51)	0.7071(35)
χ^2/d.o.f	0.667/4	4.104/4	7.039/4	0.565/2
C.L.	0.954	0.392	0.134	0.754

Table 4.6: Thermal critical exponents for the pure O(3) model. In the last column we have disregarded data with $L < 16$.

	η		η_T	
L	χ	M	χ_T	M_T
8	0.0346(26)	0.0345(28)	1.4154(36)	1.4176(37)
12	0.0360(24)	0.0360(26)	1.4195(34)	1.4207(36)
16	0.0371(23)	0.0374(25)	1.4207(34)	1.4218(35)
24	0.0373(22)	0.0375(24)	1.4204(32)	1.4221(34)
32	0.0383(21)	0.0383(23)	1.4219(31)	1.4227(33)
$L \to \infty$	0.0397(29)	0.0399(31)	1.4245(41)	1.4252(43)
χ^2/d.o.f	0.292/3	0.124/3	0.544/3	0.137/3
C.L.	0.962	0.989	0.909	0.987

Table 4.7: Magnetic exponents for the dilute O(3) model with $p = 0.9$. Extrapolations were carried out without disregarding data.

	ν			
L	$\partial_\beta g_4^V$	$\partial_\beta \xi^V$	$\partial_\beta g_4^T$	$\partial_\beta \xi^T$
8	0.7319(49)	0.7443(24)	0.7128(83)	0.7709(29)
12	0.7381(53)	0.7411(25)	0.7267(86)	0.7514(29)
16	0.7430(55)	0.7381(26)	0.7536(99)	0.7426(31)
24	0.7384(57)	0.7368(28)	0.7337(95)	0.7395(32)
32	0.7398(54)	0.7365(29)	0.7241(97)	0.7345(33)
$L \to \infty$	0.734(15)	0.7318(33)	0.728(17)	0.7152(39)
χ^2/d.o.f	0.134/1	0.168/3	5.468/2	3.156/3
C.L.	0.714	0.983	0.065	0.368

Table 4.8: Thermal exponents for the dilute O(3) model with $p = 0.9$. In the second and fourth columns we obtain poor results because the series are not monotonically decreasing.

	η		η_T	
L	χ	M	χ_T	M_T
8	0.0436(38)	0.0412(41)	1.3882(52)	1.3879(53)
12	0.0411(34)	0.0401(36)	1.4005(48)	1.4007(49)
16	0.0392(31)	0.0392(34)	1.4061(45)	1.4073(46)
24	0.0383(29)	0.0386(31)	1.4131(41)	1.4136(43)
32	0.0382(27)	0.0389(29)	1.4142(40)	1.4149(41)
$L \to \infty$	0.0343(57)	0.0370(58)	1.4299(72)	1.4318(76)
χ^2/d.o.f	0.232/3	0.059/3	0.472/3	0.567/3
C.L.	0.972	0.996	0.925	0.904

Table 4.9: Magnetic exponents for the dilute O(3) model with $p = 0.7$. Extrapolations were carried out without disregarding data.

	ν			
L	$\partial_\beta g_4^V$	$\partial_\beta \xi^V$	$\partial_\beta g_4^T$	$\partial_\beta \xi^T$
8	0.7888(69)	0.7881(31)	0.8256(143)	0.8422(42)
12	0.7810(74)	0.7806(33)	0.8078(140)	0.8067(41)
16	0.7633(70)	0.7760(35)	0.7739(131)	0.7897(43)
24	0.7491(66)	0.7628(37)	0.7719(146)	0.7792(47)
32	0.7400(67)	0.7521(42)	0.7656(178)	0.7627(56)
$L \to \infty$	0.7206(88)	0.723(10)	0.729(19)	0.7255(61)
χ^2/d.o.f	2.313/3	0.281/1	1.314/3	1.965/3
C.L.	0.510	0.596	0.726	0.580

Table 4.10: Thermal exponents for the dilute O(3) model with $p = 0.7$. In the third column the fit was obtained disregarding data with $L < 16$.

	η		η_T	
L	χ	M	χ_T	M_T
8	0.0505(45)	0.0461(48)	1.3435(61)	1.3431(62)
12	0.0448(39)	0.0439(42)	1.3684(54)	1.3702(56)
16	0.0421(36)	0.0417(39)	1.3877(51)	1.3896(52)
24	0.0396(32)	0.0406(35)	1.4033(46)	1.4053(48)
32	0.0399(30)	0.0414(32)	1.4126(43)	1.4152(45)
$L \to \infty$	0.0346(60)	0.0378(46)	1.446(12)	1.449(12)
χ^2/d.o.f	2.225/2	2.191/3	0.119/1	0.327/1
C.L.	0.329	0.534	0.730	0.568

Table 4.11: Magnetic exponents for the dilute O(3) model with $p = 0.5$. In the fourth and fifth columns we disregarded data with $L < 16$.

	ν			
L	$\partial_\beta g_4^V$	$\partial_\beta \xi^V$	$\partial_\beta g_4^T$	$\partial_\beta \xi^T$
8	0.8102(91)	0.8357(46)	0.9180(241)	0.9540(72)
12	0.8042(90)	0.8322(50)	0.8880(248)	0.8866(71)
16	0.7764(89)	0.7862(48)	0.8449(242)	0.8136(64)
24	0.7702(93)	0.7778(52)	0.8311(234)	0.7952(66)
32	0.7562(91)	0.7779(56)	0.7812(220)	0.7833(70)
$L \to \infty$	0.720(16)	0.764(14)	0.735(28)	0.744(17)
χ^2/d.o.f	1.149/2	0.208/1	1.565/3	0.025/1
C.L.	0.563	0.649	0.667	0.874

Table 4.12: Thermal exponents for the dilute O(3) model with $p = 0.5$. In the second column we only used data with $L > 8$ while in the third and fifth columns we only used data with $L > 12$.

	η		η_T	
	χ	M	χ_T	M_T
Our results	0.0390(9)	0.0389(10)	1.4251(13)	1.4251(14)
χ^2/d.o.f	6.675/12	5.104/15	9.151/10	13.931/11
C.L.	0.878	0.991	0.518	0.237
Ref. [124]	0.0378(6)	—	—	—

Table 4.13: Combined extrapolation with *all* p values for the magnetic exponent η compared with the results from Ref. [124]. The first three rows correspond to our $L \to \infty$ extrapolation.

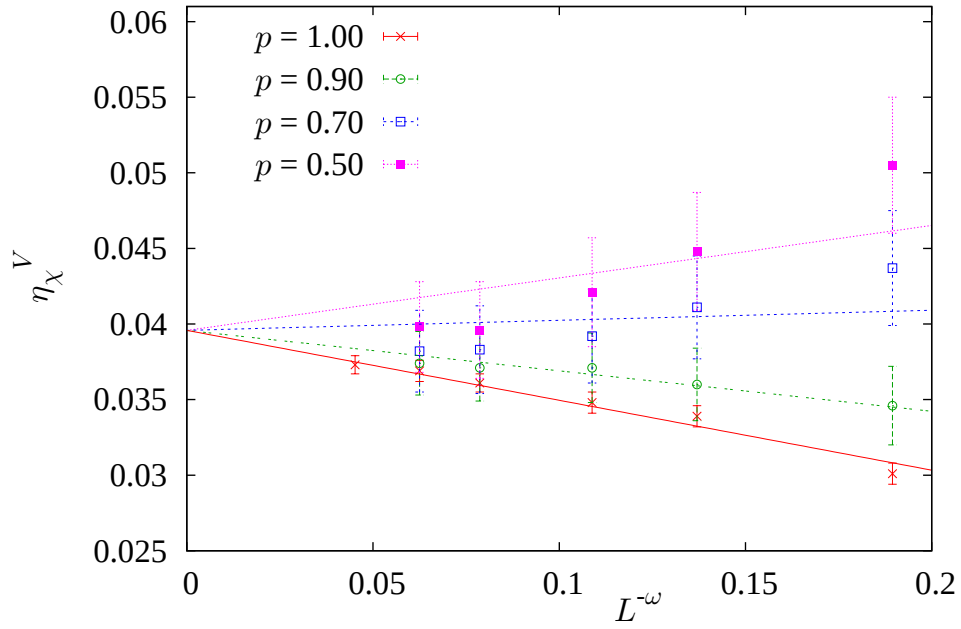

Figure 4.8: Combined extrapolation to $L \to \infty$ for the η exponent deduced from the vectorial susceptibility (χ^V). Extrapolations were carried out by choosing a common value for the first term of Eq. (4.21) for all dilutions, and by minimising the combined χ^2.

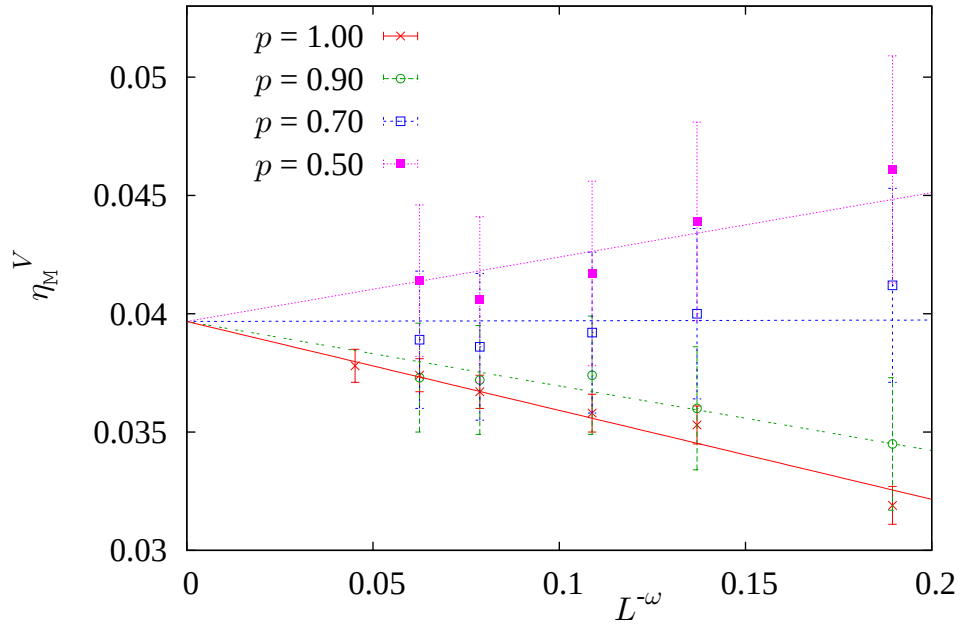

Figure 4.9: Combined extrapolation with all p values to $L \to \infty$ for the η exponent deduced from the vectorial magnetisation (M^V).

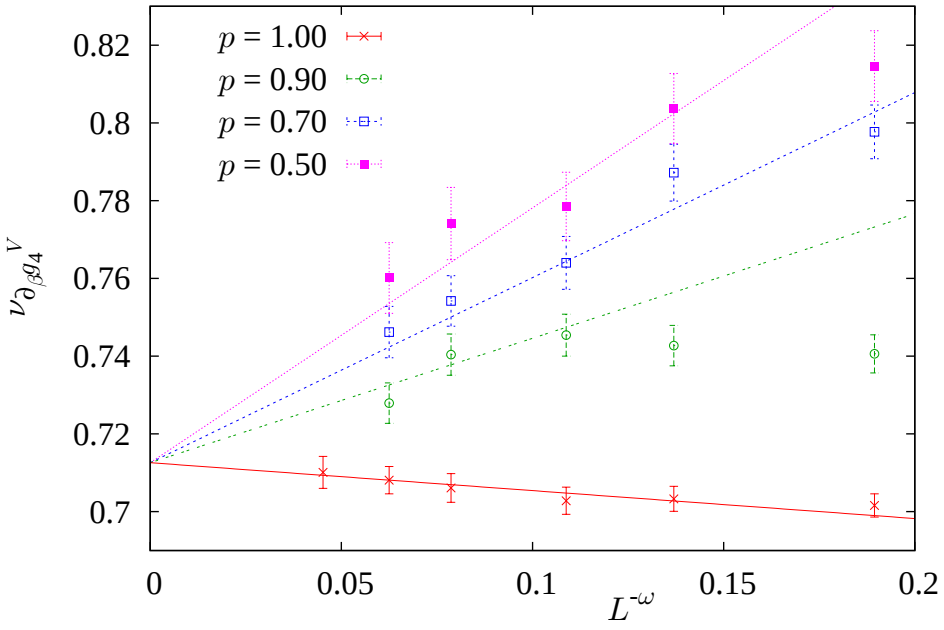

Figure 4.10: Combined extrapolation with all p values to $L \to \infty$ for the ν exponent deduced from $\partial_\beta g_4^V$.

	ν			
	$\partial_\beta g_4^V$	$\partial_\beta \xi^V$	$\partial_\beta g_4^T$	$\partial_\beta \xi^T$
Our results	0.7126(46)	0.7129(31)	0.7294(81)	0.7089(32)
χ^2/d.o.f	4.831/11	6.606/6	9.009/13	9.609/7
C.L.	0.939	0.359	0.772	0.212
Ref. [124]	0.7113(11)	—	—	—

Table 4.14: Combined extrapolation with *all* p values for the thermal exponent ν compared with the results from Ref. [124].

	g_4^V	g_4^T
Our results	0.62018(6)	0.51366(19)
χ^2/d.o.f	10.324/9	5.980/10
C.L.	0.325	0.817
Ref. [28]	0.625783	—
Ref. [124]	0.6202(1)	—

Table 4.15: Combined extrapolation to $L \to \infty$ with *all* p values for the Binder cumulant g_4 defined in Eq. (4.11), compared with results from Refs. [28] and [124].

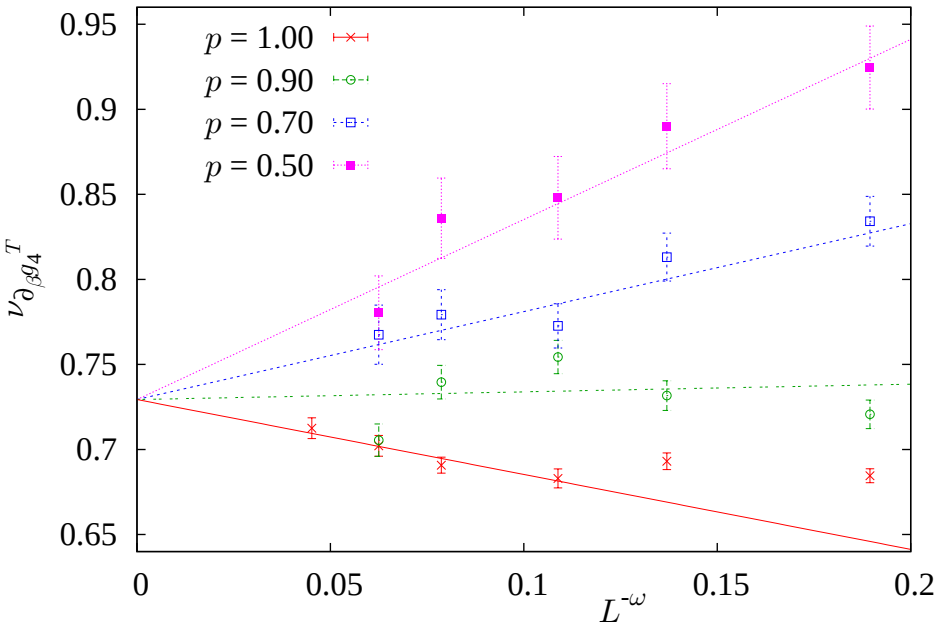

Figure 4.11: Combined extrapolation to $L \to \infty$ for the ν exponent deduced from $\partial_\beta g_4^T$.

4.5 Conclusions

We have studied the critical properties of the site-dilute Heisenberg model for different values of the dilution. Our main aims were both to re-verify the Harris criterion and to check the self-averaging properties of the susceptibility.

We studied in great detail the corrections to the scaling in the model, finding that the numerical data follow the next-to-leading correction to the scaling exponent instead of the leading one. We obtained all the critical exponents and cumulants using this next-to-leading exponent. Also, the result of this analysis was found to be fully compatible with the RG predictions and the Harris criterion: our exponents and cumulants are compatible with those of the pure model and independent of the dilution to a high degree of precision.

In addition, we showed that we obtain non-universal quantities if we assume α/ν to be the main scaling correction even if we add the ω correction to the scaling exponent, using two correction-to-scaling exponents in the analysis.

Finally, we showed strong evidence for a zero g_2 cumulant, in both the vector and the tensor channels, in the thermodynamic limit at criticality, contrasting with some analytical predictions [28], but in agreement with others [27]. The introduction of scaling corrections in the analysis was crucial to obtain the $g_2 = 0$ scenario. In addition, simulations of samples with very soft dilution ($p > 0.9$) helped us to discard the $g_2 \neq 0$ scenario.

Chapter 5

The Site-Diluted Ising Model in Four Dimensions

5.1 Introduction

One of the major achievements of statistical physics is the fundamental explanation of critical behaviour at continuous phase transitions through Wilson's Renormalization Group (RG) approach. While this has mostly provided a satisfying picture for over thirty years, certain types of phase transitions have resisted full treatment. Such stubborn cases, which have been the subject of conflicting proposals and analyses, include systems with in-built disorder.

The Ising model with uncorrelated, quenched random-site or random-bond disorder is a classic example of such systems and has been controversial in both two and four dimensions. In these dimensions, the leading exponent α which characterises the specific heat critical behaviour vanishes and no Harris prediction for the consequences of quenched disorder can be made [23], see Appendix A. In the two-dimensional case, the controversy concerns the strong universality hypothesis which maintains that the leading critical exponents remain the same as in the pure case, and the weak universality hypothesis, which favours dilution-dependent leading critical exponents (see [132] and references therein).

Since $D = 4$ marks the upper critical dimensionality of the model, the leading critical exponents there must be given by mean field theory and there is no weak universality hypothesis. However, unusual corrections to scaling characterise this model, and the precise nature of these corrections has been debated. This debate motivates the work presented in this chapter: methods similar to those employed in [132], namely a high-statistics Monte Carlo (MC) approach coupled with finite-size scaling (FSS), are used to advance our understanding of the four-dimensional version of the random-site Ising model (RSIM).

While not directly experimentally accessable, the four-dimensional RSIM is of interest for the following reasons: (i) it is closely related to the experimentally important dipolar Ising systems in three dimensions, (ii) it is an important testing ground for the widespread applicability of the RG, (iii) it presents unusual corrections to scaling, (iv) in high energy physics, the establishment of a non-trivial Higgs

sector [133] for the standard model requires a non-Gaussian fixed point and a new universality class which may, in principle, result from site dilution, and (v) it is the subject of at least *five* analytical papers which differ in the detail of the scaling behaviour at the phase transition.

5.2 Analytical Framework

5.2.1 Scaling in the RSIM in Four Dimensions

The consensus in the literature is that the following structure characterises the scaling behaviour of the specific heat, the susceptibility, and the correlation length at the second-order phase transition in the RSIM in four dimensions (up to higher-order corrections to scaling terms) [47–51, 134]:

$$C_\infty(t) \approx A - B|t|^{-\alpha} \exp\left(-2\sqrt{\frac{6}{53}|\log|t||}\right) |\log|t||^{\hat{\alpha}}\,, \tag{5.1}$$

$$\chi_\infty(t) \sim |t|^{-\gamma} \exp\left(\sqrt{\frac{6}{53}|\log|t||}\right) |\log|t||^{\hat{\gamma}}\,, \tag{5.2}$$

$$\xi_\infty(t) \sim |t|^{-\nu} \exp\left(\frac{1}{2}\sqrt{\frac{6}{53}|\log|t||}\right) |\log|t||^{\hat{\nu}}\,. \tag{5.3}$$

Here, the subscript indicates the size of the system, the reduced temperature $t = (T - T_\mathrm{c})/T_\mathrm{c}$ marks the distance of the temperature T from its critical value T_c, and A and $B > 0$ are constants. The correlation function at criticality decays as [48, 50]

$$\mathcal{G}_\infty(x) = x^{-(D-2+\eta)} |\log x|^{\hat{\eta}}\,, \tag{5.4}$$

where x measures distance across the lattice, the dimensionality of which is D. The correlation length for a system of finite linear extent L also exhibits a logarithmic correction and is of the form

$$\xi_L(t=0) \sim L(\log L)^{\hat{q}}\,. \tag{5.5}$$

The leading power-law behaviour is believed to be mean field because the fixed point is expected to be Gaussian and therefore

$$\alpha = 0\,, \quad \beta = \frac{1}{2}\,, \quad \gamma = 1\,, \quad \delta = 3\,, \quad \nu = \frac{1}{2}\,, \quad \eta = 0\,, \quad \Delta = \frac{3}{2}\,. \tag{5.6}$$

Here, β and δ are, in standard notation, the critical exponents for the magnetisation out of field and in field respectively while Δ is the gap exponent characterising the Yang-Lee edge. There is no dispute in the literature regarding these leading exponents, some of which will be re-verified in this chapter. Neither is there any dispute regarding the details of the unusual exponential correction terms in (5.1)–(5.3). However there are at least *five* different sets of predictions for the exponents

of the logarithmic terms, which differ from their counterparts in the pure model, and a principle aim of this work is to investigate these predictions numerically.

Aharony used a two-loop RG analysis to derive the unusual exponential terms in (5.1)–(5.3), and also found [47]

$$\hat{\alpha} = \frac{1}{2}\,, \quad \hat{\gamma} = 0\,, \quad \hat{\nu} = 0\,. \tag{5.7}$$

In [48], Shalaev pointed out that Aharony's results needed to be refined and, by determining the beta function to three loops, gave predictions for the specific heat and the susceptibility which differ from those in [47] in the slowly varying multiplicative logarithmic factors:

$$\hat{\alpha} = 1.2368\,, \quad \hat{\gamma} = -0.3684\,, \quad \hat{\eta} = 0.0094\,. \tag{5.8}$$

Jug studied the $\alpha = 0$ line of n-component spin models in (n, D) space where D is the system's dimensionality, and thereby worked out the logarithmic corrections for the $D = 4$ n-vector model [49]. For the case at hand ($n = 1$), he obtained

$$\hat{\alpha} = 1/2\,, \quad \hat{\gamma} = 1/212 \approx 0.0047\,. \tag{5.9}$$

In [50], Geldart and De'Bell confirmed that to obtain the correct powers of $|\log|t||$ the beta function has to be calculated to three loops, but the results of [50] differ from those of [48] in the powers of the logarithms which appear in the specific heat and in the correlation function:

$$\hat{\alpha} \approx 1.2463\,, \quad \hat{\gamma} \approx -0.3684\,, \quad \hat{\eta} = \frac{1}{212} = 0.0047\,. \tag{5.10}$$

Finally Ballesteros et al. [51] extended and corrected Aharony's computation to give the correction exponents:

$$\hat{\alpha} = \frac{1}{2}\,, \quad \hat{\gamma} = \frac{1}{106} \approx 0.0094\,, \quad \hat{\nu} = 0\,, \quad \hat{q} = \frac{1}{8}\,. \tag{5.11}$$

So the detailed analytic scaling predictions of at least five groups of workers clash, and a number of questions arise: (i) Is each set of predictions self-consistent? (ii) What is the full set of predictions (i.e., extended to all observables) originated by each set? (iii) Can a simulation approach provide numerical support for the shift in the correction terms from their counterparts in the pure model? (iv) And can such a computational approach lend support to one or other of these five different sets of analytic predictions? Here the scaling relations for logarithmic corrections developed in [135, 136] are used to answer (ii), and it is shown that the answers to questions (i) and (iii) and to some extent (iv) are affirmative. In particular, numerical support is presented for the broad scenarios presented in [47, 49, 51].

Modification of the self-consistent scaling theory for logarithmic corrections of [135, 136] to incorporate the exponential terms leads to the following forms for the behaviour of the magnetisation in the 4D RSIM:

$$m_\infty(t) = t^\beta \exp\left(-\frac{1}{2}\sqrt{\frac{6}{53}|\log|t||}\right)|\log t|^{\hat{\beta}}\,, \tag{5.12}$$

$$m_\infty(h) = h^{\frac{1}{\delta}}|\log h|^{\hat{\delta}}\,. \tag{5.13}$$

The Lee-Yang edge, denoted by $r_{LY}(t)$, is related to the locus of the Lee-Yang zeros along the imaginary h-axis, see Appendix F, and marks the end of their distribution. From Eq.(15) of [135], we also write for its scaling in the paramagnetic phase

$$r_{\rm YL}(t) \sim t^{\Delta} \exp\left(-\frac{3}{2}\sqrt{\frac{6}{53}|\log|t||}\right)|\log t|^{\hat{\Delta}}\,. \tag{5.14}$$

Besides the scaling behaviour of the Yang-Lee edge, defined in Eq. (5.14), we also consider the *density* of zeros which, for an infinitely large system, we write as $g_\infty(r)$, where r parameterises their locus along the imaginary h-axis (assuming the Lee-Yang theorem holds). In fact it is more convenient to consider the integrated, or cumulative, distribution function of zeros, defined as

$$G_\infty(r,t) = \int_{r_{YL}(t)}^{r} g_\infty(s,t)ds\ . \tag{5.15}$$

Following the approach outlined in [135], its critical behaviour can be determined as

$$G_\infty(r) \sim r^{\frac{2-\alpha}{\Delta}} \exp\left(\left(1-\frac{3\gamma}{2\Delta}\right)\sqrt{\frac{6}{53}|\log r|}\right)|\log r|^{\hat{\alpha}-(2-\alpha)\frac{\hat{\Delta}}{\Delta}}\ , \tag{5.16}$$

where the exponential term drops out by using the mean-field values $\gamma = 1$ and $\Delta = 3/2$.

The scaling relations for logarithmic corrections in this 4D model are [135, 136][1]

$$\begin{aligned}
\hat{\alpha} &= D\hat{q} - D\hat{\nu}\,, && (5.17)\\
2\hat{\beta} - \hat{\gamma} &= D\hat{q} - D\hat{\nu}\,, && (5.18)\\
\hat{\beta}(\delta-1) &= \delta\hat{\delta} - \hat{\gamma}\,, && (5.19)\\
\hat{\eta} &= \hat{\gamma} - \hat{\nu}(2-\eta)\,, && (5.20)\\
\hat{\Delta} &= \hat{\beta} - \hat{\gamma}\,. && (5.21)
\end{aligned}$$

These scaling relations are now used to generate a complete scaling picture from the fragments available in the literature [47–51]. This complete picture is given in Table 5.1, where the exponents of the logarithmic correction terms are listed. Values for the exponents in boldface come directly from the reference concerned and the remaining values are consequences of the scaling relations (5.17)–(5.21) . Each of the five papers [47–51] is self-consistent in that the exponents given within them do not violate logarithmic scaling relations. However, there are clear discrepancies *between* each of the five papers.

The presence of the special exponential corrections has recently been verified by Hellmund and Janke in the case of the susceptibility [134]. These exponential terms mask the purely logarithmic corrections, so in order to detect and measure the latter one needs to cancel the former. Certain combinations of thermodynamic functions

[1]The relation (5.17) is modified to read $\hat{\alpha} = 1 + d\hat{q} - d\hat{\nu}$ when $\alpha = 0$ and when the impact angle of Fisher zeros onto the real axis is any value other than $\pi/4$, which is not expected to be the case in this 4D model [136].

Log exp	Pure model [51, 137]	Aharony [47]	Shalaev [48]	Jug [49]	Geldart & De'Bell [50]	Ballesteros et al [51]
$\hat{\alpha}$	1/3	**0.5**	**1.237**	**0.5**	**1.246**	**0.5**
$\hat{\beta}$	1/3	0.25	0.434	0.252	0.439	0.255
$\hat{\gamma}$	1/3	**0**	**-0.368**	**0.005**	**-0.368**	**0.009**
$\hat{\delta}$	1/3	0.167	0.167	0.170	0.170	0.173
$\hat{\nu}$	1/6	**0**	-0.189		-0.187	**0**
$\hat{\eta}$	0	0	**0.009**		**0.005**	0.009
$\hat{q}$	1/4	0.125	0.120		0.125	**0.125**
$\hat{\Delta}$	0	0.25	0.803	0.248	0.807	0.245

Table 5.1: Theoretical predictions for the exponents of the logarithmic corrections to scaling for the pure Ising model in four dimensions and for its random-site counterpart. The latter exponents are listed in boldface if they come directly from the cited literature. The remaining values are extended from those of the literature using the scaling relations (5.17)–(5.21).

achieve this, but it turns out that FSS does this also. FSS therefore offers an ideal method to determine the exponents of the logarithmic corrections numerically [132].

5.2.2 Finite-Size Scaling

Fixing the ratio of $\xi_\infty(t)$ in (5.3) and $\xi_L(0)$ in (5.5) to x, one has

$$t^{-\nu} \exp\left(\frac{1}{2}\sqrt{\frac{6}{53}|\log|t||}\right) |\log|t||^{\hat{\nu}} = xL(\log L)^{\hat{q}}\,. \tag{5.22}$$

Taking logarithms of both sides, one obtains

$$|\log|t|| \approx \frac{1}{\nu}\log L\,, \tag{5.23}$$

which re-inserted into (5.22) gives

$$t \;\sim\; L^{-\frac{1}{\nu}} (\log L)^{\frac{\hat{\nu}-\hat{q}}{\nu}} \exp\left(\frac{1}{2\nu}\sqrt{\frac{6}{53}\frac{1}{\nu}\log L}\right)\left\{1+\mathcal{O}\left(\frac{1}{\sqrt{\log L}}\right)\right\} \tag{5.24}$$

$$\sim\; L^{-2} (\log L)^{-\frac{\hat{\alpha}}{2}} \exp\left(\sqrt{\frac{12}{53}\log L}\right)\left\{1+\mathcal{O}\left(\frac{1}{\sqrt{\log L}}\right)\right\}\,, \tag{5.25}$$

having used the mean-field value (5.6) for the leading exponent ν and the logarithmic scaling relation (5.17). If $\hat{\alpha} = 1/2$, this recovers a result in [51] for the FSS of the pseudo-critical point.

Inserting (5.25) into (5.3) recovers (5.5), as it should. The FSS's of the remaining functions are determined by inserting (5.25) into (5.1) to (5.3) and (5.12) to (5.14).

One finds

$$C_L(0) \approx A - B' L^{\frac{\alpha}{\nu}} \exp\left(-\left(2+\frac{\alpha}{2\nu}\right)\sqrt{\frac{6}{53\nu}\log L}\right)(\log L)^{\hat{\alpha}+\frac{\alpha}{\nu}(\hat{q}-\hat{\nu})}\,, \tag{5.26}$$

where $B' \propto B$ is a positive constant [47–51]. Inserting the mean-field values $\alpha = 0$, $\nu = 1/2$, one obtains the simpler form

$$C_L(0) \approx A - B' \exp\left(-2\sqrt{\frac{12}{53}\log L}\right)(\log L)^{\hat{\alpha}}\,. \tag{5.27}$$

Similarly, the FSS for the susceptibility is

$$\chi_L(0) \sim L^{\frac{\gamma}{\nu}} |\log L|^{\hat{\gamma}-\frac{\gamma}{\nu}(\hat{\nu}-\hat{q})} = L^2 |\log L|^{\hat{\zeta}}\,, \tag{5.28}$$

where

$$\hat{\zeta} = \hat{\gamma} - 2(\hat{\nu}-\hat{q}) = \frac{1}{2}\hat{\alpha} + \hat{\gamma}\,. \tag{5.29}$$

The FSS for the Yang-Lee edge is

$$r_1(L) \sim L^{-\frac{\Delta}{\nu}} |\log L|^{\hat{\Delta}+\frac{\Delta}{\nu}(\hat{\nu}-\hat{q})} = L^{-3} |\log L|^{\hat{\rho}}\,, \tag{5.30}$$

where

$$\hat{\rho} = \hat{\Delta} + 3(\hat{\nu}-\hat{q}) = -\frac{1}{4}\hat{\alpha} - \frac{1}{2}\hat{\gamma}\,. \tag{5.31}$$

Each of these also has sub-leading scaling corrections of strength $\mathcal{O}(1/\sqrt{\log L})$ times the leading behaviour. One notes, however, that the unusual exponential terms, which swamp the logarithmic corrections in the thermal scaling formulae (5.2) and (5.14), drop out of their FSS counterparts (5.28) and (5.30). These are therefore ideal quantities to study the logarithmic corrections. The theoretical analytical predictions of each of the five sources in the literature are now used to construct five possible FSS scenarios for the specific heat, the susceptibility, and the Lee-Yang zeros. While Jug did not calculate the critical correlator or correlation length in 4D, the FSS picture corresponding to [49] can still be constructed through the scaling relations for logarithmic corrections. The FSS scenarios are listed in Table 5.2.

The remainder of this chapter is concerned with Tables 5.1 and 5.2. The primary objective is to verify that the exponents for the logarithmic-correction terms in the RSIM are indeed different from those of the pure model. Once this is established, one would like to determine which of the five sets of analytical predictions are supported numerically. From Table 5.2, it is clear that present-day numerics can not be sensitive enough to distinguish between all five scenarios for the susceptibility or individual zeros. However, there are clear differences between the predictions from [47, 49, 51] and from [48, 50] for the specific heat (Table 5.1), and it will turn out that the numerical data is indeed sensitive enough to favour the former over the latter.

Exponent	Pure model	Aharony [47]	Shalaev [48]	Jug [49]	Geldart & De'Bell [50]	Ballesteros et al [51]
Susceptibility $\hat{\zeta}$	1/2	0.25	0.25	0.255	0.255	0.259
Lee-Yang zeros $\hat{\rho}$	-1/4	-0.125	-0.125	-0.127	-0.127	-0.130

Table 5.2: The exponents of the multiplicative logarithmic corrections to FSS for the magnetic susceptibility and for the Lee-Yang zeros coming from the literature and compared to their equivalents in the pure case. The FSS exponents are $\hat{\zeta}$ for the susceptibility and $\hat{\rho}$ for the Yang-Lee edge.

5.3 The Model

The partition function of the RSIM in a reduced magnetic field h is

$$Z_L(\beta, h) = \sum_{\{\sigma_i\}} \exp\left(\beta \sum_{\langle i,j\rangle} \epsilon_i\epsilon_j\sigma_i\sigma_j + h\sum_i \epsilon_i\sigma_i\right) , \tag{5.32}$$

where L denotes the linear extent of the lattice, the sum over configurations $\{\sigma_i\}$ is taken over Ising spins $\sigma_i \in \{\pm 1\}$, $\langle i,j\rangle$ denotes nearest neighbours, and ϵ_i are independent quenched random variables which take the value unity with probability p and zero with probability $1-p$. Below the percolation threshold ($p_c = 0.197$ in four dimensions), the phase transition is expected to disappear, while for every $p > p_c$ there exists a critical (inverse) temperature $\beta_c(p)$ for each given dilution.

In order to find the Lee-Yang zeros we define the energy, E, and the magnetisation, M, of the system as

$$E = -\sum_{\langle ij\rangle} \epsilon_i\epsilon_j\sigma_i\sigma_j \quad , \quad M = \sum_i \epsilon_i\sigma_i \, , \tag{5.33}$$

and

$$\rho_L(\beta\,; M) = \sum_E \rho_L(E, M)\exp(-\beta E) \, , \tag{5.34}$$

where the spectral density $\rho_L(E, M)$ gives the relative weight of configurations with given values of E and M, the partition function in an imaginary field ih is therefore

$$Z_L(\beta, h) = \sum_M \rho_L(\beta\,; M)\exp(ihM) = Z_L(\beta, 0)\langle\cos(hM) + i\sin(hM)\rangle \, , \tag{5.35}$$

where the thermal average $\langle(\cdots)\rangle$ is a real measure, i.e., it is taken with $Z(\beta, h = 0)$. Assuming the Lee-Yang theorem holds [138, 139], since odd moments of the magnetisation vanish in the paramagnetic phase, the zeros for a given realization of the disorder are given by the values of h for which

$$\langle\cos(hM)\rangle = 0 \, . \tag{5.36}$$

In this way we obtain the zeros of the partition function for each value of p and L. Then we average over realizations of the disorder (samples), and the resulting jth Lee-Yang zero is denoted by $r_j(L)$, the zero with $j = 1$ being the smallest.

A robust method to determine the density of zeros, defined in Eq. (5.15), from simulation data was presented in Ref. [140]. Defining the density of zeros for a finite system of size L along the singular line $r > r_{YL}(t)$ as

$$g_L(r) = L^{-D} \sum_j \delta[r - r_j(L)] \,, \tag{5.37}$$

we can insert it into the cumulative density of zeros to obtain

$$G_L(r) = \int_0^r g_L(s) ds = \frac{j}{L^D} \quad \text{for:} \quad r_j(L) < r < r_{j+1}(L) \,, \tag{5.38}$$

so that it is given at a zero by the average

$$G_L[r_j(L)] = \frac{2j-1}{2L^D} \,. \tag{5.39}$$

We also measure the non-connected susceptibility, χ_W, defined as

$$\chi_L = \frac{1}{V} \langle M^2 \rangle \,, \tag{5.40}$$

with $V = L^4$ being the volume of the system. This quantity is directly related to the average size of the clusters constructed using a Wolff algorithm [10]. We checked this point in this work. In all cases, the two definitions of the non-connected susceptibility are fully compatible.

Finally we measure the specific heat of the system, defined as

$$C = \frac{1}{V} (\langle E^2 \rangle - \langle E \rangle^2) \,. \tag{5.41}$$

5.4 Numerical Results

5.4.1 Methods

We performed extensive simulations of the model for linear lattice sizes from $L = 8$ to $L = 48$ at dilutions $p = 1$, $p = 0.8$, and $p = 0.5$. In each case, we employed a Wolff single-cluster algorithm [10] to update the spin variables using periodic boundary conditions. Thermalization tests including the comparison between cold (all spins up) and hot (all spins random) starts were carried out. We found that the plateau for the susceptibility is quickly reached by starting from cold configurations, see Fig. 5.1. Indeed, the results for the susceptibilities from hot and cold starts are fully compatible (and are less than two standard deviations away from each other, even at the level of logarithmic corrections). The information about the numerical details is given in Table 5.3. We took 1000 disorder realizations in all the cases except for $L = 48$, where only 800 samples were used. We estimate that the total simulation

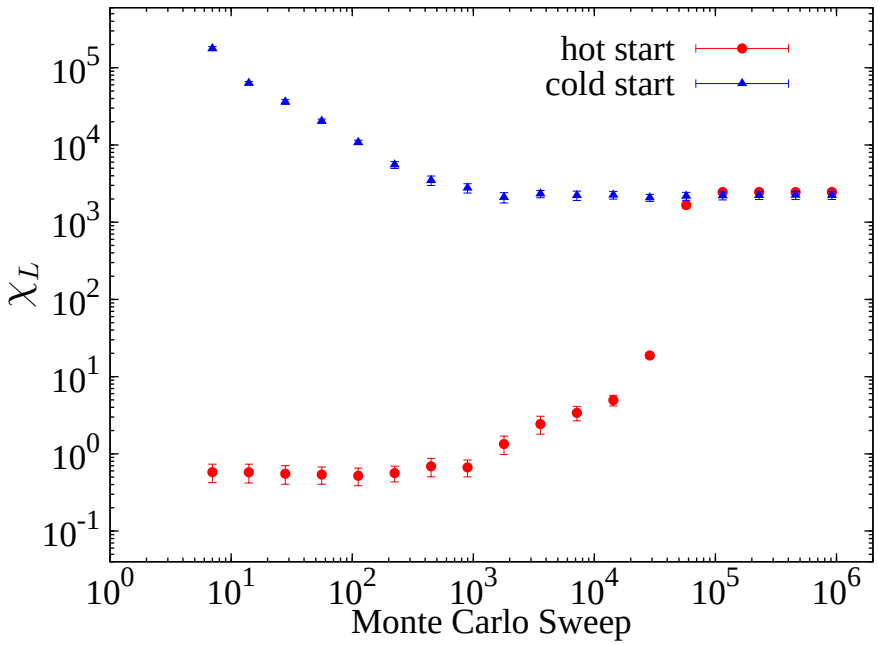

Figure 5.1: Averaged behaviour of the susceptibility with the MC time for 20 samples at $L = 32$ and $p = 0.800$. Measurements were performed after every MC sweep (Wolff update). The plateau is reached more easily starting from a cold configuration.

time was equivalent to 20 years of a single node of a Pentium Intel Core2 Quad 2.66 GHz processor. Since our aim is to estimate the scaling of quantities right at the critical point, simulations must be performed at the critical temperature of the model. We used the estimates for the critical temperature given in [51]. In terms of $\beta = 1/kT$, where k is the Boltzmann constant, these are $\beta_c = 0.149695$, $\beta_c = 0.188864$, and $\beta_c = 0.317368$, for $p = 1$, $p = 0.8$, and $p = 0.5$, respectively.

In addition we simulated the dilution $p = 0.650$ at $\beta_c = 0.235049$ [51] using the same statistics as for the other dilutions. In this case we found the behaviour of the observables to differ from the expected. For example, Fig. 5.2 shows the strong deviation of the leading scaling behaviour of the susceptibility compared with that of the other dilutions. We re-checked this point starting from different initial configurations and even using different random number generators. This deviation is surely due to a biased estimate of the critical temperature in [51]. For this reason we omit $p = 0.650$ from our analysis.

5.4.2 The Pure Case $p = 1$

To establish confidence in the present approach, the pure system is analysed first to test whether the method employed successfully quantitatively identifies the logarithmic corrections which are well established there.

Spin Concentration	L	N_{Wolff}	N_{d}
$\boldsymbol{p}$**= 1.000**	8	200	2
($\beta_{\text{c}} = 0.149695$)	12	400	8
	16	1600	32
	24	2000	128
	32	3000	400
	48	4000	1600
$\boldsymbol{p}$**= 0.800**	8	100	1
($\beta_{\text{c}} = 0.188864$)	12	200	4
	16	800	16
	24	1000	64
	32	1500	200
	48	2000	1250
$\boldsymbol{p}$**= 0.500**	8	100	2
($\beta_{\text{c}} = 0.317368$)	12	200	8
	16	800	32
	24	1000	128
	32	1500	512
	48	2000	1250

Table 5.3: Simulation details for each spin concentration p and system size L. Here, N_{Wolff} denotes the number of Wolff updates between consecutive measurements, N_{d} is the number of dropped measurements at the beginning of the MC history (in units of 10^3). We always performed 10^3 measurements within each sample after equilibration.

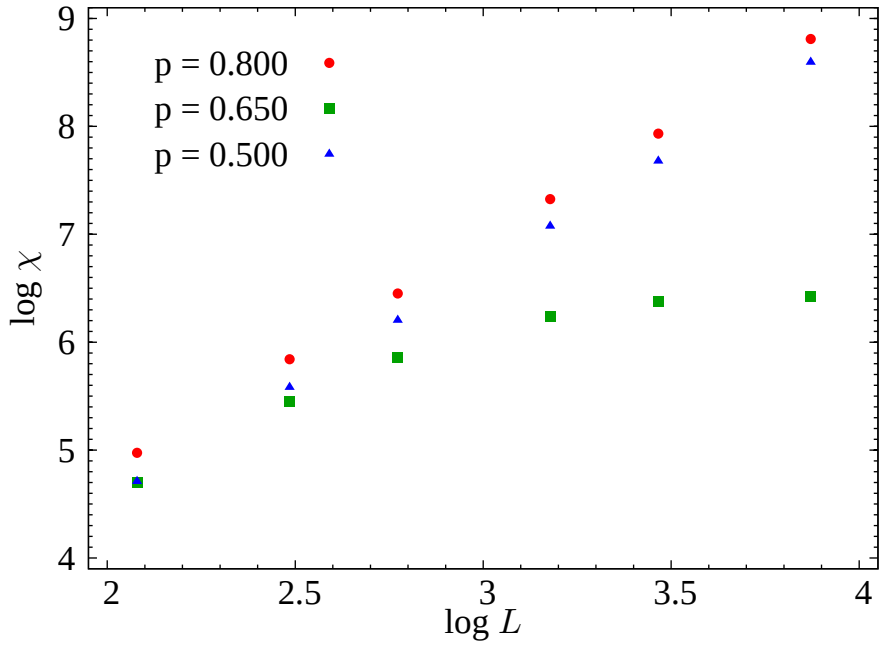

Figure 5.2: Scaling of the susceptibility comparing the $p = 0.650$ case at $\beta_c = 0.235049$ [51] with the other dilute cases (also simulated at their corresponding β_c's obtained from [51]). There can be seen the strong deviation for $p = 0.650$ from the expected leading behaviour $\chi \sim L^2$. The point size is in every case larger than the corresponding error bar.

The scaling and FSS of the pure model ($p = 1$) are well understood [51, 137]. The specific heat FSS behaviour is given by

$$C_L(0) \sim (\log L)^{\hat{\alpha}} \sim (\log L)^{1/3}\,, \tag{5.42}$$

up to additive corrections. Fitting to this form for $\hat{\alpha}$ over the full data set $8 \leq L \leq 48$, one finds the estimate $\hat{\alpha} = 0.42(4)$ with a goodness of fit given by a χ^2/d.o.f. $= 3.9/3$, C.L.=27%. The estimate is two standard deviations away from the known value 1/3. As elsewhere in this analysis, inclusion of sub-leading scaling correction terms in the fits does not ameliorate this result, which is similar to that reported in [51].

The FSS for the susceptibility is given in (5.28) with $\hat{\zeta} = 1/2$. Fitting to the leading form

$$\chi_L(0) \sim L^{\frac{\gamma}{\nu}} \tag{5.43}$$

gives $\gamma/\nu = 2.16(1)$ for $8 \leq L \leq 48$ and $\gamma/\nu = 2.13(2)$ for $12 \leq L \leq 32$, the difference from the theoretical value $\gamma/\nu = 2$ being ascribable to the presence of the logarithmic correction term. Accepting this mean-field value for γ/ν and fitting to

$$\chi_L(0) \sim L^2(\log L)^{\hat{\zeta}} \tag{5.44}$$

gives the estimate $\hat{\zeta} = 0.48 \pm 0.02$ in the range $8 \leq L \leq 48$, albeit with χ^2/d.o.f. = 12.3/3, C.L.=1%.

The FSS for the individual Lee-Yang zeros is given in (5.30) with $\hat{\rho} = -1/4$ in the pure case. Fitting to the leading form

$$r_j(L) \sim L^{-\frac{\Delta}{\nu}} \tag{5.45}$$

gives $\Delta/\nu = 3.074(5)$ for $8 \leq L \leq 48$, the difference from the theoretical mean-field value $\Delta/\nu = 3$ being due to the corrections. Accepting this value and fitting to

$$r_j(L) \sim L^{-3}(\log L)^{\hat{\rho}} \tag{5.46}$$

gives $\hat{\rho} = -0.22(2)$ in the range $8 \leq L \leq 48$. This estimate is compatible with the known value $\hat{\rho} = -1/4$. As one would expect, the higher zeros yield less accurate estimates (as they are further from the real simulation points) with $\hat{\rho} = -0.18(3)$, $\hat{\rho} = -0.17(7)$, and $\hat{\rho} = -0.10(14)$ from the second, third and fourth zeros respectively. These estimates are listed in Table 5.4.

Having established that the numerics give reasonable agreement with the pure theory at the leading and the logarithmic levels, we now perform a similar analysis in the presence of disorder.

5.4.3 The Dilute Cases $p = 0.8$ and $p = 0.5$

Since the ansatz (5.27) for the specific heat in disordered systems is somewhat more complex than that for the pure case (5.42), we begin the $p \neq 1$ analyses with the susceptibility and the Lee-Yang zeros. It will turn out that our analyses will reinforce the analytical predictions that scaling is governed by the Gaussian fixed point and that the logarithmic corrections in the RSIM differ from those in the pure model. Indeed, the results for the zeros will be seen to be broadly compatible with the analytic predictions contained in [47–51].

For the weaker dilution value $p = 0.8$, a fit using all lattice sizes to the leading form (5.43) for the susceptibility yields the estimate $\gamma/\nu = 2.14 \pm 0.01$. Ascribing the difference from the Gaussian value $\gamma/\nu = 2$ as being due to the correction terms and, as in the pure case, fitting to (5.44), one finds an estimate for the correction exponent $\hat{\zeta} = 0.39(3)$ for $8 \leq L \leq 48$. This value lies between the pure value $\hat{\zeta} = 0.5$ and the theoretical estimates for the dilute value which are $\hat{\zeta} \approx 0.25$ to 0.26. Thus, while the FSS for the susceptibility does not capture the theoretical estimates for the dilute case, the fitted values have moved away from the pure value and towards the lower value listed in Table 5.2. As elsewhere in this work, the inclusion of scaling corrections does not alter these results significantly.

A similar analysis for the FSS of the susceptibility at the stronger dilution value $p = 0.5$ gives similar results: the leading form (5.43) yields an estimate $\gamma/\nu = 2.13 \pm 0.02$ with a goodness of fit given by χ^2/d.o.f. = 1.2/3, C.L.=75%. Ascribing the difference from the mean-field value $\gamma/\nu = 2$ as being due to the logarithmic corrections, and fitting to (5.44), one obtains the estimate $\hat{\zeta} = 0.37(4)$ for $8 \leq L \leq 48$. Again this result is between the theoretical predictions for the pure ($\hat{\zeta} = 0.5$)

p		$\hat{\zeta}$	$\hat{\rho}$			
	Theory ($p=1$) $\Rightarrow$ Theory ($p\neq 1$)$\Rightarrow$	1/2 0.25 to 0.26	-1/4 -0.125 to -0.13			
			$j=1$	$j=2$	$j=3$	$j=4$
1	$L=8-48$	0.48(2)	-0.22(2)	-0.18(3)	-0.17(7)	-0.10(14)
0.8	$L=8-48$	0.39(3)	-0.15(2)	-0.16(3)	-0.20(3)	-0.17(3)
0.8	$L=12-48$	0.42(4)	-0.17(4)	-0.16(4)	-0.17(5)	-0.18(4)
0.5	$L=8-48$	0.37(4)	-0.20(4)	-0.22(4)	-0.21(4)	-0.21(4)
0.5	$L=12-48$	0.40(6)	-0.16(5)	-0.20(5)	-0.18(5)	-0.19(5)

Table 5.4: FSS estimates for the various dilution values, using a range of lattice sizes. For $p<1$ the susceptibility is expected to scale as $\chi_L \sim L^2(\log L)^{\hat{\zeta}}$ and the Lee-Yang zeros as $r_j \sim L^{-3}(\log L)^{\hat{\rho}}$, where $\hat{\zeta}\approx 0.25$ to 0.259 and $\hat{\rho}\approx -0.125$ to -0.130. (For comparison, the pure theory with $p=1$ has $\hat{\zeta}=1/2$ and $\hat{\rho}=-1/4$.)

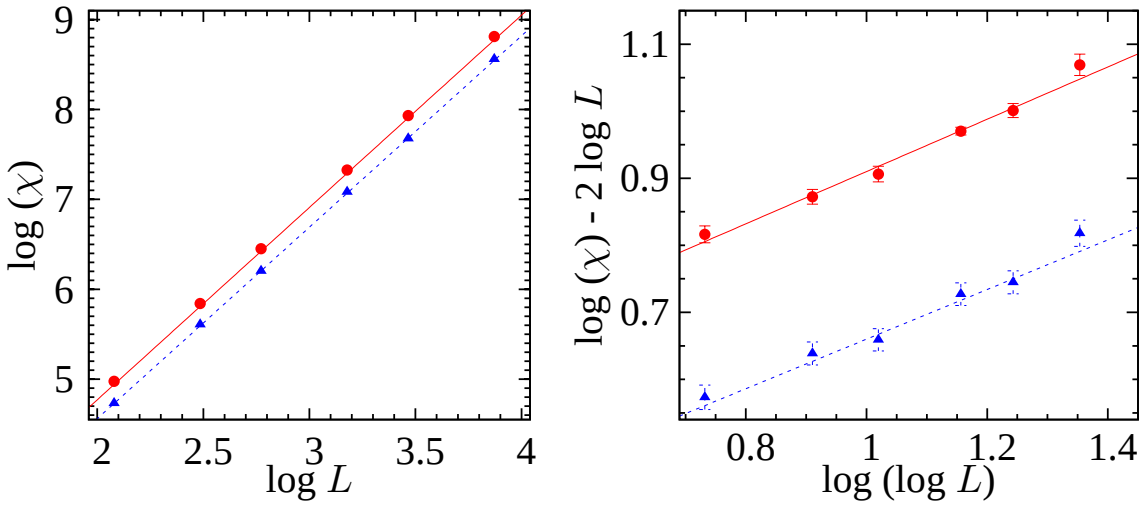

Figure 5.3: **Left**: FSS plot for χ_L at $p=0.8$ (circles) and $p=0.5$ (triangles) at the critical point. The slopes of the fitted solid and dashed lines give estimates for γ/ν of 2.14(1) and 2.13(2), respectively. **Right**: Plot of $\log\chi_L - 2\log L$ against $\log(\log L)$ at $p=0.8$ (circles) and $p=0.5$ (triangles) giving slopes 0.39(3) and 0.37(4), respectively, indicating slow crossover of multiplicative logarithmic corrections from the pure case (where $\hat{\zeta}=0.5$) to the dilute case, where the theoretical value is $\hat{\zeta}\approx 0.25$.

and the dilute ($\hat{\zeta}\approx 0.25$ to 0.26) cases. These results are summarised in Table 5.4, together with the results for the same fits but with the smallest lattices removed.

Since in each of the dilute cases the susceptibility results lie between what is expected for the pure and for the dilute theories, we appeal to the Lee-Yang zeros since they are expected to provide a cleaner signal.

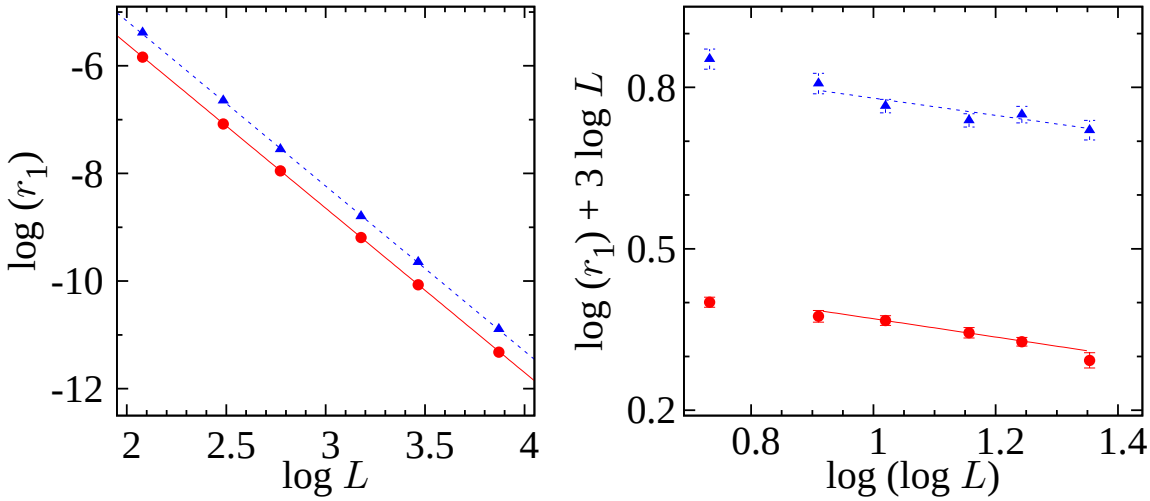

Figure 5.4: **Left**: FSS plot for the Yang-Lee edge at $p = 0.8$ (circles) and $p = 0.5$ (triangles). The slopes of the fitted solid and dashed lines give estimates for Δ/ν of 3.055(4) and 3.07(2), respectively. **Right**: Plot of $\log r_1 + 3 \log L$ against $\log(\log L)$ at $p = 0.8$ (circles) and $p = 0.5$ (triangles). Fits in the range $L = 12$ to $L = 48$ (plotted) give slopes $-0.17(4)$ and $-0.16(5)$, compatible with the literature predictions that range from $\hat{\rho} \approx -0.125$ to $\hat{\rho} \approx -0.13$. (For comparison, in the pure model, $\hat{\rho} = -1/4$.)

The leading behaviour is first examined by fitting each of the first four Lee-Yang zeros to Eq. (5.45). For the weaker dilution given by $p = 0.8$, one obtains $\Delta/\nu = 3.055(8)$, 3.056(9), 3.069(11), and 3.060(10) from fits to the first, second, third, and fourth zeros, respectively, using all lattice sizes. The equivalent results for the stronger dilution value $p = 0.5$ are $\Delta/\nu = 3.068(13)$, 3.071(15), 3.072(12), and 3.071(11), respectively. All fits are of good quality with acceptable values of χ^2/d.o.f., which we refrain from detailing. Again, these are interpreted as being supportive of the mean-field leading behaviour $\Delta/\nu = 3$ with logarithmic corrections.

The logarithmic-correction exponents are estimated by fitting to Eq. (5.46), with the various theories indicating that $\hat{\rho} = -0.125$ to -0.13. The strongest evidence supporting this comes, as it should, from the first zero (the Yang-Lee edge) for $p = 0.8$, which yields the estimate $\hat{\rho} = -0.15(2)$ (with χ^2/d.o.f. = 1.8/3, C.L.=61%). As in the pure case, and as expected, estimates for $\hat{\rho}$ deteriorate as higher-index zeros are used. Dropping the smallest lattices from the analysis, however, leads to these estimates for $\hat{\rho}$ becoming more compatible with [47–51]. These results are summarised in Table 5.4.

The equivalent analysis for the stronger dilution value $p = 0.5$ is less clear, with an estimate $\hat{\rho} = -0.20(4)$ coming from the first zero when all lattices are included in the fit (with χ^2/d.o.f. = 3.3/3, C.L.=35%). Dropping the smallest lattices, however, gives $\hat{\rho} = -0.16(5)$ (with χ^2/d.o.f. = 1.8/2, C.L.=40%), closer to the values coming

from [47–51]. Similar results are obtained for the higher zeros, and these are also summarised in Table 5.4.

As a final check of the reliability of our results, we used the spectral energy method [142, 143] to re-weight the data obtained at β_c to $\beta_c \pm \Delta\beta_c$ (taken again from [51]), finding that the new data sets are fully supportive of the previous results[2].

Having established that the leading FSS behaviour corresponds to that originating from the Gaussian fixed point, and that the logarithmic corrections to scaling are different from those in the pure model and moreover are (at least in the case of the Yang-Lee edge) broadly compatible with the literature predictions [47–51], we now attempt to distinguish *between* these broad predictions. To this end we turn to the specific heat.

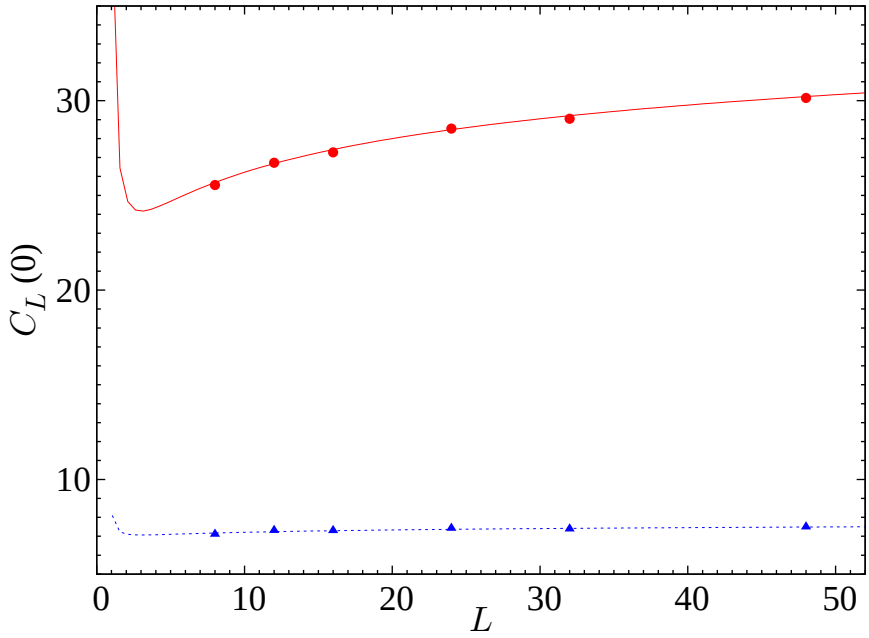

Figure 5.5: The specific heat for $p = 0.8$ (circles) and $p = 0.5$ (triangles). The error bars are in every case smaller than the point size. The solid and dashed curves are best fits to the ansatz Eq. (5.27), with $\hat{\alpha} = 1/2$.

Having established confidence in the validity of the mean-field values $\gamma = 1$ and $\Delta = 3/2$ for the 4D RSIM, we may use the scaling relation $\alpha = 2 - 2\Delta + \gamma$ to also establish the mean-field value $\alpha = 0$. The ansatz Eq. (5.27) for the specific heat may now be used. This contains information which can be used to discriminate between some of the scenarios in the literature. In Table 5.1, one observes that there is a striking difference between the estimates for the specific heat logarithmic-correction exponent $\hat{\alpha}$ coming from [48, 50] and from [47, 49, 51]. While the former have relatively large values of $\hat{\alpha}$, the latter agree on $\hat{\alpha} = 0.5$. The simulated values

[2]We followed the recipe given in Appendix D to perform the extrapolation to infinite number of measurements per sample.

of the specific heat at $p = 0.8$ and $p = 0.5$ are plotted in Fig. 5.5. The slope of the full specific heat curve (5.27) is

$$\frac{dC_L}{dL} = [A - C_L(0)]\frac{\sqrt{12/53}}{L\sqrt{\log L}}\left(1 - \frac{\hat{\alpha}\sqrt{53/12}}{\sqrt{\log L}}\right) . \tag{5.47}$$

This vanishes when $C_L(0) = A$ and when $\sqrt{\log L} = \hat{\alpha}\sqrt{53/12}$. The first of these is the asymptote $L \to \infty$, from which A can be determined for each dilution. The second occurrence of zero slope is for quite small lattice sizes, i.e., beneath lattice size $L = 8$. Therefore $\hat{\alpha} \lesssim \sqrt{12/53}\sqrt{\log 8} \approx 0.7$, which excludes the values $\hat{\alpha} \approx 1.237$ and $\hat{\alpha} \approx 1.246$ given in [48, 50]. In fact, a best fit to the ansatz Eq. (5.27) gives $A = 89(34)$, $B' = 142(71)$, and $\hat{\alpha} = 0.57(14)$ for $p = 0.8$, and $A = 60(25)$, $B' = 102(54)$, and $\hat{\alpha} = 0.76(3)$ for $p = 0.5$. Fixing $\hat{\alpha} = 1/2$ in each case gives $A = 76(4)$, $B' = 115(13)$ for $p = 0.8$, and $A = 22(3)$, $B' = 19(9)$ for $p = 0.5$. These curves are plotted along with the specific heat measurements in Fig. 5.5. However, fixing the correction exponent $\hat{\alpha}$ to the value given in [48, 50] yields a best-fit value of B' which is negative in each case, contradictory to [47, 50]. Thus we can deem these values to be unlikely.

5.5 Conclusions

Numerical measurements of the leading critical exponents in the 4D RSIM have been presented, confirming that the phase transition in this model is governed by the Gaussian fixed point. We then turned to the corrections to scaling, for which there exist *five distinct sets of predictions* in the literature [47–51]. The scaling relations for logarithmic corrections were used to complete these sets, and their counterparts for finite-size systems were given.

The measured values of the susceptibility FSS correction exponent, $\hat{\zeta}$, for the site-diluted model lie between the known value for the pure model and the theoretical estimates coming from [47–51] for the disordered system. While this result illustrates slow crossover of the susceptibility, the lowest lying Lee-Yang zeros give a cleaner signal. The measured value for their logarithmic correction exponents were indeed found to be compatible with the theories.

To discriminate between the five theories, the detailed finite-size scaling behaviour of the specific heat was also examined. The analysis was clearly in favour of the analytical predictions of [47,49,51] over those of [48,50]. This was contrary to expectation since the former involve only two loops in the perturbative RG expansion, while the latter take the expansion to three loops in the beta function.

Chapter 6

Conclusions

We have presented in this work highly accurate numerical simulations of various models of phase transitions in the presence of dilution. We checked the validity of some recent work, being able to outperform their statistical accuracy.

Firstly, we checked the goodness of a recently proposed microcanonical simulation method [13] that computes entropy, rather than free energy, to derive all the thermodynamic information. The results, both for the pure four-state ($Q = 4$) Potts model in two dimensions and for the pure Ising model in three dimensions, were fully compatible with the most recent canonical simulations [8, 43]. To achieve this, we applied (for the first time, to the best of our knowledge) the Nightingale phenomenological renormalization [69] (also called the Quotient Method [70]) within a microcanonical ensemble. In addition we obtained the critical exponents in the microcanonical ensemble, checking the validity of the Fisher renormalization [58] for models with a constraint in the internal energy.

Once we had set up a correct microcanonical simulation method, we used it to study the (inherently complicated) strong first-order phase transition of the three-dimensional Potts model with $Q > 3$ states. We confirmed that dilution dramatically smooths the transition up to a tricritical point, with spin concentration p_c, where it becomes of second order [44–46]. We were able to claim that p_c is definitely less than unity, having obtained $p_c = 0.954(3)$ and $p_c = 0.922(1)$ in the $Q = 4$ and $Q = 8$ cases, respectively. We also obtained that within the first order region in the $Q = 4$ case the latent heat is a self-averaging quantity while the surface tension is not. As a future development we will study the scaling of latent heat, surface tension, and critical temperature within the first-order region for the $Q = 8$ case. In this case we will have to deal with not fully equilibrated systems, so that we will have to quantify the effects of the lack of thermalization.

Within the canonical ensemble, we studied the critical properties of the Heisenberg dilute model in three dimensions for different values of the dilution. Using the next-to-leading scaling correction, we obtained results fully compatible with the Renormalization Group predictions and with the Harris criterion: our exponents and cumulants in the dilute cases were compatibles with those of the pure model and independent of the dilution. We also obtained strong evidence for a zero g_2 cumulant, in both the vector and the tensor channels, in the thermodynamic limit

at criticality, contrasting with some analytical predictions [28], but in agreement with others [27]. The introduction of scaling corrections into the analysis was found to be crucial to obtain the $g_2 = 0$ scenario.

We also studied the site-diluted version of the Ising model in four dimensions, confirming that the phase transition in this model is governed by the Gaussian fixed point. The logarithmic corrections to scaling were analysed to try to discriminate between five distinct sets of predictions [47–51]. The measured values of the susceptibility logarithmic correction exponent in the dilute case lie between the known value for the pure model and all the theoretical estimates for the disordered system, indicative of a slow crossover to the dilute universality class. We were able to discriminate between the five theories by a detailed study of the finite-size scaling behaviour of the specific heat. The analysis is clearly in favour of the analytical predictions of [47,49,51] over those of [48,50]. Further theoretical effort should be made in this field because the favoured scenerio stems from computation up to two loops in the perturbative RG expansion, while the rejected scenario involves expansion up to three loops in the beta function.

The numerical results of this thesis were only made possible by the intensive use of important supercomputing facilities. We obtained from their resources more than the equivalent of 400 years of computation time of a single last generation Pentium 2.5 GHz CPU. Specifically, we used the clusters at the "Instituto de Biocomputación y Física de Sistemas Complejos" (BIFI) and the "Barcelona Supercomputing Centre" (BSC). In addition, we exploited the volunteer computing platform IBERCIVIS, for which we are in debt with all its developers and volunteers.

Capítulo 6

Conclusiones

En el presente trabajo hemos realizado simulaciones numéricas de alta precisión de varios modelos de transiciones de fase en presencia de desorden. Con dichas simulaciones hemos logrado comprobar la validez de los trabajos más recientes y hemos mejorado la precisión de sus resultados.

En primer lugar, hemos comprobado la validez de un método de simulación dentro del colectivo microcanónico propuesto recientemente [13]. Dicho método utiliza la entropía, en lugar de la energía, para obtener toda la información termodinámica del sistema. Los resultados obtenidos, tanto para el modelo de Potts puro con cuatro estados ($Q = 4$) en dos dimensiones como para el modelo de Ising puro en tres dimensiones, son completamente compatibles con las simulaciones dentro del colectivo canónico más recientes [8, 43]. Para lograrlo hemos aplicado por primera vez, que nosotros sepamos, la renormalización fenomenológica de Nightingale [69] (también llamada Método de los Cocientes [70]) dentro del colectivo microcanónico. Además hemos obtenido los exponentes críticos microcanónicos comprobando la validez de la renormalización de Fisher [58] para un modelo con una ligadura en la energía.

Una vez que hemos asegurado la bondad de nuestro método de simulación microcanónico, lo hemos utilizado para el estudio de la (inherentemente complicada) transición de primer orden fuerte que tiene lugar en el modelo de Potts tridimensional con $Q > 3$ estados. Hemos comprobado que la dilución suaviza drásticamente la transición hasta llegar a un punto tricrítico, con concentración de espines p_{c}, donde la transición pasa a ser de segundo orden [44–46]. Podemos afirmar que p_{c} es definitivamente más pequeña que la unidad, habiendo obtenido $p_{\mathrm{c}} = 0.954(3)$ y $p_{\mathrm{c}} = 0.922(1)$ en los casos $Q = 4$ y $Q = 8$ respectivamente. También hemos obtenido que dentro de la región de primer orden para el caso $Q = 4$ el calor latente es una magnitud autopromediante mientras que la tensión superficial no lo es. Como una futura investigación se pretende estudiar el escalado del calor latente, la tensión superficial y la temperatura crítica dentro de la región de primer orden para el caso con $Q = 8$, para ello tendremos que tratar con estados no completamente equilibrados por lo que tendremos que cuantificar los efectos debidos a la falta de termalización.

Dentro del colectivo canónico hemos estudiado las propiedades críticas del modelo de Heisenberg diluido en tres dimensiones para diferentes valores de la dilución. Usando hasta segundo orden en correcciones de escala hemos obtenido resultados

completamente compatibles con las predicciones del Grupo de Renormalización y con el criterio de Harris: los exponentes y cumulantes obtenidos son compatibles con los del modelo puro e independientes de la dilución. Además hemos obtenido evidencias importantes de un cumulante g_2 nulo, tanto en el canal vectorial como en el tensorial, en el límite termodinámico y en el punto crítico. Éste último resultado contrasta con algunas predicciones analíticas [28] y concuerda con otras [27]. La introducción de correcciones al escalado en nuestro análisis ha sido fundamental para obtener el escenario con $g_2 = 0$.

También hemos estudiado la versión con dilución por sitios del modelo de Ising en cuatro dimensiones, confirmando que la transición de fase de este modelo está gobernada por el punto fijo Gaussiano. Las correcciones logarítmicas al escalado fueron analizadas para tratar de discriminar entre cinco conjuntos distintos de predicciones [47–51]. Los valores medidos del exponente de correcciones logarítmicas de la susceptibilidad en el caso diluido se sitúan entre el valor conocido del modelo puro y todos los valores teóricos estimados para el modelo diluido, esto es un signo de la existencia un fenómeno de paso (*crossover*) muy lento hacia la clase de universalidad del modelo diluido. Hemos logrado discriminar entre las cinco teorías en conflicto haciendo un estudio detallado de comportamiento de escalado con el tamaño del sistema del calor específico. El análisis claramente favorece las predicciones analíticas propuestas en [47, 49, 51] sobre las propuestas en [48, 50]. Un esfuerzo teórico adicional parece necesario ya que el escenario favorecido procede de un cálculo hasta dos "loops" de la expansión perturbativa del Grupo de Renormalización mientras que el escenario descartado procede de una expansión hasta tres "loops".

Los resultados numéricos de esta tesis doctoral solo han sido posibles debido al uso exhaustivo de importantes infraestructuras de supercomputación. Hemos obtenido el equivalente a más de 400 años de tiempo de cómputo de un único procesador Pentium 2.5 GHz de última generación. Específicamente hemos usado los *clusters* del "Instituto de Biocomputación y Física de Sistemas Complejos" (BIFI) y del "Barcelona Supercomputing Centre" (BSC). Además hemos explotado la plataforma de computación voluntaria IBERCIVIS, por lo que estamos en una deuda profunda con los desarrolladores y voluntarios.

Appendices

Appendix A

The Harris Criterion

Given the fact that real systems are almost always impure, it is crucial to quantify to what extent, if any, disorder affects their critical behaviour. A criterion, the so-called Harris criterion, makes it possible to predict quantitatively the effect of disorder by using the critical exponents of the pure system only [23]. According to this criterion, the impurities change the critical behaviour only if the specific heat exponent α of the pure system is positive (the specific heat of the pure system is divergent). In the opposite case, $\alpha < 0$ (the specific heat is finite), the impurities appear to be irrelevant, i.e. their presence does not alter the critical behaviour. We will derive the criterion following the approach of Ref. [141].

Let us consider a system with quenched disorder. This can be for example the presence of impurities at random sites in a crystal lattice. In the pure case, this system undergoes a continuous phase transition at a temperature $T_{\rm c}$. This critical temperature is expected to change in presence of disorder because it introduces spatial inhomogeneities in the coordination number[1]. The thermodynamics of second-order phase transitions is dominated by large-scale fluctuations. The dominant scale, or the correlation length, $\xi \sim |t|^{-\nu}$ goes to infinite as $t \to 0$, with $t = (T - T_{\rm c})/T_{\rm c}$ being the reduced temperature.

The strength of the disorder (in our example, the impurity concentration) is denoted by ρ, with $\rho = 0$ being the pure case. As T_c is approached the following change of scale length takes place. First the correlation length of the fluctuations becomes much larger than the lattice spacing, and the system 'forgets' about the lattice. The only relevant scale that remains in the system is $\xi(t)$. When we move closer to the critical point, ξ grows and becomes larger than the average distance between impurities, so that the effective concentration of impurities, measured with respect to the correlation length, becomes larger. It should be stressed that such a situation is reached for an arbitrary small initial concentration ρ. If $\xi^D \rho \gg 1$ there is no reason for believing that the effect of impurities will be small.

We will discuss, for the sake of simplicity, the Harris criterion using a particular model: the D-dimensional Ising-like system described in terms of the scalar field

[1]This is by definition the number of interacting neighbours of a given spin. In a mean field calculation, one obtains that the critical temperature of the Ising model is $T_{\rm c} = 2qJ/k_B$, where q is the coordination number, J the coupling, and k_B the Boltzmann constant.

Ginzburg-Landau Hamiltonian, see for example [141]:

$$H = \int \mathrm{d}^D x \left[\frac{1}{2}(\nabla\phi(x))^2 + \frac{1}{2}(t - \delta t(x))\phi^2(x) + \frac{1}{4} g\phi^4(x) \right] , \tag{A.1}$$

where the quenched disorder is described by random fluctuations of the effective transition temperature $\delta t(x)$ whose probability distribution is taken to be symmetric and Gausssian:

$$P[\delta t] = p_0 \exp\left(-\frac{1}{4\rho} \int \mathrm{d}x \, (\delta t(x))^2 \right) , \tag{A.2}$$

where p_0 is the normalisation constant. For notational simplicity, the sign of $\delta t(x)$ in Eq. (A.1) is defined such that positive fluctuations lead to locally ordered regions.

Configurations of the fields $\phi(x)$ that correspond local minima in H satisfy the saddle-point equation:

$$-\Delta\phi(x) + t\phi(x) + g\phi^3(x) = \delta t(x)\phi(x) \, , \tag{A.3}$$

Such localised solutions exist in regions of space where $t - \delta t(x)$ assumes negative values. Clearly, the solutions of Eq. (A.3) depend on a particular configuration of the function $\delta t(x)$ being inhomogeneous. Let us estimate under which conditions the quenched fluctuations of the effective transition temperature are the dominant factor for the local minima field configurations.

Let us consider a large region Ω_L of linear size $L \gg 1$. The spatially average value of the function $\delta t(x)$ in this region can be defined as follows:

$$\delta t(\Omega_L) = \frac{1}{L^D} \int_{x \in \Omega_L} \mathrm{d}x \, \delta t(x) \, . \tag{A.4}$$

Correspondingly, for the characteristic values of the temperature fluctuations (averaged over realizations) in this region we get:

$$\delta t_L = \sqrt{\overline{\delta t^2(\Omega_L)}} = \sqrt{2\rho} L^{-D/2} \, . \tag{A.5}$$

Then, according to Eq. (A.3) the average value of the order parameter $\phi(\Omega_L)$ in this region can be estimated from the equation:

$$t + g\phi^2 = \delta t(\Omega_L) \, . \tag{A.6}$$

One can obtain that if the value of t is sufficiently small, i.e. if

$$\delta t(\Omega_L) \gg t \, , \tag{A.7}$$

then the solutions of Eq. (A.6) are defined only by the value of the random temperature fluctuation

$$\phi(\Omega_L) \simeq \pm \left(\frac{\delta t(\Omega_L)}{g} \right)^{1/2} \, . \tag{A.8}$$

Now let us estimate up to which sizes of locally ordered regions this may occur. According to Eq. (A.5) the condition $\delta t_L \gg t$ yields:

$$L \ll \frac{\rho^{1/D}}{t^{2/D}}\,. \tag{A.9}$$

On the other hand, the estimation of the order parameter in terms of the saddle-point equation (A.6) can be correct only at scales much larger than the correlation length $\xi \sim t^{-\nu}$. Thus one has a lower bound for L

$$L \gg\ t^{-\nu}\,. \tag{A.10}$$

Therefore, quenched temperature fluctuations are relevant only when

$$t^{-\nu} \ll \frac{\rho^{1/D}}{t^{2/D}}\,, \tag{A.11}$$

or

$$t^{2-\nu D} \ll \rho\,. \tag{A.12}$$

According to the Josephson scaling relation, $\alpha = 2 - \nu D$, see for example [1]. Thus one recovers the Harris criterion: if the specific heat critical exponent of the pure system is positive, then in the critical interval:

$$t < t_* \equiv \rho^{1/\alpha} \tag{A.13}$$

the disorder becomes relevant. This argument identifies $1/\alpha$ as the crossover exponent associated with randomness. In this case, the critical exponents of the disordered systems differ from those of the pure one. In particular, the value of α for the disordered systems is never positive [2].

On the other hand, if the exponent $\alpha = 2 - \nu D < 0$, the condition (A.13) can not be satisfied near T_c (at $t \ll 1$), and therefore in this case a weak disorder remains irrelevant in the critical region.

In the marginal situation, i.e. $\alpha = 0$, which is the case, for instance, in the four-dimensional Ising model (Chapter 5) or in the two-dimensional Ising model [132], it can be demonstrated [141] that although the specific heat exponent in the disordered model remains zero, the forms of the logarithmic singularities are affected by the disorder.

[2] A rigorous argument for $\alpha < 0$ in the disordered case, applicable to many situations, is given in [106].

Appendix B

Finite Size Scaling and the Quotient Method

When doing numerical simulations we are restricted to finite systems and therefore we will never obtain infinite specific heats or susceptibilities at the critical point. Nonetheless, there exist different methods to study the critical behaviour of a physical system, working with a finite number of degrees of freedom.

Probably the most popular approach is the use of Finite Size Scaling (FSS) techniques. They are based on the study of the evolution of observables with the system size in order to obtain information about the behaviour of the system at the Thermodynamic Limit (TL). FSS is based on the scaling hypothesis [128], which states that the behaviour of the system is governed by the ratio $L/\xi(\infty,t)$, where L is a characteristic scale of the system (for example its linear dimension) and $\xi(\infty,t)$ is the correlation length of the infinite system. If this ratio is large, the system is basically in its TL; if it is small, it will be in the FSS regime.

One of the consequences of the above statement is that the evolution of the mean value of a given observable, O, with the system size will follow the functional form

$$\frac{\langle O(L,t)\rangle}{\langle O(\infty,t)\rangle} = f_O(L/\xi(\infty,t)) + \mathcal{O}(\xi^{-\omega}, L^{-\omega}) \;, \tag{B.1}$$

with $t = (T - T_c)/T_c$ being the reduced temperature and f_O is a smooth function depending on the observable. The leading correction term exponent, ω, is minus the eigenvalue of the first irrelevant operator of the theory, in terms of RG language. In the following we assume that we are in the critical region, so that $\xi \gg L$. Then in the last term we can neglect $\xi^{-\omega}$ compared with $L^{-\omega}$. The above equation is one of the multiple forms of the FSS ansatz, which can also be derived from a pure RG analysis, see for example [7] or [56] for detailed explanations.

There exist more practical forms of the ansatz. The observable O diverges in the TL according to:

$$\langle O(\infty,t)\rangle = t^{-x_O} + \cdots \;. \tag{B.2}$$

For the correlation length, $x_\xi = \nu$, so that we can make the change

$$t^{-x_O} = t^{-\frac{x_O}{\nu}\nu} \propto \xi(\infty,t)^{x_O/\nu} L^{-x_O/\nu} L^{x_O/\nu} = g(L/\xi(\infty,t)) L^{x_O/\nu} \;, \tag{B.3}$$

and Eq. (B.1) can be rewritten as

$$\langle O(L,t)\rangle = L^{x_O/\nu}[\hat{F}_O(L/\xi(\infty,t)) + L^{-\omega}\hat{G}_O(L/\xi(\infty,t)) + \cdots]\,, \tag{B.4}$$

where it can be shown that the correction term is also a function of $L/\xi(\infty,t)$. Given that $\xi(\infty,t) \propto t^{-\nu}$, the scale variable can be written in terms of the reduced temperature to obtain an alternative form of the ansatz:

$$\langle O(L,t)\rangle = L^{x_O/\nu}[\tilde{F}_O(tL^{\frac{1}{\nu}}) + L^{-\omega}\tilde{G}_O(tL^{\frac{1}{\nu}}) + \cdots]\,. \tag{B.5}$$

Moreover, since we can use Eq. (B.4) for the correlation length and $\hat{F}_O$ is smooth, we can invert it to obtain $\xi(\infty,t)$ as a function of $\xi(L,t)$, and thus arrive at the most useful form of the ansatz:

$$\langle O(L,t)\rangle = L^{x_O/\nu}[F_O(L/\xi(L,t)) + L^{-\omega}G_O(L/\xi(L,t)) + \cdots]\,. \tag{B.6}$$

All the quantities in the above equation can be measured on a finite lattice, so that this will be our starting point for the explanation of the quotient method [70].

If we form the quotient, Q_O, of a given observable, O, measured for two lattice sizes $L_1 = L$ and $L_2 = sL$, with $s > 1$, at just such a temperature that $Q_\xi = s$, or explicitly

$$\frac{\xi(sL,t)}{sL} = \frac{\xi(L,t)}{L}\,, \tag{B.7}$$

the result will be the elimination of the scaling function F_O in Eq. (B.6),

$$Q_O|_{Q_\xi = s} = s^{x_O/\nu} + \mathcal{O}(L^{-\omega})\,. \tag{B.8}$$

Typically one chooses $s = 2$. The critical exponent x_O can easily be derived from the above equation. The fact that there are strong statistical correlations between the quotients in Eqs. (B.7) and (B.8) can be used via a jack-knife method to decrease the statistical errors in the numerical estimates of critical exponents, see Appendix C or Ref. [7].

In the present work we used the quantities:

$$\chi \;\rightarrow\; x_o = \nu(2-\eta)\,, \tag{B.9}$$

$$\mathcal{M} \;\rightarrow\; x_o = \frac{\nu}{2}(D-2-\eta)\,, \tag{B.10}$$

$$\partial_\beta\xi\ ,\ \partial_e\xi \;\rightarrow\; x_o = \nu + 1\,, \tag{B.11}$$

$$\partial_\beta g_4 \;\rightarrow\; x_o = 1\,. \tag{B.12}$$

In addition, the crossing points of the correlation length, i.e. the temperatures where the condition of Eq. (B.7) is satisfied, provide an estimate of the critical temperature of the transition. By applying Eq. (B.5) to the correlation length, assuming that the scaling functions are smooth, we can obtain for the (inverse) temperature of the crossing the following behaviour:

$$\beta_c^{L,s} - \beta_c \propto \frac{1-s^{-\omega}}{s^{1/\nu}-1}L^{-\omega-\frac{1}{\nu}}\,. \tag{B.13}$$

The method can be also applied in a microcanonical context if a valid FSS ansatz is available. In this case the role of the reduced temperature t is played by $e - e_{\rm c}$, where e is the energy density of the system and $e_{\rm c}$ is the energy density at the critical point, see Sec. 2.2.3 for more details.

The quotient method can be improved to speed up convergence if logarithmic corrections are present. In particular, if a given quantity, O, behaves in the TL as

$$O(L,z) = L^{x_O/\nu}(\log L)^{\widehat{x}_O}\left[F_O\left(\frac{L}{\xi(L,z)}\right) + \mathcal{O}(L^{-\omega})\right], \tag{B.14}$$

where z can be either the reduced temperature t or $e - e_{\rm c}$, the critical canonical or microcanonical exponent calculated using Eq. (B.8) must be corrected according to:

$$\frac{x'_O}{\nu} = \frac{x_O}{\nu} - \frac{\widehat{x}_O}{\log(L_2/L_1)}\log\left(\frac{\log L_2}{\log L_1}\right), \tag{B.15}$$

where we use primes to label corrected exponents.

If we have enough analytical information about the logarithmic term exponents we can apply the correction exactly. For example, for the two-dimensional four-state Potts model the values of the logarithmic correction exponents are known analytically [43, 86]. Thus we can calculate the corrections accurately. The susceptibility behaves as

$$\chi \sim L^{7/4}(\log L)^{-1/8} \tag{B.16}$$

and we easily arrive at

$$\eta' = \eta - \frac{1}{8\log(L_2/L_1)}\log\left(\frac{\log L_2}{\log L_1}\right). \tag{B.17}$$

For the correlation length it is known that

$$\xi \sim |t|^{-2/3}(-\log t)^{1/2} \qquad ; \qquad t \sim L^{-3/2}(\log L)^{3/4}, \tag{B.18}$$

and therefore its temperature derivative scales as

$$\partial_\beta \xi \sim L^{5/2}(\log L)^{-3/4}, \tag{B.19}$$

resulting in a ν canonical exponent correction of

$$\nu' = \nu\left[1 - \frac{3}{4}\frac{\nu}{\log(L_2/L_1)}\log\left(\frac{\log L_2}{\log L_1}\right)\right]. \tag{B.20}$$

For the microcanonical ν exponent, $\nu_{\rm m}$, we use that

$$e \sim L^{-1/2}(\log L)^{-3/4}, \tag{B.21}$$

so that

$$\partial_e \xi \sim L^{3/2}(\log L)^{3/4}, \tag{B.22}$$

and

$$\nu'_{\rm m} = \nu_{\rm m}\left[1 + \frac{3}{4}\frac{\nu_{\rm m}}{\log(L_2/L_1)}\log\left(\frac{\log L_2}{\log L_1}\right)\right]. \tag{B.23}$$

Appendix C

Data Analysis: Autocorrelations and Error Estimation

The goal of this appendix is to provide a brief resume of the main ideas for the data analysis of the output of a dynamic Monte Carlo (MC) simulation. For a more detailed study see for example Refs. [7, 115]. Our aim is to describe the modern techniques that avoid the usual error sources in this kind of numerical study.

Given that the output of a dynamic MC simulation is a sequence of system configurations[1], $\{\phi\}_0, \{\phi\}_1, \{\phi\}_2, \ldots, \{\phi\}_N$, we have to take two crucial issues into account:

1. *The initial bias:* We have to start every simulation from a physically unrepresentative configuration (usually "hot", all the spins in random configurations, or "cold" , every spin in the same state). The first configurations are thus not representative of the equilibrium distribution (the Boltzmann weight). There will be an initial transient regime which must be discarded to avoid a systematic source of error. If we discard the $n_{\rm d}$ initial data in estimating the mean value $\langle O \rangle_\beta$ at the inverse temperature β, then:

$$\langle O \rangle_\beta \approx \bar{O} \equiv \frac{1}{N - n_{\rm d}} \sum_{t=n_{\rm d}+1}^{N} O_t \ , \tag{C.1}$$

   where we have distinguished the true mean value $\langle O \rangle$ from its estimate $\bar{O}$.

2. *Error estimates in equilibrium:* The output of every MC simulation must be a confidence interval around the estimated mean value. The true mean value must lie within this interval at a reasonable level of confidence if the correct procedures have been applied. Once equilibrium is reached, correlations between consecutive system configurations make the statistical error a factor $2\tau_{{\rm int},O}$ larger than that of the corresponding independent sampling case, where $\tau_{{\rm int},O}$ is the integrated correlation time of the observable O, see below.

[1] As one does not need to store all the configurations, but only the values of a few functions of them (observables), what one really has is a sequence of numbers $O_0, O_1, O_2, \ldots, O_N$, where O is a generic observable.

Both these issues are related to the same object, namely the *autocorrelation function*.

The Autocorrelation Function

By definition, the equilibrium autocorrelation function of the observable O at time t is [7]:

$$C_{OO}(t) \equiv \langle O_s O_{s+t} \rangle_\beta - \langle O \rangle_\beta^2 \tag{C.2}$$

$$= \sum_Y \sum_X O(Y) \left[[T^t]_{YX} - \frac{e^{-\beta H(Y)}}{Z} \right] \frac{e^{-\beta H(X)}}{Z} O(X) \,, \tag{C.3}$$

where:

- $O(Y)$ is the value of the observable O for the system configuration Y.
- $[T]^t_{YX}$ is the probability of reaching the configuration Y starting from the configuration X in t steps; i.e., it is a sum over all possible paths connecting X and Y in t steps.
- $\exp(-\beta H(Y))/Z$ is the Boltzmann weight of the configuration Y, with β being the inverse temperature, H the Hamiltonian, and Z the partition function.

A normalised form is often used, defined as:

$$\rho_{OO}(t) \equiv \frac{C_{OO}(t)}{C_{OO}(0)} \,. \tag{C.4}$$

Typically, for long times, $C_{OO}(t)$ decays exponentially with time.

The *exponential autocorrelation time* is defined by

$$\tau_{\exp,O} = \lim_{t \to \infty} \sup \frac{t}{-\log \rho_{OO}(t)} \,. \tag{C.5}$$

It is useful to define the maximum over all the measured observables,

$$\tau_{\exp} = \sup_O \tau_{\exp,O} \,. \tag{C.6}$$

In Ref. [115] it is demonstrated that the rate of convergence to equilibrium from an initial non-equilibrium distribution can be bounded in terms of $\tau_{\exp}$. In particular:

$$\left| \sum_Y O(Y) [T^t]_{YX} - \langle O \rangle_\beta \right| \sim e^{-t/\tau_{\exp}} \,, \tag{C.7}$$

From this, it can be said that setting $n_{\mathrm{d}} = 20\tau_{\exp}$ in Eq. (C.1) is enough for all practical purposes. Hence, waiting for this time before starting to save the measurements for averaging, we can avoid the initial bias of the MC simulation. The problem with this approach is the difficulty in estimating $\tau_{\exp}$ in some cases.

Usually the convergence to equilibrium is determined *empirically* by plotting certain observables as a function of time and noting when the initial transient seems to end. This includes the comparison between hot and cold starts. The main objection to this is the possibility of metastability, especially for first-order phase transitions. In such cases the equilibrium appears to be reached but really the system has just settled down into a long-lived metastable region of the configuration space. One has to be extremely careful in these cases, see Chapter 3.

Once in equilibrium, to what extent are the measurements taken in the system representative? This issue reflects the fact that consecutive measurements are usually close in configuration space (and are thus *correlated*) so they do not provide the same information as if they were independent.

We can resolve this question in terms of the *integrated autocorrelation time*, defined as:

$$\tau_{\mathrm{int},O} = \frac{1}{2} + \sum_{t=1}^{\infty} \rho_{OO}(t)\,. \tag{C.8}$$

This time controls the error estimates in MC simulations. In particular, the sample mean

$$\bar{O} \equiv \frac{1}{N} \sum_{t=1}^{N} O_t\,, \tag{C.9}$$

assuming for brevity that the data at $t = 1$ are already good, has a variance

$$\begin{aligned}
\langle (\bar{O} - \langle O\rangle_\beta)^2 \rangle_\beta &= \frac{1}{N^2} \sum_{r,s=1}^{N} \langle (O_r - \langle O\rangle_\beta)(O_s - \langle O\rangle_\beta) \rangle_\beta && \text{(C.10)}\\
&= \frac{1}{N^2} \sum_{r,s=1}^{N} C_{OO}(r-s) && \text{(C.11)}\\
&= \frac{1}{N} \sum_{t=-(N-1)}^{N-1} \left(1 - \frac{|t|}{N}\right) C_{OO}(t) && \text{(C.12)}\\
&\approx \frac{2\tau_{\mathrm{int},O}}{N} (\langle O^2\rangle_\beta - \langle O\rangle_\beta^2)\,. && \text{(C.13)}
\end{aligned}$$

To derive these last relationships, we made use of $C_{OO}(t) = C_{OO}(-t)$ in equilibrium and assumed that N is large enough to neglect $C_{OO}(t)$ for $|t| \sim N$ – recall that $C_{OO}(t) \to 0$ exponentially for increasing t.

Therefore the variance of $\bar{O}$ is a factor $2\tau_{\mathrm{int},O}$ larger that it would be if all the configurations $\{\phi\}_i$ were statistically independent. In other words, the number of effective measurements in a MC simulation of length N is reduced to $N/(2\tau_{\mathrm{int},O})$. Roughly speaking, the error bars will be of order $(\tau_{\mathrm{int},O}/N)^{1/2}$, so that if we want an error bar for our simulation of around 1% precision we will need a run of length $\approx 10000\tau_{\mathrm{int}}$.

Now we will define a more practical estimate of the correlation times [115]. The direct estimate from a run of length N (supposing again that at $t = 1$ the data are

already good) is:

$$\overline{C_{OO}(t)} = \frac{1}{N-|t|}\sum_{s=1}^{N-|t|}(O_s - \bar{O})(O_{s+|t|} - \bar{O})\,, \tag{C.14}$$

$$\overline{\rho_{OO}(t)} = \overline{C_{OO}(t)}/\overline{C_{OO}(0)}\,. \tag{C.15}$$

At first sight, one would estimate the integrated autocorrelation time as

$$\overline{\tau_{\mathrm{int},O}} = \frac{1}{2} + \sum_{t=1}^{N-1}\overline{\rho_{OO}(t)}\,. \tag{C.16}$$

But this is wrong because this estimator has a variance that does not go to zero for large N. Each of the terms $\rho_{OO}(t)$ decreases exponentially with t but is a random variable obtained by averaging $N-t$ data. For $t > \tau_{\mathrm{int},O}$ each $\rho_{OO}(t)$ is very small, but its error is not null. Therefore most of the terms in the definition Eq. (C.16) carry little information but much noise for large t, and there are very many of them. The cure is the truncation of Eq. (C.16) to estimate $\tau_{\mathrm{int},O}$ self-consistently:

$$\overline{\tau_{\mathrm{int},O}} = \frac{1}{2} + \sum_{t=1}^{\alpha\overline{\tau_{\mathrm{int},O}}}\overline{\rho_{OO}(t)}\,, \tag{C.17}$$

where α is a small fixed number, around 6. Clearly $\tau_{\mathrm{int},O}$ is biased, but the contribution of the neglected terms should be negligible (at $6\tau_{\mathrm{int},O}$, it is expected that $\overline{\rho_{OO}(t)} \ll 1$). See [115] for more details about this "automatic windowing" algorithm.

For $\tau_{\mathrm{exp},O}$, one can use two different estimates, see [7]:

$$\overline{\tau_{\mathrm{exp},O_{t,A}}} = \frac{t}{|\log\overline{\rho_{OO}(t)}|}\,, \tag{C.18}$$

$$\overline{\tau_{\mathrm{exp},O_{t,B}}} = \left[\log\left(\frac{\overline{\rho_{OO}(t)}}{\overline{\rho_{OO}(t+1)}}\right)\right]^{-1}. \tag{C.19}$$

The autocorrelation functions decay as pure exponentials, $e^{-t/\tau_{\mathrm{exp},O}}$, for large t. Then both $\overline{\tau_{\mathrm{exp},O_{t,A}}}$ and $\overline{\tau_{\mathrm{exp},O_{t,B}}}$ become equal to $\tau_{\mathrm{exp},O}$. Nevertheless as was found before, the information carried by the signal decreases rapidly with t, and it can not be said which definition will first reach the t-independent region, see [7].

Error Estimation

Having demonstrated that the effective number of measurements is $N/(2\tau_{\mathrm{int},O})$, where $\tau_{\mathrm{int},O}$ is not known accurately, we will now describe the most usual method of obtaining independent quantities: *making data blocks*. This will also allow the estimate of functions of observables, and we will see that the time correlations between different observables can even be beneficial.

Starting from a set of N data, let us form N/b data blocks of size b:

$$O_{b,i} = \frac{1}{b} \sum_{t=(i-1)b+1}^{bi} O_t \,. \tag{C.20}$$

The autocorrelation times for the blocked data are divided by a factor b. The mean value of the block data, $\hat{O}$, is b-invariant, while the error can be estimated (if b is large enough) as for statistically independent data:

$$\overline{\Delta_O^2} = \frac{1}{\frac{N}{b}-1} \left[\frac{b}{N} \sum_{i=1}^{N/b} (O_{b,i})^2 - \left(\frac{b}{N} \sum_{i=1}^{N/b} O_{b,i} \right)^2 \right] . \tag{C.21}$$

The error estimate first grows with b until the data blocks become effectively independent ($b \approx 20\tau_{\mathrm{int},O}$). Then $\overline{\Delta_O^2}$ becomes b-independent (the expression in brackets in Eq (C.21) decreases as $1/b$ but the prefactor grows as b). As can be seen in Ref. [7], an assumption that the data are independent would underestimate the errors by a factor $\sqrt{2\tau_{\mathrm{int},O}}$. Once b is large enough, the error estimate reaches a plateau, but from then on the fluctuations grow as the block size is increased. Therefore N/b should be kept large enough. Typically, a ratio of between 10 and 50 is chosen.

Now we have to consider the crucial issue of the error estimation of *functions* of observables. Let $f(\langle O^{(1)} \rangle_\beta, \langle O^{(2)} \rangle_\beta, \ldots, \langle O^{(R)} \rangle_\beta)$ be a function of R observables (R could be one). The best thing we can do is estimate $f(\{\langle O^{(R)} \rangle_\beta\})$ by $f(\{\overline{O^{(R)}}\})$, although we know that this estimate is biased unless $f(x)$ is a linear function. The estimate of the error could be done by linear error propagation, but when f depends on several observables this may overestimate the size of the errors due to correlations between the observables. For some clear examples of this last point, see Ref. [7].

The fact that correlations can be beneficial is exploited by the *jack-knife* method. This allows one to estimate the error bars of derivative quantities easily and coherently. The procedure is the following [7]:

1. Estimate $f(\langle O^{(1)} \rangle_\beta, \langle O^{(2)} \rangle_\beta, \ldots, \langle O^{(R)} \rangle_\beta)$ by $f(\overline{O^{(1)}}, \overline{O^{(2)}}, \ldots, \overline{O^{(R)}})$.

2. For each observable, form the corresponding block data, as in Eq. (C.20), with large enough b (the same for every observable).

3. Make jack-knife blocks from the blocked data. This means that the i-th jack-knife block is formed by averaging all the blocks formed in the previous step except the i-th. I.e.:

$$O_{JK,b,i}^{(r)} \equiv \frac{1}{\frac{N}{b}-1} \sum_{j \neq i} O_{b,j}^{(r)} \quad , \quad r = 1, 2, \ldots, R \,. \tag{C.22}$$

4. Estimate the function value for the jack-knife blocked observables as

$$f_{JK,b,i} \equiv f(O_{JK,b,i}^{(1)}, O_{JK,b,i}^{(1)}, \ldots, O_{JK,b,i}^{(R)}) \,. \tag{C.23}$$

5. Estimate the variance of the function as

$$\overline{\Delta_f^2} = \left(\frac{N}{b} - 1\right) \left[\frac{b}{N} \sum_{i=1}^{N/b} f_{JK,b,i}^2 - \left(\frac{b}{N} \sum_{i=1}^{N/b} f_{JK,b,i}\right)^2\right] . \tag{C.24}$$

Since the expression in brackets is an average of blocked data, it is smaller than usual. This is the reason for the multiplication (instead of division) by the number of blocks minus one. In the case of correlations between observables, their jack-knife blocks will fluctuate simultaneously, thus reproducing the possible positive effect on the error.

Appendix D

Temperature Extrapolations

Within a canonical Monte Carlo method, the temperature of the system is kept fixed, and all the information about the observable corresponds to the simulation temperature. It is often very desirable to obtain an accurate estimate of a given quantity at a temperature different from the simulated one. This may be the case for example when one tries to obtain the absolute maxima in temperature of some quantities to estimate critical exponents, or when one has to fine-tune some condition as in the quotient method, see Eq. (B.7).

Using the energy histogram of the system at a given temperature, one can obtain accurate information at nearby temperatures. The method was first proposed in [142], and was recovered in [143]. If we are working with disordered systems, the temperature extrapolation must be performed before averaging over the different disorder realizations.

The following formulae allow one to calculate the thermal derivative of an observable, O, and its value at a temperature close to the simulated one:

$$\partial_\beta \overline{\langle O \rangle} = \overline{\partial_\beta \langle O \rangle} = \overline{\left\langle OE - \langle O \rangle \langle E \rangle \right\rangle}\,, \tag{D.1}$$

$$\langle O \rangle (\beta + \Delta\beta) = \frac{\langle O \mathrm{e}^{-\Delta\beta\mathcal{E}} \rangle}{\langle \mathrm{e}^{-\Delta\beta\mathcal{E}} \rangle}\,, \tag{D.2}$$

where $\beta = 1/T$ is the inverse simulation temperature.

Nevertheless, it must be borne in mind that the two above expressions involve a systematic bias whose correction can become critical. We shall follow the approach proposed in [144]. Using Eq. (D.1) with N different measurements, we are really obtaining

$$\overline{\left(1 - \frac{2\tau}{N}\right) \partial_\beta \langle O \rangle}\,, \tag{D.3}$$

where τ represents the integrated autocorrelation time, see Appendix C, between the observable O and the energy. Since the τ value is different for different samples, we shall have to obtain the disorder average.

Let us demonstrate the validity of Eq. (D.3). Consider two observables, O^a and O^b, and, using N measurements, calculate their connected correlation

$$\langle O^a O^b \rangle - \langle O^a \rangle \langle O^b \rangle\,, \tag{D.4}$$

Since the mean value of O^a is by definition

$$\langle O^a \rangle = \frac{1}{N} \sum_{i=1}^{N} O_i^a \,, \tag{D.5}$$

Eq. (D.4) can be written as

$$\frac{1}{N} \sum_{i=1}^{N} O_i^a \, O_i^b - \frac{1}{N^2} \sum_{i=1}^{N} \sum_{j=1}^{N} O_i^a \, O_j^b \,, \tag{D.6}$$

where the latter term is more complex given that the measurements of the two observable may be correlated. We can rewrite it as

$$\sum_{i=1}^{N} \sum_{j=1}^{N} O_i^a \, \mathcal{O}_j^b = \sum_{i=1}^{N} \sum_{t=1-i}^{N-i} O_i^a \, O_{i+t}^b \,. \tag{D.7}$$

Recall that the behaviour of the correlation between two observables is for large $|t|$:

$$\langle O_i^a \, O_{i+t}^b \rangle \equiv C_t = \langle O^a \rangle \langle O^b \rangle + C_0 \exp \left[-\frac{|t|}{\tau} \right] \,, \tag{D.8}$$

where

$$C_0 = \langle O^a \, O^b \rangle - \langle O^a \rangle \langle O^b \rangle \,. \tag{D.9}$$

As we are summing over i, we can replace $O_i^a \, O_{i+t}^b$ by its mean value, and in order to perform the sum we shall take $N \gg |t|$. From the exponential decay with $|t|$ in Eq. (D.8) we can extend the limit of the sum to infinity, and simplify things by replacing the sum with an integral. Therefore

$$\sum_{i=1}^{N} \sum_{j=1}^{N} O_i^a O_j^b = N^2 \left(\langle O^a \rangle \langle O^b \rangle \right) + N C_0 \int_{-\infty}^{+\infty} \mathrm{d}t \;\; \exp \left[-\frac{|t|}{\tau} \right] \,. \tag{D.10}$$

But the integral is 2τ, see again Appendix C, and replacing C_0 by the expression (D.9) one recovers Eq. (D.3).

Thus it has been shown that the derivative of the mean value of an observable is subject to a systematic bias of order $2\tau/N$, although corrections of higher order can be expected. This systematic error is not considered in general in other MC studies mainly because it is usually masked by the statistical error, of order $1/\sqrt{N}$, that is far larger than the bias.

Nevertheless, in a dilute model the situation is more complicated because there are two parameters involved: the number of measurements that we perform within each realization of the disorder (Ising average), denoted by N_I, and the number of realizations of the disorder (sample average), N_M.

We can associate with every observable σ_M, representing the deviation of this observable between different samples, and σ_I, representing the average of the deviations within each sample. Assuming statistical independence between different

samples (this is the case if there are no correlations in the random numbers) and independence between different measurements within a sample (possible using a cluster method), the variance of the mean value of an observable can be written as

$$\sigma_T^2 = \frac{1}{N_M}\left(\sigma_M^2 + \frac{\sigma_I^2}{N_I}\right) . \tag{D.11}$$

From this equation the optimal choice of N_I and N_M can be deduced if we want to optimise the simulation time to obtain a given error bar. Note that the simulation time is proportional to $N_M N_I$, because the simulation spends an approximately fixed portion of time taking measurements. For this reason the optimal value of N_I can not be much larger than σ_I^2/σ_M^2, i.e., N_I is limited by this latter expression. Therefore the best procedure to improve the statistical errors is to increase the number of samples, performing a not too large number of measurements within each one. Numerous studies on dilute models have avoided tackling this question by working in general in the regime $N_I \gg N_M$. Besides, a value of N_I that is large does not improve the result for the deviation σ_M^2 because it is only suppressed by a factor N_M.

However, if we need to obtain the temperature derivatives there is a term in the statistical error proportional to $1/\sqrt{N_M}$. If this number is of order $1/N_I$ (systematic error in the extrapolation) a detectable bias appears. Unfortunately this is indeed the scenario in some cases. For example for the Heisenberg model, see Sec. 4.4.1, we used $N_M = 10^4$ and $N_I = 100$ measurements per sample.

As a result it is necessary to find some algorithm to obtain correct results from the simulation data. The first possibility is to use fully independent measurements (by assuring $2\tau = 1$) for each disorder realization. In such a case, recalling Eq. (D.3), we could build a correct unbiased estimator by multiplying by the factor $1/(1-1/N_I)$ in the case of the derivative and by the corresponding quantity in the case of the temperature extrapolations. However this is too expensive in simulation effort, due both to the need for too wide a time interval between measurements and to the fluctuations of τ between different samples, which forces one to disregard too many measurements in samples with τ smaller than the maximum. This makes the use of this approach inefficient.

Another possibility, see Ref. [51], is to correct the systematic bias by splitting the measurements into statistically independent groups. In this way, by multiplying estimators from the different groups, correct values of $\langle O^a\rangle\langle O^b\rangle$ can be obtained. Nevertheless, in a real situation independence is complicated because, in general, consecutive measurements in MC time are used to form these groups.

In this work the approach that will be used for the dilute models, see again Ref. [51], is to extrapolate to $N_I \to \infty$ by using estimators coming from different values of N_I. We will work with $2\tau \gtrsim 1$, but the equality is not essential, as we will demonstrate in the following.

In particular, for each disorder realization we can calculate the derivative with the entire MC history (N_I measurements), obtaining the estimator, y_1, whose systematic error is proportional to $2\tau/N_I$. If we consider the two contiguous halves of the total history, we obtain two estimates for the derivative that, once averaged, produce

the estimator, y_2, whose systematic error is proportional to $4\tau/N_I$. If the history is divided into four, the derivative in each part is obtained and the average of the four parts is calculated, the estimator, y_3, will have a bias of $8\tau/N_I$. In Fig. D.1, obtained in Ref. [51], is shown the observable $\partial_\beta \chi$ for a four-dimensional site-diluted Ising model in a system with $L = 48$, $p = 0.5$. The estimator y_1 is plotted, but using only one of every k measurements of the history and averaging the results. It is obvious that doing so reduces the τ by a factor k, as also is the case for the number of measurements, N_I. Therefore the bias, proportional to $2\tau/N_I$, remains constant. This effect is maintained up to $k \approx 10$. The correlation time between energy and χ, τ, was about eight measurements.

Using the y_i values, linear and quadratic extrapolations to $N_I \to \infty$ in the variable $1/N_I$ can be obtained with the form

$$y_i = y_\infty + \frac{A}{N_I} + \frac{B}{N_I^2} \,. \tag{D.12}$$

For the linear case ($B = 0$) we obtain

$$y_L = y_\infty = 2y_1 - y_2 \,, \tag{D.13}$$

and for the quadratic case

$$y_Q = y_\infty = \frac{8}{3} y_1 - 2y_2 + \frac{1}{3} y_3 \,. \tag{D.14}$$

The procedure is repeated for each sample and averaged over the disorder. The value y_Q is used to verify that the higher-order effects are negligible compared with the statistical error of the extrapolation in temperature. If this were not the case, to obtain measurements of the observable at the shifted temperature it would be advisable to make another simulation closer to that point.

The estimate for the temperature extrapolations of the $O(3)$ model was obtained in this work in a similar way, see Chap. 4, Fig. 4.1.

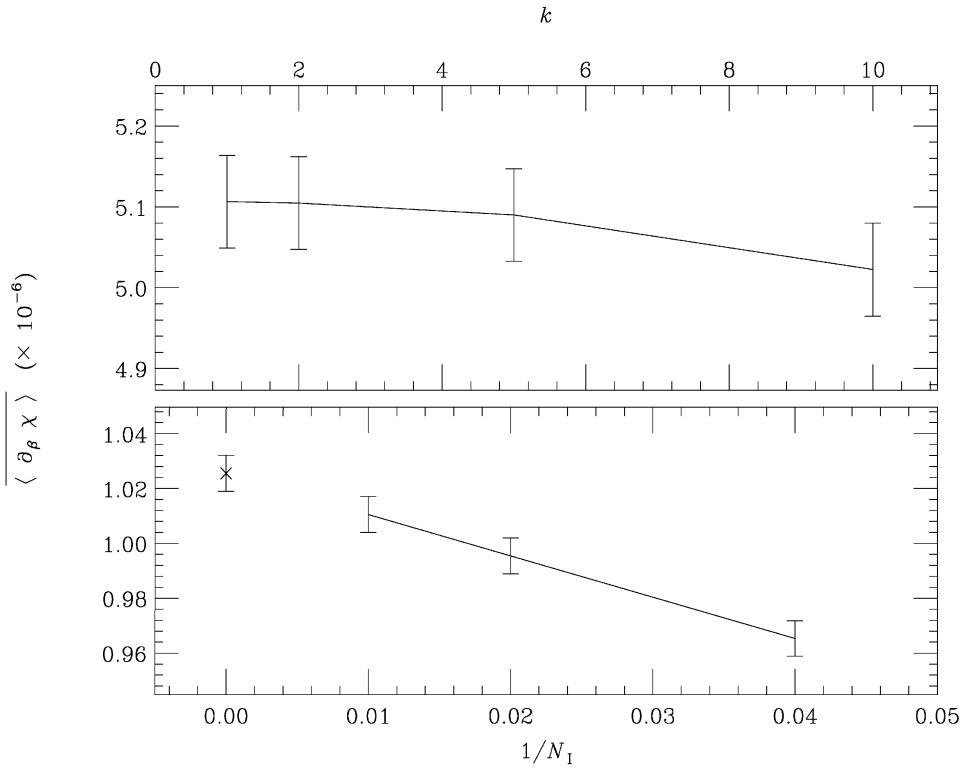

Figure D.1: *Upper part:* Sample average of the estimator y_1 corresponding to $\partial_\beta \chi$ considering just one of each k measurements, for a four-dimensional Ising model on an $L = 48$ lattice, with $p = 0.5$ and $\tau \approx 8$. *Lower part:* Sample average of y_1, y_2, and y_3 as a function of the inverse of N_I, on a lattice, with $L = 32$, $p = 0.5$, and $\tau \approx 0.8$. Figure taken from Ref. [51].

Appendix E

The Maxwell Construction

Let us consider a system with action $S[\psi]$, depending on the local variables ψ, coupled with a source J. If $\phi(\beta, J)$ is the Gibbs free energy[1] and $O(x) \equiv O(\psi(x))$ is a generic observable then

$$e^{-V\phi(\beta,J)} = \int \mathrm{d}[\psi] e^{-\beta S[\psi] - J\int \mathrm{d}^{\mathrm{D}}x\, O(x)}\,, \tag{E.1}$$

where V is the system volume and D is the spatial dimensionality. The equation of state is

$$\frac{\partial\phi}{\partial J} = \frac{1}{V}\int \mathrm{d}^{\mathrm{D}}x\, O(x) \equiv \overline{O}(J)\,, \tag{E.2}$$

relating the observable, $\overline{O}$, with its conjugate variable, J.

In the neighbourhood of the phase transition, the function $\overline{O} = \overline{O}(J)$ may be discontinuous. In other words, there may exist a range of $\overline{O}$ values that do not correspond to any J value, see Fig. E.1.

An effective potential associated with the observable O can be defined as:

$$e^{-V\Gamma(\overline{O})} = \int \mathrm{d}[\psi]\, e^{-\beta S[\psi]}\, \delta\left(\frac{1}{V}\int \mathrm{d}^{\mathrm{D}}x\, O(x) - \overline{O}\right)\,, \tag{E.3}$$

where δ is the Dirac delta function. Then it can be obtained

$$e^{-V\phi(\beta,\,J)} = \int \mathrm{d}\overline{O}\, e^{-V[\Gamma(\overline{O})+J\overline{O}]}\,. \tag{E.4}$$

But for a large volume this integral is dominated by the saddle point

$$\frac{\partial\Gamma}{\partial\overline{O}} = -J\,, \tag{E.5}$$

and we can conclude that $\phi(\beta, J)$ is the Legendre transform of Γ:

$$\phi(\beta, J) = \Gamma(\overline{O}) + J\overline{O}\,. \tag{E.6}$$

[1] We have included in its definition the β term.

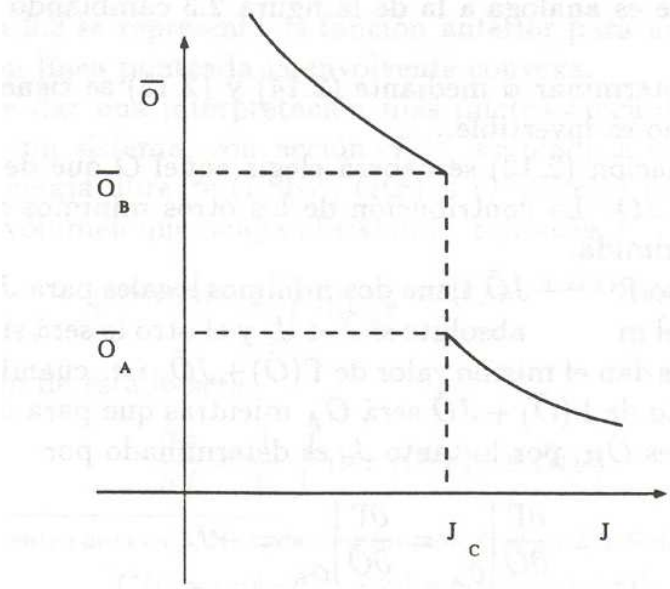

Figure E.1: Lack of continuity of the function $\overline{O} = \overline{O}(J)$ at a first-order phase transition.

In Eq. (E.6), the $\overline{O}$ must be chosen that produces a global minimum of $\Gamma(\overline{O}) + J\overline{O}$. The contribution of all other minima will be exponentially suppressed. In general $\Gamma(\overline{O}) + J\overline{O}$ has two local minima. One will be the absolute minimum for $J < J_c$, and the other will be that corresponding to $J > J_c$. Recall that $\overline{O} = \overline{O}(J)$ may be discontinuous.

The condition for a minimum located at $\overline{O}$ is

$$\frac{\partial}{\partial \overline{O}} \left(\Gamma(\overline{O}) + J\overline{O} \right) = 0 \,. \tag{E.7}$$

Let us define the two local minima as:

$$\min_{J<J_c} [\Gamma(\overline{O}) + J\overline{O}] \equiv \overline{O}_A \,, \tag{E.8}$$

$$\min_{J>J_c} [\Gamma(\overline{O}) + J\overline{O}] \equiv \overline{O}_B \,. \tag{E.9}$$

Therefore

$$\left. \frac{\partial \Gamma}{\partial \overline{O}} \right|_{\overline{O}_A} = \left. \frac{\partial \Gamma}{\partial \overline{O}} \right|_{\overline{O}_B} = -J_c \,. \tag{E.10}$$

Just at J_c both minima will result in the same value of $\Gamma(\overline{O}) + J\overline{O}$, i.e.,

$$\Gamma(\overline{O}_A) + J_c \overline{O_A} = \Gamma(\overline{O}_B) + J_c \overline{O_B} \,. \tag{E.11}$$

Given that

$$\Gamma(\overline{O}) = -\int_{\text{Cte}}^{\overline{O}} \mathrm{d}O \, J(O) \,, \tag{E.12}$$

Eq. (E.11) can be written as

$$\int_{\overline{O}_A}^{\overline{O}_B} \mathrm{d}O\, J(O) - J_c(\overline{O}_B - \overline{O}_A) = 0\,, \tag{E.13}$$

which implies that the shaded areas in Fig. E.2 must be equal (in absolute value). This represents the well-known form of the Maxwell construction.

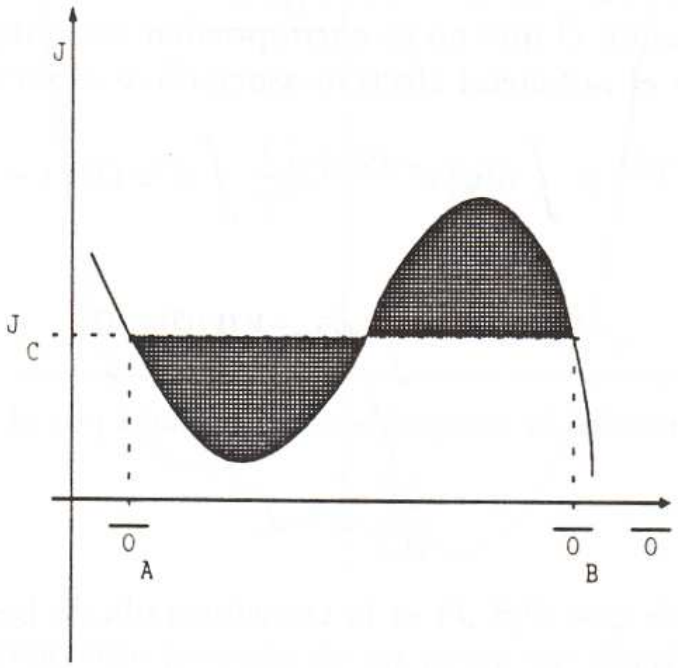

Figure E.2: Usual form of the function $J = J(\overline{O})$. Also shown is the Maxwell construction.

Appendix F

Lee-Yang Zeros

In 1952 T. D. Lee and C. N. Yang, as part of their study of the phenomenon of spontaneous symmetry breaking, wrote two impressive papers [138]. In analysing the behaviour of a lattice gas (which is equivalent to an Ising model in a magnetic field), they approached the problem of its phase transition in an absolutely novel way focusing on finding the zeros of the partition function in terms of an external field allowed to take complex values. With this new approach, the dimension, size, structure, and periodicity of the lattice play no part at all in the main result.

Their starting point is that for a real (inverse) temperature, β, the partition function of the finite system is a polynomial in the activity $\exp(-2h)$, where h is the external field. Since all the coefficients of the polynomial are positive, none of their roots can be on the real positive axis, but are in general complex.

Lee-Yang Theorem

The discovery of Lee and Yang is that the zeros of the partition function are all located on the unit circle of the complex activity plane, or equivalently on the imaginary h-axis. This was originally demonstrated for an Ising system with ferromagnetic interactions (with no need for any limit to first nearest neighbours) although the result is valid for more general models [145].

The distribution of the zeros on the unit circle will determine whether or not a phase transition exists. As the number of spins, N, approaches infinity, if the zeros do not condense onto the positive real axis the free energy, F, will remain analytic and no phase transition exists at the given β; otherwise, if the zeros condense onto the real positive axis a phase transition will exist at this $\beta = \beta_c$.

We will use the demonstration of the theorem described in [146] including the derivation of the magnetisation of the system from the angular distribution of roots on the unit circle. We will focus on a general Ising model defined on a graph of N sites (vertices of the graphs) with at most one link joining each pair of vertices, which are then defined as neighbours. The total number of links is L.

The partition function for N spins, σ_i, is:

$$Z_N = \frac{1}{2^N} \sum_{\sigma_i=\pm 1} \exp\left(\beta \sum_{(ij)} \sigma_i \sigma_j + \sum_i h_i \sigma_i \right) , \tag{F.1}$$

where $\sum_{(ij)}$ is a sum over all links and h_i denotes the magnetic site-dependent field at the site i (strictly the true external field is proportional to h_i/β). Let us define

$$\rho_i = e^{-2h_i} \qquad ; \qquad \tau = e^{-2\beta} . \tag{F.2}$$

Then the partition function can be recast in the form

$$Z_N = \frac{1}{2^N} \exp\left(\beta L + \sum_i h_i \right) P(\tau, \rho_i) , \tag{F.3}$$

where P is a polynomial in τ and ρ obtained as

$$P = \sum_{\sigma_i=\pm 1} \exp\left[\beta \sum_{(ij)} (\sigma_i \sigma_j - 1) + \sum_i h_i (\sigma_i - 1) \right] . \tag{F.4}$$

For τ and ρ_i real and positive, P is always positive and cannot vanish. We assume in the following $0 < \tau < 1$, i.e., we are in the ferromagnetic regime.

It is easy to find that the polynomials P corresponding to the simplest graphs are:

$$P_{12} = 1 + \tau(\rho_1 + \rho_2) + (\rho_1 \rho_2) \tag{F.5}$$

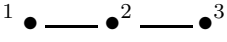

$$P_{123} = (1 + \rho_1 \tau)(1 + \rho_3 \tau) + \rho_2 (\tau + \rho_1)(\tau + \rho_3) \tag{F.6}$$

It can then be seen that P is a polynomial of degree one in each ρ_i individually and of degree N in all of them.

We will analyse how the polynomials are generated by building a graph step by step. First, one observes that for any disjoint union of subsets of the graph, the polynomial P factorizes, $P = P_1 P_2$, where P_1 and P_2 are the corresponding polynomials of the two separate subsets. With this in hand, we generate a new polynomial by identifying a site a from the subset 1 with a site b from subset 2. We call $P_{(12)}$ the corresponding (contracted) polynomial of the union. Since P_1 is linear in ρ_a and P_2 is linear in ρ_b we can write

$$P_1 = A_+ + \rho_a A_- \qquad ; \qquad P_2 = B_+ + \rho_b B_- , \tag{F.7}$$

where $A_+(B_+)$ correspond to the contribution with spin up, $\sigma_a = +1$ ($\sigma_b = +1$), and $A_-(B_-)$ correspond to the contribution with spin down, $\sigma_a = -1$ ($\sigma_b = -1$). When the identification of a and b is made, a new activity variable, ρ_{ab}, is attached to the new site and we have the following contraction process, see Fig. F.1:

$$P_1 P_2 \equiv A_+ B_+ + \rho_a A_- B_+ + \rho_b A_+ B_- + \rho_a \rho_b A_- B_- \quad \longrightarrow \tag{F.8}$$

$$P_{(12)} \equiv A_+ B_+ + \rho_{ab} A_- B_- . \tag{F.9}$$

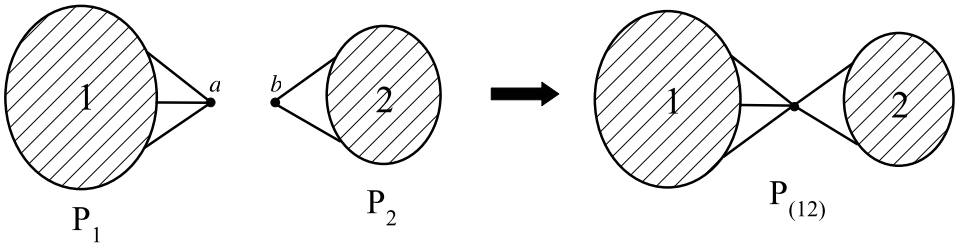

Figure F.1: The contraction process obtained by identifying a and b from two disjoint subsets of the whole graph.

Using this process, one can obtain for example the expression of Eq. (F.6) by joining two unconnected two-vertex graphs, such as that of Eq. (F.5), and by identifying two of the four points. It is a good exercise to obtain the expression for a cyclic graph of three vertices by first obtaining that corresponding to a graph of four vertices (by joining a graph of two with a graph of three) which is

$^1\bullet\!\!-\!\!-\bullet^2\!\!-\!\!-\bullet^3\!\!-\!\!-\bullet^4$

$$\begin{aligned} P_{1234} \;=\; & 1+\tau\{\rho_1[1+\rho_2(1+\rho_3)]+\rho_4[1+\rho_3(1+\rho_2)]\}+ \\ & \tau^2[\rho_1\rho_4(1+\rho_2+\rho_3)+\rho_2(1+\rho_3)+\rho_3]+ \\ & \tau^3(\rho_1\rho_3+\rho_2\rho_4)+\rho_1\rho_2\rho_3\rho_4\,, \end{aligned} \tag{F.10}$$

and then identifying the outer vertices (1 and 4 in the above equation) to obtain for the cyclic graph:

$$P_{\rm cyclic} = 1+\tau^2(\rho_1+\rho_2+\rho_3+\rho_1\rho_2+\rho_1\rho_3+\rho_2\rho_3)+\rho_1\rho_2\rho_3\,. \tag{F.11}$$

The contraction process can be applied to a single connected part, where at first the sites a and b are different, then they are identified as a single site ab with activity variable ρ_{ab} and

$$P \equiv A_{++}+A_{-+}\rho_a+A_{+-}\rho_b+A_{--}\rho_a\rho_b \quad\longrightarrow\quad P_{ab}\equiv A_{++}+\rho_{ab}A_{--}\,. \tag{F.12}$$

As in the initial set, in the contracted graph no pair of vertices can be joined by more than one link.

Thus we have demonstrated that the contraction process allows the polynomial P of any arbitrary graph to be obtained by starting from the elementary result of the simplest graph of two vertices joined by a link. In this case, from Eq. (F.5), the zero of the polynomial is obtained for:

$$\rho_1 = -\frac{1+\tau\rho_2}{\tau+\rho_2}\,, \tag{F.13}$$

which defines a one-to-one mapping between the complex planes ρ_1 and ρ_2. For τ real it leaves the unit circle invariant while for $0<\tau<1$ exchanges the interior and the exterior of this circle. Therefore it can be stated that if $|\rho_1|<1$ and $|\rho_2|<1$, or $|\rho_1|>1$ and $|\rho_2|>1$, the polynomial can not vanish.

The previous property for a graph of two vertices is generalised in the following: For an arbitrary graph, if all ρ_i lie inside, or all ρ_i lie outside the unit circle, P is different from zero.

To demonstrate the foregoing statement, it is sufficient to verify that the property survives the contraction process. Let us assume that for a given graph $P(\rho_i) \neq 0$ when $|\rho_i| < 1$ for all i, and apply the contraction process: When the dependence on the two points (a and b) to be identified is made explicit, P is given by Eq. (F.12), while if the identification is already made P_{ab} is a function only of the subset $\{\rho_i\} - \{\rho_a, \rho_b\}$ and a new variable ρ_{ab}. We fix all the ρ_i's distinct from ρ_a and ρ_b within the unit circle. We want to show that $|A_{++}| > |A_{--}|$, in which case P_{ab} will be non-vanishing for $|\rho_{ab}| < 1$. Recalling that $P \neq 0$ for $|\rho_a| < 1$, $|\rho_b| < 1$, the polynomial $A_{++} + \rho(A_{+-} + A_{-+}) + \rho^2 A_{--}$ must have its two roots equal to or greater than unity, which means that $|A_{++}| \geq |A_{--}|$. Thus P_{ab} is different from zero when all its ρ's are within the unit circle, and this property holds for any graph.

If we set now all $\rho_i \equiv \rho$, corresponding to a uniform external field, from the symmetry property under reversal of the field $h \to -h$, $\rho \to \rho^{-1}$, and $Z(h) = Z(-h)$, we have:

$$\mathrm{e}^{+Nh} P(\tau, \rho) = \mathrm{e}^{-Nh} P(\tau, \rho^{-1}) \,, \tag{F.14}$$

or equivalently:

$$P(\tau, \rho) = \rho^N P(\tau, \rho^{-1}) \,. \tag{F.15}$$

As a result if $P \neq 0$ for $|\rho| < 1$, it follows that also $P \neq 0$ for $|\rho| > 1$. The Lee-Yang theorem has thus been demonstrated – the partition function can (and does) only vanish on the unit circle $|\rho| = 1$.

Distribution of Roots on the Unit Circle

Using the definition of P in Eq. (F.4) we can obtain the two extreme cases of the distribution of the zeros on the unit circle:

- For a system at infinite temperature ($\tau = 1$):

$$P(\tau, \rho) = P(1, \rho) = (1 + \rho)^N \,. \tag{F.16}$$

- For a system at zero temperature ($\tau = 0$):

$$P(\tau, \rho) = P(0, \rho) = 1 + \rho^N \,. \tag{F.17}$$

Then, decreasing the temperature from infinity, one goes from a degenerate zero with multiplicity N located at $\rho = -1$ to a uniform distribution $\rho_k = \mathrm{e}^{i\pi(2k+1)/N}$. In addition, if N remains finite, no zero will be located on the real positive axis ($\rho = 1$, $h = 0$).

Let us obtain the general result for a lattice of N sites, with coordination number q, see footnote in Appendix A, when taking the infinite volume limit. According to Eq. (F.1), the free energy per site in a uniform field is:

$$F \equiv \frac{1}{N} \ln Z = \frac{1}{2} q\beta + h + \ln 2 + \lim_{N \to \infty} \frac{1}{N} \ln P_N(\tau, \rho) \,, \tag{F.18}$$

where we have used that $L = Nq/2$, with L being the total number of links in the lattice. P_N can be factorized in terms of its roots

$$P_N = \prod_{a=1}^{N} \left(1 - \frac{\rho}{\rho_a(\tau)}\right) . \tag{F.19}$$

As was demonstrated in the previous section, the zeros will accumulate for $N \to \infty$ on the unit circle, $\rho = e^{i\varphi}$, with a (τ-dependent) angular density $N\mu(\varphi)$ satisfying

$$\mu(\varphi) = \mu(-\varphi) \geq 0 \qquad ; \qquad \int_{-\pi}^{+\pi} \mathrm{d}\varphi \mu(\varphi) = 1 \,, \tag{F.20}$$

where the above property is a consequence of the invariance under field reversal, $h \to -h$. Making the change

$$\frac{1}{N} \ln P_N(\tau, \rho) = \frac{1}{N} \sum_{a=1}^{N} \ln \left(1 - \frac{\rho}{\rho_a(\tau)}\right) \longrightarrow \frac{1}{N} \int_{-\pi}^{\pi} \mathrm{d}\varphi N\mu(\varphi) \ln \left(1 - \frac{\rho}{\rho(\varphi)}\right) , \tag{F.21}$$

and using the symmetry property of the angular distribution to join the contributions of the conjugate zeros we arrive at

$$F = \frac{1}{2} q\beta + h + \ln 2 + \frac{1}{2} \int_{-\pi}^{+\pi} \mathrm{d}\varphi \mu(\varphi) \ln(1 + \rho^2 - 2\rho \cos\varphi) \,, \tag{F.22}$$

which is valid over the whole range $0 < \tau < 1$. Below the critical temperature, where the support of $\mu(\varphi)$ is the full circle, this defines in general two different analytic functions, one for $|\rho| < 1$ and another for $|\rho| > 1$. At $\rho = 1$ ($h = 0$), F is continuous. Nevertheless, let us consider the behaviour of its derivative with respect to h, i.e. the magnetisation, as the temperature varies. By definition

$$M = \frac{\partial F}{\partial h} = 1 + \int_{-\pi}^{+\pi} \mathrm{d}\varphi \mu(\varphi) \frac{\partial}{\partial h} \left[\ln(1 - \rho \mathrm{e}^{-i\varphi})\right] , \tag{F.23}$$

but

$$\frac{\partial}{\partial h} = \frac{\partial \rho}{\partial h} \frac{\partial}{\partial \rho} = -2\rho \frac{\partial}{\partial \rho} \,, \tag{F.24}$$

thus

$$M = 1 + 2 \int_{-\pi}^{+\pi} \mathrm{d}\varphi \mu(\varphi) \frac{\rho}{\mathrm{e}^{i\varphi} - \rho} = \int_{-\pi}^{+\pi} \mathrm{d}\varphi \mu(\varphi) \frac{1 + \rho \mathrm{e}^{-i\varphi}}{1 - \rho \mathrm{e}^{-i\varphi}} \,, \tag{F.25}$$

$$= \int_{-\pi}^{+\pi} \mathrm{d}\varphi \mu(\varphi) \frac{1 - \rho^2}{1 - 2\rho \cos\varphi + \rho^2} \,, \tag{F.26}$$

where we made use of the normalisation of $\mu(\varphi)$, Eq. (F.20). The magnetisation vanishes as $h \to 0$ ($\rho \to 1$) for $\tau > \tau_\mathrm{c}$ and becomes discontinuous for $\tau < \tau_\mathrm{c}$. The above equation is not zero for $\rho = 1$ only if $\cos\varphi = 1$. Therefore the value of the

magnetisation is directly related to the value of the density of zeros on the real positive axis ($\varphi = 0$), as a simple contour integration summing the residues shows:

$$\tau < \tau_{\mathrm{c}} \qquad ; \qquad M_{\pm} \equiv \lim_{h \to \pm 0} M = \pm 2\pi\mu(0) \tag{F.27}$$

We have therefore demonstrated that in the Thermodynamic Limit the spontaneous magnetisation is directly related to the existence of zeros on the real positive axis.

Appendix G

IBERCIVIS

During the year 2007, the BIFI (Institute for Biocomputation and Physics of Complex Systems) and the National Fusion Laboratory of the CIEMAT (Centro de Investigaciones Energéticas, Medioambientales y Tecnológicas), collaborating with the city council of Zaragoza (Spain), leadered the ZIVIS project. The scope of the project was to develop a volunteer supercomputing platform, based on individual computers located in both private homes and public buildings, to be used by the scientific community in the University of Zaragoza. This network of individual computers would make it possible to perform calculations as a single installation. The project converted Zaragoza into the first city with a large and stable computing structure based only on the volunteer effort of its citizens in a non-profit contribution to science and research. The scientific goal of the project was the analysis of plasma trajectories in the next-generation nuclear fusion reactors.

The ZIVIS project was based on the BOINC (Berkeley Open Infrastructure for Network Computing) software. BOINC was originally developed in the *SETI@home* project for analysing the electromagnetic radiation received from outer space in the search for extra-terrestrial intelligence. The software every volunteer downloaded has the form of a simple-to-instal program (client) that works as a screensaver during idle times of the computer (on average, some 80% of total CPU time). This means that the user does not notice any inconvenience when using the computer. A server sends tasks via Internet to the clients, which return the results of the computations as they are performed and when their Internet connection is enabled.

ZIVIS was an impressive success that even took its promoters aback. Around 3000 volunteers offered more than 5000 computers resulting in around 850 000 hours of CPU time. It allowed the analysis of more than 4.2×10^6 ion trajectories. During the short life of the project (40 days), it achieved a performance comparable with a large "traditional" supercomputing facility (in fact it became one of the five most important supercomputing facilities in Spain).

After the marvellous experience of ZIVIS, and the interest it raised in the rest of the country, an extension of the project to a higher level was designed. The result was called IBERCIVIS [147]. It was predicted that it would include more than 50 000 nodes (only in Spain) resulting in the largest computer of this kind all around the world. The project was officially launched in June 2008 and it has helped the

scientific community since then. The project is becoming a major achievement both scientifically (now six applications are producing high-precision numerical results) and socially (more than 6000 users are sharing their computers and getting involved with scientific research daily). It differs from ZIVIS in some major points:

- There is not just one scientific application running within IBERCIVIS. Scientists all around the world are invited to use the infrastructure created to run their programs. The "machine" is an open structure where any research group could in principle execute their programs. The diagram of the process an application must follow to run in IBERCIVIS is outlined in Fig. G.1. While at first IBERCIVIS started just running three different applications (plasma trajectories in fusion reactors, protein folding, and phase transitions in disordered systems), it is today running simultaneously six scientific programs (the former three plus neuronal amino acid simulations, adsorption in porous media, and light behaviour at the nanoscale) [147]. Every volunteer can choose which application they prefer to run on their computer.

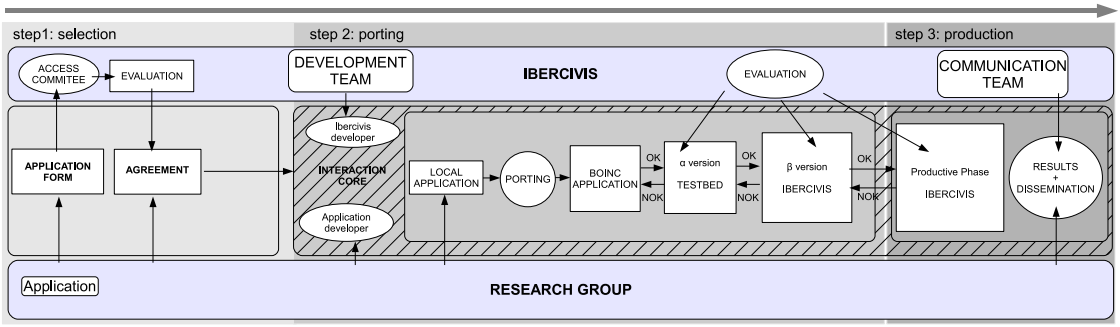

Figure G.1: An IBERCIVIS application road map from the beginning of the collaboration up to the dissemination of the results.

- IBERCIVIS is not a temporary project (unlike ZIVIS or many other BOINC-based volunteer computing projects), so it will be possible to submit applications indefinitely. This implies that IBERCIVIS is seen by scientists as a stable structure like traditional supercomputing centres on which they can run their programs via a user-friendly interface with a typical queueing system, launch their simulations from their personal computers, and receive the output on a special server with high storage capability.

Advantages and Disadvantages versus Other Structures

On the one hand, the strong points of the project are the following:

- Apart from the huge scientific interest that nowadays every supercomputing facility produces, this one has the additional feature of its extremely low cost.

As it mainly uses existing infrastructure (both computers and networks), it only requires the effort of the development and support of the specific software and servers, apart from an effort in publicity to persuade people to join the project (for example, there are periodically competitions between individual clients or between teams of clients with prizes for the winners).

- It provides an excellent way for bringing science close to people; the best way to make someone interested in something is to get them involved with it. People feel themselves to be part of the solution of a hard research problem and learn about the subject. Channels of communication can be established between volunteers and scientists through blogs and social networks [147]. In this way, the most advanced scientific knowledge is spread to society using modern information technologies.

On the other hand, the main objections to the project, and generally to any kind of distributed volunteer computation, are the following:

- Every node of the supercomputing facility is located, in principle, away from other nodes making the communication between nodes very expensive. This fact makes direct parallelisation of the computing problem impossible if communication between nodes is a must. The range of applicability is therefore lower than for "one-room" supercomputers. Nevertheless, there exists a large class of problem for which communication between nodes is irrelevant. These are the so-called *embarrassingly parallel problems*. Within this class, problems can be split into independent simulations whose outputs can be joined later.

- Given that all the data necessary for the job must be transferred to the volunteer's computer via the Internet, the input/output of the program cannot be too massive. Otherwise, it would interfere with the volunteers' network traffic and they would naturally become upset. Typically the size of the transfered I/O files should not be greater than a few megabytes.

- Volunteers' computers are not as stable as computers within a traditional supercomputing facility – they are more likely to be restarted or even turned off. Therefore, in order to increase the probability for a task to be finished, a long computation (say of a week) must be divided into short portions (say of one hour). This produces an increase both in the network traffic and in the probability of corruption of transferred data as they undergo several iterations from computer to computer. The implementation of a bulletproof system for the validation of the output of each task becomes crucial in order to ensure reliability of the final data.

The Numbers of the Project

As was said before, the project is being a success both in scientific results and in citizen contributions. The number of users and of available nodes are both increasing

continuously, see Fig G.2. The number of registered users is today (May 2009) around 11 000 and every day around 5500 of them share their computers with the scientists. The cluster equivalence of the IBERCIVIS structure is currently of 900 nodes located in a classical supercomputing facility.

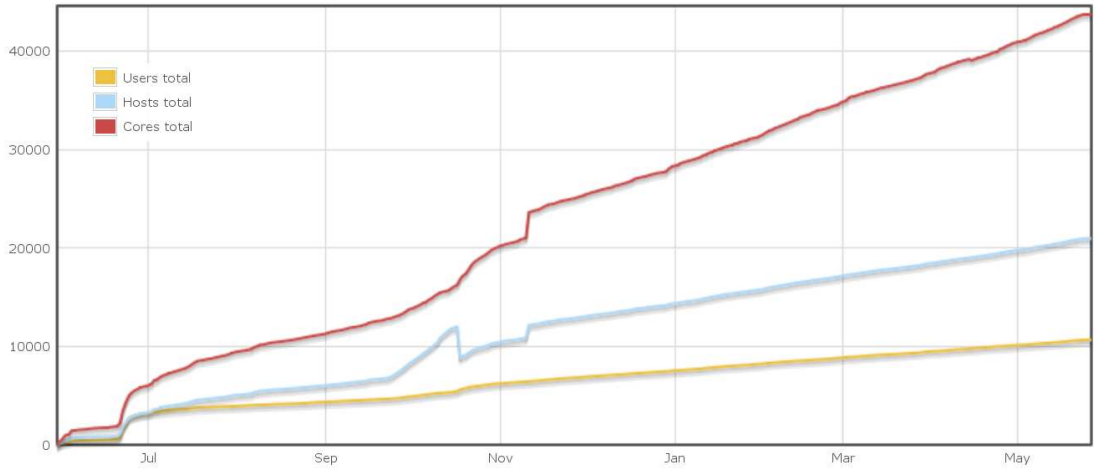

Figure G.2: Evolution in time (from June 2008 to June 2009) of the number of volunteers, computers, and cores involved in the project.

Only during the project's first year it has produced around eight millions hours of CPU time. The total economic cost has been around 270 000 euros, which is not too much taking into account that the first year of life will be surely the most expensive.

At present, six research groups are running simultaneously on the platform, and three new applications are in the porting process. This is indicative of the interest that the project is producing in the scientific community.

The publicity campaign of the project has also been really important. Apart from appearances in newspapers, magazines, and TV [147], more than 200 000 entries can be found using the Google search engine for the word "ibercivis".

Our Experience

In our case we have been using IBERCIVIS for approximately a year to simulate disordered magnetic systems defined in lattices through Monte Carlo methods. In particular, we have studied the three-dimensional eight-state Potts model [82] in the presence of dilution. The results of these simulations are presented in Sec. 3.4.3.

We started running on IBERCIVIS from its earliest stages (around May 2008) so that we have followed all the evolutional process of the project, thus suffering its teething problems but also experiencing its gratifying educational advances.

Our starting point was code written in C that we had been running during the previous year on different supercomputing facilities. The code was neither too complex nor did it make use of any exotic C libraries – facts which made the porting

process simpler, ensuring compatibility between the different platforms of the volunteer's computers (Windows, Mac, or Linux operating systems with 32 or 64 bit processor architectures).

Our application is the perfect example of an embarrassingly parallelisable one. We parallel in four fully independent ways: Firstly we have to simulate different system sizes. Secondly, for each size, we have to simulate different values of the dilution of the system. Thirdly, for each dilution, we have to simulate different realizations of the random spatial hole distribution (each one is called a *sample*). And fourthly, we have to simulate each sample at different values of its internal energy.

Our application does not have strong requirements of RAM within the volunteer nodes (around 40 megabytes for the most demanding case) or of disk storage (around 2 megabytes to store the I/O configurations of the largest systems). The main problem of our simulations is that, as the system size is increased, the run time grows exponentially. This fact forced us to design a continuity system allowing the division of long simulations into small (in terms of time) parts. In particular, the process that one of our runs for a given dilution and system size follows is:

1. For each sample (typically there will be around 1000 of them), a random spatial hole configuration is generated depending on the system dilution. The holes will remain fixed in time (quenched disorder).

2. For each energy (typically there will be around 30 of them), to each non-empty site of the lattice a spin variable is assigned. The assignation can be or a random Potts state, or a fixed one, or even a value depending on the system's energy. The result is called a configuration and saved into a file.

3. Each configuration is sent to a volunteer's machine and updated there using a MC method. In addition, some measurements are taken into the system during the update process and saved into a measurement file. It has been calculated that the optimal time for a run on each volunteer machine (in order to minimise both the errors due to unexpected shutdowns and the web traffic) is around half an hour. Therefore the number of MC updates of the configuration must be set to last around this amount of time.

4. When the specified number of MC updates have been made, both the output configuration and the measurement file are uploaded from the volunteer's computer to a server, where they are checked properly in order to avoid corruption.

5. If the total desired simulation time is longer than half an hour, the continuity system takes over control: It will resend both the configuration and the measurement file to another volunteer (step 3), who will continue updating the system from the last configuration. The process is repeated until the total number of desired MC updates is performed. The number of continuity iterations of a given job must be specified a priori in our application.

For example, for the smallest simulated system (with 24^3 sites) the configurations travel only twice between the IBERCIVIS server's and the volunteer's computers while for the largest system (with 128^3 sites) the continuity process is repeated twenty times. See Fig. G.3 for a full sketch of the process.

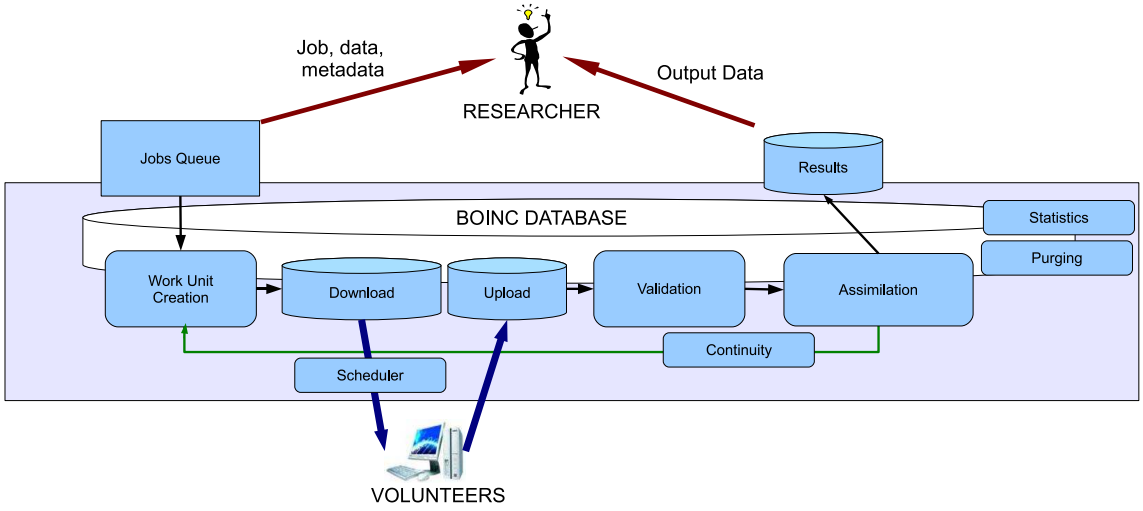

Figure G.3: Different stages of a simulation from the user submission to the results download. The term "work unit" is used the define each small portion of the whole job that is sent to a single client (each work unit should last around half an hour). Both validation and assimilation stages are crucial in order to avoid data corruption. The continuity stage is only used if the required time for the job is much longer than half an hour.

The implementation of the continuity systems is by no means naive. Each file must be univocally identified in order to avoid misdirections. If only a single file is lost or misplaced, the rest of the continuity process will fail for this configuration making the analysis of the corresponding sample impossible. In addition, if there were a temporary failure in the servers, some files would surely fail to be transferred, resulting in a breakdown of the continuity process. This sometimes happened in the early stages of the project: due to some server crashes, the continuity process was unstable and simulation of the largest systems was impossible. Finally, by building paranoid assimilation-validation systems and by developing a univocal nomenclature for each file we decreased the failure rate of the continuity system to less than 0.5%.

Using IBERCIVIS, we have simulated the site-diluted three-dimensional Potts model with a precision never reached before. We obtained more than 2.5×10^6 hours of CPU time. A more detailed description of our usage of the infrastructure is given in Table G.1.

L	# dilutions	# samples	# iterations	# energies	CPU time ($\times 10^3$ hours)
24	14	7000	2	40	280
32	13	6500	2	30	195
48	12	24000	2	30	720
64	8	10000	3	30	450
128	4	2000	20	30	900

Table G.1: Approximate statistics of our simulations in IBERCIVIS for each linear lattice size L. The fourth column gives the number of continuity iterations used to obtain enough MC time for each simulated energy.

Bibliography

[1] N. Goldenfeld, *Lectures on Phase Transitions and the Renormalization Group*, Addison-Wesley Publishing Company (1992).

[2] J. Zinn-Justin, *Quantum Field Theory and Critical Phenomena*, Oxford University Press (2004).

[3] L. P. Kadanoff, Physics (Long Island City, NY) **2**, 263 (1966).

[4] K. G. Wilson, Phys. Rev. B **4**, 3174 (1971); *ibid* **4**, 3184 (1971).

[5] K. G. Wilson, Rev. Mod. Phys. **47**, 773 (1975).

[6] M. E. Fisher, Rev. Mod. Phys. **70**, 653 (1998).

[7] D. Amit and V. Martín-Mayor, *Field Theory, the Renormalization Group and Critical Phenomena*, 3rd. edition, World Scientific (2005).

[8] A. Pelissetto and E. Vicari, Phys. Rep. **368**, 549 (2002).

[9] D. P. Landau and K. Binder, *A Guide to Monte Carlo Simulations in Statistical Physics*, Cambridge (2000).

[10] U. Wolff, Phys. Rev. Lett. **62**, 361 (1989).

[11] R.H. Swendsen and J.-S. Wang, Phys. Rev. Lett. **58**, 86 (1987).

[12] J. Salas and A. D. Sokal, J. Stat. Phys. **87**, 1-2 (1997).

[13] V. Martín-Mayor, Phys. Rev. Lett. **98**, 137207 (2007).

[14] A. P. Young (editor), *Spin Glasses and Random Fields*, World Scientific (1998).

[15] M. Mezard, G. Parisi, and M. A. Virasoro, *Spin Glass Theory and Beyond*, World Scientific (1987).

[16] M. Dudka, R. Folka, and Y. Holovatch, J. Magn. Magn. Mater. **294**, 305 (2005).

[17] R. Harris, M. Plischke, and M. J. Zuckermann, Phys. Rev. Lett. **31**, 160 (1973).

[18] R. Stinchcombe, *Theory of Dilute Anisotropic Magnets*, in *Disordered Systems and Localization*, Springer (1981).

[19] R. Stinchcombe, *Dilute Magnetism*, in *Phase Transitions and Critical Phenomena*, vol. 7, edited by C. Domb and J. L. Lebowitz, Academic Press (1983).

[20] W. Janke, B. Berche, C. Chatelain, and P. E. Berche, *Quenched disordered ferromagnets*, PoS(LAT2005)018.

[21] R. Folk, Yu. Holovatch, and T. Yavors'kii, Physics-Uspekhi **46**, 169 (2003).

[22] G. Parisi, *Field Theory, Disorder and Simulations*, World Scientific (1994).

[23] A. B. Harris, J. Phys. C **7**, 1671 (1974).

[24] S. Wiseman and E. Domany, Phys. Rev. E **58**, 2938 (1998).

[25] C. Deroulers and A. P. Young, Phys. Rev. B **66**, 014438 (2002).

[26] A. Malakis and N. G. Fytas, Phys. Rev. E **73**, 016109 (2006); see also *arXiv:0810.5438*.

[27] A. Aharony and A. B. Harris, Phys. Rev. Lett. **77**, 3700 (1996).

[28] H. Chamati, E. Korutcheva, and N. S. Tonchev, Phys. Rev. E **65**, 026129 (2002).

[29] A. Aharony, A. B. Harris, and S. Wiseman, Phys. Rev. Lett. **81**, 252 (1998).

[30] A. Gordillo-Guerrero and J. J. Ruiz-Lorenzo, J. Stat. Mech. **P06014** (2007).

[31] L. A. Fernández, A. Gordillo-Guerrero, V. Martín-Mayor, and J. J. Ruiz-Lorenzo, Phys. Rev. Lett. **100**, 057201 (2008).

[32] L. A. Fernández, A. Gordillo-Guerrero, V. Martín-Mayor, and J.J. Ruiz-Lorenzo, AIP Conference Proceedings **1071**, 46 (2008).

[33] L. A. Fernández, A. Gordillo-Guerrero, V. Martín-Mayor, and J.J. Ruiz-Lorenzo, Phys. Rev. E **80**, 051105 (2009).

[34] A. Gordillo-Guerrero, R. Kenna, and J. J. Ruiz-Lorenzo, Phys. Rev. E **80**, 031135 (2009).

[35] A. Gordillo-Guerrero, R. Kenna, and J. J. Ruiz-Lorenzo, proceedings of the "3rd Conference on Statistical Physics: Modern Trends and Applications", Lviv, Ukraine (2009), in press.

[36] F. Belletti, M. Cotallo, A. Cruz, L. A. Fernández, A. Gordillo, M. Guidetti, A. Maiorano, F. Mantovani, E. Marinari, V. Martín-Mayor, A. Muñoz-Sudupe, D. Navarro, G. Parisi, S. Pérez-Gaviro, M. Rossi, J. J. Ruiz-Lorenzo, S. F. Schifano, D. Sciretti, A. Tarancón, R. Tripiccione, and J. L. Velasco, Computing in Science and Engineering **11**(1), 48 (2009).

[37] F. Belletti, M. Cotallo, A. Cruz, L. A. Fernández, A. Gordillo, M. Guidetti, A. Maiorano, F. Mantovani, E. Marinari, V. Martín-Mayor, A. Muñoz-Sudupe, D. Navarro, G. Parisi, S. Pérez-Gaviro, M. Rossi, J. J. Ruiz-Lorenzo, S. F. Schifano, D. Sciretti, A. Tarancón, R. Tripiccione, and J. L. Velasco, Nuovo Cimento B **123**, 6-7, 972 (2008).

[38] F. Belletti, M. Cotallo, A. Cruz, L. A. Fernández, A. Gordillo, A. Maiorano, F. Mantovani, E. Marinari, V. Martín-Mayor, A. Muñoz-Sudupe, D. Navarro, S. Pérez-Gaviro, J. J. Ruiz-Lorenzo, S. F. Schifano, D. Sciretti, A. Tarancón, R. Tripiccione, and J. L. Velasco, Comp. Phys. Comm. **178** (3), 208 (2008).

[39] F. Belletti, A. Cruz, L. A. Fernández, A. Gordillo, M. Guidetti, A. Maiorano, F. Mantovani, E. Marinari, V. Martín-Mayor, A. Muñoz-Sudupe, D. Navarro, G. Parisi, S. Pérez-Gaviro, J. J. Ruiz-Lorenzo, S. F. Schifano, D. Sciretti, A. Tarancón, R. Tripiccione, and D. Yllanes, AIP Conference Proceedings **1091**, 228 (2009).

[40] A. Cruz, L.A. Fernández, A. Gordillo-Guerrero, M. Guidetti, A. Maiorano, F. Mantovani, E. Marinari, V. Martín-Mayor, A. Muñoz-Sudupe, D. Navarro, G. Parisi, S. Perez-Gaviro, J. J. Ruiz-Lorenzo, S. F. Schifano, D. Sciretti, A. Tarancón, R. Tripiccione, J. L. Velasco, D. Yllanes, and A. P. Young, Phys. Rev. B **79**, 184408 (2009).

[41] F. Belletti, M. Cotallo, A. Cruz, L.A. Fernández, A. Gordillo-Guerrero, M. Guidetti, A. Maiorano, F. Mantovani, E. Marinari, V. Martín-Mayor, A. Muñoz-Sudupe, D. Navarro, G. Parisi, S. Pérez-Gaviro, J. J. Ruiz-Lorenzo, S. F. Schifano, D. Sciretti, A. Tarancón, R. Tripiccione, J. L. Velasco, and D. Yllanes, Phys. Rev. Lett. **101**, 157201 (2008).

[42] F. Belletti, A. Cruz, L.A. Fernández, A. Gordillo-Guerrero, M. Guidetti, A. Maiorano, F. Mantovani, E. Marinari, V. Martín-Mayor, J. Monforte, A. Muñoz Sudupe, D. Navarro, G. Parisi, S. Pérez-Gaviro, J. J. Ruiz-Lorenzo, S. F. Schifano, D. Sciretti, A. Tarancon, R. Tripiccione, and D. Yllanes, J. Stat. Phys. **135**, 1121 (2009).

[43] J. Salas and A. D. Sokal, J. Stat. Phys. **88**, 567 (1997).

[44] H. G. Ballesteros, L. A. Fernández, V. Martín-Mayor, A. Muñoz Sudupe, G. Parisi, and J. J. Ruiz-Lorenzo. Phys. Rev. B **61,** 3215 (2000).

[45] C. Chatelain, B. Berche, W. Janke, and P. E. Berche, Phys. Rev. E **64**, 036120 (2001).

[46] C. Chatelain, B. Berche, W. Janke, and P. E. Berche, Nucl. Phys. B **719**, 275 (2005).

[47] A. Aharony, Phys. Rev. B **13** 2092 (1976).

[48] B. N. Shalaev, Zh. Eksp. Teor. Fiz. **73** 2301 (1977) [Sov. Phys. JETP **46**, 1204 (1977)].

[49] G. Jug, Phys. Rev. B **27**, 4518 (1983).

[50] D. J. W. Geldart and K. De'Bell, J. Stat. Phys. **73**, 409 (1993).

[51] H. G. Ballesteros, L. A. Fernández, V. Martín-Mayor, A. Muñoz-Sudupe, G. Parisi, and J. J. Ruiz-Lorenzo, Nucl. Phys. B **512**, 681 (1998).

[52] W. Janke, Nucl. Phys. B (Proc. Suppl.) **63**, 631 (1998). Similar ideas, although less explicit in their use of a microcanonical language, were developed in [105].

[53] D. H. E. Gross, *Microcanonical Thermodynamics: Phase Transitions in "Small" Systems,* Lectures Notes in Physics **66**, World Scientific (2001).

[54] R. Lustig, J. Chem. Phys. **109**, 8816 (1998).

[55] K. Binder, Z. Phys. B **43**, 119 (1981).

[56] M. N. Barber, *Finite Size Scaling* in *Phase Transitions and Critical Phenomena*, vol 8, edited by C. Domb and J.L. Lebowitz, Academic Press (1983).

[57] V. Privman (editor), *Finite Size Scaling and Numerical Simulations of Statistical Systems*, World Scientific (1990).

[58] M. E. Fisher, Phys. Rev. **176**, 257 (1968).

[59] V. Dohm, J. Phys. C **7**, 174 (1974).

[60] R. Kenna, H-P. Hsu, and C. von Ferber, J. Stat. Mech. **L10002** (2008).

[61] R. C. Desai, D. W. Heermann, and K. Binder, J. Stat. Phys. **53**, 795 (1988).

[62] M. Kastner, M. Promberger, and A. Hüller, J. Stat. Phys. **99**, 1251 (2000).

[63] A. D. Bruce and N. B. Wilding, Phys. Rev. E **60**, 3748 (1999).

[64] M. Kastner and M. Promberger, J. Stat. Phys. **103**, 893 (2001).

[65] H. Behringer and M. Pleimling, Phys. Rev. E **74**, 011108 (2006).

[66] A. Tröster, Phys. Rev. Lett. **100**, 140602 (2008).

[67] S. Caracciolo, R. G. Edwards, S. J. Ferreira, A. Pelissetto, and A. D. Sokal, Phys. Rev. Lett. **74**, 2969 (1995).

[68] F. Cooper, B. Freedman, and D. Preston, Nucl. Phys. B **210**, 210 (1982).

[69] M.P. Nightingale, Physica A, **83**, 561 (1975).

[70] H. G. Ballesteros, L. A. Fernández, V. Martín-Mayor, and A. Muñoz Sudupe, Phys. Lett. B **378**, 207 (1996); **387**, 125 (1996); Nucl. Phys. B **483**, 707 (1997).

[71] A. Aharony, J. Mag. Magn. Mater. **7**, 215 (1978).

[72] P-Z. Wong, Phys. Rev. B **34**, 1864 (1985).

[73] R. Caflisch and P-Z. Wong, Phys. Rev. B **34**, 8160 (1986).

[74] Y. Deng and H. W. J. Blöte, Phys. Rev. E **70**, 046111 (2004).

[75] M. O. Kimball and F. M. Gasparini, Phys. Rev. Lett. **95**, 165701 (2005).

[76] Y. Imry, Phys. Rev. Lett. **33**, 1304 (1974).

[77] G. A. Baker and J. W. Essam, Phys. Rev. Lett. **24**, 447 (1970).

[78] A. Tröster, Phys. Rev. Lett. **100**, 140602 (2008).

[79] C. W. Garland and B. B. Weiner, Phys. Rev. B **3**, 1634 (1971).

[80] S. Duane, A. D. Kennedy, B. J. Pendleton, and D. Roweth, Phys. Lett. B **195**, 216 (1987).

[81] M. Fukugita, H. Mino, M. Okawa, and A. Ukawa, J. Phys. A: Math. Gen. **23**, L561 (1990).

[82] F. Wu, Rev. Mod. Phys. **54**, 235 (1982).

[83] M. Hasenbusch and K. Pinn, J. Phys. A: Math. Gen. **31**, 6157 (1998).

[84] H. G. Ballesteros, L. A. Fernández, V. Martín-Mayor, A. Muñoz Sudupe, G. Parisi, and J. J. Ruiz-Lorenzo, J. Phys. A: Math. Gen. **32**, 1 (1999).

[85] M. Campostrini, A. Pelissetto, P. Rossi, and E. Vicari, Phys. Rev. E **65**, 066127 (2002).

[86] M. Nauenberg and D. J. Scalapino, Phys. Rev. Lett. **44**, 13 (1980); J. L. Cardy, M. Nauenberg, and D. J. Scalapino, Phys. Rev. B **22**, 2560 (1980).

[87] R. J. Baxter, J. Phys. C **6**, L445 (1973).

[88] B. A. Berg and T. Neuhaus, Phys. Rev. Lett. **68**, 9 (1992).

[89] F. G. Wang and D. P. Landau, Phys. Rev. Lett. **86**, 2050 (2001); Phys. Rev. E **64**, 056101 (2001).

[90] Q. Yan and J. J. de Pablo, Phys. Rev. Lett. **90**, 035701 (2003).

[91] J. Lee, Phys. Rev. Lett. **71**, 211 (1993); W. Janke and S. Kappler, Phys. Rev. Lett. **74**, 212 (1995); Y. Wu, et al., Phys. Rev. E **72**, 046704 (2005); S. Trebst, D. A. Huse, and M. Troyer, Phys. Rev. E **70**, 046701 (2004); S. Reynal and H. T. Diep, Phys. Rev. E **72**, 056710 (2005); J. Viana-Lopes, M. D. Costa, J. M. B. Lopes-dos-Santos, and R. Toral, Phys. Rev. E **74**, 046702 (2006).

[92] T. Neuhaus and J. S. Hager, J. Stat. Phys. **113**, 47 (2003).

[93] M. Biskup, L. Chayes, and R. Kotecký, Europhys. Lett. **60**, 21 (2002); K. Binder, Physica A **319**, 99 (2003); L. G. MacDowell, P. Virnau, M. Müller, and K. Binder, J. Chem. Phys. **120**, 5293 (2004); A. Nußbaumer, E. Bittner, T. Neuhaus, and W. Janke, Europhys. Lett. **75**, 716 (2006).

[94] K. T. Leung and R. K. P. Zia, J. Phys. A **23**, 4593 (1990).

[95] L. G. MacDowell, V. K. Shen, and J. R. Errington, J. Chem. Phys. **125**, 034705 (2006).

[96] E. Domany, M. Schick, and J. S. Walker, Phys. Rev. Lett. **38**, 1148 (1977).

[97] E. Domany, Y. Shnidman, and D. Mukamel, J. Phys. C **15**, 495 (1982).

[98] L. Schwenger, K. Budde, C. Voges, and H. Pfnür, Phys. Rev. Lett. **73**, 296 (1994); Phys. Rev. B **52**, 9275 (1995).

[99] E. Dagotto, Science, **309**, 258 (2005); J. Burgy et al., Phys. Rev. Lett. **87**, 277202 (2001); **92**, 097202 (2004); C. Sen, G. Álvarez, and E. Dagotto, Phys. Rev. Lett. **98**, 127202 (2007).

[100] M. Aizenman and J. Wehr, Phys. Rev. Lett. **62**, 2503 (1989); K. Hui and A. N. Berker, *ibid* **62**, 2507 (1989).

[101] J. Cardy and J.L. Jacobsen, Phys. Rev. Lett. **79**, 4063 (1997); J. Cardy and J.L. Jacobsen, Nucl. Phys. B **515**, 701 (1998); J. Cardy, at STATPHYS20 conference, North-Holland (1999), *arXiv:9806355*.

[102] B. Widom, J. Chem. Phys. **43**, 3892 (1965).

[103] H. Rieger, Phys. Rev. B **52**, 6659 (1995).

[104] H. Rieger and A. P. Young, J. Phys. A: Math. Gen. **26**, 5279 (1993); J. Machta, M. E. J. Newman, and L. B. Chayes, Phys. Rev. E **62**, 8782 (2000).

[105] M. S. S. Challa, D. P. Landau, and K. Binder, Phys. Rev. B **34**, 1841 (1986); J. Lee and J.M. Kosterlitz, Phys. Rev. Lett. **65**, 137 (1990).

[106] J. T. Chayes, L. Chayes, D. S. Fischer, and T. Spencer, Phys. Rev. Lett. **57**, 2999 (1986).

[107] A. Maiorano, V. Martín-Mayor, J. J. Ruiz-Lorenzo, and A. Tarancón, Phys. Rev. B **76**, 064435 (2007).

[108] G. Parisi and N. Sourlas, Phys. Rev. Lett. **43**, 744 (1979).

[109] A. J. Bray and M. A. Moore, J. Phys. C **18**, 927 (1985).

[110] Y. Imry and S. K. Ma, Phys. Rev. Lett. **35**, 1399 (1975).

[111] K. Binder, Z. Phys. B **50**, 343 (1983).

[112] W. Kinzel and E. Domany, Phys. Rev. B **23**, 3421 (1981).

[113] D. Stauffer, Z. Phys. B **22**, 161 (1975).

[114] D. Stauffer and A. Aharony, *Introduction to Percolation Theory*, Taylor and Francis (1984).

[115] A. D. Sokal, *Functional Integration. Basis and Applications*, (1996 Cargèse summer school), edited by C. DeWitt-Morette, P. Cartier, A. Folacci, Plenum (1997).

[116] S. N. Kaul and M. Sambasiva Rao, J. Phys.: Condens. Matter **6**, 7403 (1994).

[117] M. Sambasiva Rao and S. N. Kaul, J. Magn. Magn. Mater. **140-144**, 1567 (1995).

[118] M. Sambasiva Rao and S. N. Kaul, J. Magn. Magn. Mater. **147**, 149 (1995).

[119] P. D. Babu and S. N. Kaul, J. Phys.: Condens. Matter **9**, 7189 (1997).

[120] M. R. Said, Y. A. Hamam, I. Abu-Alyarayesh, and S. Mahmood, J. Magn. Magn. Mater. **195**, 679 (1999).

[121] V. Tsurkan, M. Baran, A. Szewczyk, and R. Szymczak, J. Phys.: Condens. Matter **11**, 7907 (1999).

[122] A. Perumal, V. Srinivas, V. V. Rao, and R. A. Dunlap, Physica B **292**, 164 (2000).

[123] A. Perumal, V. Srinivas, K. S. Kim, S. C. Yu, V. V. Rao, and R. A. Dunlap, J. Magn. Magn. Mater. **233**, 280 (2001).

[124] M. Campostrini, M. Hasenbusch, A. Pelissetto, P. Rossi, and E. Vicari, Phys. Rev. B **65**, 144520 (2002).

[125] E. Brezin and J. Zinn-Justin, Nucl. Phys. B **257**, 867 (1985).

[126] H. G. Ballesteros, L. A. Fernández, V. Martín-Mayor, and A. Muñoz-Sudupe, Phys. Lett. B **387**, 125 (1996).

[127] M. Hasenbusch, F. P. Toldin, A. Pelissetto, and E. Vicari, J. Stat. Mech. **P02016** (2007).

[128] M. E. Fisher and M. N. Barber, Phys. Rev. Lett. **28**, 1516 (1972).

[129] R. Guida and J. Zinn-Justin, J. Phys. A **31**, 8103 (1998).

[130] M. Hasenbusch, J. Phys. A: Math. Gen. **34**, 8221 (2001).

[131] H. G. Ballesteros, L. A. Fernández, V. Martín-Mayor, A. Muñoz-Sudupe, G. Parisi, and J. J. Ruiz-Lorenzo, Phys. Rev. B **58**, 2740 (1998).

[132] R. Kenna and J. J. Ruiz-Lorenzo, Phys. Rev. E **78** 031134 (2008).

[133] R. Fernández, J. Frölich, and A. Sokal, *Random Walks, Critical Phenomena and Triviality in Quantum Field Theory*, Springer-Verlag (1992).

[134] M. Hellmund and W. Janke, Phys. Rev. B **74**, 144201 (2006).

[135] R. Kenna, D. A. Johnston, and W. Janke, Phys. Rev. Lett. **96**, 115701 (2006).

[136] R. Kenna, D. A. Johnston, and W. Janke, Phys. Rev. Lett. **97**, 155702 (2006).

[137] R. Kenna and C. B. Lang, Phys. Lett. B **264** , 396 (1991); Nucl. Phys. B **393**, 461 (1993); Phys. Rev. E **49**, 5012 (1994).

[138] T. D. Lee and C. N. Yang, Phys. Rev. Lett. **87**, 404 (1952); **87**, 410 (1952).

[139] J. J. Ruiz-Lorenzo, J. Phys. A **30**, 485 (1997).

[140] W. Janke and R. Kenna, J. Stat. Phys. **102**, 1211 (2001); in *Computer Simulation Studies in Condensed Matter Physics XIV*, edited by D. P. Landau, S. P. Lewis, and H.B. Schuettler, Springer (2001); Nucl. Phys. B (Proc. Suppl.) **106-107**, 905 (2002); Comp. Phys. Comm. **147**, 443 (2002); W. Janke, D. A. Johnston, and R. Kenna, Nucl. Phys. B (Proc. Suppl.) **119**, 882 (2003); Nucl. Phys. B **682**, 618 (2004); Comp. Phys. Comm. **169**, 457 (2005).

[141] V. Dotsenko, *Introduction to the Replica Theory of Disordered Statistical Systems*, Cambridge University Press (2001).

[142] M. Falcioni, E. Marinari, M. L. Paciello, G. Parisi, and B. Taglienti, Phys. Lett. B **108**, 331 (1982).

[143] A. M. Ferrenberg and R. H. Swendsen, Phys. Rev. Lett. **61**, 2635 (1988).

[144] H. G. Ballesteros, *Transiciones de Fase en Sistemas Desordenados*, PhD thesis, Universidad Complutense de Madrid (1998).

[145] B. Simon and R. B. Griffiths, Comm. Math. Phys. **33**, 145 (1973); M. Newman, Comm. Pure Appl. Math. **27**, 143 (1974); E. H. Lieb and A. D. Sokal, Comm. Math. Phys. **80**, 153 (1981).

[146] C. Itzykson and J. M. Drouffe, *Statistical Field Theory*, vol. 1, Cambridge University Press (1989).

[147] For more information visit: *www.ibercivis.es* .